In Situ Molecular Analysis using Two-Step Laser Mass Spectrometry

Scott Jason Wright

A thesis presented for the degree of
Doctor of Philosophy in the Faculty of
Science at the University of Edinburgh,
1997

In memory of my father.

... we shall have an open mind, and not let a little bit of truth check the rush of a big truth, like a small rock does a railway truck. We get the small truth first. Good! We keep him, and we value him; but all the same we must not let him think himself all the truth in the universe.

— Abraham Van Helsing
in *Dracula*, by Bram Stoker

Abstract

The work described in this thesis is concerned with the development of laser desorption laser photoionisation mass spectrometry (L2MS) towards spatially resolved analysis of real complex molecular systems. A broad overview of the main elements of the technique is presented. In addition, the experimental procedures and equipment used to carry out this work are described in some detail.

Photoionisation mass spectra recorded for a series of azo dyes and porphyrin pigments revealed a marked wavelength dependence in their ionisation and fragmentation channels. The relationship between this behaviour and the known photochemical and photophysical properties of these molecules is discussed. The photochemistry of these molecules has been exploited to aid the differentiation between isomeric species.

The selectivity inherent in the L2MS technique has been exploited for *in situ* studies of a number of real systems. Polymer additives, such as antioxidants and ultraviolet stabilisers, have been successfully detected directly from their host polymer matrices without recourse to extraction, separation or pre-concentration. The technique has been shown to be surface specific, suggesting that the long-term goal of spatially resolved analysis to monitor, for example, additive aggregation and migration to the surface are feasible. In further *in situ* studies, polycyclic aromatic hydrocarbons, an important class of priority pollutants, adsorbed onto aerosol particulates have been detected. Electrochemically polymerised indoles, known to form conducting films, have also been identified directly from the electrode surface.

Finally, current limitations of the L2MS technique are discussed. It is suggested that many of the problems identified are inextricably linked to the laser desorption process. It is shown that energy imparted to neutral molecules during the desorption event can lead to fragmentation. This has implications for both the ionisation of high mass molecules and for quantitative studies. Possible ways of circumventing these problems are discussed. The future outlook for the technique, both for fundamental studies, and as an analytical tool, is also discussed.

Acknowledgments

The completion of this thesis would not have been possible without help and support from many sources. Firstly, I would like to thank my supervisor, Pat Langridge-Smith for introducing me to the area of laser mass spectrometry, and for his help and encouragement throughout the course of this thesis. I would also like to thank my second supervisor, Anita Jones, for many valuable discussions on all aspects of this work. I would also like to thank the BMSS, who in addition to funding me throughout the last three years via a John Beynon Studentship, also contributed greatly to sending me to several conferences, both at home and abroad.

I would also like to thank Professor Renato Zenobi for allowing me to work for three weeks in his laboratory at the ETH Zürich during my final year. I enjoyed the experience immensely and learnt a great deal during my time there. Thanks must also be extended to the rest of Renato's group for making me feel most welcome.

This work would not have been possible without considerable help from my co-workers. Mike Dale deserves special thanks for showing me how to operate the experimental apparatus and for sharing with me his unique views on life. Jon, Kevin, Craig, Robert, Alison and Angela were always willing to help, and often provided a useful sounding board from which to bounce ideas. Ally, Cameron, Colin, Graham, Bob and Gill, although not directly involved with this work, helped to provide a pleasant atmosphere in Room 6 which was not always conducive to working. The social life within the laser group has always been prolific, and for this Neil, Andy and Trevor deserve much praise over the last three years. Thanks to Andy for buying more beers than he needed to, and to Neil for putting up with incessant football chat. Thanks to Trevor for keeping the football chat going.

Finally, I would like to thank my mother, father and brother, Simon, for their support during my time at university. In particular, thanks to mum for her financial support over the last few grantless months of my PhD.

Table of Contents

1. Introduction 1

2. Two-Step Laser Mass Spectrometry: Background Theory 12

2.1 Introduction 12

2.2 Laser Desorption 13

2.2.1 Laser Induced Thermal Desorption 15

2.2.2 Resonant Desorption 21

2.2.3 Shock-Wave and Mechanical Desorption 25

2.2.4 Laser Desorption of Neutral Molecules in L2MS 26

2.3 Laser Photoionisation 30

2.3.1 Modes of Laser Photoionisation 31

2.3.2 Competing Processes in MPI 36

2.3.3 MPI as an Analytical Tool 45

2.4 Time-of-Flight Mass Spectrometry. 52

2.4.1 Basic Principles of TOF-MS. 54

2.4.2 Factors Affecting Mass Resolution 57

2.5 Reflectron TOF Mass Spectrometer. 65

2.5.1 Effect on Resolution upon Removing the Molecular Beam 67

2.6 Concluding Remarks 68

3. Experimental 79

3.1 Introduction 79

3.2 Vacuum System 81

3.3 Generation of Gas Phase Neutrals 83

3.3.1 Laser Desorption with Entrainment 83

3.3.2 Laser Desorption with Non-Entrainment 85

3.4 Time-of-Flight Ion Optics 89
3.5 Ion Signal Detection 92
3.6 Laser Systems 93
3.6.1 Alltec 854MS CO_2 Laser 93
3.6.2 JK HyperYAG HY750 Nd^{3+}:YAG Laser 94
3.6.3 Lumonics TE - 861T-4 Excimer Laser 95
3.6.4 Vacuum Ultra Violet (VUV) Generation 96
3.7 Experimental Control and Data Acquisition 97
3.7.1 Control Hardware 99
3.7.2 Kinetic Systems 3655 Pulse Delay Generator 99
3.7.3 Transient Digitiser 100
3.7.4 Control Software 101
3.8 Data Acquisition Modes 102
3.8.1 TOF Mode — Acquisition of Mass spectra 102
3.8.2 Timescan Mode 102
3.8.3 Frequency Scan Mode 104

4. L2MS of Azo Dyes and Porphyrin Pigments 108

4.1 Introduction 108
4.2 L2MS of Azo Dyes 109
4.2.1 L2MS of Simple Azo Dyes 112
4.2.2 L2MS of Isomeric Azo Dyes 124
4.3 L2MS of Porphyrin Pigments 139
4.3.1 Evidence of Class B Behaviour in MetalloTPPs 141
4.3.2 Effect of Ionising Wavelength on Class B Behaviour 143
4.4 Concluding Remarks 151

5. Analysis of Polymer Systems Using L2MS 157

5.1 Introduction 157
5.2 L2MS of Pure Polymer Additives 162
5.2.1 Antioxidants 162
5.2.2 UV Stabilisers 166

5.2.3 Isomeric UV Stabilisers 168
5.2.4 Discussion — Photofragmentation of UV Stabilisers 172
5.3 *In situ* Analysis of Additives Directly From Polymers 174
5.4 L2MS of Non-Aromatic Polymers 180
5.4.1 Non-Resonant MPI 181
5.4.2 Single-Photon Ionisation (SPI) 181
5.4.3 Laser Induced Photoelectron Ionisation (LIPEI) 187
5.5 Concluding Remarks 191

6. More Analytical Applications of L2MS 197

6.1 Introduction 197
6.2 *In Situ* Analysis of PAHs from Aerosol Particulates 198
6.2.1 Introduction 198
6.2.2 Sample Collection and Preparation 200
6.2.3 Screening of Filtrates for PAHs using L2MS 200
6.2.4 Quantitative Assessment of PAH Concentration using L2MS 207
6.2.5 Concluding Remarks 212
6.3 L2MS of Electrochemically Polymerised Indoles 213
6.3.1 Introduction 213
6.3.2 L2MS of 5-Substituted Indole Copolymers 215
6.3.3 *In Situ* Detection of Polyindole Directly from the Electrode 221
6.3.4 Concluding Remarks 224

7. Current Limitation of L2MS as an Analytical Technique 228

7.1 Introduction 228
7.2 Desorption Issues 229
7.2.1 Unexpected Experimental Observations 231
7.2.2 Tryptophan as a Chemical Thermometer 241
7.3 Ionisation of High Mass Molecules 256
7.3.1 Geminate Charge-Pair Formation and Ionisation 258
7.3.2 Efficient Photofragmentation as a Result of Internal Energy 260
7.3.3 Experimental Tests 262

7.4 Limitations on *in Situ* Analysis.....265

7.5 Concluding Remarks.....267

8. L2MS – Concluding Remarks.....272

8.1 Thesis Summary.....272

8.2 Future Outlook.....275

Appendix A. Courses and Conferences Attended.....282

Appendix B. Publications and Official Reports.....284

List of Figures

2-1: Schematic diagram illustrating the "bottleneck model" of IR laser desorption. 18

2-2: Schematic diagram illustrating various laser photoionisation schemes; (a) Single photon ionisation, (b) non-resonant multi-photon ionisation, (c) [1 + 1] REMPI and (d) [2 + 1] REMPI. 32

2-3: Schematic diagram illustrating the possible competing photophysical and photochemical process occurring at the excited intermediate state. 39

2-4: Schematic diagram illustrating the ladder switching model of multiphoton ionisation 42

2-5: Schematic diagram illustrating the Molecular Ion and Autoionisation models for photoionisation using picosecond and femtosecond pulsed laser systems..... 44

2-6: Time-of-flight mass spectrum of trytophan in a matrix of PEG, obtained using 10.6 μm laser desorption and 300 nm photoionisation. The only peaks in the spectrum correspond to the molecular ion and the dehydroindole fragment ion. There is no evidence of any signal from the non-absorbing PEG. 49

2-7: Time-of-flight mass spectra of perylene obtained under (a) soft, and (b) hard ionisation conditions using 266 nm photoionisation. The power densities were 0.5×10^6 Wcm^{-2} and 5×10^6 Wcm^{-2}, respectively. 51

2-8: Schematic diagram illustrating the ionisation and fragmentation mechanisms in electron impact ionisation. 53

2-9: Schematic diagram illustrating the (a) single field, and (b) double field Wiley-McLaren type, linear TOF mass spectrometers..... 56

2-10: Schematic diagram illustratint the effects of ions created (a) with different initial locations, (b) with different initial velocities, and (c) at the (I) leading and (ii) trailing edges of the ionising laser pulse. These illustrate the limits of spatial, energy and timing resolution, respectively. 60

2-11: Schematic diagram illustrating the Reflectron TOF mass spectrometer..... 66

2-12: Schematic diagram illustrating the effects of desorbing (a) parallel, and (b) orthogonal to the axis of extraction. 69

3-1: Schematic diagram of the L2MS instrument. This shows a side view of the instrument as set up for the entrainment mode. When used in the non entrainment mode, desorption is carried out in the ionisation chamber, as illustrated in Figure 3-3. 80

3-2: Schematic illustration of the laser desorption source used in the entrainment mode. The molecular beam valve is mounted on an XYZ translator, not shown, which allows alignment of the molecular beam with the skimmer aperture. 84

3-3: Schematic diagram of the laser desorption source as used in the non-entrainment mode. Desorption is carried out within the ion extraction optics, with ionisation occurring just above the sample surface. 87

3-4: Time-of-flight mass spectra of cloud water filtrate, obtained using 10.6 μm laser desorption and 193 nm photoionisation using (a) entrainment mode, and (b) non-entrainment mode 88

3-5: Schematic diagram of ion extraction optics, situated in the ion source chamber. Typical operating potentials are shown, and all dimensions are given in mm. 90

3-6: Schematic diagram of the ion mirror which is mounted from the rear flange of the reflectron chamber. It is tilted at 4^{o} to the normal in order to deflect the ions down the second field free drift region. All dimensions are given in mm, and typical operating potentials are shown. 91

3-7: Schematic illustration of the VUV generation assembly, where 355 nm radiation is frequency tripled in a gas cell of xenon to give 118 nm (10.4 eV) radiation. 98

3-8: Schematic diagram of the CAMAC-based experimental control system. 100

3-9: Typical trigger pulse timing set-up for an L2MS experiment in (a) the non-entrainment mode, and (b) the entrainment mode 103

3-10: Desorption profile of coronene obtained in the timescan mode by varying the time of the UV laser relative to the desorption laser. 105

3-11: Fixed frequency scan of Parsol1789, demonstrating the decay of the ion signal as the sample is depleted by repeated exposure to the desorption laser. The sample has been effectively removed after approximately 2000 laser shots. 106

4-1: L2MS spectra of (a) 4-phenylazoaniline (paa), and (b) 4-phenylazophenol (pap), obtained using 10.6 μm laser desorption and 193 nm laser photoionisation. 113

4-2: Proposed scheme of major ionisation channels for (a) paa, and (b) pap, following 193 nm photoionisation. 115

4-3: L2MS spectra of (a) paa, and (b) pap, obtained using 10.6 μm laser desorption and 266 nm photoionisation. 117

4-4: Proposed scheme of major ionisation and fragmentation pathways for (a) paa, and (b) pap, following 266 nm photoionisation. 119

4-5: Schematic illustration of trans-cis isomerisation of azobenzene, and proposed cyclic intermediate required for N_2 elimination. 122

4-6: Schematic illustration of azo-hydrazone tautomerism 124

4-7: L2MS of the isomeric azo dyes (a) ahp, and (b) hap, obtained using 10.6 μm laser desorption and 266 nm laser photoionisation. The peaks denoted "*" are due to an internal mass standard, carbazole, m/z = 167. 125

4-8: Proposed fragmentation scheme for (a) ahp, and (b) hap, following 266 nm photoionisation 127

4-9: L2MS of mr1 obtained using 10.6 μm laser desorption and 266 nm laser photoionisation. Spectra (b), (c) and (d) were obtained at low, medium and high ionising laser power density, respectively, and illustrate the behaviour of the major fragmentation products with ionising laser power density..... 131

4-10: Proposed fragmentation pathways for mr1 following 266 nm photoionisation.... 132

4-11: L2MS of mr2 obtained using 10.6 μm laser desorption and 266 nm laser photoionisation. Spectra (b), (c) and (d) were obtained at low, medium and high ionising laser power density, respectively, and illustrate the behaviour of the major fragmentation products with varying ionising laser power density..... 133

4-12: Proposed ionisation and fragmentation pathways for mr2 following 266 nm photoionisation of mr2. 134

4-13: L2MS of mr3 obtained using 10.6 μm laser desorption and 266 nm laser photoionisation. Spectra (b), (c) and (d) were obtained at low, medium and high ionising laser power density, respectively, and illustrate the behaviour of the major fragmentation products with ionising laser power density..... 136

4-14: Proposed ionisation and fragmentation pathways for mr3 following 266 nm photoionisation. 137

4-15: L2MS of ZnTPP obtained using 10.6 μm laser desorption and 235 nm laser photoionisation. This spectrum was obtained under partially hard ionising laser conditions in order to induce some fragmentation processes. 144

4-16: L2MS of ZnTPP obtained using 10.6 μm laser desorption and (a) 240 nm, (b) 250 nm, (c) 260 nm, and (d) 270 nm laser photoionisation. There is no evidence of demetallation of the porphyrin macrocyle at any of these ionisation wavelengths. 145

4-17: Enlargement of molecular ion region of ZnTPP, illustrating near-unit mass resolution. The solid "spiked lines" indicate the calculated isotope fingerprint of ZnTPP. This fits the experimental data very well. 146

4-18: L2MS of VOTPP obtained using 10.6 μm laser desorption and 250 nm laser photoionisation. This spectrum was obtained using partially hard ionisation conditions in order to induce some fragmentation. 147

4-19: L2MS of VOTPP obtained using 10.6 μm laser desorption and (a) 235 nm, (b) 245 nm, (c) 255 nm, and (d) 266 nm laser photoionisation. It can clearly be observed that as the laser wavelength is increased, demetallation of the porphyrin macrocycle is increased. 148

4-20: Plot of $M^{+\cdot}$:$[M\text{-}VO+2H]^{+}$ versus ionising laser wavelength. This clearly shows that as the laser photon energy is increased, Class A photoionisation behaviour begins to dominate over Class B behaviour. 150

5-1: L2MS spectra of Irganox 1330 using (a) 266 nm and (b) 193 nm photoionisation; Irganox 1076 using (c) 266 nm and (d) 193 nm photoionisation. 163

5-2: L2MS spectra of Irgafos 168 using (a) 266 nm and (b) 193 nm photoionisation; Santo White powder using (c) 266 nm and (d) 193 nm photoionisation. 165

5-3: L2MS spectra of Tinuvin P using (a) 266 nm and (b) 193 nm photoionisation; Tinuvin 326 using (c) 266 nm and (d) 193 nm photoionisation; Tinuvin 327 using (e) 266 nm and (b) 193 nm photoionisation. Peaks marked with an

asterisk (*) are due to the internal mass standards indole (m/z=117) and carbazole (m/z=167)..... 167

5-4: L2MS spectra obtained using 266 nm photoionisation of the isomeric UV stabilisers (a) Tinuvin 320, (b) Tinuvin 343 and (c) Tinuvin 329..... 169

5-5: L2MS spectra obtained using 193 nm photoionisation of the isomeric UV stabilisers (a) Tinuvin 320, (b) Tinuvin 343 and (c) Tinuvin 329..... 170

5-6: In situ L2MS spectra of a polypropylene (PP) sample containing Irganox 1330 (0.15wt%) and Irgafos 168 (0.05wt%). Photoionisation was carried out using (a) 266 nm and (b) 193 nm radiation. $[M1]^+$ and $[M2]^+$ denote the molecular ions of Irganox 1330 and Irgafos 168, respectively. 175

5-7: In situ L2MS spectrum of an injection moulded sample of polyoxymethylene (POM) containing 0.3wt% Tinuvin 320. Photoionisation was carried out using 193 nm radiation. Photoionisation using 266 nm radiation produced no signal... 177

5-8: In situ L2MS spectra of an injection moulded POM sample containing 0.1wt% Santo White powder. The desorption laser was used interrogate (a) the finished exterior surface and (b) the unfinished interior surface..... 179

5-9: L2MS spectrum of an injection moulded sample of pure POM. The ionisation laser power density used was increased from 0.8 x $10^6 Wcm^{-2}$ to 3.4 x 10^6 Wcm^{-2} in order to promote non-resonant MPI. 182

5-10: L2MS mass spectrum of a PDMS sample, M_w=770. The peaks labeled n=1-13 correspond to the siliconium series of ions, $[Me_3Si(O\text{-}SiMe_2)]^+$. The peaks labeled with an asterisk (*) correspond to the $[(O\text{-}SiMe)()\text{-}SiMe_2)_m]^+$ ion series.. 184

5-11: SPI L2MS spectra of higher average molecular weight PDMS samples, where (a) M_w = 3780 and (b) M_w = 93 700. Peaks denoted by an asterisk (*) are members of the $[O\text{-}SiMe(O\text{-}SiMe_2)_m]^+$ ion series, whilst the peaks marked "n" are members of the $[Me_3Si(O\text{-}SiMe_2)_n]^+$ series. These ion series are illustrated in Table 5-2. 186

5-12: (a) Schematic illustration of the experimental arrangement for generation of laser induced photoelectrons. (b) Photoelectron trajectories as simulated by the SIMION programme, version 6.0. The electron emitter is grounded, and all other electrode potentials are at typical values as shown in Chapter 2. 189

5-13: LIPEI L2MS spectrum of PDMS, M_w=770. The estimated photoelectron energy is approximately 100 eV. Peaks denoted by an asterisk (*) are members of the $[O\text{-}SiMe(O\text{-}SiMe_2)_m]^+$ ion series, whilst the peaks marked "n" are members of the $[Me_3Si(O\text{-}SiMe_2)_n]^+$ series. These ion series are illustrated in Table 5-2. 191

6-1: Schematic diagram of the conical passive Harp-Wire device used to collect cloud water samples. 201

6-2: L2MS spectrum of cloud water filtrate obtained directly from the polycarbonate filter using 10.6 μm laser desorption and 193 nm photoionisation. The transient digitiser (TD) sampling interval used was 40 ns 203

6-3: L2MS spectrum of cloud water filtrate obtained directly from the polycarbonate filter using 10.6 μm laser desorption and 193 nm photoionisation. The TD sampling interval used was 20 ns, resulting in improved mass mass resolution: (a) shows the full mass spectrum, whereas (b) shows the same spectrum expanded into two regions..... 206

6-4: L2MS spectrum of cloud water filtrate obtained directly from the polycarbonate filter using 10.6 μm laser desorption and 248 nm photoionisation. The TD sampling interval used was 20 ns: (a) shows the full mass spectrum, whereas (b) shows the same spectrum expanded into two regions. 208

6-5: Postulated structure for the cyclic trimer formed during electropolymerisation of 5-substituted indoles..... 216

6-6: (a) L2MS spectrum of DMF soluble fraction of copolymer film produced by electroxidation of an equimolar mixture of CI and ICA, using 10.6 μm laser desorption and 266 nm photoionisation. (b) Proposed structures for asymmetric trimers and cotrimers produced by electroxidation of CI and ICA. It should be noted that each cotrimer shown is only one of three possible stuctures, since the three indole groups are not in identical environments. 217

6-7: L2MS spectrum of an equimolar mixture of 3CI and 3ICA trimers obtained using 10.6 μm laser desorption and 266 nm photoionisation. This demonstrates that the different substituent groups on each of these molecules does not induce significant changes in their absorption cross-sections at 266 nm. 219

6-8: L2MS spectra of the four fractions of the original CI/ICA copolymer mixture which eluted from the Sephadex column. These spectra were obtained using 10.6 μm laser desorption and 266 nm photoionisation, and demonstrate that the individual trimer species can be partially separated.....220

6-9: (a) L2MS spectrum of the DMF soluble fraction of a polyindole film recovered from the electrode, and applied to a stainless steel sample probe in concentrated form: (b) *in situ* L2MS spectrum of a polyindole film directly from the gold electrode. In both cases, 10.6 μm laser desorption and 266 nm photoionisation were used.....223

7-1: Time-of-flight mass spectra of Parsol 1789 using 10.6 mm laser desorption and 193 nm photoionisation; (a) with a low desorption power density of 7 x 10^6 Wcm^{-2}, and (b) with a higher desorption power density of 12 x 10^6 Wcm^{-2}.....233

7-2: Fixed frequency scans of the three major ion peaks of 4-phenylazoaniline. Scans 1 and 2 were obtained using identical laser conditions, but at different locations on the sample. The three major ion peaks correspond to the molecular ion, (a) and (d), elimination of N_2 from the molecular ion, (b) and (e), and the aniline fragment ion, (c) and (f).....234

7-3: Time of flight mass spectrum of Parsol 1789 using 10.6 μm laser desorption, with entrainment of the desorbed neutrals in a supersoni molecular beam of helium. Photoionisation was carried out at 193 nm radiation.....236

7-4: Time-of-flight mass spectra of Parsol 1789 using 10.6 μm laser desorption and 193 nm photoionisation; (a) using a low ionising laser power density, and (b) a high ionising laser power density.....237

7-5: Simple "bar" mass spectra of 4-phenylazoaniline. Spectra (a) and (b) correspond to the first and last laser shots of Scan 1, respectively. Spectra (c) and (d) correspond to the first and last laser shots of Scan 2, respectively.....239

7-6: Time-of-flight mass spectrum of tryptophan obtained using 532 nm laser desorption in conjunction with a supersonic expansion. Photionisation was carried out at 286.5 nm.....245

7-7: Time-of-flight mass spectrum of tryptohan obtained using 10.6 μm laser desorption and 290 nm photoionisation, without the use of molecular beam entrainment. 246

7-8: Time-of-flight mass spectra of tryptophan obtained using 10.6 μm laser desorption. The photoionisation wavelength is varied between 250 nm and 340 nm. All spectra are normalised relative to the dehydroindole ion. The peak at m/z = 220 corresponds to an oxide of tryptophan, produced in the solution phase. 248

7-9: Time-of-flight mass spectra of tryptophan obtained using 10.6 μm laser desorption and 300 nm photoionisation; (a) desorption of a thin layer of tryptophan from a glass substrate; (b), (c) and (d) desorption of tryptophan dispersed in a PEG matrix. The desorption power density is systematically increased from spectra (b) to (d). 250

7-10: Energy level diagram for the photoionisation of tryptophan under three different experimental conditions: (a) photoionisation at 286.5 nm of internally cool neutral molecules, as would be expected with the use of molecular beam entrainment. (b) photoionisation at 290 nm of vibrationally excited neutral molecules. (c) photoionisation using 250 nm of vibrationally excited neutral molecules 253

7-11: Time-of-flight mass spectra of tryptophan obtained under three different experimental conditions. This Figure should be read in conjunction with Figure 7- 10: (a) shows 286.5 nm photoionisation of tryptohan desorbed into a molecular beam. (b) shows photoionisation of tryptophan at 290 nm without seeding in a molecular beam. (c) shows photoionisation at 250 nm, without seeding in a molecular beam. 254

List of Tables

3-1: Power supplies and typical operating potentials of ion extraction and reflectron electrodes 92

4-1: Names, structures and molecular weights of azo dyes studied by L2MS 111

4-2: Names, structures and molecular weights of the metalloTPPs studied in this work 142

5-1: Nomenclature and Structure of Polymer Additives 161

5-2: Major ion series observed in the SPI L2MS spectra of PDMS, M_W = 770. Members of these two ion series, $[Me_3Si(O\text{-}SiMe_2)_n]^+$ and $[O\text{-}SiMe(O\text{-}SiMe_2)_m]^+$, are characteristic of PDMS samples 185

6-1: Representative structures and molecular weights of PAHs detected in cloud-water particulate samples using L2MS 204

Chapter 1

Introduction

Currently, there is an increasing demand for the development of techniques capable of carrying out advanced measurements on a wide variety of materials. Historically, mass spectrometry has proved to be a very powerful method for identifying and studying the structure of molecules, and for the characterisation of matter. However, many mass spectrometric techniques suffer due to the requirement for the sample to be either initially present in, or introduced into, the gas-phase. This is no great problem for low molecular weight or volatile materials. Even some larger, less volatile molecules are amenable to mass spectroscopic analysis, simply by heating the sample, provided it is thermally stable. Unfortunately, the mass spectroscopic analysis of high mass, involatile and thermally labile molecules is problematic, and the identification and structural characterisation of such samples has presented the analytical chemist with a major challenge.

An ideal mass spectrometric technique must be flexible in the type of data it produces. If the technique is to be used to identify many components in a complex mixture, then clearly soft ionisation is desirable so that only molecular ions are generated. This would result in simple mass spectra, which are readily interpretable. However, the same technique, if it is to be generally applicable, should also be capable of yielding structural information on single component systems. This would require hard ionisation in order to break the molecule down into its constituent parts. It is evident, therefore, that the mass spectrometric technique of choice should provide some control over the degree of fragmentation, either to reduce congestion mass spectra of complex mixtures, or to yield structural information on single component systems. In addition to these features, the ideal mass spectrometric

technique should enable measurements to be made in the high mass range with good resolution and reasonable mass measurement accuracy. Also, since many samples of interest will be minor components of mixtures, the technique must be both sensitive and selective.

A wide variety of mass spectrometric techniques are now available that can fulfill some, but unfortunately not all, of these demands. As yet, there is no universally applicable mass spectroscopic technique, and, at present, a combination of techniques must be used to fully characterise a given system. The scope of these techniques has been increased by coupling them with various separation methodologies, yielding an array of so-called hyphenated techniques. However, although very useful, they are also time consuming and so severely limit the number of systems which can be fully characterised.

The principal difficulty in the analysis of thermally labile and highly polar molecules is that the mass spectroscopic characterisation must be preceded by sample evaporation into the gas-phase. Traditionally, resistive heating of the sample has been used to produce an appreciable vapour pressure of sample for ionisation. However, the energy required for evaporation frequently exceeds the level that induces thermal degradation, thereby limiting the amount of useful information. This has been the principal reason why many molecular species have previously eluded satisfactory mass spectroscopic characterisation. Another approach that has often been used is to chemically derivatise the sample, in order to produce a more volatile material that is readily amenable to mass spectrometric analysis [1]. However, in addition to being extremely time consuming and empirical, there is no guarantee that the chemical integrity of the sample remains uncompromised.

The development of flash desorption techniques in the 1970s proved to be an important advance [2,3]. This demonstrated that thermolability was a relative concept, and that it is the heating rate, and not the absolute temperature, which is important in influencing the degree of sample decomposition. Using such techniques, heating rates of 5000 Ks^{-1} were achieved, compared to the more conventional heating rate of 10 Ks^{-1} possible using traditional resistive heating. It

was also discovered that these faster heating rates favoured the desorption of intact neutral species over decomposition products. However, although this was an important advance, the attainable heating rates were insufficiently high to completely preclude decomposition.

The advent of so-called desorption/ionisation techniques such as fast atom bombardment (FAB) [4], secondary ion mass spectrometry (SIMS) [5,6] and Cf-plasma desorption mass spectrometry (Cf-PDMS) [7] proved to be another significant advance. In these techniques, a thin layer of solid material is bombarded with beams of energetic particles, leading to the desorption of ions and neutral species into the gas-phase. In addition to these desorption/ionisation processes, there are a variety of others which have been developed, including laser desorption (LD) [8,9,10], matrix assisted laser desorption ionisation (MALDI) [11], field desorption (FD) [12], direct chemical ionisation (DCI) [13], thermal desorption (TD) [14], thermospray ionisation (TSI) [15] and electrospray ionisation (ESI) [16]. These have all been used for the investigation of large involatile molecules.

Although there is a great diversity in the experimental procedures employed in these techniques, they all have one central theme in common; the evaporation of the solid sample and the production of gas-phase ionic species are carried out in a single step. Therefore, the overall efficiency is limited by the combined efficiencies of both processes. Since the energy available for ionisation is directly coupled to the energy required for desorption, the ionisation process is very difficult to control. This necessarily makes it difficult to control the degree of fragmentation observed in the mass spectrum. For example, in these single step desorption/ionisation techniques, very often little or no molecular ion signal is observed, the spectra being dominated instead by fragment ions. In addition, it is rare for radical molecular cations to be formed; it is far more common to see protonated molecular ions and alkali metal adducts. A further difficulty is that these techniques tend to be non-selective, so any matrix species or impurities present will also be ionised. This can often lead to extremely complex mass spectra. Therefore, whilst useful structural data on large polar, involatile molecules can be obtained using these techniques, their use for the

analysis of complex mixtures is clearly limited due to the relative lack of selectivity and the abundance of fragment ions and adduct species observed in typical spectra.

In other sample introduction techniques, such as electrospray and thermospray, sample evaporation and ionisation also occurs in a single step. However, with these processes, it is particularly difficult to induce fragmentation. These techniques are inherently soft ionisation methods, and whilst useful for complex mixture analysis, provide little structural information. Also, in common with MALDI and FD, these techniques have found only limited application in the analysis of "real-world" systems. The spraying techniques require sample dissolution, and, as a result, much information is lost, such as the spatial distribution of material in the sample. This is also true of MALDI, which requires dispersion of the sample within a suitable matrix.

The most significant disadvantage of these single step techniques, in particular, methods such as FAB and SIMS, is that they are not tremendously efficient at ion production. In many cases, the abundance of neutral species generated is orders of magnitude greater than that of the desorbed ionic species [17,18]. An alternative approach, therefore, is to ignore the nascent ions produced during the desorption event, and to exploit the vast excess of gas phase neutrals generated by ionising them in a second step. This separation of the desorption and ionisation steps enables each process to be independently optimised, which can provide a large increase in sensitivity and allows the use of an ionisation technique which best suits the particular application. The work presented in this thesis concerns the development of such a two-step mass spectrometric approach, which combines laser desorption with postionisation by laser multi-photon ionisation (MPI), followed by time-of-flight (TOF) mass analysis of the resulting photoions. The key advantage of this technique is the spatial and temporal separation of the desorption and ionisation events. Not only does this allow each process to be independently optimised; most importantly, a wide array of selective *and* general ionisation techniques can be employed, which can be tailored to particular applications.

In common with both FAB and SIMS, infrared (IR) laser desorption generally results in the production of a vast excess of neutrals over ions. At typical power densities of 10^6 Wcm^{-2}, about 10^5 neutrals are produced for every ion [19,20]. Also, the heating rates attainable using pulsed IR laser desorption can be in excess of 10^8 Ks^{-1} [21], which favours the desorption of intact molecules over decomposition. These features make IR laser desorption an ideal tool for producing intact gas-phase molecules from thermally labile samples for analysis by a suitable mass spectroscopic technique.

A particularly powerful and flexible means by which ionic species can be produced from gas-phase neutrals is laser photoionisation. Most organic molecules have ionisation potentials in the range 7-10 eV [22]. In order for sample photoionisation to occur by single photon absorption, energetic vacuum ultraviolet (VUV) radiation is required. Laser radiation at such short wavelengths is technically difficult to generate. It is also extremely inconvenient to work with in the laboratory since oxygen in the atmosphere absorbs VUV light very strongly. Therefore, evacuated or purged beam paths are required, along with expensive VUV transmitting optics.

The development of high power pulsed laser systems, however, has led to the use of alternative techniques such as multiphoton ionisation (MPI). Such techniques involve the target molecule absorbing two or more photons of energy less than the ionisation potential in order to achieve ionisation. These laser wavelengths tend to lie in the visible and UV regions of the electromagnetic spectrum, and consequently are much more convenient to work with. A huge increase in the ionisation efficiency can be achieved if the laser wavelength is tuned to coincide with a real excited intermediate state of the molecule under study. This is known as resonance enhanced multi-photon ionisation (REMPI). It is this feature of the technique which furnishes two step laser mass spectrometry (L2MS) with its high selectivity. At low laser power densities, only molecules with a significant absorption cross-section at the ionising laser wavelength will be ionised. Therefore, by judicious choice of laser wavelength, it is, in principle, possible to selectively ionise a single component in a

complex mixture, thereby simplifying what would be an extremely congested mass spectrum if produced by conventional FAB or SIMS. Also, at low power densities, REMPI is an inherently soft ionisation technique, generally producing radical molecular cations. Another significant advantage of this ionisation technique is that hard ionisation can be induced simply by increasing the ionising laser power density. Therefore, this ionisation technique is well suited for analysis of both complex mixtures and single component systems. By tuning the laser wavelength to a resonance in a particular molecule, even if it is present only in trace quantities in a mixture, it is possible to observe only the molecular ion of this species. Once this has been achieved, it is then possible to generate structural information and promote fragmentation by increasing the ionising laser power density.

This experimental approach of laser desorption combined with laser postionisation and TOF mass spectrometry was developed primarily by three independent research groups in the mid 1980s. Two of these groups, Schlag's [23] and Lubman's [24], made use of a pulsed supersonic expansion to transport the desorbed neutrals from the point of desorption to the ionisation source. Zare's group [25], on the other hand, carried out laser desorption within the ionisation source and photoionised directly above the sample. Each approach has distinct advantages in particular applications.

The use of a supersonic expansion allows the inherent optical selectivity of the ionisation technique to be exploited to the full, by cooling the internal degrees of freedom of the desorbed molecules. This has the effect of sharpening the vibronic features of the absorption spectrum of the target molecules. This combination of laser desorption with jet-cooling has previously been employed for biomolecules and complex organic molecules [26,27,28]. Additional information can be obtained by varying the wavelength of the ionisation laser, thereby adding a second dimension to the technique. However, the downside of this approach is that the entrainment step is inherently inefficient. It has been estimated that as little as 0.1% of all desorbed species are entrained into the molecular beam [29]. Therefore, although the cooling which can be achieved in the molecular beam renders the technique analytically powerful, it is only at the expense of loss of sensitivity. This, ironically, limits its use

as an analytical technique for real systems, where the target species may be present in very small quantities.

Zare's group, by dispensing with the molecular beam, have sacrificed an element of selectivity in favour of greatly enhanced sensitivity. Under optimum jet-cooling conditions, it is possible to selectively ionise a single component in a mixture, even if the absorption spectrum differs from that of another component by only 1-5 cm^{-1}. Optical resolution on this scale is sufficient for isotopic shifts to be resolved, which, for example, would allow a molecule and its isotopomer to be distinguished. In dispensing with the supersonic expansion, this level of selectivity is lost, although it is still possible to achieve functional group selectivity. Therefore, it is still possible to selectively ionise UV absorbing species (e.g. aromatics) over non-UV absorbers (e.g. aliphatics). This often proves sufficient to greatly simplify mass spectra, and this approach has enabled "real-world" samples to be studied more easily.

The principal objective of the work described in this thesis was to develop an existing instrument, which was set up to carry out molecular beam spectroscopy on laser desorbed species, into one which was capable of carrying out L2MS studies on "real-world" systems. The overall aim was to assess the long-term feasibility of developing a new laser mass microscope. By reducing the desorption laser spot-size to ~ 10 μm, it may be possible to carry out spatially resolved analysis of surfaces. Moving the sample relative to this laser spot, may allow two-dimensional images of the sample surface to be obtained.

In Chapter 2, the background and theory behind the three fundamental components of L2MS, namely laser desorption, laser photoionisation and TOF-MS, are described in more detail and the reasons why they are well suited in combination are discussed. Each of the processes are considered individually, as well as their suitability for the analysis of real systems. Chapter 3 contains a discussion of the experimental equipment and methodologies employed in carrying out this work. A discussion of both the entrainment and non-entrainment modes of operation is presented, which illustrates the analytical advantages of dispensing with the molecular beam.

The main body of this thesis, presented in Chapters 4 to 7, is devoted to discussion of experimental results obtained using L2MS on a wide variety of systems. As briefly outlined below, it is demonstrated that the technique is well suited to the analysis of real systems, and that ultimately the development of a laser mass microscope is feasible. In addition, it is also shown that important fundamental information can be obtained about large molecular systems which would otherwise be impossible, or at least very difficult, to obtain.

Chapter 4 presents the photoionisation mass spectra of a variety of azo dyes and porphyrin pigments. These experiments demonstrate the use of L2MS for probing photochemical and photophysical properties in large molecular systems. They also show that wavelength dependent fragmentation can be useful in identifying unknown species from real systems.

Chapter 5 shows how diverse a technique L2MS can be for the *in situ* analysis of polymers and polymer additives. It is shown that the use of two fixed ionisation laser wavelengths, 266 nm and 193 nm, yield characteristic molecular weight and structural information on a variety of polymer additives, including UV stabilisers and antioxidants. The selectivity of the REMPI process is exploited to effectively discriminate against non-UV absorbing host polymers, whilst selectively ionising the aromatic additive components. It is also demonstrated that the separation of the desorption and ionisation events allows general, non-selective ionisation techniques to be used, which allow the non-UV absorbing host polymers to be characterised. Non-resonant multiphoton ionisation (MPI), single-photon ionisation (SPI) and laser induced photoelectron ionisation (LIPEI) have been used to successfully characterise poly(ethyleneglycol) and poly(dimethysiloxanes), neither of which contain UV chromophores.

Chapter 6 illustrates the use of L2MS for the study of a wide variety of real systems. It is shown that IR laser desorption can be used to volatilise intact target molecules directly from extremely complex matrices without recourse to time consuming purification and separation techniques. This allows the selectivity of the REMPI process to be exploited for the selective detection of aromatic components in

non-UV absorbing matrices, for example, polycyclic aromatic hydrocarbons (PAHs) adsorbed onto aerosol particulate matter. It is also demonstrated that conducting poly(indole) films can be characterised directly from the electrode surfaces on which they are produced.

In Chapter 7, some of the limitations of L2MS are examined and discussed. In particular, it is shown that the desorption conditions used can have a considerable influence on the resultant mass spectra. Internal energy transferred to the molecules during the desorption event is shown to have a marked effect on the degree of fragmentation observed. A discussion on why there is an apparent high mass "ceiling" using MPI is also presented, and again, the desorption process is implicated. The future of L2MS as an analytical technique is discussed in the light of these problems, with a special emphasis on the contentious issue of quantitation. Ultimately, the data presented in this chapter will show that in order for further significant analytical advances to be made, considerable fundamental research into the desorption process will have to be undertaken.

Finally, in Chapter 8, a summary of the advances made during the course of this work is presented, together with an outlook of where further advances are likely to be made. Areas of the technique that need to be improved are illustrated, and possible ways in which this may be achieved are suggested.

References

[1] V. Parameswaren, A. V. Rama Rao, K. Venkateraman, *Indian J. Chem.*, **12**, 785, (1974)

[2] G. D. Daves, T. D. Lee, W. R. Anderson, D. F. Barofsky, G. A. Naissey, J. C. Johnson, P. A. Pincus, *Adv. Mass Spectrom.*, **8**, 1012, (1980)

[3] R. J. Beuhler, E. Flanigan, L. J. Greene, L. Friedman, *J. Am. Chem. Soc.*, **96**, 3990, (1974)

[4] A. Benninghoven, Ed., *Ion Formation from Organic Solids*, Springer-Verlag, Berlin, Part 3, 1983

[5] A. Benninghoven, W. K. Sichtermann, *Anal. Chem.*, **50**, 1180, (1978)

[6] A. Benninghoven, R. J. Colton, D. S. Simmons, H. W. Werner, Eds., *Secondary Ion Mass Spectrometry SIMS V, Springer Series in Chemical Physics 44*, Springer-Verlag: Berlin, 1986

[7] A. Benninghoven, Ed., *Ion Formation from Organic Solids*, Springer-Verlag, Berlin, Part 2, 1983

[8] M. A. Posthumus, P. G. Kistemaker, H. L. C. Meuzelaar, M. C. Ten Noever de Brauw, *Anal. Chem.*, **50**, 985, (1978)

[9] J.-C. Tabet, R. J. Cotter, *Anal. Chem.*, **56**, 1662, (1984)

[10] M. G. Sherman, J. R. Kingsly, J. C. Hemminger, R. T. McIver Jr., *Anal. Chim. Acta*, **79**, 178, (1985)

[11] R. C. Beavis, *Org. Mass Spectrom.*, **27**, 653, (1992)

[12] H. D. Beckey, *Field Ionisation Mass Spectrometry*, Pergamon Press, Oxford, 1971

[13] M. A. Baldwin, F. W. McLafferty, *Org. Mass Spectrom.*, **7**, 1353, (1973)

[14] T. R. Rizzo, Y. D. Park, L. A. Peteanu, D. H. Levy, *J. Chem. Phys.*, **84**, 2534, (1986)

[15] M. L. Vestal, G. J. Fergusson, *Anal. Chem.*, **57**, 2373, (1985)

[16] C. M. Whitehouse, R. N. Dreyer, M. Yamashita, J. B. Fenn, *Anal. Chem.*, **57**, 675, (1985)

[17] E. Schroder, H. Munster, H. Budzikiewicz, *Org. Mass Spectrom.*, **21**, 707, (1986)

[18] R. B. Frees, A. M. Ross, J. E. Campana, *J. Am. Chem. Soc.*, **107**, 6195, (1985)

[19] R. J. Cotter, *Anal. Chim. Acta*, **195**, 45, (1987)

[20] R. B. Van Breeman, M. Snow, R. J. Cotter, *Int. J. Mass Spectrom. Ion. Phys.*, **49**, 35, (1983)

[21] R. N. Zare, R. D. Levine, *Chem. Phys. Letters*, **136**, 593, (1987)

[22] R. Boschi, E. Clar, Wi Schmidt, *J. Chem. Phys.*, **60**, 4406, (1974)

[23] H. v. Weyssenhoff, H. L. Selze, E. W. Schlag, *Z. Naturforsch.*, **40a**, 674, (1985)

[24] R. Tembruell, D. M. Lubman, *Anal. Chem.*, **58**, 1299, (1986)

[25] F. Engelke, J. H. Hahn, W. Henke, R. N. Zare, *Anal. Chem.*, **59**, 909, (1987)

[26] J. Grotemeyer, U. Boesl, K. Walter, E. W. Schlag, *Org. Mass Spectrom.*, **21**, 645, (1986)

[27] D. M. Lubman, *Anal. Chem.*, **59**, 31A, (1987)

[28] R. Tembruell, D. M. Lubman, *Appl. Spectrosc.*, **41**, 431, (1987)

[29] K. F. Costello, *PhD Thesis, The University of Edinburgh*, 1991

Chapter 2

Two-Step Laser Mass Spectrometry: Background Theory

2.1 Introduction

Two-step laser mass spectrometry, or laser desorption laser photoionisation mass spectrometry (L2MS) has evolved over the last decade or so into a very powerful technique for the study of large, involatile and thermally labile molecular species. Not only does L2MS permit studies of these "difficult" molecules from the purely mass spectrometric point of view, the use of laser desorption enables such compounds to be analysed directly from their native environments. In the recent literature, much is made of the power of laser photoionisation and the variety of advantages that it provides, especially for *in situ* analysis. Whilst this is true, it is the first stage of the technique, namely laser desorption, which underpins the effectiveness of this two-step methodology as both a mass spectrometric and an analytical tool. The coupling of this novel and flexible mode of volatilisation with both laser multiphoton ionisation and time-of-flight mass spectrometry makes the analysis of a vast array of large involatile and/or thermally labile molecules possible.

This chapter is split into three main sections, covering the theoretical aspects of each of the main processes involved in the L2MS technique. Special emphasis will be placed on the first section covering laser desorption. Various models for the underlying mechanisms of LD, for both ionic and neutral species, will be discussed.

This section concludes with a discussion on which combination of these processes are likely to be prevalent in the domain in which L2MS is usually employed, and the problems and shortcomings of our current understanding. In the following section the principles of laser multiphoton ionisation (MPI) are described. Factors affecting the appearance of MPI mass spectra will be discussed, along with the advantages of this ionisation technique, over other methods, for use as an analytical tool. The final section outlines the basic principles of time-of-flight (TOF) mass spectrometry, and why in particular it is ideally suited to coupling with pulsed laser ion sources.

2.2 Laser Desorption

Many techniques have been developed over the last twenty years or so, in order to facilitate the analysis of high mass, involatile and thermally labile molecules with varying degrees of success. Laser desorption (LD) is one such technique [1,2]. The generic term LD, as commonly used, encompasses an entire range of diverse experimental conditions and methodologies. A wide variety of laser systems are now available which can be used to desorb solid phase material into the gas-phase. These lasers produce different wavelengths, pulse durations (from cw to femtoseconds) and power densities. Also, solid phase samples can be presented in a variety of different ways; the analyte can be dispersed either in some suitable matrix material or placed as a film on a range of substrates. The relative amounts of matrix and sample, or the thickness of the film laid down on a particular substrate are all important parameters. Also, the degree of interaction between the sample and its surroundings can produce vast differences in the amount and type of species which are liberated into the gas-phase.

All of these experimental parameters can cause one or more alternative mechanisms of desorption to contribute to the production of gas-phase material. Therefore, the term LD is simply not specific enough to describe the diverse range of phenomena which can occur during the desorption event.

What is clear, however, is that the use of pulsed laser radiation can lead to the *intact* desorption of large, involatile and thermally labile molecules and ions into the

gas-phase with little decomposition, for analysis by an appropriate MS technique. In many ways, it is surprising that these large organic molecules can survive the energetic environment created by the laser pulse. This poses several questions. Why do molecules desorb instead of decomposing? How does desorption occur? What controls the internal energy of the desorbed molecule? Which parameters determine the efficiency of the desorption event, and what controls the degree of decomposition? Answers to these questions are critical to our understanding of the desorption process, and yet the exact role of many of the above parameters in the mechanism of laser desorption remain very controversial. Various models have been proposed in an attempt to explain the wide variety of experimental data produced by these diverse LD experiments. These include resonant [3] and thermal [4] desorption, through to shock-wave [5] and non-thermal [6] desorption mechanisms. It is generally accepted that mass spectrometric information generated by a particular LD event is likely to be a result of one or more of these processes. The experiments carried out in this thesis generally employed a pulsed infrared laser for desorption, and it is believed that infrared laser desorption proceeds predominantly via a thermal mechanism. Therefore, the following section is mainly concerned with the discussion of thermal desorption mechanisms. Other models, and their relevance or otherwise to the desorption conditions used in these experiments, will also be discussed briefly.

A common feature in all of these desorption models discussed in the following sections, is that the energy from the laser radiation somehow has to induce processes which allow the analyte material to leave the sample bulk and be desorbed into the gas-phase. There are two principle routes by which energy can be imparted to the analyte in order to effect volatilisation. These are direct and indirect energy transfer mechanisms [7]. With direct energy transfer, the laser energy is absorbed by the analyte itself. The effectiveness of this process is determined by the coupling of the photon energy with a suitable transition in the solid material, and is, therefore, very dependent on the wavelength of the laser radiation. For infrared LD, either phonon or vibrational modes can be excited, whereas with UV LD, it is generally electronic excitation which occurs. However, since the energy is deposited into the molecules

themselves, it is more difficult to liberate internally cold molecules, making the desorption of large intact molecules less likely.

The indirect method of energy deposition is generally perceived as being somewhat more flexible. In this case, some mediator, usually an absorbing matrix or substrate which absorbs at the desorbing laser wavelength, is used as a chromophore. This then transfers energy to the analyte molecules, causing them to volatilise. The use of a mediator in this way allows at least some control over the coupling mechanism for energy transfer, and therefore, also over the desorption. The precise mechanisms by which the energy is transferred to the analyte depends on many experimental factors, and will be discussed for each model individually.

Even nowadays, in most LD experiments, the ions produced directly from the desorption event are detected and analysed. It is, therefore, surprising that little attention has been paid to the actual mechanisms of ion formation. Most studies have concentrated on how the material actually gets into the gas-phase, and have focused less on how the ions are formed. Under normal conditions, it is found that only a small fraction of the desorbed species are ionic [8,9]. However, in the context of the present discussion, the main aim in L2MS is postionisation of laser desorbed *neutral* species. It is worth noting that LD in general does produce ionic species as well as neutrals, and so this process will be mentioned where appropriate.

2.2.1 Laser Induced Thermal Desorption

As early as the 1970s, fast heating was perceived as having potential for promoting intact vapourisation over decomposition processes in large organic molecules [10]. However, until fast pulsed laser systems became widely available, it was not possible to attain the heating rates required to completely avoid fragmentation. Thermolability of large organic molecules is a relative concept; it is the heating rate which controls the degree of decomposition. Therefore, the liberation of intact thermally labile molecules from the solid state is not necessarily compromised at high surface temperatures, provided the heating rate is fast enough.

This was demonstrated by Daves et al. [10] and Beuhler et al. [4] using the flash desorption technique, which was developed as an alternative to conventional resistive heating. Here, instead of heating rates of 10 Ks^{-1}, rates of up to 5000 Ks^{-1} were achieved, resulting in enhanced molecular ion signals. This phenomenon can be rationalised by assuming that the desorption of intact neutrals and the generation of thermal degradation products show a different temperature dependence and behave according to an Arrhenius-type relationship.

$$k = A\exp\left(\frac{-E_a}{RT}\right) \tag{2.1}$$

The parameter k is the rate coefficient for desorption or thermal degradation, E_a is the activation energy for the desorption/degradation process, T is the temperature and A is the pre-exponential factor. A thermally labile molecule is defined as one in which the activation energy for decomposition is lower than the activation energy for vapourisation. However, since the A factor is lower for the degradation process than for intact desorption, the Arrhenius plots for both of these processes must intersect at some value of T^{-1} [10]. This implies that intact molecular species will be relatively more abundant in the gas-phase at temperatures above the point of intersection than at lower temperatures where decomposition is favoured. If the opposite were true, then there is no gaurantee that the curves will intersect, with the result that thermal decomposition will be favoured. Essentially, the fast-heating approach minimises the time spent in the low temperature range, where decomposition prevails, thereby increasing the relative contribution of the intact molecules in the gas-phase.

When a solid is irradiated by a pulsed infrared laser it is rapidly heated. Zare et al. [11] have measured the heating rates induced in a series of insulating material such as glass and quartz by a pulsed CO_2 laser to be of the order of 10^8 Ks^{-1} using a time-resolved platinum resistance thermometer. It therefore seems reasonable that desorption using infrared radiation should proceed via thermal heating of the sample. In the case of infrared laser desorption, as discussed earlier, there are two main mechanisms by which energy deposition can occur; heating of the sample and heating of the substrate. The latter method of energy deposition is indirect, where the energy

is initially deposited into the substrate, after which energy transfer to the adsorbate takes place. The former process is a direct method of energy deposition, which would involve direct multiphoton absorption by the adsorbate molecules. However, anharmonicity of the vibrational modes of the adsorbate makes this process highly unlikely, and so direct desorption becomes increasingly difficult.

Evidence for laser induced thermal desorption of thin organic films proceeding via heating of the substrate is shown in work carried out by Kistemaker et al. [2]. It is assumed that for a substrate with a high thermal absorptivity, the presence of the thin organic film does not influence the substrate temperature distribution. In other words, the organic film is considered to be optically transparent. It was observed that the laser power required to desorb a non-absorbing analyte from a given substrate was dependent upon the thermal properties of that substrate. Substrates with poor heat transfer properties required the use of greater laser desorption power densities. This suggested that the laser energy is absorbed mainly in the substrate and then transferred to the organic layer resulting in desorption of the analyte molecules.

Other experiments have shown that the rapid heating of a surface facilitates the desorption of internally cool molecules [12,13,14]. This led Zare and Levine to propose a mechanism which attempts to rationalise the internal energies of thermally desorbed molecules [15]. This is discussed below, and illustrated schematically in Figure 2-1.

Traditionally, it has not been possible to localise energy in a molecule, since it dissipates on a rapid timescale. As a result, the molecule will gradually approach equipartition of the excitation energy amongst all of the available degrees of freedom. Deviations from this statistical behaviour require some means of restricting the energy flow within the molecule, i.e., the existence of a "bottleneck". Zare and Levine's model uses this principle to rationalise the production of relatively cool gas-phase molecules upon desorption from a substrate with a fast laser pulse.

A molecule physisorbed on a surface is bound by a weak van der Waals (vdw) type bond. In comparison to the stronger chemical bonds within the molecule, this bond has a very low vibrational frequency. Rapid heating of the substrate surface

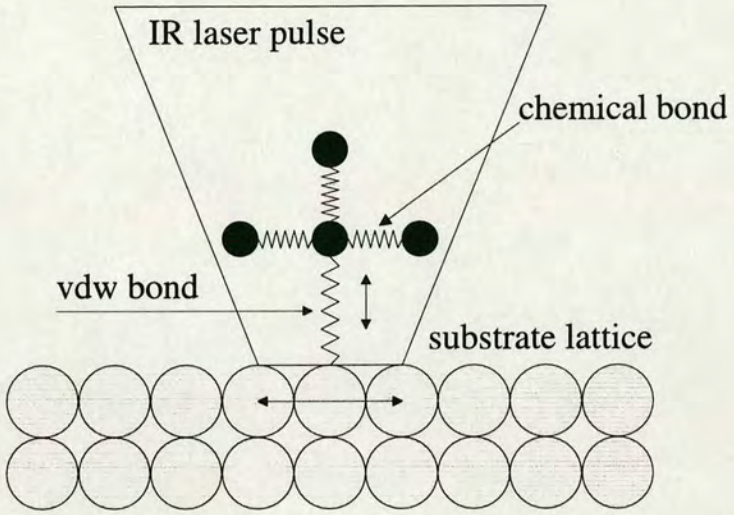

Figure 2-1: Schematic diagram illustrating the "bottleneck model" of IR laser desorption.

will excite the surface phonons, which are well matched in frequency to the weak vdw bond, leading to this bond being efficiently pumped. However, since the bonds within the molecule are much stronger, and of much higher frequency, a "bottleneck" can occur in the transfer of energy from the substrate into the molecule. Therefore, the energy transfer out of this vdw bond and into the molecule is slower than the rate at which energy can be supplied from the substrate. This can result in the vdw bond being broken before significant amounts of energy has transferred into the adsorbed molecule, resulting in its intact desorption with minimal internal energy, i.e., the desorption of internally "lukewarm" molecules occurs.

Zare and Levine defined the criterion for "lukewarm" desorption from a surface as

$$\tau\nu \exp(-\varepsilon) < 1 \qquad (2.2)$$

where τ is the timescale of the desorption event, ν is the frequency of the vdw physisorption bond and ε is the so called adiabaticity parameter, which represents the

ability of the adsorbate molecule to resist changes in vibrational excitation. The parameter ε is related to the ratio of the vibrational frequency of a chemical bond in the adsorbate to that of the vdw physisorption bond. If the criterion in Equation 2.2 is not satisfied, then it will still be possible for the molecule to leave the surface. However, it will take with it some internal energy resulting from energy transfer via the physisorption bond. It has been shown from studies on the unimolecular decomposition of vdw adducts that values of $\varepsilon > 11$ are not uncommon [16,17,18]. With values of $\varepsilon > 10$, heating rates of 10^{11} - 10^{12} Ks^{-1} can be used to desorb even relatively strongly bound molecules with reasonably low internal energies. In fact, surface heating rates of up to 10^{15} Ks^{-1} have been reported using femtosecond laser pulses [19], which suggests that selective desorption of tightly bound molecules may be possible.

The early flash desorption work suggested that the role of the heating rate was of prime importance for the desorption of intact species. This was corroborated by experimental evidence from several groups [10,4]. This interpretation is based entirely on thermal equilibrium arguments, in that it is assumed that the surface-adsorbate system is in complete thermal equilibrium at all times. However, in contrast, the "bottleneck" model proposed by Zare and Levine [15] suggests that sufficiently rapid surface heating, such as that achieved using pulsed lasers, is very much in the non-equilibrium regime. The "bottleneck" model also explains much of the experimental observations, and has the added advantage that it is qualitatively illustrative.

It would, therefore, appear that both equilibrium and non-equilibrium approaches have been used to rationalise experimental data which show that fast heating can lead to the desorption of large intact molecules. Zenobi and Zare attempted to clarify this confusing situation by studying low coverages of naphthalene vapour condensed onto a cooled quartz surface using L2MS [20]. Their approach was to measure the temporal evolution of the surface temperature, determine the temperature at which the molecules left the surface and compare this to the kinetic and internal energy distributions of the desorbed species. It was found that the velocity distributions

were extremely dependent on the surface coverage as well as the laser power densities and subsequent heating rates. For sub-monolayer coverage, it was found that the velocity distribution was well fitted by a Maxwell-Boltzmann distribution. However, for higher coverages, a fit to a Maxwell-Boltzmann distribution proved to be inadequate, until it was modified by a stream velocity parameter. This suggested that molecular collisions above the surface were beginning to dominate. However, although different desorption fluences resulted in similar desorption temperatures, the maximum velocity increased with desorption fluence. Although the velocity distributions were consistent with collisions taking place above the sample surface, this fluence dependence is not consistent with a thermal equilibrium model, since in such a model molecules would be expected to desorb at a given temperature governed by desorption kinetic parameters.

Therefore, it is still not entirely clear whether laser-induced thermal desorption is an equilibrium process or not. It is not unreasonable, however, to assume that since both the laser pulse duration and the sample coverage are crucial to the desorption process, both factors may contribute at some stage to the total desorbed signal.

So far, only the desorption of intact neutral species into the gas-phase have been considered in detail. However, as mentioned earlier, most LD experiments measure nascent ions. There is also a considerable body of evidence that a thermal mechanism is responsible for ion production in single-stage infrared LDMS. Ion production has been observed by many workers using both pulsed [1,8] and cw [21] laser systems. For thin layer coverages, the efficiency of ion production seems to be almost independent of the infrared laser wavelength employed. In most cases, mass spectra are dominated by cationised molecular ions. Alkali metal cations are also always abundant in IR-LD mass spectra. It is well known that production of alkali metal cations occurs due to ordinary thermal ionisation resulting from sufficiently strong heating of the sample surface. The frequently observed Na^+ and K^+ ion peaks usually result from heating of the sample surface to over 700 ^{o}C, at which point impurities in the probe surface are ionised, or ions in the surface are mobilised [2]. It has been proposed that $[M + alkali]^+$ ions are likely to be formed as the result of the

attachment of an alkali metal cation to the intact neutral molecule [1,22,23]. It is most likely that this occurs as a gas-phase ion-molecule reaction. Most of the evidence for this has come from work carried out by Kistemaker and co-workers [2]. They noted that at low laser fluences, no cationised molecular ions were formed. However, neither were any cation signals observed. As the laser fluence, and hence the surface temperature was increased, the formation of K^+ ions occurred first, at which point the onset of $[M + K]^+$ ions was observed. Therefore, it is evident that the high surface temperature was required in order to produce the K^+ ions and not the $[M + K]^+$ ions, and so the quasi-molecular ions are formed in the gas-phase. Subsequent to this work van der Peyl [24] showed that cationised molecular ions could still be observed if the source of the K^+ was kept physically separated from the desorbed species.

2.2.2 Resonant Desorption

Some of the early work on laser desorption with nanosecond lasers, in both the visible and UV, reported that the influence of laser wavelength was a relatively minor effect, and consequently of little importance. However, more recent work by Hillenkamp et al. [25] showed that significant differences in threshold irradiances for ion detection were obtained for desorption of a series of amino acids, dependent on their classical absorption of the incident laser radiation. Further work on laser desorption of amino acids has shown that the use of a desorption wavelength which coincides with a molecular absorption band in the analyte can dramatically improve the molecular ion to fragment ion ratio [26,27,28]. Similar effects have also been demonstrated for resonant desorption of neutral molecules [29]. Non-resonant laser desorption required the use of significantly higher desorption powers, and produced less intact molecular ion species upon photoionisation. Resonant laser desorption, on the other hand, produced intact neutrals more efficiently and at lower laser powers by coupling the laser energy directly into the sample bulk. Also, the observation of predominately molecular radical cations generated from polycyclic aromatic hydrocarbons when desorbed at 266 nm provides additional support for a resonant desorption mechanism initiated by electronic excitation of the sample [30].

At near threshold irradiances, linear energy absorption by individual molecules may play an important role. Such linear processes are, in principle, easier to control with respect to total energy deposition than the non-linear ones necessary for non-absorbing samples. As a result, the degree of internal excitation of desorbed quasi-molecular ions may remain limited. However, as discussed in the previous section, direct excitation of this type offers only limited possibilities for the desorption of large involatile species. This can be transformed, however, into an efficient means by which to transfer energy to non-absorbing analyte species which are dispersed within this material or matrix. This is the basic principle underpinning the new technique of matrix assisted laser desorption (MALD).

In this technique, the large uptake of energy which can be achieved by resonantly absorbing media is exploited and used as an indirect means of transferring energy to the analyte. This has lead to one of the most significant recent developments in laser mass spectrometry, if not mass spectrometry as a whole. The new technique of matrix assisted laser desorption ionisation (MALDI), uses the MALD part of the technique to generate quasi-molecular ions of non-absorbing analyte materials by dispersing them in absorbing matrices prior to analysis. This was first reported in 1987 by Tanake and co-workers [31],who reported the mass spectra of intact high mass proteins following their irradiation at 337 nm whilst dispersed in a matrix of powdered cobalt. This was subsequently confirmed by several groups [32,33] [34,35], and has led to an entire new field in laser mass spectrometry, with several commercial instruments now available, capable of generating ions of mass well in excess of 100 000 u. MALDI has found particular use in biomolecular analysis on species such as proteins and peptides, and is currently being developed for the analysis of high molecular weight polymers.

When the surface of an organic crystal is exposed to UV radiation, the range of physical processes which can occur is far wider than for excitation with IR radiation. Excitation with a resonant wavelength allows direct energy transfer to the target molecules. The absorption of UV radiation leads primarily to electronic excitation of the molecules. This, however, can lead in turn to the occurrence of many other

physical processes, such as the formation of excitons, electrons and holes in the conduction band of organic crystals, and the emission of electrons from the surface. Also, direct photofragmentation can occur as a consequence of electronic singlet state excitation. It is believed that non-radiative relaxation processes, such as internal conversion, leads to transfer of the electronic excitation energy to vibrational molecular energy, which allows desorption to occur [7]. However, since the most common use of resonant desorption is simply as a means of indirectly transferring energy to some non-absorbing guest molecule, this begs the question "What prevents the guest molecules from heating up?", especially since they are in an environment where both the host matrix molecules and lattice vibrations are both highly excited.

This led to the proposal of the so-called homogeneous bottleneck model (HBM) [7], for the description of MALD of large molecules. This is very similar to the model proposed by Zare and Levine for laser induced thermal desorption from a surface using IR lasers (see previous section). In the HBM it is suggested that there is an obstacle to energy flow into the embedded guest molecules caused by a frequency mismatch between the guest-host interaction frequency and the internal vibrations of the guest molecule. A simple kinetic model of energy transfer [36] shows that guest molecules can be liberated intact and internally cold. This concept of restricted energy flow appears to be a recurring theme in the description of LD. Although it is unlikely to be the only process occurring, it certainly appears to be very important, and has the added advantage of providing a useful visual picture of how large molecular species are desorbed into the gas-phase.

Once again, this discussion on resonant desorption has centred predominantly on the volatilisation of large intact molecules. However, in most resonant (UV) LD techniques, such as MALDI, it is generally nascent ions which are detected rather that postionised neutrals. Generally, radical cations are not formed in UV LD or MALDI. In the positive ion mode, it tends to be cationised or protonated species which are detected, whereas in negative ion mode, deprotonation is favoured over electron attachment.

The mechanism for ion formation in MALDI is still a matter of some conjecture. It is generally believed that gas-phase processes are the most dominant means of ion production, but there are several mechanisms by which this may occur. Karas et al. [37] substantiated the idea that the photochemical activity of the matrix species plays an important role in the ionisation of the analyte as well as its desorption into the gas-phase. They proposed that upon desorption into the gas-phase, the first step is the production of radical molecular ions, which being very reactive, undergo many chemical reactions with neutral molecules in the dense plume of desorbed material. However, they do acknowledge that there is still no hard experimental evidence for such a model.

Beavis et al. [38] have suggested that a disproportionation ionisation mechanism is acting, involving non-ionised matrix molecules as intermediates. They also noted the possibility of proton generation from the matrix as a first step, followed by efficient transfer to the analyte material. However, again this was not verified experimentally. A further model [39] linked the ionisation propensity to the relative magnitudes of the proton affinity of the matrix and analyte. This model proposed that an analyte with a suitably high proton affinity would capture all free protons, as well as abstracting protons from the matrix molecules. However, this model does not explain how the protons are generated, and none of the above account for the presence, often at base peak levels, of alkali metal adducts. Recent work by Zenobi et al. [40] has led them to propose a model in which singly excited matrix molecules are the common precursor for all subsequent ion products. Simultaneous neighbouring presence of two such excited species are required for ionisation. The authors claim that this model can account for both cationised species and protonated molecular ions, and in addition rationalises the often observed effect of matrix suppression.

At higher still laser desorption power densities, the situation can become even more complex. At power densities of around 10^{10} Wcm^{-2}, such as those used in LAMMA and LIMA experiments, photoionisation processes in the vapour phase during the laser pulse can lead to rapid plasma formation. This allows ion-molecule

reactions to occur before the system equilibrates. Hercules [41] has, in fact proposed that there are four different spatial regions around the desorption event which can lead to ion formation. Small molecular fragments are produced by direct ionisation in the region impacted by the focused laser beam, as a result of the high temperatures generated (3000-6000 K). A region of high temperature gradient is established immediately adjacent to the hottest part of the sample, which is subjected to both the shock-wave generated by the laser and the collapsing plasma. It is thought that heavier neutrals and ions are emitted from this region. The formation of heavy ions, including molecular and quasi-molecular ions, is thought to occur at the surface of the sample adjacent to the laser beam, as well as in the gas-phase over the impacted region. This gas-phase ion formation can be the result of ion-molecule reactions or by the absorption of UV photons by desorbed neutral species. Evidence seems to suggest that both solid-state and gas-phase ionisation processes occur, although the relative importance of the two processes is still the topic of some debate.

2.2.3 Shock-Wave and Mechanical Desorption

An alternative model which has been proposed to account for the liberation of intact molecular species from surfaces is shock-wave desorption. This was proposed by Lindner and Seydel [5], who observed extensive fragmentation of sacharides when a laser fluence of 10^8 Wcm^{-2} was incident on a 1μm film, whereas cationised signals were predominant upon irradiation of 20 μm layers at a laser fluence of 10^{11} Wcm^{-2}. Desorption under the first set of conditions seems to conform well to a thermal equilibrium model for desorption, whilst under the latter, apparently more severe conditions, a shock-wave driven desorption model seems to fit.

The heating rate in these experiments of 10^{11} Ks^{-1} is greater than the minimum limit of 10^9 Ks^{-1} required to induce explosive vapourisation (phase explosion). The result of this thermal ablation is a shock wave which traverses the solid and leads to desorption of intact molecules and alkali ions. The criterion which must be met to ensure the desorption of cold molecules from the surface, is that the velocity of the shock wave must exceed the velocity of heat conduction in the sample. Therefore, if

the molecules are not coupled to the surface long enough to absorb sufficient internal energy, thermally labile molecules can be ejected intact.

A similar phenomenon is that of desorption induced by mechanical stress [6]. In this case, it is proposed that the energy from the laser causes inhomogeneous heating of the sample surface. Thermal expansion of the illuminated region produces mechanical stress in certain areas, which if this exceeds some critical value induces mechanical fragmentation leading to desorption of gas-phase material. The criterion for desorption of intact species is that the time required to form a crack must be much less than the time required for the guest molecule to heat up significantly above the initial temperature. Therefore, artificial methods of inducing crack formation will aid in the desorption of internally cool species. This is one possible explanation of why introducing fine metal powder into samples improves the desorption efficiency [42].

Some evidence for such phenomena have also been reported by Zare and Zenobi [20]. Asymmetric velocity distributions were observed when several monolayer coverages of naphthalene were desorbed from a quartz substrate. The velocity distributions were also peaked to lower velocity than expected. They proposed that a thin layer of molecules close to the surface is vapourised, subsequently propelling a thicker layer away from the surface. This hypothesis may also account for the observation that the velocity distributions are shifted to higher velocity with increasing laser desorbing powers. Both of these effects are anomalous with the thermal equilibrium model which fits for sub-monolayer coverages, and so appear to be plausible explanations.

2.2.4 Laser Desorption of Neutral Molecules in L2MS

The mass spectrum observed for a particular laser desorption experiment can be seen to rely on a variety of experimental parameters such as laser wavelength, power density and the way in which the sample is presented. In the experiments described in this thesis, an IR laser at power densities between 10^6 and 10^8 Wcm^{-2} was used to desorb relatively thin layers of material from a surface. The reason that IR laser desorption was predominantly used was because it was believed that most organic

molecules would be optically transparent at this wavelength, and that for the most part, photochemical decomposition and fragmentation would be negligible. It is widely believed that if any mechanism is dominant in the case of IR LD of thin organic films, it is likely to be that of thermal desorption. However, in most cases, although thin layers are used, there will be many hundreds of monolayers present, and so the situation will be far removed from the "ideal" cases described in many mechanistic discussions such as Zare and Levine's bottleneck model [15]. In most cases, there will be far more adsorbate-adsorbate interactions than adsorbate-substrate interactions. So, if the molecules are in fact transparent to the incoming radiation, perhaps desorption of the first layer does occur, and propels the remaining layers away from the from the surface. This would be rather like a mixture between the bottleneck [15] and shock wave models [5,6,20].

Also, there is an added degree of complexity in analysing real systems such as contaminants in soils, additives in polymers and so forth, where the analyte molecules are not in well characterised layers, or in homogeneous matrices; rather they constitute layers of varying thickness, or consist of aggregated clusters in an irregular matrix. In cases such as these, a single desorption mechanism is clearly inappropriate, and a combination of several of the aforementioned models, as well as perhaps others, may prevail.

The original LD experiment by Vastola and Pirone [8] was carried out to look at the nascent ions produced during the desorption event. However, they found that neutral species were the major desorption product, and that these were produced over a much longer period of time than ions. This is actually predicted by the thermal model of desorption which states that the rate of desorption of neutrals (or ions) depends only on the provision of sufficient energy to remove them from the surface:

$$\frac{dn^{(+)}}{dt} \propto [c] \exp\left(\frac{-E_d}{kT}\right) \qquad (2.3)$$

where $n^{(+)}$ is the number of neutrals (or ions) in the gas-phase, $[c]$ is the concentration of surface species, E_d is the activation energy for desorption of neutrals

(or ions) and T is the surface temperature. The activation energy for the desorption of neutrals will generally be lower than that for ions, and therefore, neutrals will be emitted at a lower surface temperature and over longer periods of time [43].

The ratio of ions to neutrals produced during a laser desorption pulse is determined by the rapid jump in surface temperature. This ratio can be calculated to a first approximation by the Langmuir-Saha equation [44]:

$$\frac{n^+}{n^o} = \exp\left(\frac{W-I}{kT}\right) \tag{2.4}$$

where n^+ is the number of ions, n^o the number of neutrals, W is the work function of the substrate, I the ionisation potential of the sample molecules, and T the surface temperature. This equation describes a gas-phase equilibrium process between ions and neutrals, but has also been applied with some success to non-equilibrium systems. The surface temperature is dependent upon laser power density, and so consequently the ratio of ions to neutrals is also affected. Cotter et al. [45,9] have demonstrated that at power densities of 10^8 Wcm^{-2}, similar to those used in L2MS experiments, the ratio of ions to neutrals is as low as 10^{-5}, but at elevated power densities of around 10^9 Wcm^{-2}, this ratio was found to be as high as 0.01-0.1 They also reported that ions were emitted from a surface for approximately 1 μs upon irradiation by a CO_2 laser, with a power density of 10^8 Wcm^{-2}. On the other hand, neutrals were observed for around 100 μs. Therefore, it is obvious that at these sort of laser power densities, the desorption of neutrals is clearly favoured over ions. Therefore, purely on sensitivity grounds, it clearly makes sense to neglect the nascent ions produced during the desorption event in order to postionise the vast excess of neutral species. In addition, this allows the use of extremely effective multiphoton ionisation techniques, which in principle, can enable spectroscopic investigations to be carried out as well as providing inherent selectivity in ionisation.

L2MS was principally developed in the mid-1980s [46,47,48], and since then, many researchers have realised the power of this two-step approach for the ionisation of large molecular species, and have developed the technique still further [49,50,51,52,53]. In most cases, a CO_2 laser at 10.6 μm has been used for desorption

of neutral species, although some workers have used the fundamental and harmonic outputs from an Nd:YAG laser (1064 nm, 532 nm, 355 nm and 266 nm) as well as other visible and UV wavelengths to good effect.

The common problem all workers in this field have experienced is the difficulty in obtaining a stable desorption signal. This has led to much experimentation on methods of presenting samples for analysis. Initially, Lubman [46] and Grotemeyer [48] both used relatively thick samples deposited from solution followed by evaporation. Lubman then tried to use samples dispersed in a glycerol matrix, as is commonly done in FAB, to improve shot to shot stability. Zare et al. [47] have tended to use very thin layers deposited onto highly absorbing substrates such as glass, MACOR and quartz, whilst Levy has used samples pressed into pellets doped with dye which absorbs very strongly at the desorption laser wavelength [51], before settling on thin films of approximately 10 μm. Zenobi et al. [54] have recently demonstrated the use of IR absorbing polymers as effective matrices for aiding the desorption of neutral analytes. Clearly, the use of such diverse sample preparations makes mechanistic interpretations difficult. However, to more fully understand processes occurring for *in situ* analysis, further studies of the desorption process is required. This is discussed further in Chapter 7.

Initially, most groups used L2MS in tandem with a supersonic molecular beam capability in order to carry out spectroscopy on laser desorbed species. This involved laser desorption of the neutral target into an expanding molecular beam, which was also used to transport the neutrals into the ion source region. However, as the analytical potential of the technique became apparent, many groups dispensed with this inefficient entrainment step in order to increase their sensitivity to the levels required for trace analysis. Recently, a number of groups have taken this a stage further, and have begun investigating the potential of the technique as a microanalytical tool. Here, the desorption laser spot is tightly focused to spot sizes between 1 and 50 μm, enabling the analysis of small features on particulates and surfaces. De Vries et al. [50] have used a waveguide excimer laser at 248 nm with reflective cassegranian optics to achieve a spatial resolution of 1 μm. Similarly, Zare

et al. have dispensed with the entrainment step [55] and have used a pulsed CO_2 laser to achieve spot sizes of less than 40 μm, to investigate features on meteorite residue particulates. Zenobi et al. have also used spatially resolved IR desorption to analyse a number of systems, including aerosol particulates [56] and chemical additives in polymers [54].

The principal objective of the work described in this thesis was to develop an existing instrument, set up to carry out molecular beam spectroscopy on laser desorbed species, into one capable of carrying out L2MS on real systems. The overall aim was assess the long-term feasibility of developing a new laser mass microscope. Reduction of the laser spot size to ~10μm may allow spatially resolved analysis of surfaces to be carried out. Preliminary experiments have shown that in the long term this is a feasible project, although to realise the ultimate goals, some fundamental issues must be addressed before further significant analytical advances can be made. These points will be discussed in Chapters 4 to 7.

2.3 Laser Photoionisation

The use of light as an ionisation source in mass spectrometry was demonstrated as early as 1929, when Ditchburn and Arnot used an iron arc lamp to photoionise potassium vapour in a magnetic sector instrument [57]. However, most organic molecules have ionisation potentials (IP) in the region of 7-11 eV. Photon energies of 10 eV and above lie in the vacuum ultra violet (VUV) region of the spectrum, and there are several difficulties associated with the use of VUV radiation which restricted research activities in using light to ionise molecular species. Firstly, VUV lamps produce low output intensities, resulting in inefficient ionisation. However, more importantly, the use of VUV sources from a practical point of view is non-trivial. VUV radiation is efficiently absorbed by oxygen in the atmosphere, and so in order to generate appreciable light intensity at the ion source, evacuated or purged beam paths must be used at all times. This made VUV radiation a cumbersome and expensive option.

However, the development of high powered laser systems signaled a renaissance in photoionisation in mass spectrometry. The high photon fluxes generated using these sources provided a new method of photoionising organic molecules, namely multiphoton ionisation (MPI). This was quickly recognised as a powerful new technique. The attraction of MPI is that photons of lower energy than the ionisation potential can be used to ionise the molecule. Typically, these wavelengths are in the visible and UV, and are more convenient to use in the laboratory. This, in conjunction with the many available ionisation schemes quickly established MPI as a useful ionisation technique.

The following sections will briefly describe some of the various ionisation schemes which are possible using laser photoionisation. A discussion of which physical processes affect the appearance of MPI mass spectra will also be given. Finally, the advantages of this ionisation source as an analytical tool will be discussed along with some details as to why it is suitable for coupling with both laser desorption and time-of-flight mass spectrometry.

2.3.1 Modes of Laser Photoionisation

Laser photoionisation of gas-phase neutral molecules can proceed via a variety of different schemes. The most common of these are illustrated schematically in Figure 2-2. Conceptually, the simplest photoionisation methodology is single photon ionisation (SPI), in which one photon with an energy in excess of the IP of the molecule is required to achieve ionisation. This is shown in Figure 2-2a. As was discussed in the previous section, this generally requires VUV radiation, and traditional sources such as discharge lamps provided insufficient photon intensities to enable sensitive mass spectrometry to be carried out. Recently, however, the use of VUV laser sources has dramatically increased the potential photoion yield. Many workers have now demonstrated the use of frequency tripling the third harmonic of an Nd:YAG laser (355 nm) in xenon or a phase matched mixture of xenon and argon to produce 118 nm radiation [58,59,60]. These photons have an energy of 10.4 eV, and so offer the potential to ionise most organic species using single-photon ionisation. However, the technological and practical difficulties previously

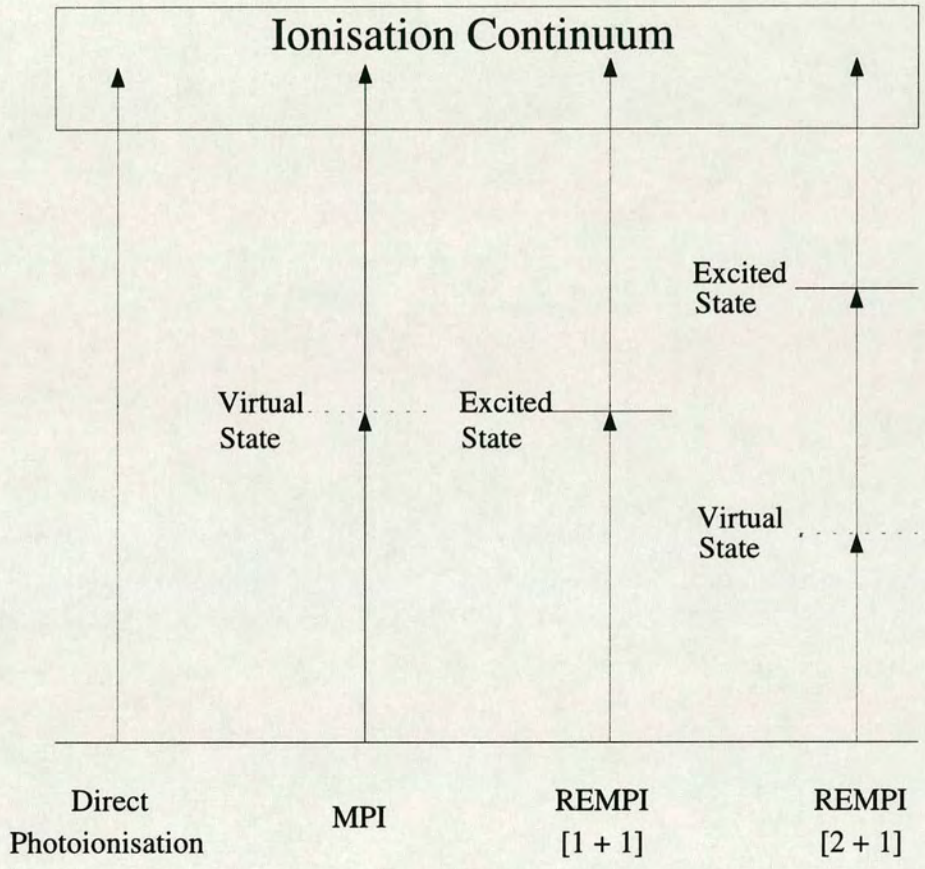

Figure 2-2: Schematic diagram illustrating various laser photoionisation schemes; (a) Single photon ionisation, (b) non-resonant multi-photon ionisation, (c) [1 + 1] REMPI and (d) [2 + 1] REMPI.

experienced using VUV radiation remain, and it is still a non-trivial matter to routinely use VUV radiation in the laboratory. A more widespread and routine methodology for photoionisation is multiphoton ionisation (MPI).

The MPI technique depends upon the absorption of two or more photons by a molecule upon irradiation with intense visible or UV light. A molecule will only be ionised if the sum of energies of the absorbed photons is greater than the IP. This makes MPI much more practical, since visible and UV laser wavelengths can be used routinely in a laboratory, with no significant reduction in intensity from absorption by the atmosphere.

The rate equation for an *n*-photon absorption process, W_n is generally given as

$$W_n = \sigma_n I^n \tag{2.5}$$

where σ_n is the absorption cross-section for an *n*-photon process ($cm^{2n}s^{n-1}$), and *I* is the radiation flux (photons cm^{-2} s^{-1}). The simplest MPI process is non-resonant MPI, which involves the simultaneous absorption of two photons, as illustrated in Figure 2-2b. The transition rate in this case reflects the requirement for a coherent two-photon interaction with the molecule,

$$W_2 = \sigma_2 I^2 \tag{2.6}$$

where σ_2 is the two-photon absorption cross-section (cm^4s^1), and *I* is the radiation flux (photons cm^{-2} s^{-1}). Cross sections for strongly allowed single photon transitions are typically on the order of 10^{-17} to 10^{-18} cm^2. However, for allowed two photon transitions, this is dramatically reduced to only 10^{-50} cm^4s. Therefore, it is apparent that the simultaneous absorption of two photons is much less probable. In order for this coherent two-photon absorption to occur, the photon density in the ionisation region must be sufficiently large to offset the very small probability of absorption. UV lamps providing 10^{15} photons cm^{-2} are not sufficiently powerful to drive such processes. However, narrow bandwidth pulsed lasers can provide photon fluxes of around 10^{28} photons cm^{-2}, which translates to a power density of 1 GW cm^{-2} when tightly focused. This is sufficiently intense to overcome the low probability of the

absorption of the second photon. Unfortunately, at these high laser intensities, even background gases in the ion source will be ionised, and furthermore such high power densities make control of further absorption by the molecular ion almost impossible, and so therefore fragmentation processes predominate. Both of these effects obviously limit the use of non-resonant MPI as an analytical tool.

A common, although not theoretically rigorous, way of describing this is to consider what happens following absorption of the first photon. In order to rationalise a simultaneous two-photon absorption, it is proposed that a "virtual" state at the one-photon energy level must exist. This "virtual" state is not a real eigenstate of the system, in that it has no measurable lifetime. It can be considered to be a state which has a lifetime on the order of the fly-by time of a photon past the molecule, ca. 1 fs.

Consider now the case where a real eigenstate of the molecule exists at the one photon level. This is the regime of resonance enhanced multiphoton ionisation (REMPI), and is illustrated in Figure 2-2c. A more general definition states that an MPI process is resonant when the energy of an integral number of photons, n, approaches closely the energy of an n-photon allowed transition. In contrast to non-resonant processes, real eigenstates have much longer lifetimes than the so-called "virtual" states, typically between 10^{-9} and 10^{-6} seconds. This is six or more orders of magnitude longer than the fly-by time of a photon, or the "lifetime" of the virtual state [61,62]. This, therefore, increases the probability of absorbing the next photon, and so the absorption process is resonantly enhanced. The consequence of the increased efficiency of this resonantly enhanced process is that much lower photon densities can be used than for non-resonant ionisation. Typically, these are on the order of 1 $MWcm^{-2}$ cf. 1 GW cm^{-2} for non-resonant MPI. These lower power densities also allow some control over the degree of fragmentation, to the extent that in most cases, only the molecular ion is observed.

This resonant enhancement is very important in L2MS, especially in the analysis of mixtures. At these low ionising power densities, processes which are resonant dominate the mass spectra, with little or no contribution from non-resonant

ionisation. This, therefore, results in great potential for selectivity of ionisation, where in principle, the laser wavelength can be tuned to a particular resonance in one species in a mixture such that only that species is ionised and detected. As the laser power density is increased, non-resonant contributions dominate and any selective spectroscopic information present in the data is lost or greatly confused. However, non-resonant processes can still be useful for deriving structural information.

The general definition of a resonantly enhanced process states only that an integral number of photons, n must approach the energy of an n-photon allowed transition. This includes, therefore, in principle, coherent absorption of n non-resonant photons to a real state, followed by ionisation out of that state. However such processes are much less efficient than for completely resonant processes, since there is at least one non-resonant step, as shown in Figure 2-2d. Although this methodology can be useful in probing electronic states not accessible in single-photon transitions [63,64], it is experimentally difficult and less efficient than the equivalent resonant processes. Therefore, no such process has been used in these studies.

The most commonly used REMPI methodology is a two-photon resonant process (R2PI). In this case, one photon excites a molecule from the ground state to a singlet excited state, $S_1 \leftarrow S_0$. A second photon is then used to ionise the molecule. There are two subtly different means by which this can be done. The first is a so-called (1 + 1) REMPI process, where both photons have the same energy. This is generally the methodology which was adopted during this work. However, the same process can be driven using photons of different wavelength. This is called a (1 + 1') REMPI process, or a two colour ionisation experiment. Experimentally, however, this can prove to be much more difficult since it requires both spatial and temporal overlap of two laser beams. However, this is often used in spectroscopic studies. Also, as will be discussed in Chapter 7, this can be used to probe fragmentation processes.

Since most organic molecules have IPs between 7 and 11 eV, R2PI requires photons with wavelengths in the far to near UV range. In the one colour experiments carried out during this work, generally fixed laser wavelengths were used for ionisation. However, although these wavelengths were not selected purposely to

coincide with specific molecular resonances, the ionisation process can still be considered resonant to some extent due to the high density of vibronic states available in the large aromatic systems studied. This is especially true when the molecular beam was not used, since the electronic spectra for large molecules are broad and overlap in the absence of cooling provided by an adiabatic expansion. Therefore, in the experiments carried out during this work, although the identity of particular vibronic states accessed by the laser radiation are not known, specific broad band electronic transitions can be excited, for example $\pi \rightarrow \pi^*$ and $n \rightarrow \pi^*$.

The usual way of describing this is to say that the molecule contains a chromophore at the ionising laser wavelength. A chromophore is a functional group of the molecule, which may be present in many molecules, giving rise to an absorption band at approximately the same wavelength. An aromatic group based on the benzene molecule is such an example. Benzene itself has three major bands in the UV region of the spectrum [65], resulting from transitions involving the π-electrons of the aromatic system. Therefore, any molecules containing an aromatic group can be said to contain a UV chromophore which has a strong absorption at some region of the UV spectrum. If the correct wavelength (within a few nm) is chosen, this molecule can, in principle, be efficiently ionised via a two-photon resonance enhanced process.

2.3.2 Competing Processes in MPI

There are three distinct stages in an MPI event. These are:

- Excitation
- Ionisation
- Fragmentation

The common feature in all of these processes, is that there is a kinetic competition between further excitation in order to proceed to the "next stage" (up-pumping), and one of several decay channels for the various excited state populations. In all cases,

this competition seeks to minimise the molecular ion intensity. Each of these stages is described in more detail below.

Excitation

REMPI mass spectrometry relies on the ability to tune the laser wavelength to a real excited state of the molecule, as a platform from which to ionise the molecule. In general, excitation proceeds via the first excited singlet state of the molecule, S_1. This state is usually the most accessible, and generally has the simplest and best characterised spectroscopic features. In a real excited intermediate state, such as that accessed in REMPI, one of various photophysical and photochemical processes may occur. These are illustrated schematically in Figure 2-3.

- The excited molecule may absorb a second photon, resulting in its excitation above the IP. This is the "desired result" for efficient ionisation.
- The excited state may decompose to form neutral fragment. This neutral fragment may then be photoionised to produce a fragment ion, but molecular ion production is prevented.
- The excited state may undergo intersystems crossing (ISC) to a triplet electronic state. This, in general, cannot be ionised by a photon of the same energy, and thus, once again, detection of the molecular ion is prevented.
- The excited state may decay via fluorescence on a timescale which competes effectively with up-pumping to the molecular ion. This has the net effect of reducing the overall molecular ion yield.
- Intramolecular rearrangement may occur, which can lead to products which may or may not be distinguishable from the molecular ion.

These processes have been the subject of much study, and Gedanken et al. [66] have classified two extremes of characteristic behaviour at the first excited intermediate state. These extremes can be characterised according to the relative rates of up-pumping, leading to ionisation and dissociation. Molecules belonging to "Class A" are defined as being those in which the molecule is ionised out of its

intermediate state, and is subsequently fragmented. Generally, though, the molecular ion can be detected. Molecules belonging to "Class B", on the other hand, are those in which dissociation to neutral fragment species occurs at the excited state, after which one, or both, of these fragments is ionised. For most of the molecules studied in this work, Class A behaviour was found to prevail. Examples of compounds which exhibit Class B behaviour include inorganic complexes and organometallic species [67]. Some species, however, have been shown to exhibit *both* Class A and Class B behaviour, depending on the ionising laser wavelength used (and hence the excited intermediate state accessed). Such behaviour was observed in porphyrin pigments, and is presented in Chapter 4.

However, the observation of fragment ions with no evidence of the molecular ion *does not* necessarily signify Class B behaviour. The occurrence of thermal or photodissociation during the desorption process cannot be ruled out at this stage [68,69]. This was illustrated by work previously carried out in this laboratory [69]. Initially, L2MS studies on a series of organo-lead compounds appeared to exhibit classic Class B behaviour. However, by using an ionising wavelength resonant with an atomic transition in lead, it was shown that lead was already present in the ionisation source, suggesting that dissociation had already occurred prior to ionisation. Further confirmation of neutral dissociation during desorption was achieved by desorbing the material into a high pressure environment, which is known to promote clustering. Clusters of lead up to n = 7 were observed. This makes it clear that care must be taken to avoid inferring photochemical processes which are in fact not there.

Much work has been carried out on benzene, which along with many of its derivatives, is known to exhibit Class A behaviour. Benzene itself has been the molecule of choice for mechanistic studies of MPI and fragmentation processes in large molecules. Most organic molecules such as those studied in this thesis display predominantly Class A behaviour. However, for molecules which possess substituent groups which can induce radiationless transitions, obviously the ionisation efficiency can drop off dramatically. Molecules containing Cl and Br

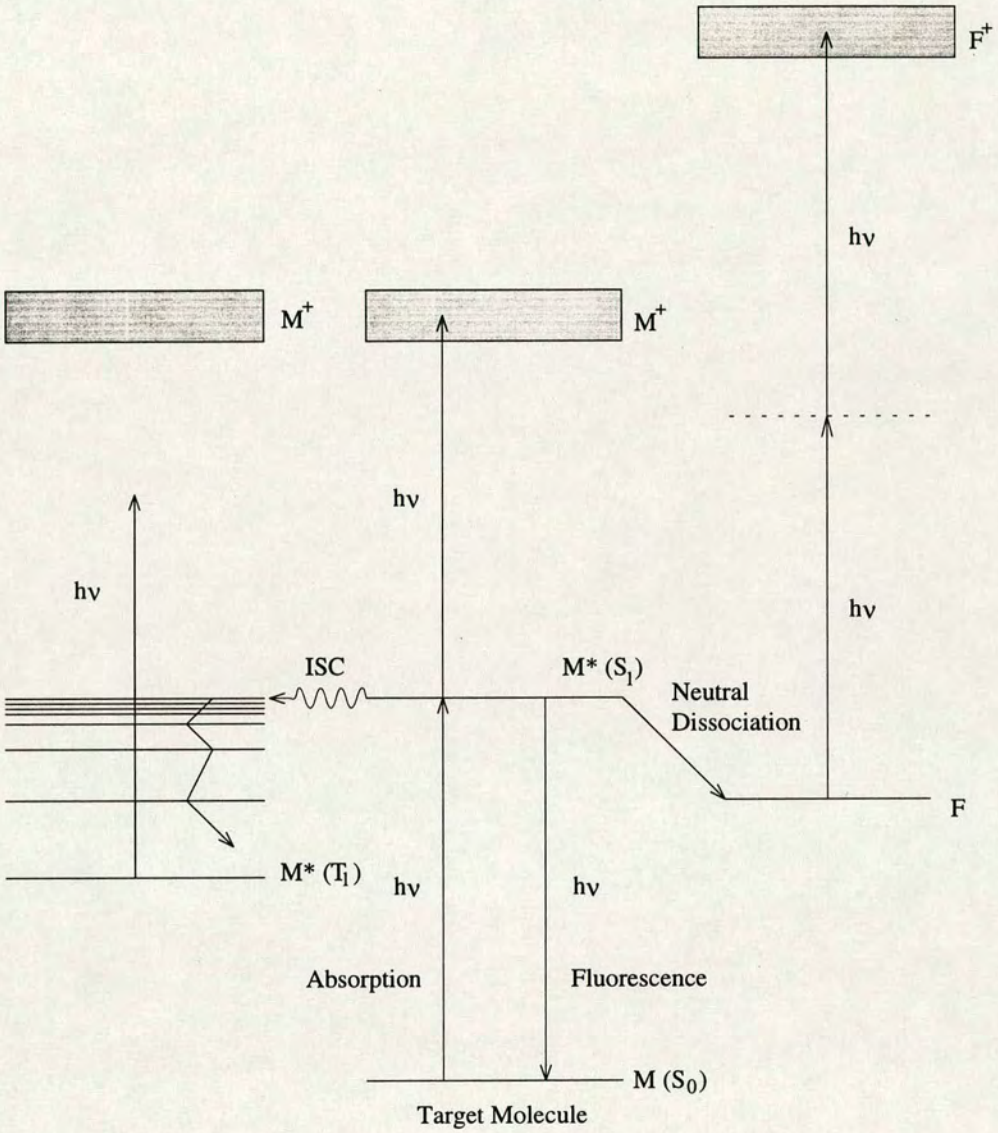

Figure 2-3: Schematic diagram illustrating the possible competing photophysical and photochemical process occurring at the excited intermediate state.

substituents are prone to this type of behaviour. These substituents enhance the intersystems crossing rate to highly excited rovibrational states of the first excited triplet manifold. The Franck-Condon factors for subsequent absorption from such states into the ion are too low for R2PI to occur. Alternatively, efficient relaxation down the triplet manifold can mean that the second photon is insufficiently energetic to induce ionisation.

Many workers have also documented that there appears to be a mass limit above which it is difficult to photoionise large molecules [42,70,71,72]. Above 2000 u, ionisation efficiency seems to drop off very rapidly. There are several possible reasons for this, one of which is efficient relaxation at the first excited intermediate state. However, this will be dealt with in some detail in Chapter 7. In general, however, for molecules below 1500 u, vibronic states near the origin band of the S_1 system do not dissociate and display relatively slow non-radiative relaxation processes. Thus, the predominant process following excitation to S_1 is further absorption by this state, leading to excitation into the ionisation continuum.

Ionisation

For the ionisation process itself, two processes must be considered. The most obvious process to consider is direct ionisation, whereby the molecule is excited directly from the S_1 state into the ionisation continuum, instantaneously ejecting an electron to leave the molecular ion in either its ground state or an electronically excited state. However, this may not be the most likely scenario, as it may take a finite time for the system to localise enough energy to eject any one electron. What is more likely to occur, is the process of autoionisation. In this case, although the total energy of the system is greater than the IP, no single electron has sufficient energy to be ejected. A super-excited state of the molecule, known as an autoionising state, is populated above the IP. After a finite time, a spontaneous change in the electronic configuration can occur, such that one electron acquires enough energy to enable ionisation to occur. This is known as electronic autoionisation. It is widely believed that this results in the production of molecular ions formed in well defined vibronic levels, usually the vibrationless ground state

[73]. Any excess energy is removed as kinetic energy of the ejected electron, resulting in molecular ions with a very narrow energy spread.

Fragmentation

It is possible to induce fragmentation processes in the mass spectrum by increasing the ionising laser power density. However, an important consideration is whether these further photons are absorbed by the neutral super-excited state or by the molecular ion. A simple calculation, assuming an autoionising rate of 10^{13} s^{-1} and an absorption cross-section of 10^{-16} cm^{-2} by the superexcited state, suggests that autoionisation will dominate under typical laser conditions ($I < 10^{29}$ photons cm^{-2} s^{-1}) [74]. This calculation is corroborated by experimental evidence by Boesl et al. [75], where it was shown that the molecular ion was the precursor of all observed fragment ions. This was done using a UV laser to produce benzene ions via the S_1 state. After a delay of 0 - 17 ns, the resulting species were then irradiated using a second UV laser yielding fragment ions. In 17 ns, any super-excited state would have had sufficient time to autoionise. The total ion current with and without the fragmentation laser was identical, and so it was concluded that the molecular ion was the exclusive pre-cursor to ion formation. It also showed that photoionisation of neutral fragments could be neglected.

The dissociation of most polyatomic molecular ions can be described by statistical models. Several such mechanisms have been proposed, and work well in specific cases [76,77,78,79,80]. However, in most cases the successive uptake and decrease of energy content in the molecular ion ensemble during the light pulse was not considered. The generally accepted model is the so-called "ladder-switching" model of Dietz et al. [80]. This is illustrated schematically in Figure 2-4 and described below.

This model allows for fragmentation and subsequent photon absorption by fragment ions during the period of the laser pulse. It assumes that unimolecular decomposition can occur on very short timescales on the order of 10^{-10} to 10^{-11} s, and is able to compete effectively with photon absorption during ns light pulses. As the excitation energy increases, the rates of decomposition become so fast that further

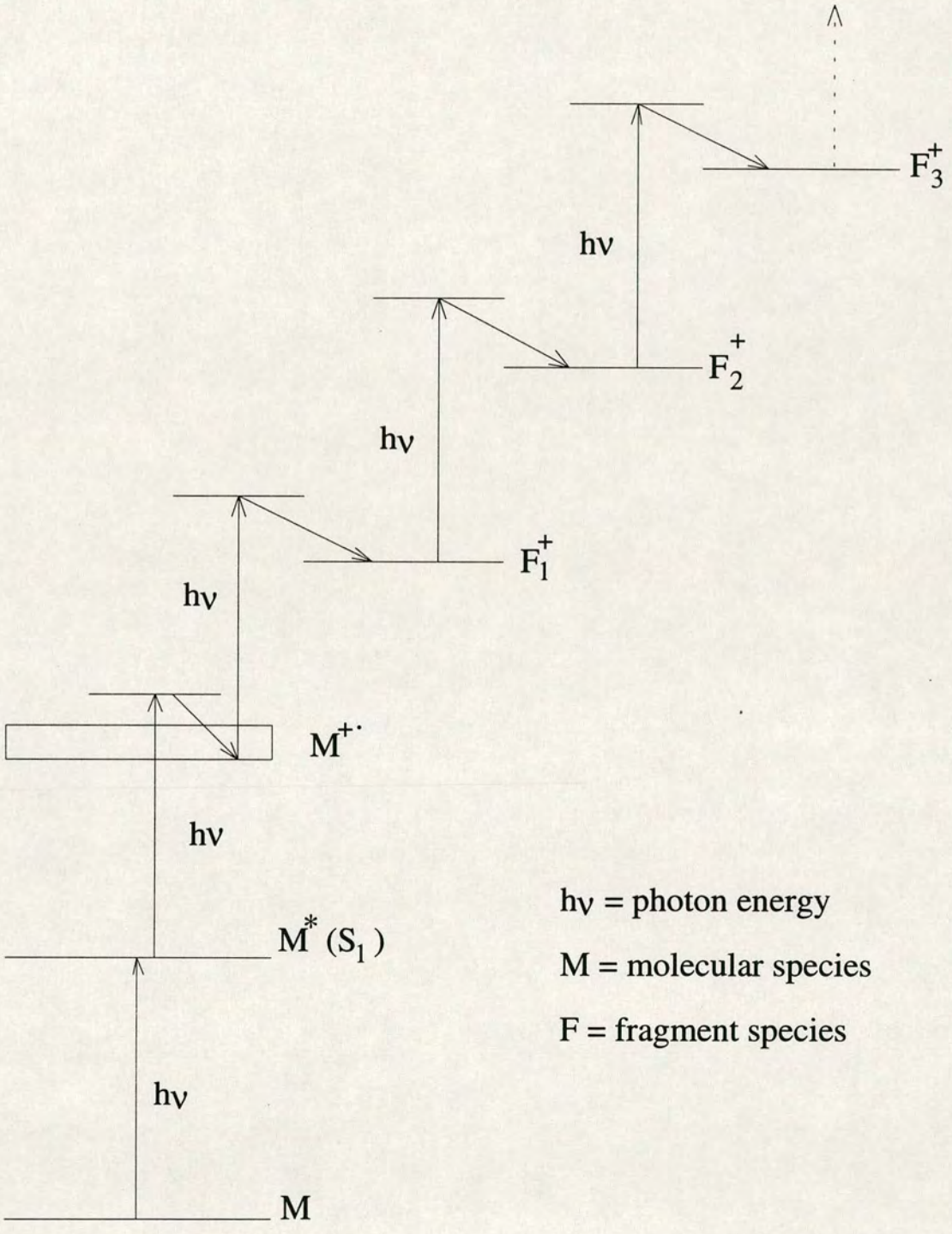

Figure 2-4: Schematic diagram illustrating the ladder switching model of multiphoton ionisation

optical excitation in the ladder cannot compete, thus placing an effective maximum on that absorption ladder. This leads to a "switch" to an alternative ladder of product ions, which in turn can absorb photons during the same light pulse and undergo analogous reactions until its maximum is reached, and so on. This means that an ion cannot climb indiscriminately high on its own absorption ladder, thereby restricting the possible fragmentation pathways.

This model has been verified experimentally by Boesl et al. [81] Again, for benzene, they mass selectively irradiated fragment ions with a second laser and observed a mass spectrum similar to those generated in a single photoionisation experiment. They concluded that the fragmentation pathways involved absorption by these fragment ions, directly supporting the ladder switching model. More recently, Schlag et al. have followed this fragmentation ladder step by step using a tandem time-of-flight mass spectrometer [82,83].

This fragmentation model is not universally applicable to all photoionisation experiments. Recent developments in laser technology have seen femtosecond (fs) laser systems come to the fore. Weinkauf et al. [84] have shown that under near identical conditions, nanosecond (ns) and femtosecond laser pulses induce different fragmentation channels in large decapeptides. They observed local fragmentation at the absorbing chromophore upon fs excitation and not the typical ladder switching-type fragmentation observed by ns laser irradiation. This was the first direct demonstration of the breakdown of a statistical description of MPI fragmentation processes. The assumption in the ladder switching scenario, is that unimolecular decomposition occurs on a timescale competitive with optical up-pumping. Presumably, therefore, in the case of fs excitation, the rate of optical pumping dominates over decomposition, and so there is no longer necessarily a maximum on this ladder of products. Therefore, the fragmentation is more localised at the absorbing chromophore. This fits a molecular ion ladder model [85], which is illustrated in Figure 2-5. It may even be that for very short pulses, an autoionising model may prevail [86], in that the optical pumping rate can dominate over ionisation. There is, therefore, speculation that femtosecond lasers may eventually

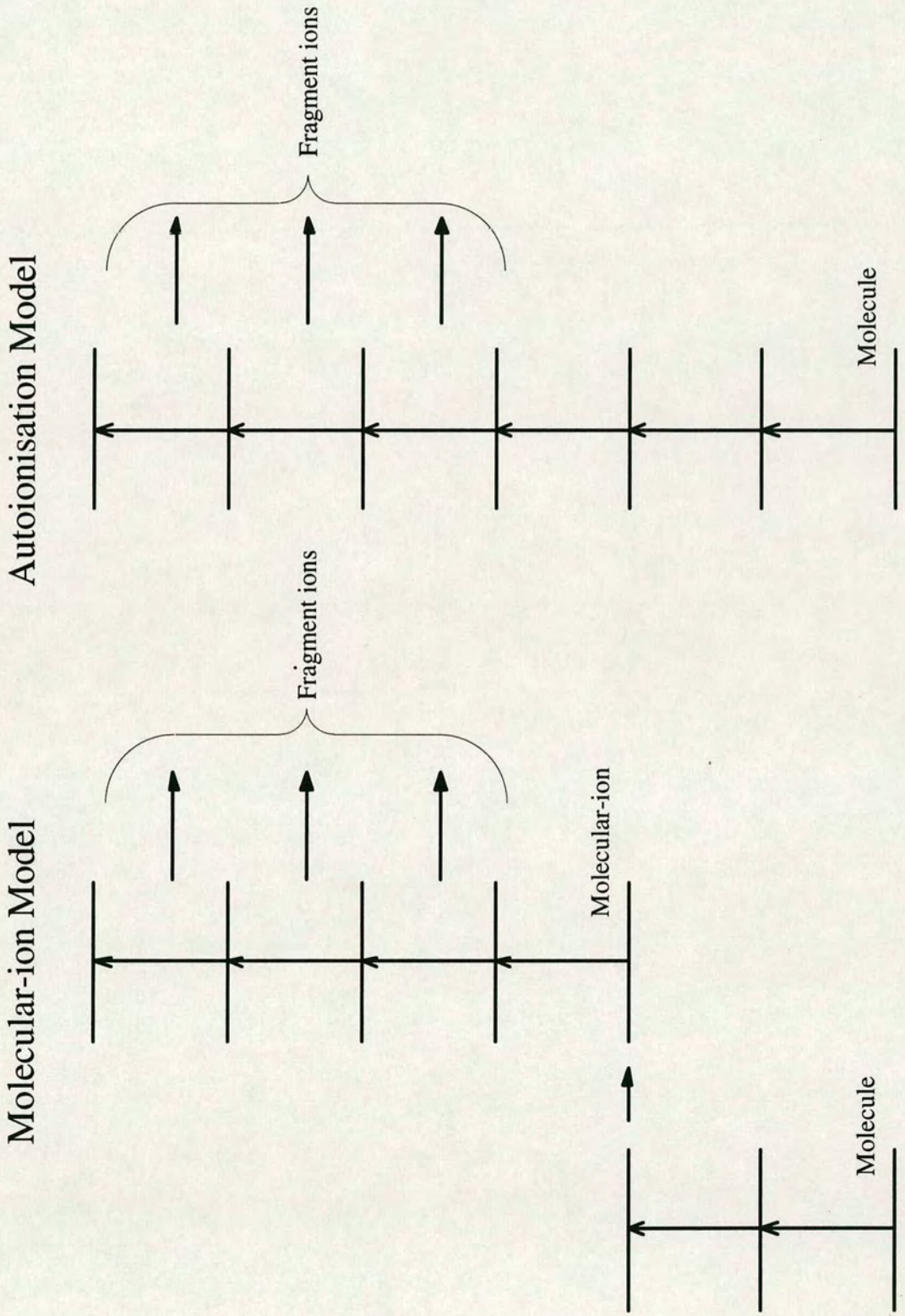

Figure 2-5: Schematic diagram illustrating the Molecular Ion and Autoionisation models for photoionisation using picosecond and femtosecond pulsed laser systems.

find applications for inducing site-specific fragmentation, such as in peptide sequencing.

Another advantage of fs laser ionisation, is that it has been demonstrated to be more efficient than ns ionisation [87]. This is due to the high rate of optical pumping from the first excited intermediate state, which dominates over decay processes such as intersystem crossing and internal conversion. This has been used to good effect in tackling the topical issue of photoionising high mass molecules. This will be elaborated on in Chapter 7.

2.3.3 MPI as an Analytical Tool

MPI, as well as having been extensively used over the last fifteen years as a means of studying the spectroscopy of small, and in some cases quite large molecules, is now being increasingly used as an ionisation source for many analytical applications. For example, in addition to being used by many groups as a means of postionising laser desorbed neutral species, some researchers have demonstrated the use of MPI to postionise neutral species produced during desorption in secondary ion mass spectrometry (SIMS) experiments [88,89,90,91]. For example, Winograd et al. [88] have used a YAG pumped dye laser system to postionise neutral tryptophan and benzo[a]pyrene molecules desorbed using a liquid metal ion gun. The postionisation methodology produces more efficient ionisation, resulting in higher ion yields than usually obtained in SIMS. This allows high spatial resolution to be achieved in the desorption, whilst maintaining static conditions.

In terms of ionising laser desorbed neutrals, there are four main advantages in utilising MPI, namely:

- efficient ion production
- selective ionisation
- tunable fragmentation
- wavelength dependent fragmentation

These will be discussed in more detail below.

Efficiency

As mentioned previously, non-resonant MPI is not a particularly efficient means of molecular ion production from neutral target species. However, when the photon energy is in resonance with a real excited intermediate electronic state, the ionisation efficiency can increase dramatically.

Several workers have reported estimates of between 10 % to 100 % ionisation efficiency, for molecules that interact with the laser beam volume during the light pulse [92,93,94,95,86]. Although the absolute efficiency is limited by the duty cycle of the ionisation laser (10 ns pulse at 10 Hz, typical desorption plume of 50 μs) and the ionisation volume, the ionisation efficiency is ultimately determined by the absorption and ionisation cross sections at any particular ionisation wavelength.

Boesl et al. [92] have measured the ionisation cross-sections for a number of organic aromatic molecules in an effusive molecular beam. For broad band excitation (1 cm^{-1}) at 10^7 Wcm^{-2}, approximately 25 % of the ground state population resonant within the laser bandwidth could be ionised. More recently, picosecond and femtosecond laser pulses have been used to enhance the ionisation efficiency for species with short excited state lifetimes [96,97,81]. These impressive ionisation efficiencies should be compared to those of typical EI efficiencies. Generally, only one molecule in 10^4 is ionised under typical (70 eV) EI conditions. Also, in order to avoid fragmentation, low electron beam energies must be used, which causes the ionisation efficiency to be diminished by several orders of magnitude further. Therefore, it is clear that the high efficiency of REMPI, coupled with its inherent selectivity (see below) and its propensity for molecular ion production makes it ideally suited to analytical applications, where multi-component analysis is important.

Selectivity

Perhaps the greatest single advantage of using resonantly enhanced MPI for analytical applications is the great selectivity achievable in the ionisation. Since only

molecules with a real excited intermediate state at the ionisation wavelength are resonantly ionised, then by controlling the laser power density, complete discrimination against non-absorbing molecules can be achieved. Thus, in a mixture of many components, judicious choice of the ionising laser wavelength makes it possible to selectively ionise only one component, which greatly simplifies the resulting mass spectra. This introduces a degree of two-dimensionality to the technique, in that by scanning over a range of ionising laser wavelengths it is possible to record the molecular gas-phase absorption spectrum. This, coupled with simultaneous mass information makes L2MS, at least in principle, a truly two-dimensional technique.

The gas-phase R2PI spectra of polyatomic molecules at room temperature show only broad features as a result of thermal population of the rovibronic states. Therefore, in order to observe all of the spectral structure, and hence maximise the optical selectivity, it is necessary to reduce the thermal population of these states. This is generally done using supersonic beam technology [98], which allows adiabatic cooling of the internal degrees of freedom of the molecules to occur. The essence of this facet of the technique, is that atoms or molecules (usually He, Ar, N_2 or CO_2) in a high pressure reservoir are allowed to expand through a small orifice into a vacuum. These molecules undergo many two-body collisions during this expansion, which has the effect of collapsing the room temperature Maxwell-Boltzmann velocity distribution to a narrow range centred on the directed mass flow velocity. The translational temperature describing the width of the "jet-cooled" distribution can be as low as 0.1 K. Rotational and vibrational temperatures are less effectively cooled, but typical temperatures of 10 K and 100 K respectively can be achieved. The analyte molecules are seeded into this molecular beam at low concentration, undergoing many collisions themselves, thereby reducing their internal temperatures. This has the effect that the broad features of the room temperature spectra are narrowed, and the optical absorption spectrum is more readily interpretable.

Whereas at room temperature the broad features in the UV spectra may make it difficult to distinguish even between different classes of molecules, at very low internal temperatures, it is possible even to distinguish between contributions from different isotopes within molecules. For example, Costello [99] obtained R2PI jet-cooled spectra for the origin band ($S_1 \leftarrow S_0$) of two aniline isotopes (mass 93 u and 94 u). It was demonstrated that careful tuning of the ionising laser wavelength to the absorption maximum of one isotope made it possible to discriminate between them.

Therefore, in order to achieve maximum optical selectivity and maximise the two-dimensional UV/MS capabilities of the technique, a supersonic expansion must be used. However, for analytical purposes, this is unfortunately far from ideal. The entrainment procedure is remarkably inefficient, with as little as 0.1 % of the desorbed species reaching the ionisation region [99]. Therefore, in terms of trace analysis, a trade off between internal cooling by supersonic expansion and its associated advantages, and sensitivity must be made. This is now generally done by many workers in the field by dispensing with the molecular beam and ionising directly above the sample. Although much is lost in terms of optical selectivity (i.e., isotopic differentiation), semi-selectivity is still possible. As discussed in Section 2.3.1, when the spectroscopic features are broadened as they are in the absence of a supersonic expansion, a wide range of vibronic states can be accessed simultaneously by the ionising laser. For UV wavelengths, this typically corresponds to having some aromatic group in the molecules. Molecules which do not contain such a chromophore, e.g. aliphatics, will not be efficiently ionised and so aromatic species in a mixture of compounds are selectively detected in preference to non-aromatics.

Although some selectivity is lost, aromatic molecules can routinely be differentiated from non-aromatic species. An example of this is found in the L2MS spectrum of a 1:100 mixture of the amino acid tryptophan and polyethylene glycol (PEG). Tryptophan is a strong UV absorber with the $S_1 \leftarrow S_0$ origin band at 287 nm [100]. The ionisation wavelength in this experiment was 300 nm, and although this is not tuned to a specific resonance in the molecule, there is a sufficiently high density of states for the ionisation process to be resonantly enhanced. PEG, on the

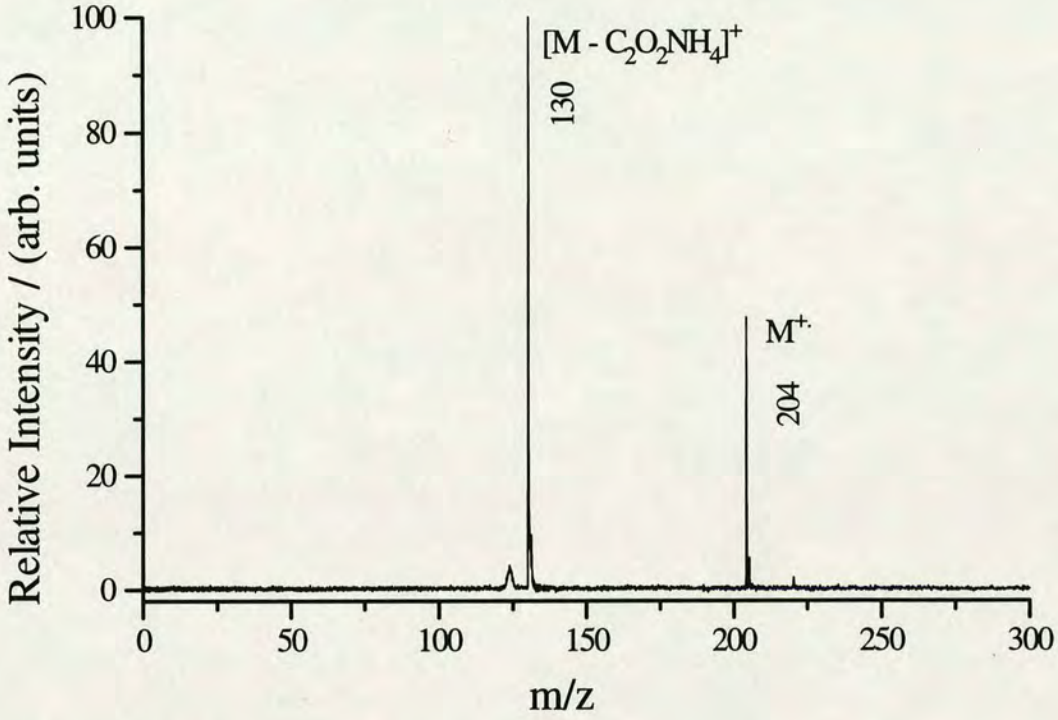

Figure 2-6: Time-of-flight mass spectrum of tryptophan in a matrix of PEG, obtained using 10.6 μm laser desorption and 300 nm photoionisation. The only peaks in the spectrum correspond to the molecular ion and the dehydroindole fragment ion. There is no evidence of any signal from the non-absorbing PEG.

other hand, does not absorb UV radiation strongly. The spectrum in Figure 2-6 clearly shows that at 300 nm, only the molecular ion of tryptophan and one of its associated fragments is detected. There is no evidence of signal corresponding to PEG, even though it is present in great excess. This shows that by using UV wavelengths for ionisation, aromatic species can be selectively detected with respect to non-absorbing species. In addition, trace quantities of UV absorbing polymer additives have been selectively ionised with respect to using non-absorbing bulk polymers using this approach [101,54]. This will be discussed in detail in Chapter 5. Also, it has even proved possible to differentiate between different classes of aromatic molecules in much the same way as in UV-VIS spectroscopy. This has in fact been done to identify which isomers of polycyclic aromatic hydrocarbons are present in an atmospheric aerosol particulate, by linking there solution phase molar absorptivities to the intensities in the mass spectrum at particular ionisation wavelengths [102]. This is described in Chapter 6. Therefore, by dispensing with the molecular beam, although some selectivity is lost, an element of UV absorption

information is retained. More importantly, however, the potential for real system analysis is greatly enhanced by the increase in sensitivity.

Tunable Fragmentation:

Although the efficient production of molecular ions is a requirement for mixture analysis, in many situations, structural information is also desirable. As was mentioned earlier, at low ionising laser fluence, soft ionisation mass spectra of a wide range of organic aromatic analytes can routinely be obtained. An increase in the ionising laser power density promotes further absorption in the ion, which can induce a series of fragmentation reactions. This was described earlier as the ladder switching mechanism [80]. At high laser powers, extensive fragmentation can occur, producing ions all the way down to C^+. Figure 2-7a shows the soft photoionisation mass spectrum of perylene. The molecular ion is the base peak in the mass spectrum, and no associated fragment ions are observed. Figure 2-7b shows the hard ionisation spectrum, where the ionising laser power density has been increased by one order of magnitude. Here, the molecular ion is no longer the base peak in the mass spectrum, with a series of low mass ions beginning to dominate. This clearly shows the flexible nature of MPI as an ionisation technique.

The fragmentation induced by MPI can be used to differentiate between different molecular classes, as well as between isomeric species. Examples of such cases will be given throughout Chapters 4 to 8.

Fragmentation patterns obtained using MPI can be radically different from those obtained using EI. With EI, typically 70 eV electrons are directed at the gas-phase molecules. This induces a large perturbation in the molecule, which results in many states in the ion being populated. The energy is deposited instantaneously in the molecule, with the result that all possible fragmentation channels compete with each other [103]. This is illustrated schematically in Figure 2-8. Conversely, in the case of MPI, the open fragmentation channels are somewhat restricted. The fragments produced are induced by absorption of UV photons. These transitions are Franck-Condon controlled, in that no significant changes in geometry can occur. Therefore, only transitions to certain states in the ion are allowed, limiting the number of

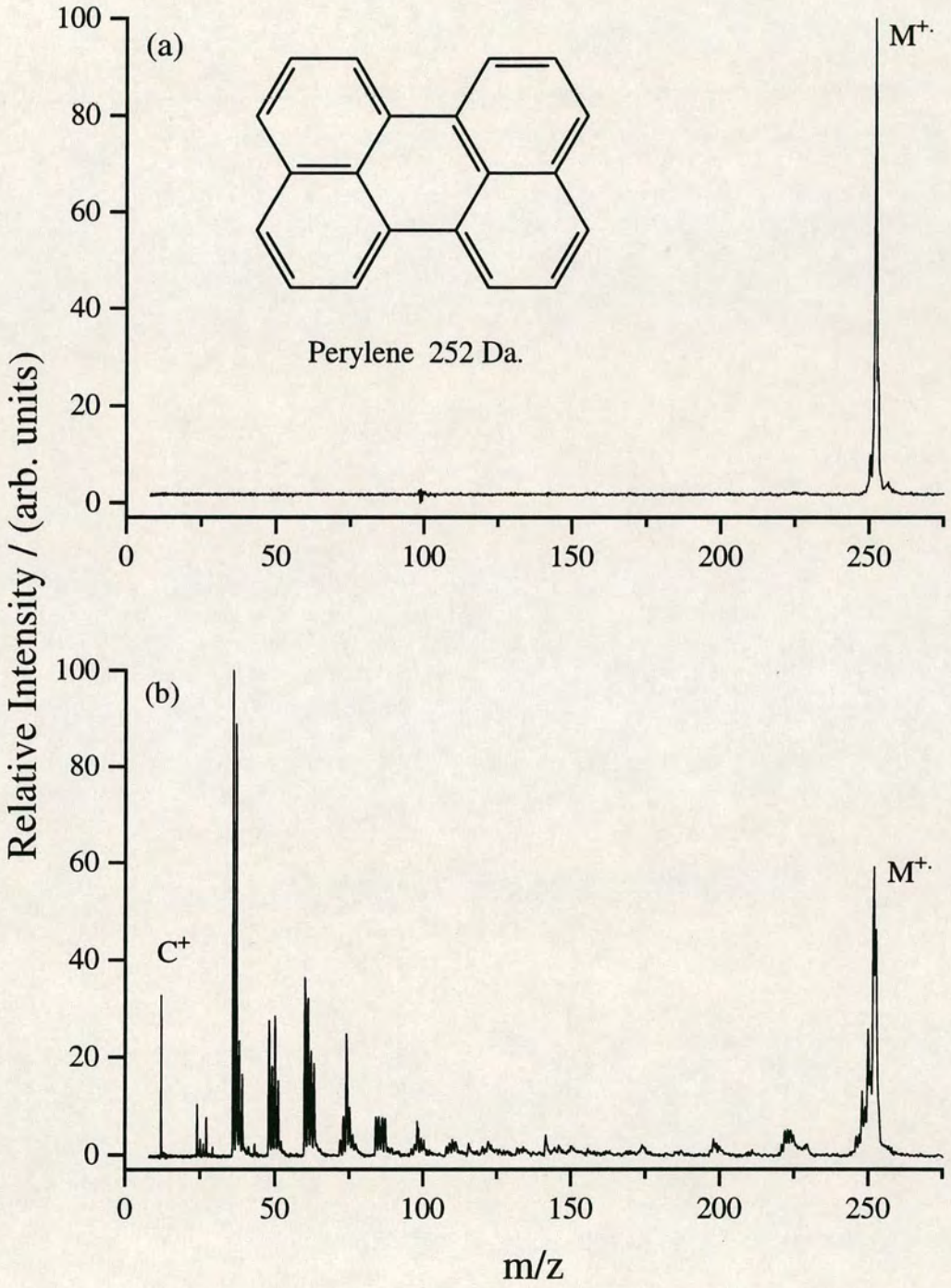

Figure 2-7: Time-of-flight mass spectra of perylene obtained under (a) soft, and (b) hard ionisation conditions using 266 nm photoionisation. The power densities were 0.5 x 10^6 Wcm^{-2} and 5 x 10^6 Wcm^{-2}, respectively.

fragments observed in the mass spectra. The available fragmentation channels are also limited due to kinetic factors in the ladder switching fragmentation mechanism.

Wavelength Dependent Fragmentation:

In addition to the wavelength of radiation being responsible for selectively ionising particular components in a mixture with different efficiencies, it can also have a drastic effect on the appearance of the mass spectra [53,104,101]. There are several possible explanations as to why this may occur, and examples of this wavelength dependent fragmentation will appear at various points during this thesis. Therefore, detailed explanations as to why this may occur will be given where appropriate. However, in general terms, it will be shown that both the nature of the first excited intermediate state, and the amount of energy deposited into the molecular ion contribute to the various differences in mass spectra caused by different ionising wavelengths.

2.4 Time-of-Flight Mass Spectrometry.

This section is devoted to the third and final element of the L2MS technique, namely time-of-flight mass spectrometry (TOF-MS). The first part of this section will describe why TOF-MS is ideally suited to coupling with the other elements of L2MS, and the basic principles will briefly be outlined. The physical processes which limit the mass resolving power of TOF mass spectrometers will be discussed, as well as how some of these problems can be addressed. Following this, a commonly used extension of TOF-MS, reflecting geometry TOF mass spectrometers (RETOF) will be described, and the advantages that this brings to TOF analysis will be illustrated. Finally, as will be discussed in Chapter 3, there are two configurations in which this L2MS instrument can be used, namely with and without a supersonic molecular beam. The ramifications of this with respect to mass resolution in TOF-MS will be addressed, including how the degradation in mass resolution may be minimised by carefully considering the desorption and extraction geometry. A more complete theoretical description of TOF instruments, along with a consideration of their operational limitations can be found elsewhere [99].

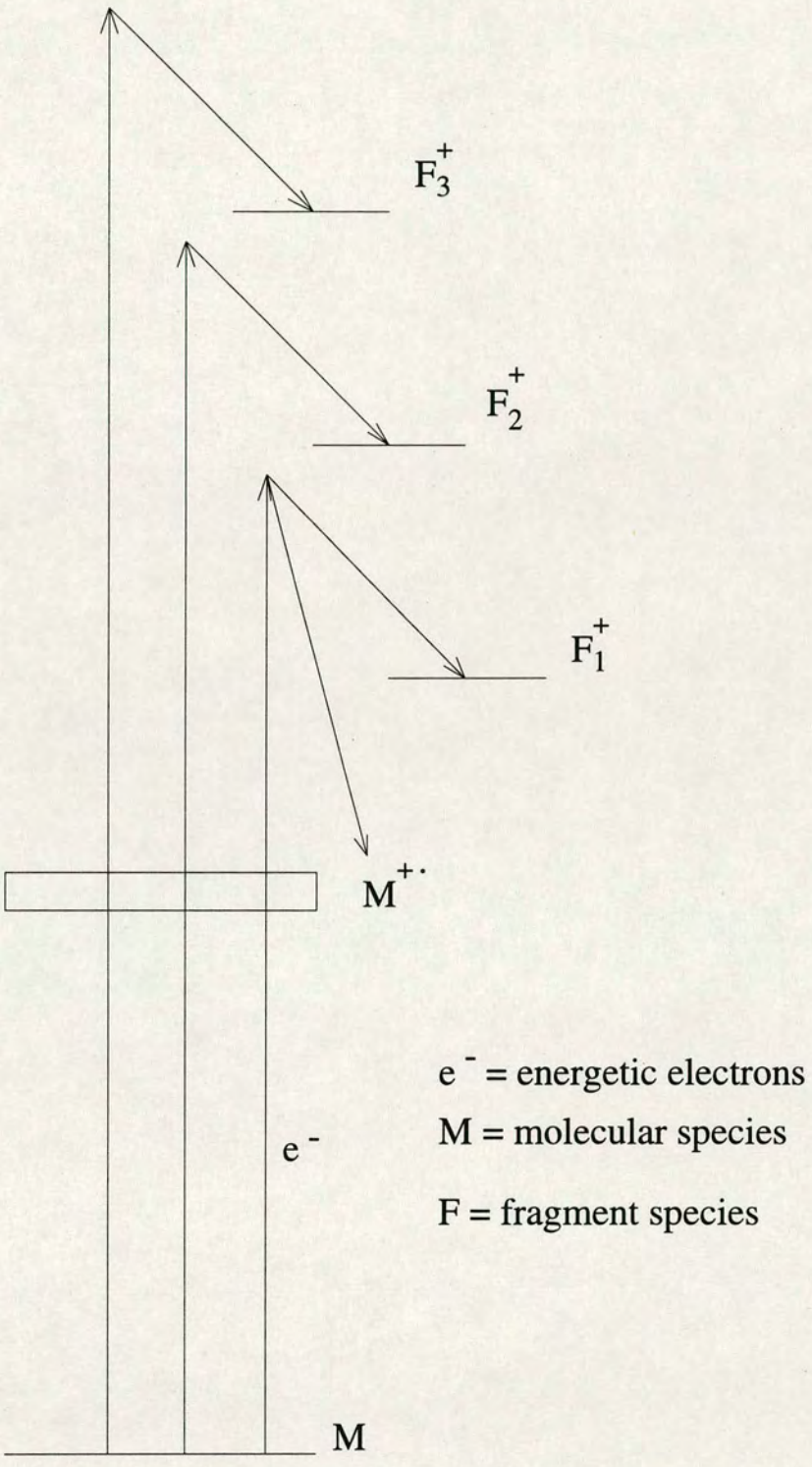

Figure 2-8: Schematic diagram illustrating the ionisation and fragmentation mechanisms in electron impact ionisation.

2.4.1 Basic Principles of TOF-MS.

The preceding sections have considered the background and mechanisms behind laser desorption and laser photoionisation. Since both of these techniques are pulsed in nature, then the obvious type of mass analyser to employ is one which efficiently processes ions created in short pulses. Scanning mass spectrometers (magnetic and electric sector instruments, and more commonly quadrupoles) have previously been used with pulsed ion sources such as MPI, however, there are a number of disadvantages. Sector and quadrupole instruments are designed for use with continuous ion sources, with the separation of ions being achieved by scanning the appropriate fields in order to spatially disperse ions of different masses. This is clearly inappropriate for the low duty cycle pulsed laser experiments employed in this work. A mass spectrometric method which does take advantage of the pulsed nature of the ion source is TOF-MS. The principal advantages of TOF-MS over other methods is that it:

- offers a theoretically unlimited mass range
- allows a complete mass spectrum to be recorded for each laser shot
- has a high transmission

Using TOF-MS is probably the most obvious way of separating ions by mass, and was first proposed fifty years ago by W. E. Stevens [105]. However, TOF-MS also has a serious disadvantage compared to scanning sector instruments, in that it suffers from very poor mass resolution. As a result of the high resolution attainable using sector instruments and the lack of fast pulsed ionisation sources, high speed detectors and poor data processing capabilities, TOF-MS was abandoned for quite some time, and so research into tackling the poor resolution problems was severely curtailed. However, the emergence of pulsed ionisation sources such as FAB, SIMS and LD sparked a renaissance in TOF-MS, and this renewed interest allowed some considerable advances to be made. The small size, low cost and ease of construction of TOF instruments has now made them the mass analyser of choice for many workers using pulsed ionisation sources.

The fundamental components of a TOF mass spectrometer are the ion source, the drift region (or flight tube) and the detector. The simplest type of TOF mass spectrometer is shown schematically in Figure 2-9a. In this single stage linear TOF, the ions are formed in the ion source and are immediately extracted by a fixed potential. This electric field accelerates the ions into a longer, field free drift region, where the ions are directed onto a detector. In the ideal case, all ions enter the drift region with the same kinetic energy (KE), given by

$$KE = zeE_s s = \frac{1}{2}mv^2 \tag{2.7}$$

where e is the charge on an electron, z is the number of charges, E_s is the electric field, s is the distance between the repeller and the field free region, m is the mass of the ion and v is the velocity with which the ion moves in the field free region. Ions enter the drift region with the same kinetic energy, and as such, will have mass dependent velocities:

$$v = \left(\frac{2zeE_s s}{m}\right)^{\frac{1}{2}} \tag{2.8}$$

Therefore, the time required to travel the fixed flight path also has a mass dependence according to

$$t = \left(\frac{m}{2zeE_s s}\right)^{\frac{1}{2}} D \tag{2.9}$$

The mass spectrum recorded over time can therefore be converted directly to mass:

$$\frac{m}{z} = 2eE_s s\left(\frac{t}{D}\right)^2 \tag{2.10}$$

Therefore, lighter faster moving ions reach the detector before the slower heavier ones. Recording the ion intensity as a function of time leads to the generation of a TOF mass spectrum. As might be expected, mass resolution using such a simple

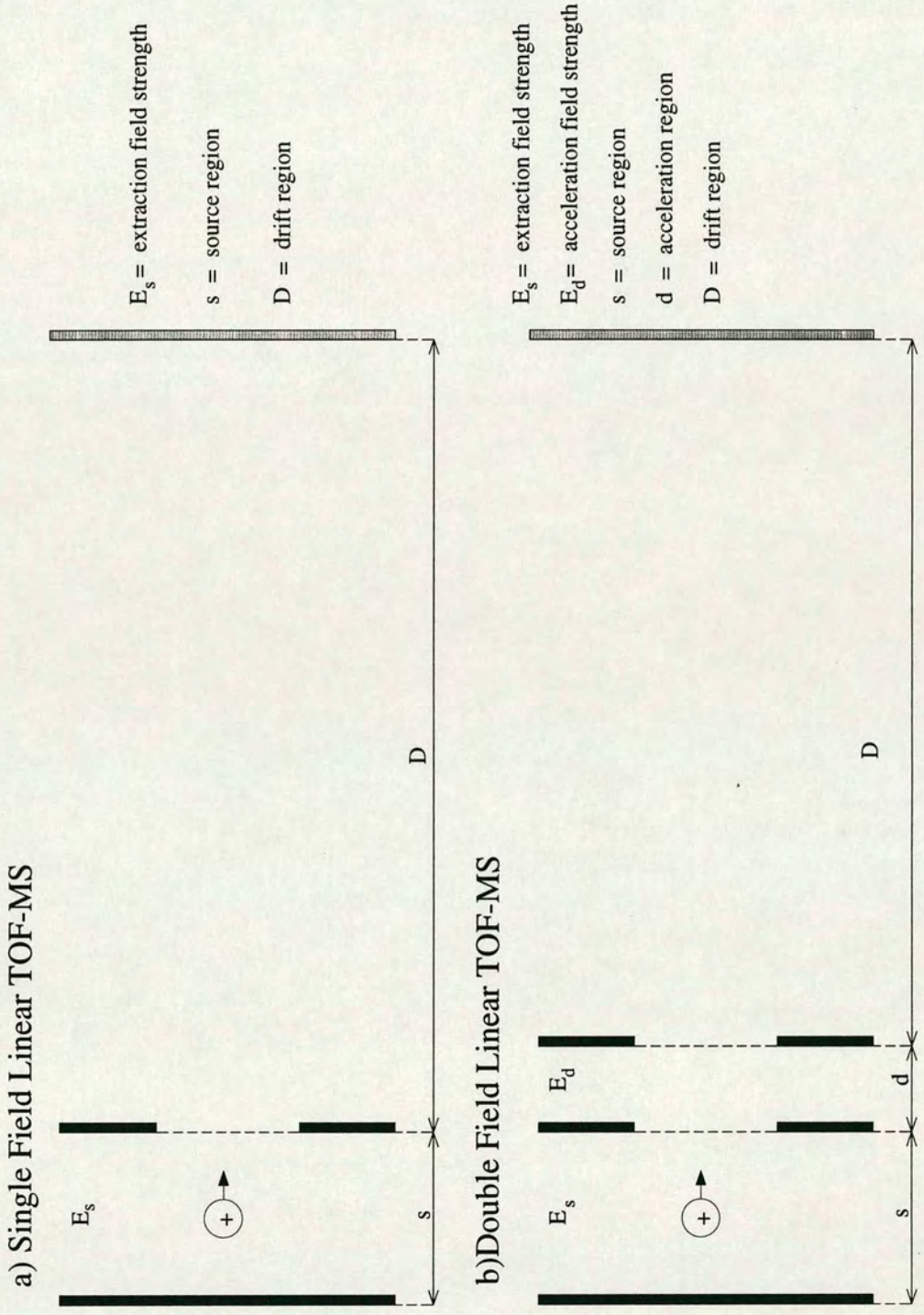

Figure 2-9: Schematic diagram illustrating the (a) single field, and (b) double field Wiley-McLaren type, linear TOF mass spectrometers.

linear TOF mass spectrometer is rather poor. This will be discussed more fully in the next section. Instead, a Wiley-McLaren ion extraction set-up, as shown in Figure 2-9 b, is generally used. This was first proposed in 1955 [106], and is still the most common means of ion extraction used in TOF instruments today. In this case, a two-step acceleration field is used, which provides a first-order focusing of the ion packets. This means that ions created at slightly different positions in the source region can be focused simultaneously at the detector, thereby increasing the resolving power of the instrument. This is discussed in Section 2.4.2 under spatial resolution.

As well as a complete mass spectrum being generated for each experimental cycle, TOF-MS has improved sensitivity in comparison with sector and quadrupole instruments. This results from temporally rather than spatially separating ions of differing mass. In scanning instruments, most of the ions are neglected at each field setting, with only the ions at one mass being focused onto the detector at any one time. The transmission in a TOF device is potentially much higher, since a mass spectrum is recorded with static fields, and all ions are extracted along the same trajectory, at least to a first approximation. The sensitivity, therefore, is enhanced, being limited only by the physical transmission efficiency of the grids employed in the extraction optics. In a real TOF mass spectrometer, there are several other mechanisms which can lead to reduced ion transmission. For example, ions may collide with background gas molecules and be deflected, or their velocity component perpendicular to the direction of extraction due to the velocity distribution of the neutral precursors, may be sufficient for them to miss the detector. This latter effect can be corrected for to some extent by using a reflecting geometry TOF mass analyser. This corrects for differences in initial kinetic energy and velocity by acting as an electrostatic hill, as described in Section 2.4.3.

2.4.2 Factors Affecting Mass Resolution

As mentioned previously, TOF-MS is directly compatible with MPI as an ionisation source. However, a major problem with TOF-MS is that it generally only provides relatively low mass resolving power. In a TOF mass spectrometer, the

resolution is determined by the temporal width of the signal produced on detection of ion packets.

The resolving power, or resolution, of a TOF instrument is defined as

$$R = \frac{m}{\Delta m} = \frac{t}{2\Delta t} \tag{2.11}$$

where m is the ion mass, Δm is the FWHM spread in the ion packet mass, t is the ion flight time and Δt is the FWHM temporal width of the ion packet. An alternative definition of mass resolution introduced by Schlag et al. [107] is:

$$R = m\frac{(t_2 - t_1)}{\Delta t} \tag{2.12}$$

where $(t_2 - t_1)$ is the difference in the time-of-flight for two neighbouring mass peaks, of mass m and $m + 1$, and Δt is the temporal width of the ion packets. From equations (2.9) and (2.10), it can be seen that the two main factors which determine the mass resolution are:

- the temporal width of each individual ion packet, and
- the differences in arrival times at the detector of two adjacent mass peaks.

The flight time of an ion is given by

$$t = \kappa m^{1/2} \tag{2.13}$$

where κ is a proportionality constant controlled by instrumental design parameters. Therefore, as mass increases, the flight times of two adjacent mass peaks converge, until the temporal width of the ion packets is equal to the difference in their flight times. This causes the peaks to become unresolvable.

Therefore, in order to maximise resolution, Δt must be minimised and $(t_2 - t_1)$ must be maximised. In order to increase the difference in arrival times of neighbouring peaks, it is evident that a large value of κ is required in order to achieve high resolution. This can be accomplished, for example by increasing the length of

the flight tube. However, there are obvious practical constraints as to how long a flight tube can be. The transmission of the instrument (and therefore the sensitivity) decreases with increasing length, unless additional focusing optics are used, due to off axis velocity components of the ions becoming more significant. The width of an ion packet, Δt is limited by several broadening mechanisms. These are outlined below.

Spatial Resolution

In the "perfect" TOF mass spectrometer, all ions will be created in a single narrow source plane perpendicular to the electric field. If this were the case, and no other broadening mechanisms were acting on the ion packet, each ion of the same mass to charge ratio would gain an equivalent amount of kinetic energy from the extraction field and arrive at the detector at the same time. In a real TOF instrument, the ionisation source plane is defined by the outer limits of the ionising laser beam. Unfortunately, it is impossible to focus or aperture a laser beam down to a single point, and so there exists a finite region in space over which ions will be formed.

Consider two ions of same mass-to-charge ratio and initial kinetic energies, created at precisely the same time. Figure 2-10a illustrates the scenario where two ions are formed at the outer limits of a region in space defined by the edges of the ionising laser. The ion formed closest to the higher potential repeller plate gains more kinetic energy from the field than does the other ion, and for an appropriate length of flight tube, is detected first. Thus, ions of the same mass-to-charge ratio, formed at the slightly different points in space are temporally separated. In the absence of all other broadening mechanisms, the temporal separation of ions of the same nominal mass due to their being created at different locations is known as the limit of spatial resolution. It is evident that effects of spatial resolution will be minimised by the focusing or aperturing of the beam in order to limit the range in potentials over which ions are created. However, the tight-focusing of the ionisation beam introduces another broadening mechanism due to space charge effects, which will be discussed later in this section.

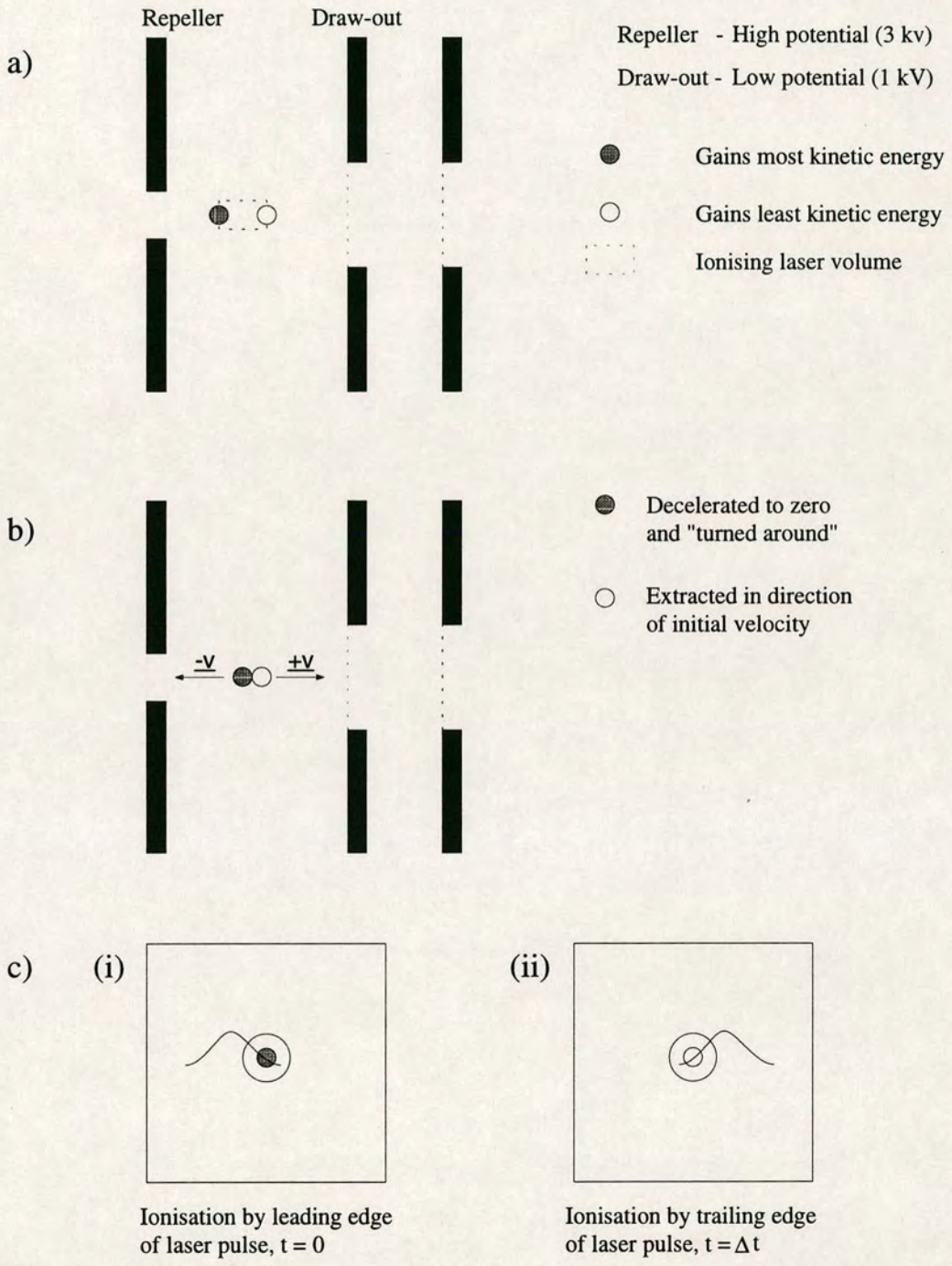

Figure 2-10: Schematic diagram illustrating the effects of ions created (a) with different initial locations, (b) with different initial velocities, and (c) at the (I) leading and (ii) trailing edges of the ionising laser pulse. These illustrate the limits of spatial, energy and timing resolution, respectively.

Spatial resolution is the main limiting factor on the attainable mass resolution in a simple linear TOF instrument, such as that illustrated in Figure 2-9a. The dependence of ion flight times on the initial position of the ions can, at least partially, be eliminated by introducing ion focusing capabilities into the TOF spectrometer. One means of doing this was first demonstrated by Wiley and McLaren in 1955 [106]. They developed a two-field acceleration region which produced first-order focusing of the ion packets, so that ions created at different points in the source arrive at the detector at approximately the same time.

In a simple single-stage accelerating field, there is a point in the drift-region where the faster moving ion catches up to the slower moving one. At this point, these ions are said to be spatially focused, and if the detector is placed at this point, a very narrow ion packet should be detected, in the absence of other broadening mechanisms. However, in practice, this is usually not the case. For this simple two-electrode system, it is generally found that the position of this space focus is at a position much too close to the point of ion formation for adequate separation. Additionally, the only way to achieve spatial focusing should the position of ionisation change, would be to physically move the detector. Wiley and McLaren noted that a much more versatile TOF device could be constructed by the addition of a second field to the extraction region. This results in much longer flight times and allows the mass spectrometer to be refocused by simply adjusting the extraction fields. Therefore, the double field extraction region allows spatial resolution to be improved with respect to that of the single field device.

Kinetic Energy Resolution

The resolution of a TOF instrument will also be affected by the velocity distribution of the ions parallel to the spectrometer axis. The initial velocities of these ions are derived from the velocities of the neutral precursor molecules. The most instructive way of illustrating this effect is to consider the extreme case of two ions of the same mass-to-charge ratio, formed at identical points in space and time but possessing oppositely directed velocities, $+\underline{v}$ and $-\underline{v}$ parallel to the spectrometer

axis (see Figure 2-10b). These two ions will obviously not impinge on the detector at the same time; the ion moving in the opposite direction to the detector must be decelerated to zero before being accelerated back towards its initial position, where it will follow the same trajectory as the other ion, "starting again" at a later time with velocity $+\underline{v}$. The separation in time of the detection of these two ions is the so-called "turn-around time". Similarly, if two ions have the same mass-to-charge ratio, and are formed in the same location but with different kinetic energies, the differences in their flight times increases with flight tube length. Essentially, a distribution of kinetic energies for the neutral pre-cursors results in the detection of ion packets of finite width. In the absence of all other broadening mechanisms, the temporal distribution of the ion packet caused by this effect is known as the limit of energy resolution.

The magnitude of this turn-around time is influenced by the initial velocity distribution the ions and the electric field strengths in the ion-source. This effect can be minimised in a number of ways. It is possible to reduce the turn-around time by minimising the ratio of the initial kinetic energy of the ions to the extraction potential. This can be achieved by increasing the value of the accelerating potential. However, this is only feasible to a certain degree since a longer flight tube would be required in order to maintain the same time-of-flight. It is also possible to attenuate the effect of energy resolution by reducing the initial spread in velocities of the neutral precursor molecules. This can be achieved by seeding the desorbed species in a pulsed supersonic molecular beam propagating parallel to the spectrometer axis, thus cooling the translational degrees of freedom by a series of two-body collisions. The narrow velocity distribution afforded by such a molecular beam can substantially reduce the temporal broadening of the ion packet.

In their 1955 paper [106], Wiley and McLaren described a way of energy focusing in their double-field ion source called "time-lag-focusing". Here, a time delay between the ionisation pulse and the application of a pulsed extraction field was introduced, such that the ions spread out in the zero field ion source. If the extraction field was switched on at the correct time, then most of the initial kinetic energy

spread could be corrected for. This was because ions initially moving away from the detector would be extracted at a higher potential, thereby attaining higher kinetic energies. However, any gain in energy resolution was offset by a degradation in spatial resolution, since the device had to be operated away from spatial focusing conditions. An alternative method for overcoming the effects of the nascent kinetic energy distribution is "impulse field focusing" [108]. In this case, a fast, short, high voltage pulse accelerates the ions in a very short time to a velocity that is much greater than their initial velocity, before switching on the extraction potentials. Further novel methods have been reviewed by Boesl et al. [109].

However, all of these attempts to energy focus within the ion source have their drawbacks. Nowadays, the method of choice is to maximise the spatial resolution as described before, and to use the resultant first-order space focus as a pseudo-ion source. Therefore, the ions can be considered to have originated from the same point in space, with only their kinetic energy distribution uncorrected. It is then possible to correct for flight-time broadening using a secondary energy compensating device. The most popular means of doing this is to use a reflectron mass spectrometer. This will be described in more detail in Section 2.4.3. The separation of the ion source and mass spectrometer in this way allows optimisation for spatial resolution in the ion source, and for kinetic energy resolution in the reflectron mass spectrometer.

Temporal Resolution

A further limit on the resolution of a TOF mass spectrometer is the temporal width of the ion packet resulting from the limiting pulse duration of the ionisation technique. Figure 2-10c shows the case where two ions of equal mass-to-charge ratio are formed at the same point in the ion source, but at the leading and trailing edges of the ionising pulse. They acquire the same velocity and travel the same trajectory, but arrive at the detector separated by Δt, the duration of the ionising pulse. This remains a constant separation throughout the drift region in the absence of all other broadening mechanisms, and is known as the limit of temporal resolution. Historically, poor temporal resolution was the principal cause of the poor mass

resolving power of TOF instruments. However, the advent of pulsed laser systems, which are now routinely available with pulse widths of less than 10 ns, has alleviated this problem.

Obviously, the effects of temporal resolution can be minimised by using shorter and shorter ionisation pulses. This is now possible using picosecond and femtosecond laser systems. However, this is a rather expensive solution to improving mass resolution. Similar improvements can also be made by increasing the flight time, either by reducing the accelerating potential or by increasing the length of the flight tube. However, not surprisingly, there are trade-offs to be made. Reducing the accelerating potential reduces the ion transmission, and brings the effects of energy resolution back into play; increasing the flight path reduces transmission as a result of off-axis velocity components becoming more significant. In all cases, it is best to reach a compromise solution. Fortunately, broadening due to the pulse duration of the ionising laser, even for nanosecond sources, is by no means the major resolution limiting factor, and so consequently is of less concern than spatial and energy resolution.

Space Charge Effects

As was mentioned previously, a tightly focused laser beam will assist in the reduction of the effects of spatial resolution. However, this can result in very high ionising laser power densities, which leads to the production of large numbers of ions in a small volume. This causes each ion to influence the others via electrostatic interactions. The effect of these repulsive forces is to move the ions to different regions of the ion source, where they will be extracted with varying amounts of kinetic energy. This results in broad ion peaks of the same nominal mass being observed at the detector.

It has been estimated that these effects become significant at ion number densities of 10^7 to 10^8 ions cm^{-3} [110]. Generally, under the experimental conditions used in

this work, ion number densities never exceeded 10^5 to 10^6 ions cm^{-3} [99], and so space charge effects were considered negligible.

2.5 Reflectron TOF Mass Spectrometer.

A reflectron mass spectrometer may be used to correct for the effects of initial kinetic energy distributions of ions. This was first introduced by Mamyrin in 1973 [111], although the reflectron used in this work is based upon a design by Boesl et al. [112]. The characteristic features of a reflectron mass spectrometer are illustrated schematically in Figure 2-11, and the basic operating principles are outlined below.

As was described in Section 2.4.2, a Wiley-McLaren two-field ion source is used to extract ions to the first-order space focus. This space focus can be considered as a pseudo ion-source for the reflectron mass spectrometer. These ions have a mean velocity defined by the ion-source, but still have a spread in kinetic energy, and continue to travel along the first field-free drift region until they enter the ion mirror. For ions of the same mass, those with the highest kinetic energies enter the ion mirror first, followed by the less energetic ions. The former penetrate deeper into the reflecting field, and spend more time in the mirror. By choosing appropriate potentials and geometries (d_t, d_k, L, U_t and U_k) the shorter flight time of the high energy ions in the field free region is compensated for by their longer residence times within the mirror. An added advantage of the reflectron is that it now has a second field free drift region, effectively doubling the flight path of the ions. This increases the separation of neighbouring mass peaks, thereby helping to increase mass resolution. There is point at which the ions are decelerated to zero, and it can be seen that the reflector acts as a second space focus or pseudo-ion source. The simplest case, is where the flight distance from the original space focus to the reflector, and the reflector to the detector are identical. This means that the detector acts as a third space focus.

What must be stressed is that the reflectron can *only* compensate for the spread in flight time resulting from differences in kinetic energy. It cannot correct for temporal

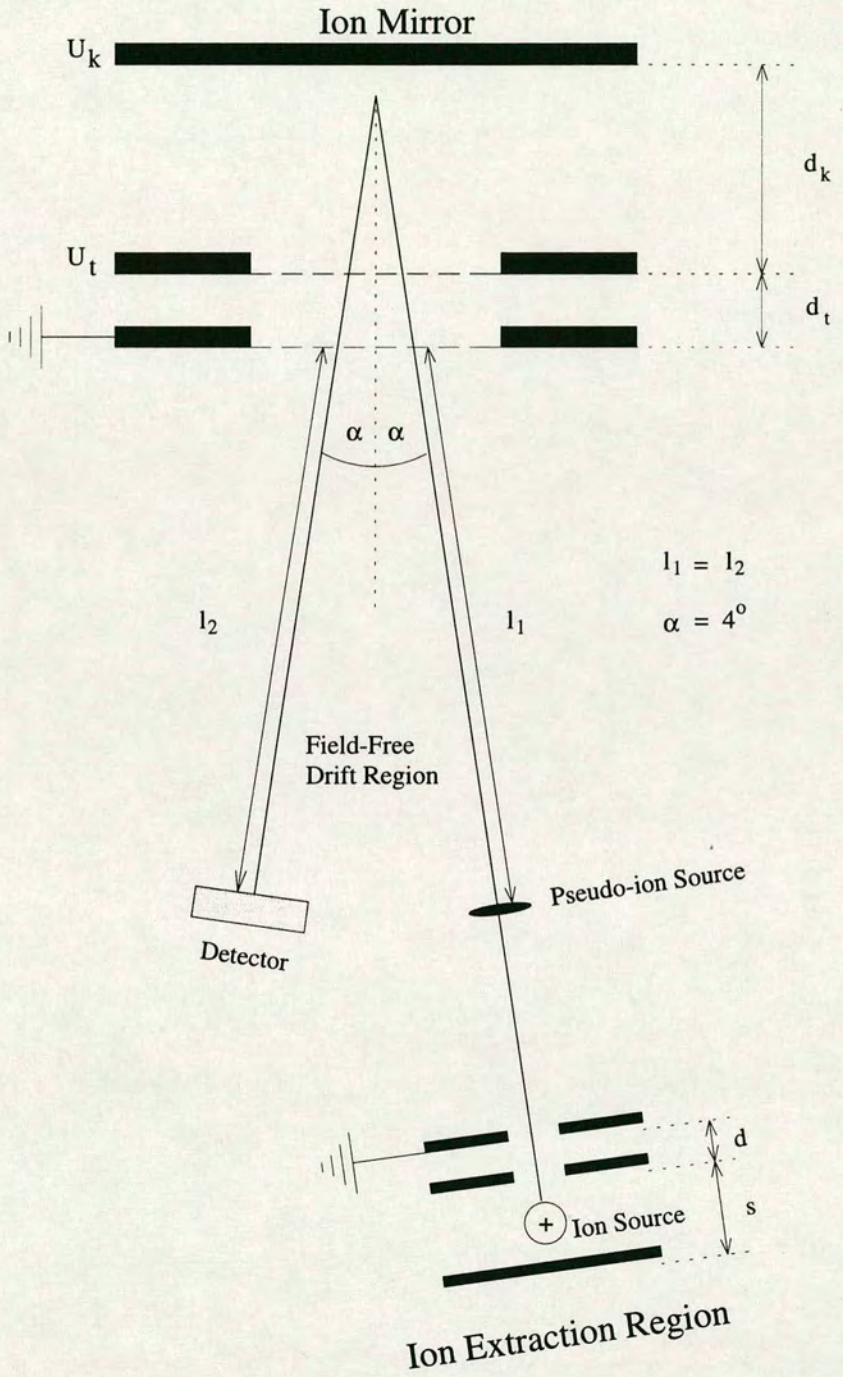

Figure 2-11: Schematic diagram illustrating the Reflectron TOF mass spectrometer.

distributions since ions are extracted at the same potential, and as such receive the same kinetic energy.

The temporal distribution at the pseudo ion source, or time interval over which ions of single mass pass the pseudo ion-source is due to:

- an incompletely corrected energy distribution at the space focus (i.e., only first order space focusing), or
- the time spread in the ion source due to ion formation time and the turn around time.

The turn around time can be effectively reduced by using high extraction fields, with the kinetic energy distribution being corrected for by the reflector.

2.5.1 Effect on Resolution upon Removing the Molecular Beam

Initially, most workers who coupled laser desorption and laser photoionisation with TOF-MS used a molecular beam to transport the neutral species from the desorption source to the ionisation region. If the appropriate experimental conditions were used, this could result in a significant cooling of the internal degrees of freedom. In addition to facilitating spectroscopic studies, this also has the effect of improving the mass resolving power of the instrument.

When a supersonic expansion is used, very low translational temperatures as low as 0.1 K can be achieved. This means that the velocity distribution of the neutral molecules at the point of ionisation is very narrow, and well directed down the axis of extraction. Therefore, in terms of the previous discussion on energy resolution, there will be a very small initial kinetic energy distribution, resulting in narrow ion packets being observed at the detector. However, in order to use L2MS effectively as an analytical tool, it is necessary to dispense with the inefficient entrainment step in favour of high sensitivity. In the absence of the molecular beam, however, it is believed that the initial velocity distribution of the desorbed species could approach thermal values, and so a concomitant degradation in mass resolving power will

result. This can be minimised by carefully considering the desorption and extraction geometries.

When a desorption laser is incident on a sample surface, a plume of material is ejected predominantly normal to that surface. Given that the major velocity component is directed away from the surface, then for a thermal velocity distribution, most of the spread in kinetic energy will be in that direction also. Therefore, if the desorption laser is incident on the sample surface, but parallel to the axis of extraction, then the neutrals will be desorbed with their main velocity component directed along the extraction axis, resulting in relatively poor mass resolution. This is shown in Figure 2-12a. However, Figure 2-12b shows the case where the desorption laser is directed onto the sample surface perpendicular to the axis of extraction. In this case the spread in kinetic energy of the desorbed neutrals along the axis of extraction should be less than in the previous case, resulting in a less severe degradation in mass resolution. It therefore appears that the most sensible desorption geometry to adopt is that illustrated in Figure 2-12b. This is a similar argument to "orthogonal injection" of ions, which is used in electrospray TOF-MS [113]. It has been reported that injection of ions perpendicular to the extraction axis minimises the initial spatial and velocity spread, and so also improves mass resolution with respect to "parallel injection". Also, given that one of the ultimate goals of the project is to achieve spatially resolved desorption, then smaller spot sizes can be achieved using the latter geometry. On the instrument used in this work, there is no access port which allows a desorption laser beam to be directed along the plane of extraction normal to the sample surface, and so it is necessary to introduce the desorption laser at an angle of 45° from the normal. This results in an elliptical desorption spot being produced, which obviously limits the maximum attainable spatial resolution.

2.6 Concluding Remarks

The L2MS technique comprises the three fundamental processes of laser desorption, laser photoionisation and time-of-flight mass spectrometry, which when

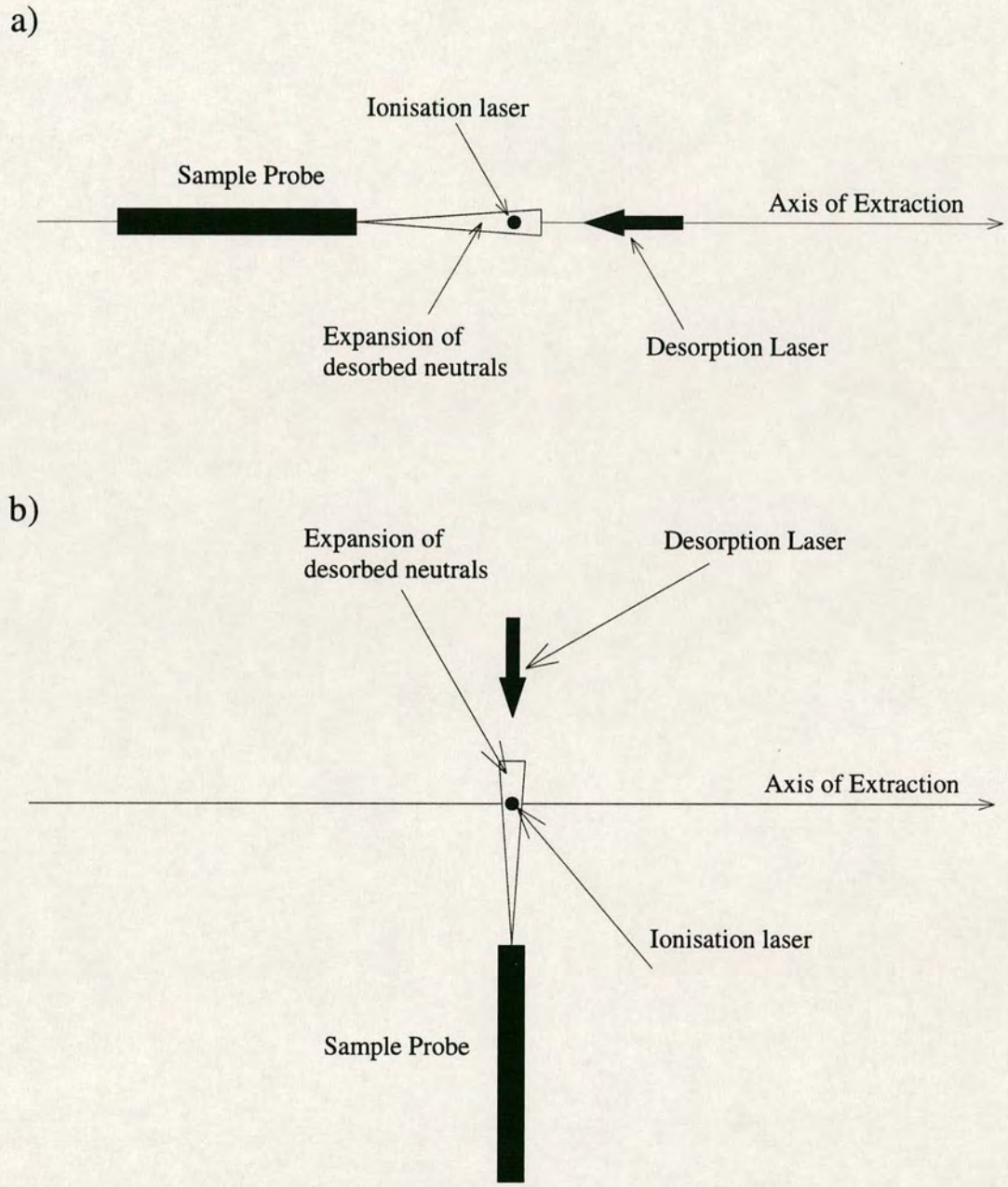

Figure 2-12: Schematic diagram illustrating the effects of desorbing (a) parallel, and (b) orthogonal to the axis of extraction.

coupled together, provide a uniquely powerful tool for the analysis of large molecular systems, both in their pure form and directly from their native environments.

Laser desorption facilitates the production of intact gas-phase, involatile, thermally labile molecules. The use of IR laser radiation at power densities around 10^8 Wcm^{-2} results in a vast excess of neutral species over ions, and therefore a huge increase in sensitivity can be achieved by neglecting nascent ions in favour of postionising the neutral species. Although laser desorption of neutrals was originally carried out in a supersonic molecular beam, this severely limited the sensitivity of the technique, and so has now largely been dispensed with. The laser desorption stage of the technique also underpins the effectiveness of L2MS as an analytical tool for the investigation of real systems. Even for very complex systems, laser desorption can still produce intact neutral molecules, which are available for postionisation by a second laser. This temporal and spatial separation of the desorption and ionisation events allows both processes to be independently optimised, thereby allowing tremendous control over the appearance of the mass spectra.

The second stage of the technique, resonant laser multi-photon ionisation, has a number of unique advantages. Judicious choice of the ionisation wavelength can permit the selective detection of single components in a complex mixture, thereby greatly simplifying the resultant mass spectra. Also, the unambiguous identification of target molecules can be achieved by utilising the UV absorption information, along with often observed wavelength dependent fragmentation processes. It is also possible to obtain structural information, simply by increasing the laser power density and inducing fragmentation. Although the selectivity of ionisation makes L2MS very powerful for *in situ* analysis, obviously this puts a severe limit on the molecular classes which may be studied. However, for molecules which do not contain a UV chromophore, the two-step methodology is not redundant. It will be shown in the subsequent chapters that strategies for analysing non-UV absorbers are available, with minimal changes to the experimental configuration, including VUV single-photon ionisation (SPI) and laser induced photoelectron ionisation (LIPEI).

Finally, a time-of-flight mass spectrometer is the ideal mass analyser for coupling to a laser desorption and laser photoionisation ion source. The principal advantages of such a mass analyser are the potentially unlimited mass range, the high transmission and sensitivity which can be achieved, and the ability to record a complete mass spectrum for each experimental cycle. Although mass resolution has previously been an important issue in TOF-MS, the coupling of Wiley-McLaren ion extraction optics and a reflectron TOF mass spectrometer have enabled adequate resolving power to be achieved.

References

[1] M. A. Posthumus, P. G. Kistemaker, H. L. C. Meuzelaar, M. C. Ten Noever de Brauw, *Anal. Chem.*, **50**, 985, (1978)

[2] G. J. Q. van der Peyl, J. Haverkamp, P. J. Kistemaker, *Int. J. Mass Spectrom. Ion Phys.*, **42**, 125, (1982)

[3] F. Hillenkamp, M. Karas, R. C. Beavis, B. T. Chait, *Anal. Chem.*, **63**, 1193A, (1991)

[4] R. J. Beuhler, E. Flanigan, L. J. Greene, L. Friedman, *J. Am. Chem. Soc.*, **96**, 3990, (1974)

[5] B. Lindner, U. Seydel, *Anal. Chem.*, **57**, 895, (1985)

[6] R. C. Beavis, J. Lindner, J. Grotemeyer, E. W. Schlag, *Z. Naturforsch*, **43a**, 1083, (1983)

[7] A. Vertes, in *"Methods and Mechanisms for Producing Ions from Large Molecules"*, Eds. K. G. Standing, W. Ens, Plenum, New York, 1990

[8] F. J. Vastola, A. J. Pirone, *Adv. Mass Spectrom.*, **4**, 107, (1968)

[9] R. B. van Breeman, M. Snow, R. J. Cotter, *Int. J. Mass Spectrom. Ion. Proc.*, **49**, 35, (1983)

[10] G. D. Daves, *Acc. Chem. Res.*, **12**, 359, (1979)

[11] R. Zenobi, J. H. Hahn, R. N. Zare, *Chem. Phys. Lett.*, **150**, 361, (1988)

[12] D. Burgess Jr., R. Viswanathan, I. Hussla, P. C. Stair, E. Weitz, *J. Chem. Phys.*, **79**, 5200, (1983)

[13] C. J. S. M. Simpson, J. P. Hardy, *Chem. Phys. Lett.*, **130**, 175, (1986)

[14] G. Wedler, H. Ruhmann, *Surf. Sci.*, **121**, 464, (1982)

[15] R. N. Zare, R. D. Levine, *Chem. Phys. Lett.*, **136**, 593, (1987)

[16] R. E. Smalley, D. H. Levy, L. Wharton, *J. Chem. Phys.*, **64**, 3266, (1976)

[17] K. C. Janda, *Adv. Chem. Phys.*, **60**, 201, (1985)

[18] J. C. Drobits, J. M. Skere, M. I. Lester, *J. Chem. Phys.*, **84**, 2896, (1986)

[19] C. V. Shank, R. Yen, C. Hirlimann, *Phys. Rev. Letters*, **50**, 454, (1983)

[20] R. Zenobi, R. N. Zare in *"Advances in Multi-Photon Processes and Spectroscopy"*, Ed. S. H. Lin, World Scientific, Singapore, 1991

[21] P. G. Kistemaker, M. M. Lens, G. J. Q. van der Peyl, A. J. H. Boerboom, *Adv. Mass Spectrom.*, **8A**, 928, (1980)

[22] R. Stoll, F. W. Rollgen, *Org. Mass Spectrom.*, **14**, 642, (1979)

[23] G. J. Q. van der Peyl, W. J. van der Zande, K. Bederski, A. J. H. Boerboom, P. J. Kistemaker, *Int. J. Mass Spectrom. Ion Phys.*, **47**, 7, (1983)

[24] 24 G. J. Q. van der Peyl, K. Isa, P. G. Kistemaker, *Org. Mass Spectrom.*, **18**, 416, (1981)

[25] M. Karas, D. Bachmann, F. Hillenkamp, *Anal. Chem.*, **57**, 2935, (1985)

[26] F. Hillenkamp, M. Karas, D. Holtkamp, P. Klusever, *Int. J. Mass Spectrom. Ion Proc.*, **67**, 265, (1986)

[27] F. Hillenkamp, U. Bahr, M. Karas, B. Spengler, *Scanning Microsc. Suppl.*, **1**, 33, (1987)

[28] B. Spengler, M. Karas, U. Bahr, F. Hillenkamp, *J. Phys. Chem.*, **91**, 6502, (1987)

[29] G. R. Kinsel, J. Lindner, J. Grotemeyer, E. W. Schlag, *J. Phys. Chem.*, **95**, 7824, (1991)

[30] H. J. Heinen, *Int. J. Mass Spectrom. Ion Phys.*, **38**, 309, (1981)

[31] K. Tanaka, Y. Ido, S. Akita, Y. Yoshida, T. Yoshida, *Proc. of Second Japan-China Joint Symposium on Mass Spectrometry*, Osaka, Japan, 1987

[32] M. Karas, F. Hillenkamp, *Anal. Chem.*, **60**, 2299, (1988)

[33] R. C. Beavis, B. T. Chait, *Rapid Commun. Mass Spectrom.*, **3**, 233, (1989)

[34] M. Salehpour, I. Perera, J. Kjellberg, A. Hedin, M. A. Islamian, P. Hakansson, B. U. R. Sundqvist, *Rapid Commun. Mass Spectrom.*, **3**, 259, (1989)

[35] B. Spengler, R. J. Cotter, *Anal. Chem.*, **62**, 793, (1990)

[36] A. Vertes, R. Gijbels, R. D. Levine, *Rapid Commun. Mass Spectrom.*, **4**, 228, (1990)

[37] H. Ehring, M. Karas, F. Hillenkamp, *Org. Mass Spectrom.*, **27**, 472, (1992)

[38] R. C. Beavis, T. Chaudhary, B. T. Chait, *Org. Mass Spectrom.*, **27**, 156, (1992)

[39] T. -W. D. Chan, A. W. Colburn, P. J. Derrick, *Org. Mass Spectrom.*, **26**, 342, (1991)

[40] R. Knochenmuss, F. Dubois, M. J. Dale, R. Zenobi, *Rapid Commun. Mass Spectrom.*, **8**, 871,(1996)

[41] D. M. Hercules, R. J. Day, K. Balasangmugam, T. A. Dang, C. P. Li, *Anal. Chem.*, **54**, 280A, (1982)

[42] G. R. Kinsel, J. Lindner, J. Grotemeyer, *Org. Mass Spectrom.*, **26**, 1052, (1991)

[43] J. -C. Tabet, R. J. Cotter, *Int. J. Mass Spectrom. Ion Proc.*, **54**, 151, (1983)

[44] I. Langmuir, K. H. Kingdon, *Proc. Roy. Soc. London (Series A)*, **61**, 107, (1925)

[45] R. J. Cotter, *Anal. Chem.*, **52**, 1767, (1980)

[46] R. Temruell, D. M. Lubman, *Anal. Chem.*, **58**, 1299, (1986)

[47] F. Engelke, J. H. Hahn, W. Henke, R. N. Zare, *Anal. Chem.*, **59**, 909, (1987)

[48] J. Grotemeyer, U. Boesl, K. Walter, E. W. Schlag, *J. Am. Chem. Soc.*, **108**, 4233, (1986)

[49] T. L. Weeding, R. J. J. Steenvorden, P. G. Kistemaker, J. J. Boon, *J. Anal. and Applied Pyrolysis*, **20**, 47, (1991)

[50] M. S. de Vries, D. J. Elloway, H. R. Wendt, H. E. Hunziker, *Rev. Sci. Instrum.*, **63**, 3321, (1992)

[51] J. R. Cable, M. J. Turbergen, D. H. Levy, *J. Am. Chem. Soc.*, **109**, 6198, (1987)

[52] P. Voumard, Q. Zahn, R. Zenobi, *Rev. Sci. Instrum.*, **54**, 2215, (1993)

[53] M. J. Dale, A. C. Jones, P. R. R. Langridge-Smith, K. F. Costello, P. G. Cummins, *Anal. Chem.*, **65**, 793, (1993)

[54] Q. Zahn, R. Zenobi, S. J. Wright, P. R. R. Langridge-Smith, *submitted to Macromols.*, (1996)

[55] L. J. Kovalenko, C. R. Maechling, S. J. Clemett, J-M. Philippoz, R. N. Zare, *Anal. Chem.*, **64**, 682, (1992)

[56] Q. Zhan, P. Voumard, R. Zenobi, *Rapid Comm. Mass Spectrom.*, **9**, 119, (1995)

[57] 57 R. W. Ditchburn, F. L. Arnot, *Proc. Roy. Soc. London (Series A)*, **A123**, 516, (1929)

[58] A. H. Kung, J. F. Young, S. E. Harris, *Appl. Phys. Lett.*, **22**, 301, (1976) and A. H. Kung, J. F. Young, S. E. Harris, *Appl. Phys. Lett.*, **28**, 294, (1976)

[59] R. J. J. M. Steenvorden, P. G. Kistemaker, A. E. DeVries, L. Michalak, N. M. M. Nibbering, *Int. J. Mass Spectrom. Ion Proc.*, **107**, 475, (1991)

[60] C. Koster, J. Grotemeyer, *Org. Mass Spectrom.*, **27**, 463, (1992)

[61] P. M. Jonson, C. E. Otis, *Ann. Rev. Phys. Chem.*, **32**, 139, (1981)

[62] G. Petty, C. Tai, F. W. Dalby, *Phys. Rev. Letters*, **34**, 1207, (1975)

[63] P. M. Johnson, *J. Chem. Phys.*, **62**, 4562, (1975)

[64] K. Krogh-Jespersen, R. P. Rava, L. Goodman, *Chem. Phys.*, **44**, 295, (1975)

[65] P. W. Atkins, *Molecular Quantum Mechanics, 2nd Edition*, Oxford University Press, Oxford, 1983.

[66] A. Gedanken, M. B. Robin, N. A. Kuebler, *J. Phys. Chem.*, **86**, 4096, (1982)

[67] M. A. Duncan, T. G. Dietz, R. E. Smalley, *Chem. Phys.*, **44**, 415, (1979)

[68] G. R. Kinsel, J. Lindner, J. Grotemeyer, J. *Chem. Phys.*, **96**, 3162, (1992)

[69] M. J. Dale, *PhD Thesis, The University of Edinburgh*, 1994.

[70] M. Dey, W. Böhm, S. Prinke, J. Grotemeyer, *Proceedings of the 40th ASMS Conference*, 1992.

[71] R. Frey, A. Holle, F. J. Mayer, R. Schäfer, *Proceedings of the 40th ASMS Conference*, 1992.

[72] T. Huthe-Fehre, C. H. Becker, *Rapid Commun. Mass Spectrom.*, **5**, 378, (1991)

[73] J. Grotemeyer, E. W. Schlag, *Angew. Chem. Int. Ed. Engl.*, **27**, 447, (1988)

[74] T. G. Blease, *PhD Thesis, The University of Edinburgh*, 1985.

[75] U. Boesl, H. J. Neusser, E. W. Schlag, *J. Chem. Phys.*, **72**, 4327, (1980)

[76] J. Silberstein, R. D. Levine, *Chem. Phys. Letters*, **74**, 6, (1980)

[77] J. Silberstein, N. Omichi, R. D. Levine, *J. Phys. Chem.*, **89**, 5606, (1985)

[78] F. Rebentrost, K. L. Kompa, A. Ben-Shaul, *Chem. Phys. Letters*, **77**, 394, (1981)

[79] F. Rebentrost, A. Ben-Shaul, *J. Chem. Phys.*, **74**, 3255, (1981)

[80] W. Dietz, H. J. Neusser, U. Boesl, E. W. Schlag, S. H. Lin, *Chem. Phys.*, **66**, 105, (1982)

[81] U. Boesl, H. J. Neusser, E. W. Schlag, *Chem. Phys. Letters*, **87**, 1, (1982)

[82] R. Weinkauf, K. Walter, C. Weickhardt, U. Boesl, E. W. Schlag, *Z. Naturforsch*, **44a**, 1219, (1989)

[83] U. Boesl, R. Weinkauf, K. Walter, C. Weickhardt, E. W. Schlag, *J. Phys. Chem.*, **94**, 8567, (1990)

[84] R. Wenkauf, P. Aicher, G. Wesley, J. Grotemeyer, E. W. Schlag, *J. Phys. Chem.*, **98**, 8381, (1994)

[85] U. Boesl, H. J. Neusser, E. W. Schlag, *J. Chem. Phys.*, **72**, 4327, (1980)

[86] D. M. Lubman, R. Naaman, R. N. Zare, *J. Chem. Phys.*, **72**, 3034, (1980)

[87] K. P. Aicher, U. Wilhelm, J. Grotemeyer, *J. Am. Soc. Mass Spectrom.*, **6**, 1059, (1995)

[88] M. Wood, Y. Zhou, C. L. Brummel, N. Winograd, *Anal. Chem.*, **66**, 2425, (1994)

[89] M. H. Ervin, M. C. Wood, N. Winograd, *Anal. Chem.*, **65**, 417, (1993)

[90] M. E. Ervin, N. Winograd, *Surf. Int. Analysis*, **21**, 298, (1994)

[91] N. Winograd, *Anal. Chem.*, **65**, 622A, (1993)

[92] U. Boesl, H. J. Neusser, E. W. Schlag, *Chem. Phys.*, **55**, 193, (1981)

[93] J. H. Brophy, C. T. Rettner, *Opt. Lett.*, **4**, 337, (1979)

[94] T. G. Dietz, M. A. Duncan, M. G. Liverman, R. E. Smalley, *Chem. Phys. Lett.*, **70**, 246, (1980)

[95] T. G. Dietz, M. A. Duncan, M. G. Liverman, R. E. Smalley, *Chem. Phys. Lett.*, **73**, 4816, (1980)

[96] C. W. Wilkerson Jr., J. P. Reilly, *Anal. Chem.*, **62**, 1804, (1990)

[97] C. W. Wilkerson Jr., S. M. Colby, J. P. Reilly, *Anal. Chem.*, **61**, 2669, (1989)

[98] J. M. Hayes, *Chem. Rev.*, **87**, 745, (1987)

[99] K. F. Costello, *PhD Thesis, The University of Edinburgh*, 1991.

[100] T. R. Rizzo, Y. D. Park, L. A. Peteanu, D. H. Levy, *J. Chem. Phys.*, **84**, 2534, (1986)

[101] S. J. Wright, M. J. Dale, P. R. R. Langridge-Smith, Q. Zhan, R. Zenobi, *Anal. Chem.*, **68**, 3385, (1996)

[102] M. J. Dale, O. H. J. Downs, K. F. Costello, S. J. Wright, P. R. R. Langridge-Smith, J. N. Cape, *Environ. Pollut.*, **89**, 123, (1995)

[103] R. Tembruell, D. M. Lubman, *Anal. Chem.*, **59**, 1082, (1987)

[104] A. C. Jones, M/ J. Dale, G. A. Keenan, P. R. R. Langridge-Smith, *Chem. Phys, Lett.*, **219**, 174, (1994)

[105] W. E. Stevens, *Phys. Rev.*, **69**, 691, (1946)

[106] W. C. Wiley, I. H. McLaren, *Rev. Sci. Instrum.*, **26**, 1150, (1955)

[107] U. Boesl, H. J. Neusser, R. Weinkauf, E. W. Schlag, *J. Phys. Chem.*, **86**, 4857, (1982)

[108] J. A. Browder, R. L. Miller, W. A. Thomas, G. Sanzone, *Int. J. Mass Spectrom. Ion Phys.*, **37**, 99, (1981)

[109] U. Boesl, R. Wienkauf, E. W. Schlag, *Int. J. Mass Spectrom. Ion Proc.*, **112**, 121, (1992)

[110] D. H. Parker, Ch. 4 in *"Ultrasensitive Laser Spectroscopy"*, Academic Press, New York, 1983.

[111] B. A. Mamyrin, V. J. Karatajev, D. V. Schmikk, V. A. Zagulin, *Soviet Phys. JETP*, **37**, 45, (1973)

[112] U. Boesl, J. Grotemeyer, K. Walter, E. W. Schlag, *Anal. Instrum.*, **16**, 151, (1987)

[113] V. V. Laiko, A. F. Dodonov, *Rapid Commun. Mass Spectrom.*, **8**, 720, (1994)

Chapter 3

Experimental

3.1 Introduction

The experimental results presented in the following chapters were primarily performed on a purpose built time-of-flight mass spectrometer [1]. This modular differentially pumped time-of-flight mass spectrometer has two distinct modes of operation. In the first mode a molecular beam is employed in which the laser desorbed species are seeded into a supersonic expansion of helium. In the second mode of operation the molecular beam can be dispensed with. These two modes of operation will be referred to as the Entrainment Mode and Non-Entrainment Mode. The instrument, shown schematically in Figure 3-1, consists of three differentially pumped chambers: a desorption chamber, a laser ionisation chamber and third chamber housing a reflecting geometry time-of-flight (RETOF) mass analyser.

In the entrainment mode of operation, neutral molecules were laser desorbed into the gas-phase from a sample probe in the desorption chamber (DC). These neutrals were then transported into the ion source chamber (ISC) by means of a molecular beam, where the ions were then created by laser photoionisation and extracted into the RETOF mass spectrometer for analysis.

Most of the results presented in this thesis were obtained using the non-entrainment mode configuration of the instrument. In this case both the desorption and ionisation events took place in the ISC. Here, the neutral gas-phase species were photoionised directly above the surface of the sample probe, and extracted and mass analysed as before. The principal advantage of the non-entrainment mode is the large

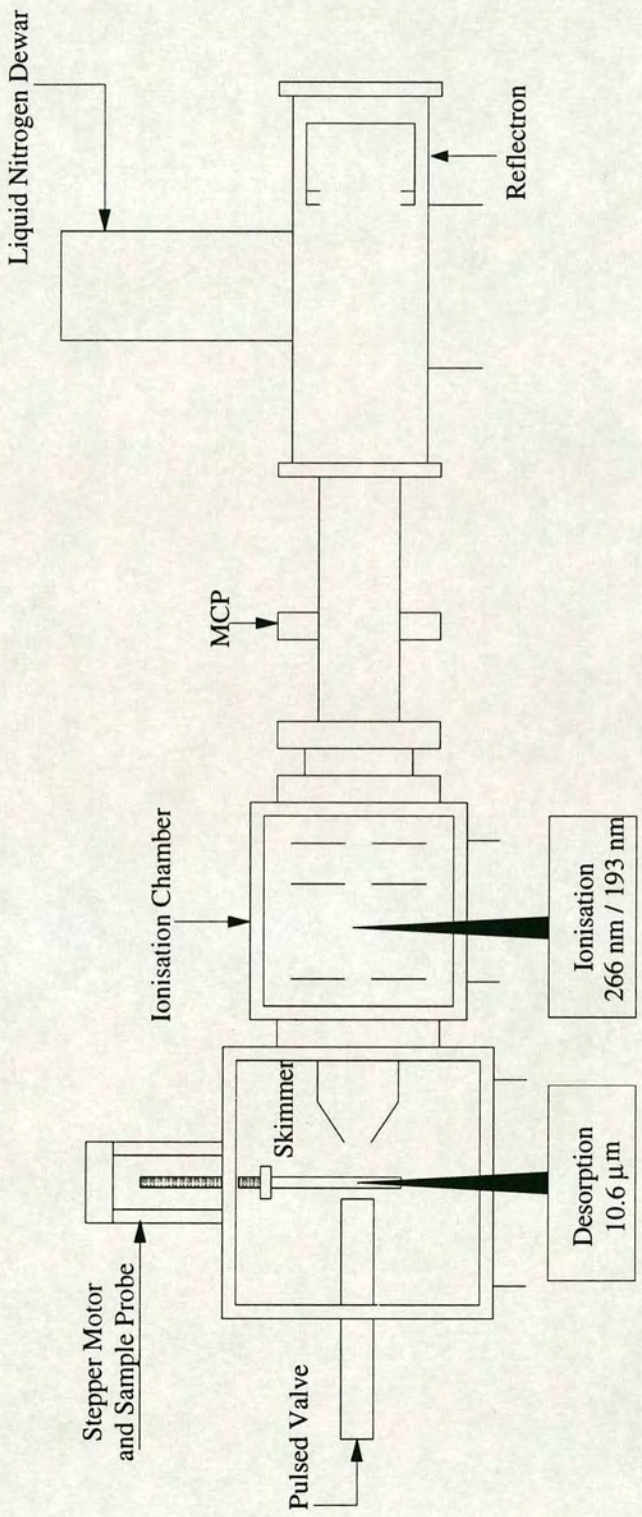

Figure 3-1: Schematic diagram of the L2MS instrument. This shows a side view of the instrument as set up for the entrainment mode. When used in the non entrainment mode, desorption is carried out in the ionisation chamber, illustrated in Figure 3-3.

increase in sensitivity which is gained by dispensing with the molecular beam. The use of each mode of operation of the instrument will be noted in the text where appropriate. A third series of experiments were performed on a similar apparatus at the ETH Zürich. This has been described in detail elsewhere [2].

In the remainder of this chapter a brief description of the vacuum systems, lasers, data acquisition and experimental control modules used in the operation of this laser mass spectrometer will be given.

3.2 Vacuum System

The vacuum system consists of two cuboidal chambers and a reflectron chamber, all of which were constructed from 304 stainless steel, and equipped with demountable flanges. In general, these flanges were also constructed from 304 stainless steel, with the exception of the flanges for the desorption chamber. These were made from aluminium in order to reduce their weight and hence make them easy to remove and handle.

The desorption chamber (DC) housed the laser desorption source for use in the entrainment mode, the molecular beam valve and skimmer. This chamber has a volume of 47.3 l and is pumped by a half-chevron baffled 10'' oil diffusion pump (CVC PMC-10, Convoil 20 pump fluid) with a pumping speed of 2600 l s^{-1} for air. In order to ensure the background pressure was kept low, and also to speed up roughing of the DC, the diffusion pump was backed by a mechanical booster/rotary pump combination (Edwards EH250 / E2M40) which has a pumping speed of 70 l s^{-1} for air at a foreline pressure of 0.3 mbar. The DC pressure was monitored by an Edwards CP25EK Penning gauge head attached to an Edwards 505 gauge readout. The base pressure in this chamber was typically 5 x 10^{-6} mbar. This rose to ca. 1 x 10^{-3} mbar upon operation of the pulsed valve with 4.5 atmospheres stagnation pressure of helium at 10 Hz repetition rate. It was possible to isolate the DC from the diffusion pump by means of a manually operated gate valve (Vacuum Research Company, LP series), and the pump itself could be isolated from the foreline using a pneumatically operated gate valve (Airco Temescal 5230). This allowed the DC to

be evacuated using the rotary pump via an independent roughing line, without requiring the diffusion pump to be cooled down and switched off. This was essential in order to ensure rapid sample turnaround.

The ion source chamber housed the ion extraction optics for the RETOF mass spectrometer. However, when the instrument was used in non-entrainment mode, it also supported the sample probe translation system. This 17 l cuboidal chamber was pumped by an Edwards Diffstack CR 160/100 diffusion pump, which has a pumping speed of 700 l s^{-1} for air. In early experiments, this diffusion pump was charged with Edwards L9 pump fluid. However, this often resulted in serious contamination being observed in the mass spectra, and so the pump fluid was changed for Santovac 5, which provided a substantial improvement. This pump was equipped with a liquid nitrogen cryotrap and quarter swing isolation valve. The pump was backed by an Edwards E2M18 rotary pump, which was also used to back the reflectron chamber via a common foreline. The pressures in this chamber were measured by an Edwards CP25K Penning gauge and a PRL 10 Pirani gauge. The background pressure in this chamber was typically < 10^{-7} mbar, however this rose to 1 x 10^{-6} when the molecular beam was in operation.

The reflectron chamber (63.5 cm long and 19 cm I.D.) was connected to the ISC by a flight-tube (31.2 cm long and 6.3 cm O.D.). This was attached to a manually operated gate valve which was used to mutually isolate these chambers. The ion mirror optics were mounted on the rear flange of the RC, and were tilted by an angle of 4° to the common molecular beam/ion extraction axis, to direct the ions down the second limb of the flight-tube. The axis of this second drift tube was angled at 8° with respect to the beam axis. This second drift tube was connected the RC to the MCP detector, and comprised two smaller tubes, the first of length 5.1 cm and 6.3 cm O.D., the second of length 8.9 cm and 5.1 cm O.D. The RC was pumped by an Edwards Diffstack 160/700 (fluid Santovac 5). A double skinned liquid nitrogen dewar was located on the top of the RC in order to provide additional cryopumping. The base pressure was measured by an Edwards CP25K Penning gauge to be below 1

x 10^{-7} mbar. However, when the molecular beam was in use, this rose to ca. 5 x 10^{-7} mbar.

3.3 Generation of Gas-phase Neutrals

The two modes of operation of this spectrometer, namely entrainment and non-entrainment, essentially only vary in the desorption stage. The remainder of the instrument and operational steps, i.e., laser postionisation and mass analysis are effectively identical.

3.3.1 Laser Desorption with Entrainment

When the entrainment mode of operation is used, the desorption source, shown schematically in Figure 3-2, is situated in the DC. This source consists of a molecular beam valve and a moveable sample probe. Desorption was carried out using radiation from a pulsed infrared laser directed mutually perpendicular to the direction of the molecular beam and the surface of the probe. This induced desorption of a plume of neutrals and ions into the gas-phase, whereupon they were entrained into a synchronised molecular beam pulse and transported through a skimmer into the ISC.

The molecular beam valve was mounted on an XYZ translator. This was important to allow alignment of the molecular beam with respect to the skimmer aperture, which defines the axis of the instrument. A commercial pulsed molecular beam valve was employed (General Valve Corporation series 9), which consisted of an iron actuator, with a Teflon plunger attached, which was seated against a 1 mm orifice. Sealing was achieved through the action of a spring. The valve was opened by the application of a current pulse to a single solenoid which pulled back the actuator. The pulse duration was determined by the length of time the current was applied to the actuator. Under normal experimental conditions, the valve was operated with a pulse duration of between 450 and 600 μs and a stagnation pressure of between 3.5 and 4.5 bar.

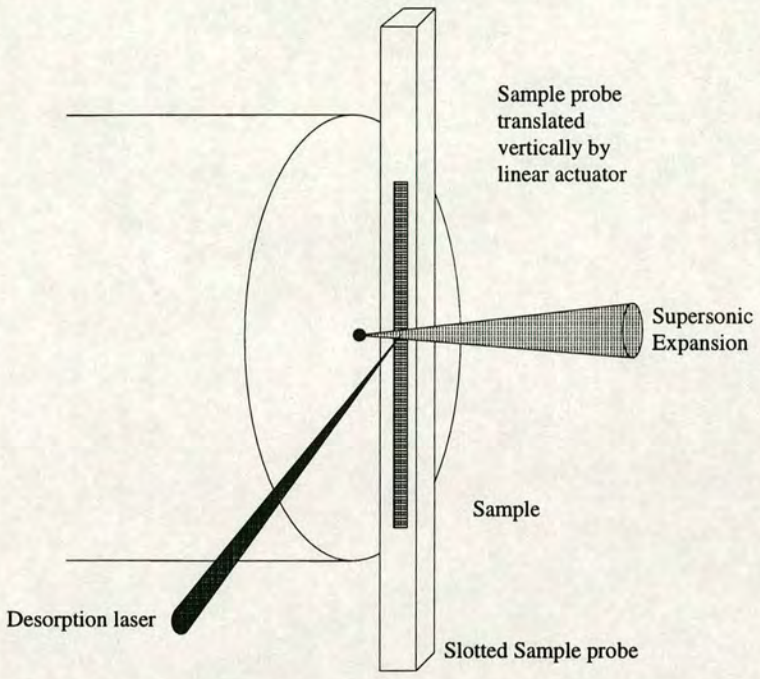

Figure 3-2: Schematic illustration of the laser desorption source used in the entrainment mode. The molecular beam valve is mounted on an XYZ translator, not shown, which allows alignment of the molecular beam with the skimmer aperture.

The majority of materials studied in this work were solid samples of low vapour pressure. These were introduced into the machine on a stainless steel sample probe. This probe was a square faced stainless steel bar, 6 mm x 6 mm, x 21 mm long. The probe had a shallow slot 1.5 mm x 40 mm^2, 0.5 mm deep. Samples were deposited using one of two methods. Generally, the sample was dissolved in a solvent and drop coated into the slot. Often, however, samples were mixed in an appropriate matrix and then pressed into the slot. The probe was suspended vertically below a stepping linear actuator, which was controlled from a free standing variable speed driver unit. This consisted of an RS unipolar 2A driver board and a type 320-24A RS power supply. This was usually operated on the slowest speed using only half-steps, in order to prolong the sample lifetime. A sample prepared in this way typically lasted between 8 and 10 minutes.

The lower section of this rod was supported by a brass guiding plate or faceplate, which was attached to the molecular beam valve faceplate. This maintained the

position of the target probe at the position of the laser focus for the duration of the experiment. The position of the sample probe relative to both the molecular beam axis and the nozzle orifice proved to be important experimental parameters. At short distances from the nozzle orifice, there is a strong likelihood of setting up shock waves in the beam as the desorbed species enter the high density region of the molecular beam. This was found to reduce the signal intensity[3]. Also, the distance from the probe to the molecular beam axis determines the ability to obtain efficient entrainment without disrupting the molecular beam. Typically, the distance between the orifice and the point of desorption was ca. 4.5 mm and the distance between the molecular beam axis and the point of desorption was ca. 5 mm.

The desorbed and entrained species then passed through a skimmer (Beam Dynamics, 5 mm orifice diameter, 50 degrees included angle[4]) before entering the ISC. This skimmer was mounted on the inner wall of the DC opposite the nozzle, at 4.5 cm from the nozzle.

3.3.2 Laser Desorption with Non-Entrainment

Although it does have its uses, the entrainment step is highly inefficient. It has been estimated that as little as 0.1 % of all desorbed neutrals reach the ISC[1]. Clearly, in order to detect trace quantities of materials, or to carry out spatially resolved analysis using small spot size desorption, where very small amounts of material will be desorbed, the sensitivity of the instrument must be greatly improved. It was therefore necessary to dispense with this inefficient entrainment step, and modify the instrument in order to enable both desorption and ionisation to be carried out within the ISC.

This was achieved by altering one of the demountable flanges on the ISC in order to allow attachment of a UHV XYZ manipulator (VG Instruments, model XYZ75). This allowed easy movement of the sample probe, with spatial resolution of 0.01 mm in both X and Y directions, and ca. 1 mm in the Z direction. The sample probe, which was attached to the XYZ manipulator via a PTFE coupling piece, consisted of a MACOR or stainless steel bar 5 mm x 6 mm, x 110 mm long. Each bar had a

series of holes 5 mm diameter, which allowed 5 mm discs to be placed into them. These inserts were fabricated from various materials, including stainless steel, MACOR and glass. The samples of interest were drop coated onto these inserts. Access to the sample probe was possible via the top flange of the ISC.

The sample probe is positioned such that the it lies horizontally along the center axis of the ISC, orthogonal to the extraction axis. This geometry was chosen in order to minimise the reduction in mass resolution expected as a result of dispensing with the supersonic expansion; this was discussed in detail in Chapter 2, Section 2.5.1. This new desorption set-up is illustrated schematically in Figure 3-3.

The increase in sensitivity obtained upon dispensing with the molecular beam capability was immediately apparent. An example which effectively illustrates this point is the screening of aerosol particulate matter for polycyclic aromatic hydrocarbons (PAHs) directly from the bulk particulate matter. A more detailed discussion of these experiments will be given in Chapter 6.

Figure 3-4a shows the result obtained when particulate matter, collected on a polycarbonate filter, was examined using the entrainment configuration of the instrument. There is a clear signal observed at m/z = 202, which corresponds to one, or both, of the isomeric PAHs pyrene and fluoranthene. A peak corresponding to pump oil contamination is also observed at higher mass. A background spectrum (not shown) obtained without the use of the desorption laser was also taken; both the m/z = 202 and the pump oil signals were still observed. This shows that these material are present in the head-space above the sample as a result of their relatively high vapour pressures. The gas-phase material is entrained in the molecular beam without the aid of the desorption laser, and subsequently photoionised. The other, less volatile PAHs present in the sample, were not detected due to the lack of sensitivity of the instrument in this configuration. The presence of the peak assigned to iron is thought to be derived from the stainless steel sample probe. This is because very high desorption power densities were used, which upon removal of the sample had drilled through the polycarbonate filter.

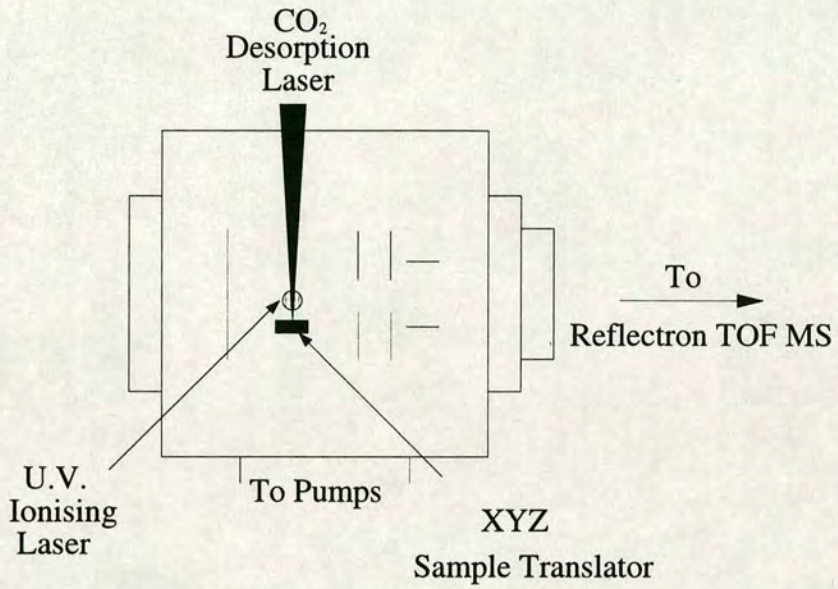

Figure 3-3: Schematic diagram of the laser desorption source as used in the non-entrainment mode. The desorption is carried out within the ion extraction optics, with ionisation occurring just above the sample surface.

A drastically different mass spectrum was obtained when the same sample was interrogated using the non-entrainment configuration of the instrument, as is shown in Figure 3-4b. It is clear from this spectrum that higher mass components were detected with significant intensity, as a result of the increased sensitivity of the instrument. Again, a background spectrum was taken, and only the peaks at m/z = 202 and that due to the pump oil were observed. This, therefore, confirms that these higher mass PAHs do result from laser desorbed species. It should also be noted that much lower desorption laser power densities were used in this case. This is reflected in the much lower intensity of the iron signal in Figure 3-4b.

These spectra clearly show that in order to carry out trace analysis on real complex systems, the desorbed material must be analysed directly above the sample, and not transported to the ion source in a molecular beam, since this compromises the sensitivity.

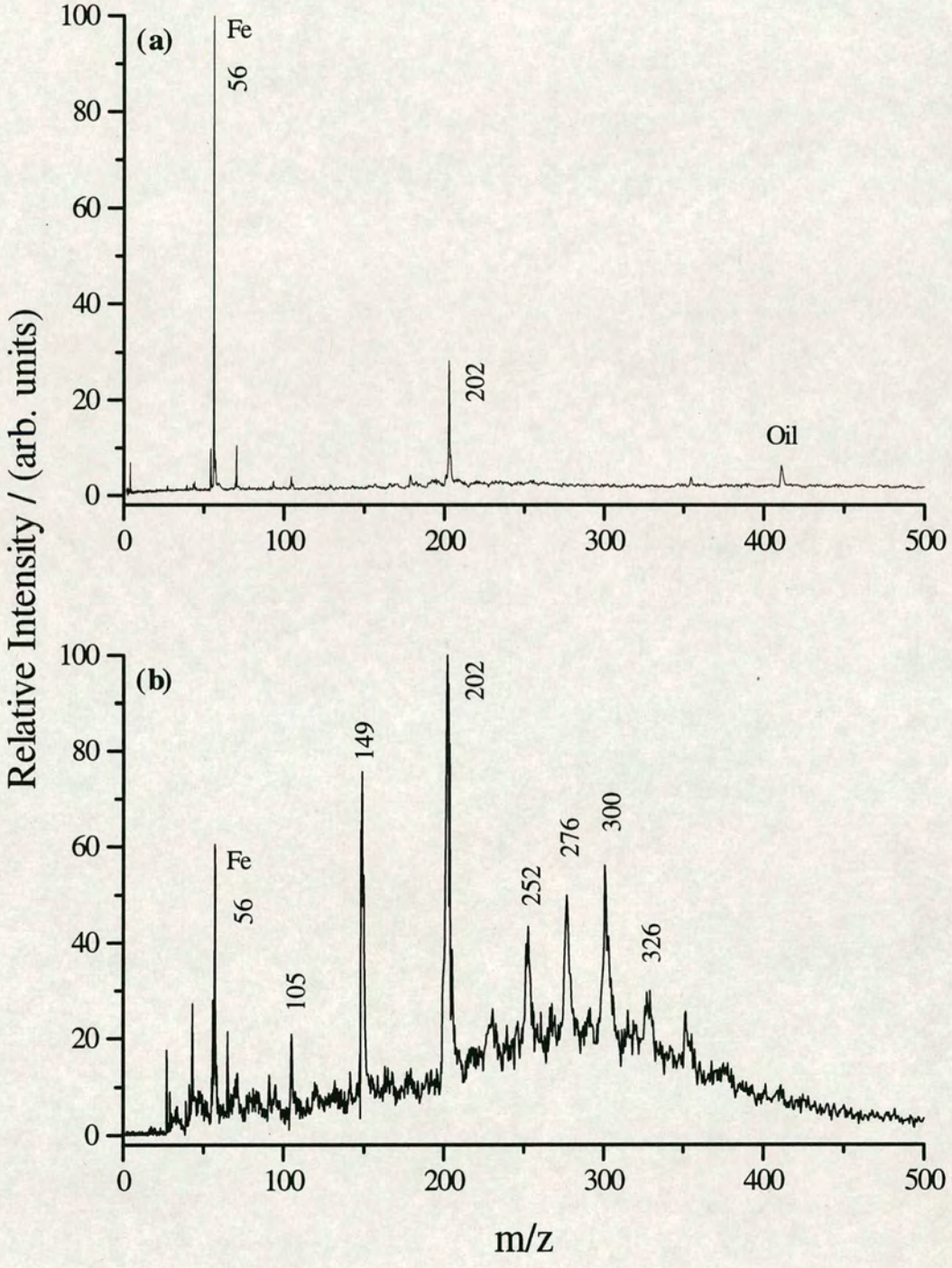

Figure 3-4: Time-of-flight mass spectra of cloud water filtrate, obtained using 10.6 μm laser desorption and 193 nm photoionisation using (a) entrainment mode, and (b) non-entrainment mode.

3.4 Time-of-Flight Ion Optics

The time-of-flight (TOF) extraction optics, shown schematically in Figure 3-5, were based upon a design for a double-field spatially focusing TOF mass spectrometer by Wiley and McLaren [5]. These fields are defined by the repeller (Rep), draw out grid (DoG) and flight grid (Fl) plates. It is also possible to fine tune the ion trajectories by means of both horizontal and vertical deflection plates. In the entrainment mode, it was not necessary to use the vertical deflectors routinely. This was because the ions had a well defined velocity along the extraction axis derived from the supersonic expansion, and so did not require further steering by deflection plates. However, when the instrument was operated in the non-entrainment configuration, vertical deflection of the ions, using potentials between 50 and 400 V, was necessary to correct for the relatively large velocity component perpendicular to the axis of extraction.

These ion optics were built in house, and were fabricated from gold-plated aluminium. The Rep, DoG and Fl plates consisted of 80 mm square plates, each 1.8 mm thick. The Rep plate has a hole 7.7 mm in diameter in the center, to allow entry of the molecular beam for the entrainment mode of operation. No mesh grid was used on this plate in order to minimise the reduction in transmission. Both the DoG and Fl plates had 22.4 mm diameter holes in their centers covered by 90 % transmission nickel mesh. This improved the homogeneity of the fields and minimised field leakage. The optics were supported on a four rod aluminium rail assembly and separated using precision machined Delrin spacers. The deflection plates consisted of four plates 30 mm square and 5 mm thick, mounted on PTFE spacers.

The ion mirror, illustrated in Figure 3-6, consisted of a series of six stainless steel rings of 12 cm O.D. and 6 cm I.D., with an additional solid plate of the same O.D. used as the backplate. The mirror consisted of two distinct regions, namely a retarding and a reflecting field defined by the distances d_t and d_k respectively. These two fields were supplied by two independent power supplies. The apertures of the first two rings were covered by nickel mesh grids (Buckbee Mears, 90 %

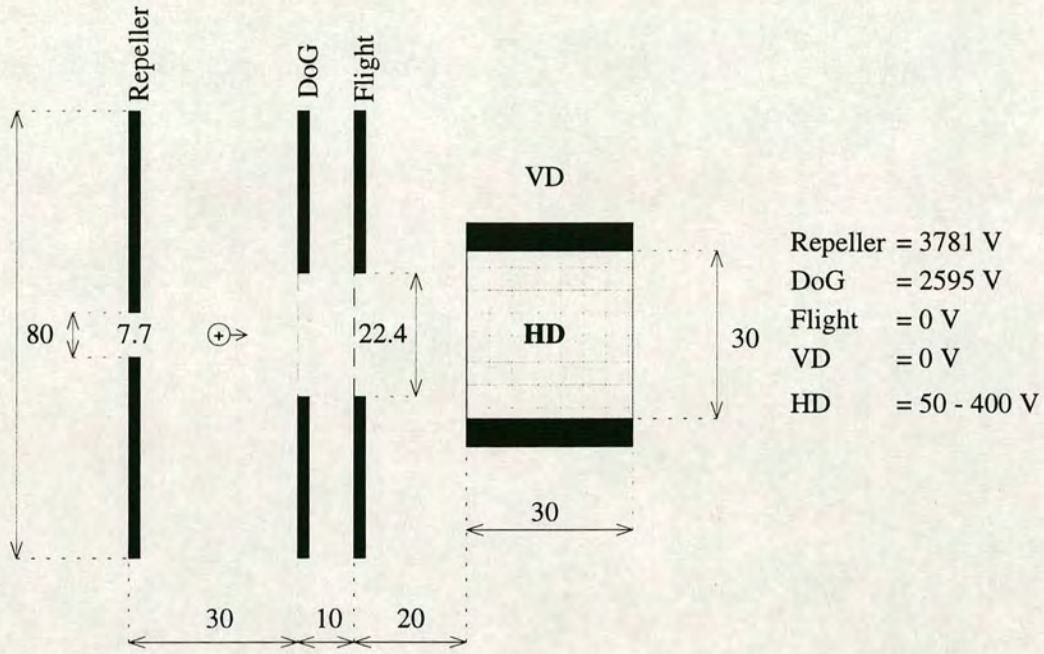

Figure 3-5: Schematic diagram of ion extraction optics, situated in the ion source chamber. Typical operating potentials are shown, and all dimensions are given in mm.

transmission), whilst the remaining rings were used as guard rings to improve the field homogeneity between the backplate and mirror entrance. The first grounded ring was designed with a cylindrical "top-hat" design to define the end of the field free region by minimising stray fields. The supply voltage on the backplate was dropped across the reflecting field rings by a resistor chain network.

When the instrument was operated in the non-entrainment mode, it was found that a large increase in signal intensity could be obtained by floating the sample probe at an appropriate potential between that used on the Rep and DoG plates. This was done by attaching a feedthrough wire to the back of the stainless steel probe by means of a small grub screw. This ensured that a definite potential was applied to the probe, meaning that other instrumental factors could then be optimised. Without this, the probe could charge up to an undetermined potential, resulting in a very unstable signal. The typical electrode potentials employed are given in Table 3-1.

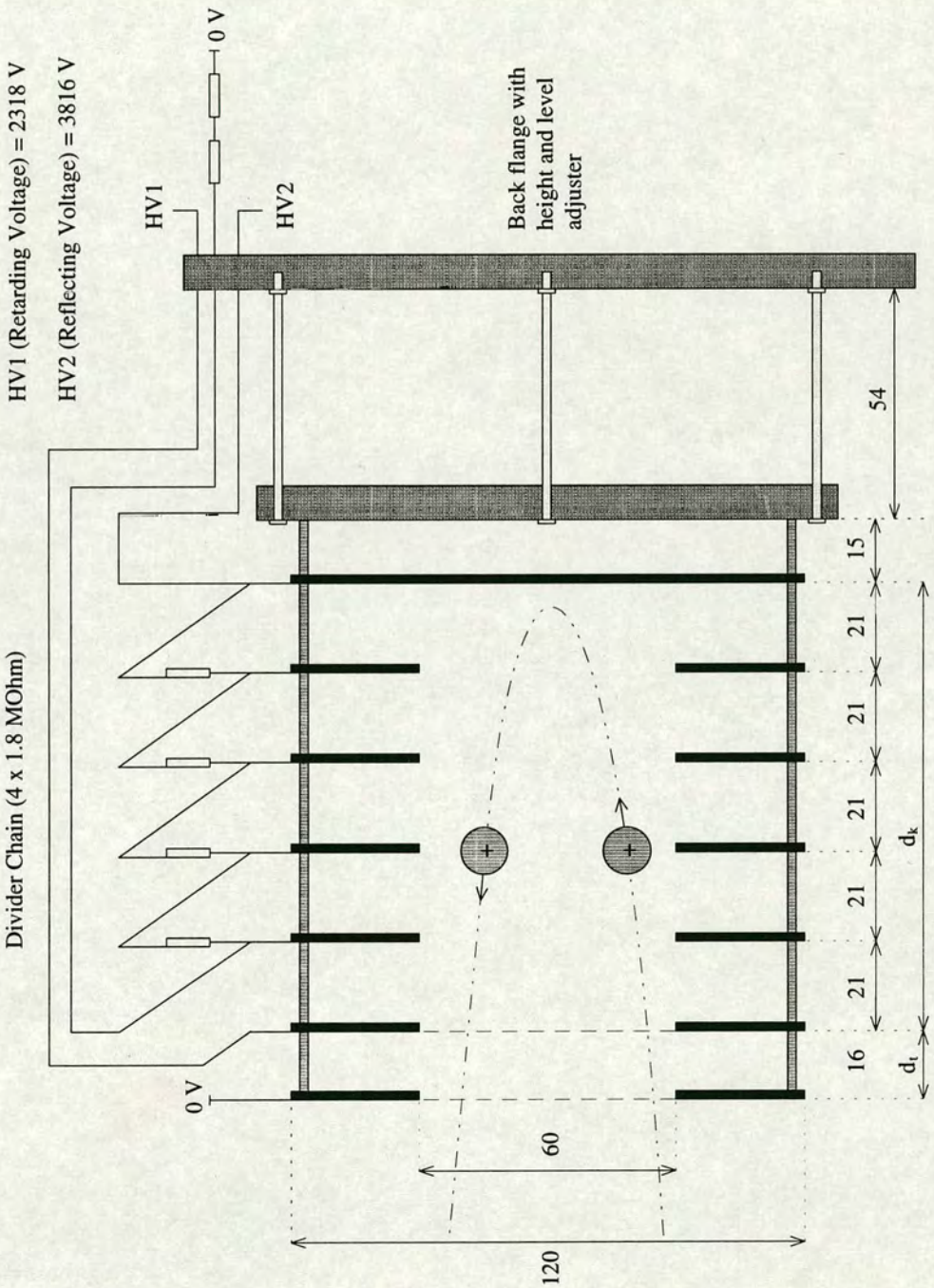

Figure 3-6: Schematic diagram of the ion mirror which is mounted from the rear flange of the reflectron chamber. It is tilted at 4° to the normal in order to deflect the ions down the second field free drift region. All dimensions are given in mm, and typical operating potentials are shown.

Electrode	Power supply	Typical operating potential / (V)
Repeller	Stanford PS 350	3781
Sample Probe	Stanford PS 350	3000 — 3500
Draw out Grid	Stanford PS 350	2595
Flight	—	0
Horizontal Deflectors	Power Designs	- 50 — 50
Vertical Deflectors	Power Designs	0 — 400
Mirror Retarder	Stanford PS 350	2318
Mirror Reflector	Stanford PS 350	3818
MCP	Stanford PS 350	- 3900

Table 3- 1: Power supplies and typical operating potentials of ion extraction and reflectron

3.5 Ion Signal Detection

The TOFMS ion signal was detected by a dual microchannel plate [6] (MCP) and amplified before being sent to a transient digitiser. This MCP (R. M. Jordan) was of a dual chevron design, with two Galilieo MCP-18B plates back to back, each having an active area of 2.5 cm^2. A divider chain was constructed to drop a maximum of 1000V across each plate, which had a gain of 10^3 at 1kV, and a gain of 10^2 at the typical working voltage of 700 V.

The detector was operated in grounded anode mode, which enabled easy coupling to the digitiser. This requires the front channel plate of the MCP to be maintained at a large negative voltage, but has the added advantage of increased gain for positive ions, which are accelerated into the first plate. The disadvantage of this arrangement is that negative ions cannot be detected, and an earth grid is required in front of the first plate of the MCP in order to define the field free drift region. In the design of

this MCP, the grid used was one of 82 % transmission. The signal at the MCP anode was amplified by a factor of ten (Ortec Model 134) prior to being sent to the low level input of a transient digitiser.

3.6 Laser Systems

The two-step approach to laser mass spectrometry obviously requires at least two laser systems: one to desorb the sample into the gas-phase, and another for photoionisation. Previous work [7] has shown that infrared laser radiation at 10.6 μm is suitable for producing large numbers of neutral species for postionisation without inducing significant photochemical effects, whilst UV laser wavelengths are required for multiphoton ionisation. More recent studies have shown that ionisation can be achieved using VUV laser wavelengths, as well as by photoelectrons generated by UV laser irradiation of metal surfaces. This experiments described in this thesis have relied primarily upon the use of three fixed laser wavelengths for photoionisation: the 193 nm and 248 nm outputs from an ArF or KrF excimer laser, and the 266 nm 4^{th} harmonic output of an Nd: YAG laser. However, single photon ionisation (SPI) using the 9^{th} harmonic of the Nd: YAG laser as well as laser induced photoelectron ionisation (LIPEI) have both been used as an extension of the technique for the analysis of non-UV absorbing species. The lasers used to perform these experiments are described in more detail below.

3.6.1 Alltec 854MS CO_2 Laser

The Alltec 854MS laser is a transverse excitation atmospheric pressure (TEA) CO_2 laser. This laser produces a pulsed infrared output at 10.6 μm with 100 ns pulse duration at a repetition rate of up to 50 Hz. A gas mixture of 12% CO_2, 4% CO balanced with He is required for stable operation of the laser. The gas fill is replenished automatically as required. The maximum power attainable on this laser fill is 400 mJ. However, a more typical output is 100 mJ operating at 10 Hz repetition rate. These pulse energies were measure using a Gentec ED-200 Joulemeter on a Tektronix 2445 (150) MHz oscilloscope. The CO_2 laser could be used in a variety of different operational modes, which could be selected using a

remote control module attached to the laser via an umbilical. External control of the laser required provision of a single trigger, (5 V amplitude, 50 μs duration).

The laser output was directed into the appropriate vacuum chamber (DC or ISC) by a series of gold plated mirrors. The side flanges of the chambers were equipped with NaCl entrance and exit windows (2" diameter, 3mm thick). The laser radiation was focused by an NaCl lens; when desorption was carried out in the DC, a 30 cm focal length lens was used, but for desorption in the ISC, a 20 cm focal length lens was employed. The laser beam was attenuated using a series of nickel mesh grids and plastic sheets. Only very slight attenuation was required for desorption within the DC, but when desorption was performed in the ISC, more extensive attenuation was required. Ultimately, the use of mesh attenuators did not prove to be subtle enough in many cases, and so a pair of counter-rotating angle tuned germanium flats attached to a stepper motor with digital position readout were used. For desorption within the DC, typical power densities were on the order of 25 x 10^6 Wcm^{-2}. For desorption in the ISC, typical power densities were between 6-10 x 10^6 Wcm^{-2}.

3.6.2 JK HyperYAG HY750 Nd:YAG Laser

The HY750 is a pulsed Nd:YAG laser which was principally used for MPI of laser desorbed neutrals using the 4th harmonic output at 266 nm. However, it was also occasionally used as a desorption laser using the 2nd harmonic at 532 nm. The laser is a Q-switched oscillator-amplifier, which produced an output of 800 mJ $pulse^{-1}$ in the fundamental (1064 nm). The second and third harmonics at 532 nm and 355 nm were generated using thermally stabilised CDA and KDP crystals. This produced optimised outputs of 320 mJ $pulse^{-1}$ and 170 mJ $pulse^{-1}$, respectively. Separation of the 532 nm radiation from the fundamental was achieved using two Brewster-angled gull wing prisms which were situated directly after the harmonic generating assembly.

The 4th harmonic output at 266 nm was produced by frequency doubling the 2nd harmonic at 532 nm using a temperature controlled KDP crystal. The fundamental and 2nd harmonic were separated from the 4th using a Pellin Broca prism assembly.

Each prism is designed to turn the 266 nm radiation through 90°, but the unwanted fundamental and 2nd harmonics are deviated by smaller angles due to wavelength dispersion in the prism. Using this arrangement, the optimised power output for the 4th harmonic was typically 70 mJ $pulse^{-1}$.

To enable external control of the laser, two 15 V trigger pulses were required in order to trigger both the flashlamps and the Q-switch. It was possible to vary the Q-switched pulse energy by changing the delay time between these two pulses. The optimum delay was 180 μs. Alternatively, the output power could be varied by altering the amplifier charging voltage.

The laser output was directed into the ISC by means of a series of quartz prisms. In order to maximise the mass resolution, the beam width along the spectrometer axis was kept as small as possible, using either an iris or vertical slits. For experiments where sensitivity was particularly important, a vertical slit was used to tighten the beam width. This was done because it gave a larger ionising volume, and hence more neutrals could be ionised and ultimately extracted and detected. The laser power was measured using a Scientec Astral AA30 power meter, and was typically between 0.5-3 mJ $pulse^{-1}$ for a 2 mm iris. The power density could be increased if necessary by means of a 30 cm quartz lens, which focused the 2mm beam to a spot of some 300 μm [1]. This allowed a range of ionising power densities from 10^5 - 10^8 Wcm^{-2} to be used routinely.

3.6.3 Lumonics TE - 861T-4 Excimer Laser

This thyratron-switched excimer laser was used to provide alternative ionisation wavelengths to the 266 nm radiation produced by the Nd:YAG laser, and can operate on a variety of halogen-noble gas mixtures. In this work, it was used predominantly on the ArF line (193 nm), although it was also possible to use the KrF line (248 nm). The laser was generally used at 10 Hz repetition rate, and typically produced pulses of 8-10 ns duration.

The laser was used throughout this work with unstable resonator optics to reduce the output beam divergence. Although this resulted in lower pulse energy than the

alternative use of stable resonator optics, it allowed the laser beam to be more tightly focused, and hence enabled more efficient MPI. The power of the laser output was measured using a Coherent 210 power meter. The ArF line at 193 nm produced a rectangular beam of cross section 3 x 15 mm^2, whereas the KrF line at 248 nm resulted in a beam of 6 x 15 mm^2. Typical pulse energies were 16 mJ $pulse^{-1}$ (ArF) and 45 mJ $pulse^{-1}$ (KrF). The beam was again collimated by a slit arrangement, and, if necessary, focused by a 30 cm focal length quartz lens.

External operation of this laser required two 15 V trigger pulses. The first pulse triggered a "charge-on-demand", which was used to initiate the capacitor charging cycle, whilst the second pulse, supplied after a delay of ca. 12 ms, was used to trigger the thyratron which ultimately caused the laser to fire. The output pulse energies were generally varied by adjusting the peak charging voltages on the capacitors, although it was also possible to do this by varying the charging period.

3.6.4 Vacuum Ultra Violet (VUV) Generation

Although not extensively used in this work, a VUV source was previously developed in this laboratory for the ionisation of non-aromatic species. The experimental setup has been described in detail elsewhere [8]. The VUV radiation was generated by frequency tripling the 3rd harmonic of the Nd:YAG laser in a gas cell filled with xenon.

The tripling cell consists of a 1'' O.D. stainless steel tube which was connected at one end to a flange assembly containing a Spectrosil B window. This allowed the 355 nm light to enter the gas cell. Another flange assembly is situated 150 mm from the first. This allows the cell to be attached to an XYZ manipulator (Vacuum Generators Model XYZ75), which facilitates fine adjustment of the VUV output within the ionisation region. The opposite end of the main tube is connected to a third flange assembly which houses the MgF_2 VUV focusing lens (Crystran Ltd). This lens is plano-convex and has a 30 mm focal length at 118 nm. This entire assembly is attached to a standard 8'' O. D. stainless steel side flange, which is in

turn mounted directly onto the side of the ISC. A schematic diagram of this arrangement for VUV generation is shown in Figure 3-7

Broad band quartz prisms were used to steer the 355 nm radiation from the Nd:YAG laser into the tripling cell. The 355 nm beam was focused using a 26 cm lens 33 mm from the MgF_2 lens . The lens system was designed such that the 118 nm radiation is focused above the sample, but the 355 nm radiation is slightly divergent. It was initially hoped that this would be sufficient to ensure that no subsequent absorption of 355 nm photons occurred by molecules ionised with the 118 nm radiation. However, in some cases, significant fragmentation was observed as a result of this process. Therefore, the 355 nm radiation was directed into the cell off-axis so that the high density region of the 355 nm laser beam was spatially moved further from the 118 nm focus. This did improve the situation, but some fragmentation was still found to occur due to excess 355 nm radiation. Currently, alterations to this design are in progress. It is hoped that by using a small MgF_2 turning prism situated after the tripling cell, the 355 nm radiation can be dispersed away from the 118 nm focus such that photodissociation of ionised molecules can be avoided.

3.7 Experimental Control and Data Acquisition

These pulsed laser desorption laser photoionisation experiments require precise control over several experimental parameters, generating large amounts of data in a short period of time. A sophisticated computer-based system was developed in order to enable both the optimisation of experimental parameters, as well as acquisition and storage of the data produced. The use of a computer-based control system in this type of experiment has a number of advantages: data can be quickly displayed during the course of the experiment, and experimental parameters can quickly and easily be altered and reset. A CAMAC (Computer Automated Measurement and Control) based system was used for these experiments [9]. This involved the use of a range of hardware, which was located in a CAMAC crate, controlled by software on the computer system. The development of the integrated data acquisition and control software was carried out by a former research student in this laboratory [10].

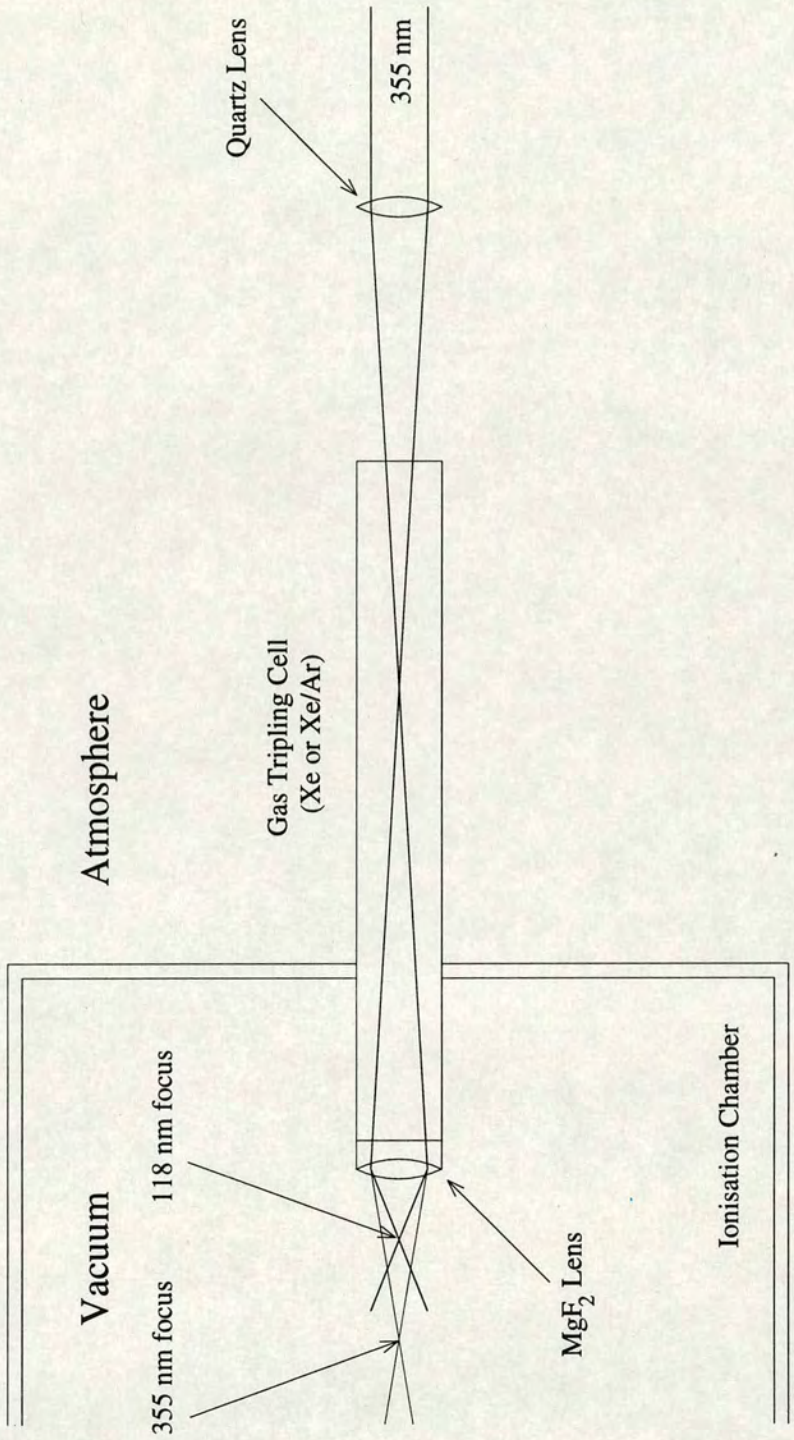

Figure 3-7: Schematic illustration of the VUV generation assembly, where 355 nm radiation is frequency tripled in a gas cell of xenon to give 118 nm (10.4 eV) radiation.

3.7.1 Control Hardware

The IEEE CAMAC standard [9] defines a common dataway to which a number of instruments can be interfaced. All CAMAC modules are located in a crate (Standard Engineering Corporation PCS 1410), which contains a backplane providing both data communication pathways and power lines to each module. A common dataway of 24 read/write lines is used to transmit data to and from each module, with further datalines being used to direct commands from the control software on a Dell Model 325 PC to the correct module (or part of a module), and transmit acknowledgment of receipt of these commands, or requests for attention, to the PC. The control set-up is illustrated schematically in Figure 3-8.

Station one of the CAMAC crate was occupied by a Hytec IBM 1331/Turbo PC Interface module. This was connected to the PC by a 3 m long interconnection cable and a Hytec IBM 1331 personality card. This module accepted commands from the computer to control the experiment, passing these on to the appropriate modules in the crate as well as passing recorded data down the dataway to the PC.

The experiment required several modules within the crate, each of which will be discussed below.

3.7.2 Kinetic Systems 3655 Pulse Delay Generator

Experimental timing control was performed using a Kinetic Systems 3655 eight channel pulse delay generator (PDG), which provided trigger pulses to the appropriate experimental hardware. This produced 200 ns TTL pulses with microsecond accuracy, and was triggered by an instruction through the dataway from the Dell 325 PC. The minimum possible interval between pulses from successive channels was 1 μs, with a minimum jitter of around 1 ns. This unit was used to provide trigger pulses for experimental devices such the pulsed valve, CO_2 laser, excimer laser and Nd:YAG laser.

The pulses produced by the PDG did not produce sufficient current to drive 50 Ω loads through long (up to 5 m) coaxial cables used in these experiments. The signals were also too narrow to trigger some of the external devices which had trigger

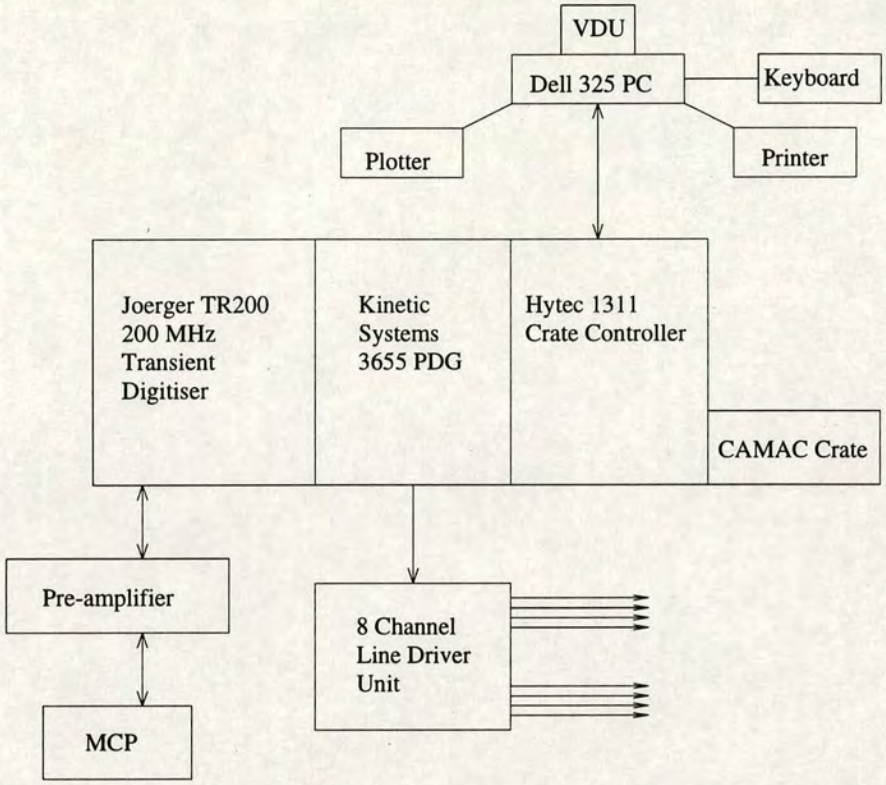

Figure 3-8: Schematic diagram of the CAMAC-based experimental control system.

thresholds of greater than 10 V, or required pulses of greater than 200 ns duration. The output signals from the PDG were therefore boosted using a custom-built 8 channel line driver unit, housed in a NIM bin, which produced either 5 V, 50 μs or 15 V, 10 μs pulses.

3.7.3 Transient Digitiser

Negative going waveforms were generated by the arrival of ions at the MCP detector. Digitisation of this signal was achieved using a fast sampling Joerger TR200 transient digitiser (TD). The digitiser has 8 bit vertical resolution, a range of 512 mV and a maximum sampling rate of 200 MHz. The module was completely programmable, and the digitising rate was set using the programming software on the PC. Input offset adjustment was set using a front panel trimpot, and could be monitored using an offset test point.

After the TD was armed by a CAMAC dataway command, the input signal was continuously sampled and stored. This data was continuously overwritten until the module received an external stop trigger pulse. The next 2048 bytes of data constituted the required mass spectral data.

Since the maximum record length was 2 Kb, only ca. 10 μs portions of the mass spectrum could be recorder using the highest resolution sampling rate of 200 MHz. For the experimental conditions employed in this work, flight times were on the order of 50-100 μs for many of the molecular species studied. Therefore, in order to record a complete mass spectrum for each laser shot, a slower sampling rate (25 or 50 MHz) was used. This resulted in the loss of spectral resolution. It was also possible that at these slower sampling speeds only ions on the extrema of the ion peaks were sampled, resulting in weaker peak intensities than expected. This was particularly undesirable when relative intensities were being compared. In order to utilise the faster digitisation rates, the effective mass window for the TD could be moved in time by varying the delay between the trigger to the ionising laser and the TD stop trigger. This, however, meant that mass spectra were recorded which did not encompass the complete mass range.

3.7.4 Control Software

The software which was used to control the experiment was written by A. M. Butler [10] using the C high level programming language (Microsoft v. 5.00), together with some assembler routines (IBM MACRO Assembler v. 2.00). This package controlled the experimental timings and acquired data via the CAMAC interface. It was necessary to run the experiment at a constant repetition rate in order to prevent thermal lensing of the Nd:YAG rods, which had the effect of detuning the laser. This was accomplished by employing the interrupt mechanism of the PC. This ensures that any changes made to the experimental parameters were executed during the dead time between experimental cycles. The interrupts were operated at twice the experimental operation rates. On alternative interrupts, the software toggled between routines for controlling the experiment and processing the data, known as TIC and TOC, respectively.

The TIC routine armed the digitiser, loaded the time delays and triggered the 3655 PDG, thereby initialising the experimental cycle. The TOC function was executed upon completion of the TIC in order to read data from the transient digitiser. This data was then inverted to give a positive going waveform and summed with that from previous shots. This experimental cycle was repeated on the next TIC call. Typical timing sequences for both the entrainment and non-entrainment modes of operation are illustrated in Figure 3-9.

3.8 Data Acquisition Modes

There are three basic modes of acquiring experimental data using this software. These are TOF mode, Timescan mode and Frequency scan mode.

3.8.1 TOF Mode — Acquisition of Mass spectra

The simplest and most frequently used mode was that used to record TOF mass spectra. These spectra were displayed on the PC monitor as soon as the data was obtained. Successive single shot mass spectra could be accumulated before the screen was refreshed, or alternatively, the mass spectra could be displayed individually as they were summed. Mass spectra were typically summed until a satisfactory signal-to-noise ratio was achieved. The display in this mode showed autoscaled intensities normalised to the most intense ion signal on the vertical axis, and time-of-flight on the horizontal axis. Once the data had been accumulated and stored, it was possible to convert this time scale to a mass axis using a simple calibration routine. However, this was not possible whilst acquiring the data.

3.8.2 Timescan Mode

In order to maximise the signal intensity in the TOF mass spectra, it was necessary to optimise several timing parameters. It was possible to experimentally determine these timing delays using the timescan mode of operation. In timescan mode, it is possible to scan one trigger pulse in time relative to the others in the timing sequence whilst monitoring the signal intensity over a particular mass channel. The time channels for a particular mass were established by running an initial non-optimised

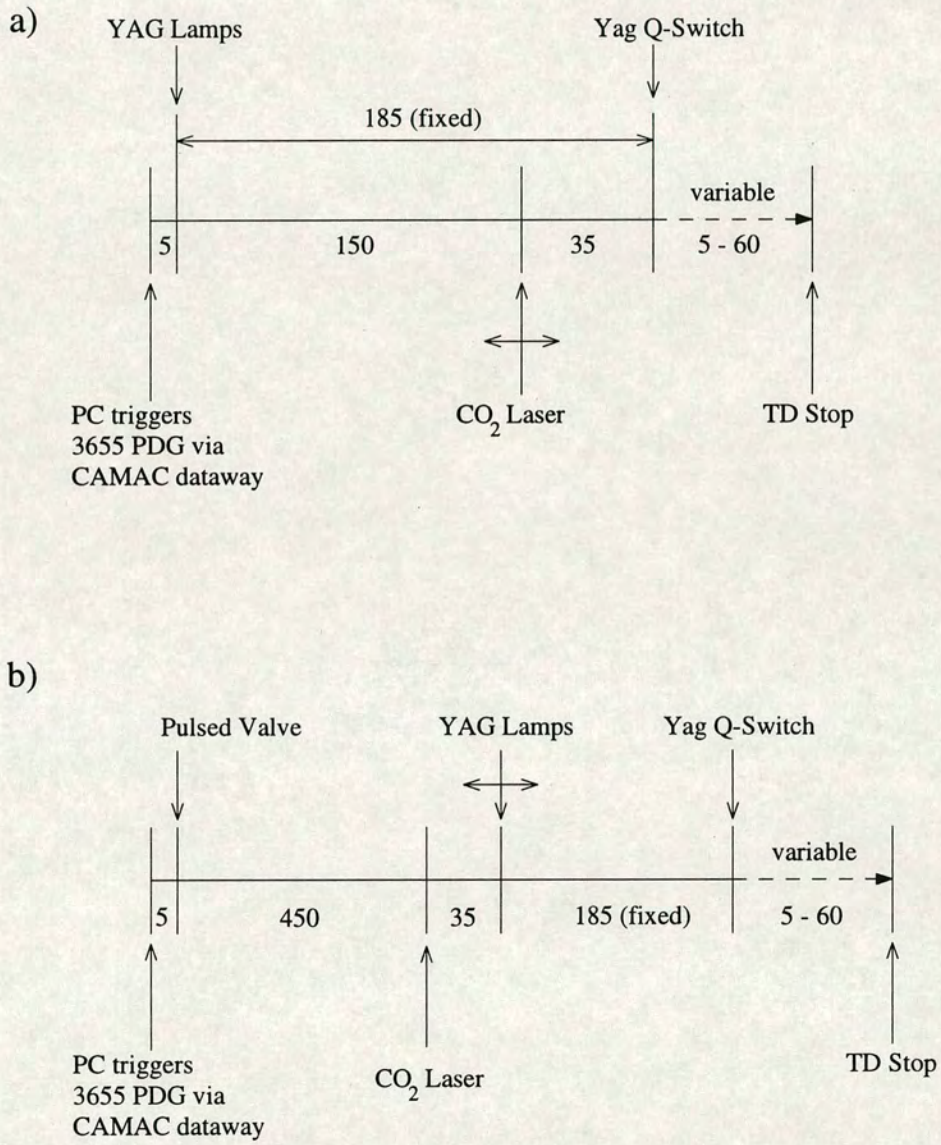

Figure 3-9: Typical trigger pulse timing set-up for an L2MS experiment in (a) the non-entrainment mode, and (b) the entrainment mode.

mass spectrum. Up to ten different mass peaks could be monitored simultaneously using this facility, whilst a single time delay was scanned. The delay showed the changing ion signal as a function of time delay.

The most common timescan carried out was to vary the delay between the desorption and ionisation lasers. In Figure 3-10, the distribution of desorbed material as it arrives in the ionisation volume is displayed by simply scanning the time at which the ionisation laser fires relative to the fixed desorption laser time. The peak of this distribution represents the optimum time for firing the ionising laser in order to obtain the maximum possible photoion signal. In the case of weak or noisy signals, it was again possible to accumulate several scans in order to build up an appreciable signal intensity. In addition, it is also possible to use this timescan facility with a higher resolution to measure the velocity distribution of laser desorbed neutrals. Since all gas-phase neutrals travel a fixed distance to the ionisation volume, then the time profile generated gives a measure of their velocities.

3.8.3 Frequency Scan Mode

The third data acquisition mode available was a frequency scan mode, which in principle operates in a similar manner to the timescan mode. Firstly, the time channels for a given mass channel of interest are obtained and loaded into the signal definition register. The original idea behind this mode of operation, was that it could be used for carrying out spectroscopy on laser desorbed species. By setting up on a particular mass channel, it is possible to monitor the signal intensity as a function of the ionising laser wavelength. Therefore, by entering the appropriate dye laser details into the frequency scanning routine a number of single shot spectra could be accumulated at each designated frequency. This mode of operation has previously been used to record the [2 + 1] REMPI spectrum for the atomic resonance of lead [3]. However, an alternative use of this data acquisition mode is to monitor the signal intensity of a given mass species over time. This is referred to as a "fixed frequency" scan. This can be used to good effect if it is important to know how long it takes for a given amount of material to be completely desorbed from a single spot. This is done by setting up the appropriate mass channel as before, and entering an extended

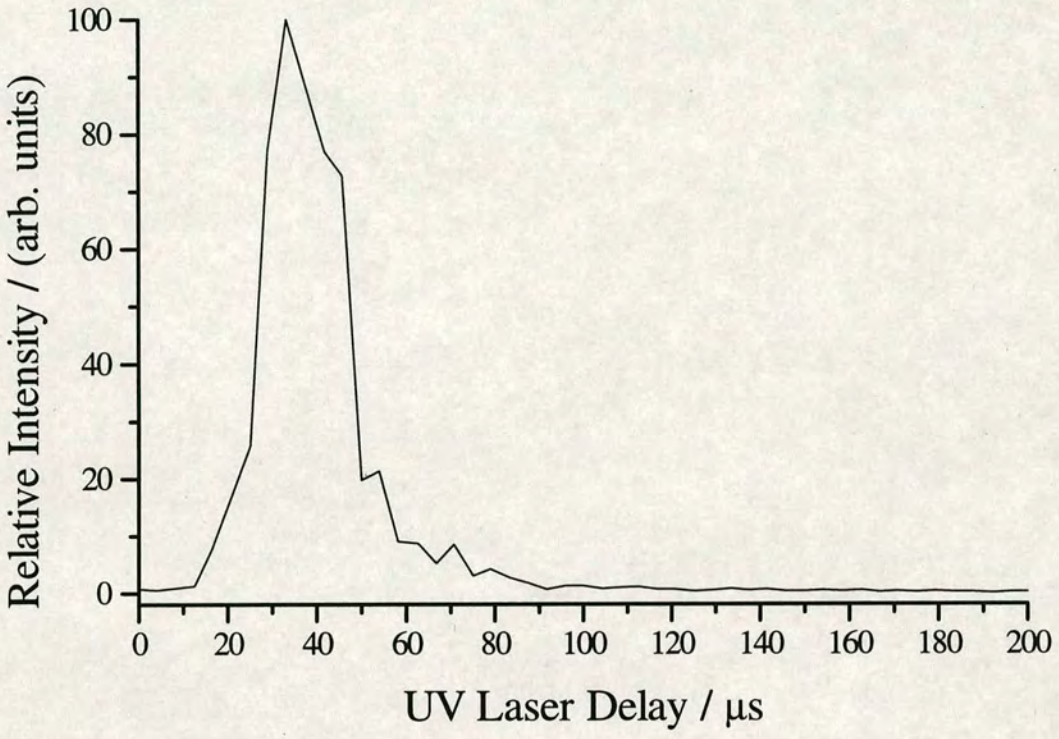

Figure 3-10: Desorption profile of coronene obtained in the timescan mode by varying the time of the UV laser relative to the desorption laser.

"dummy" frequency range. The yield of desorbed neutrals per laser shot can thereby be monitored, giving an estimate of how long it takes to remove the sample from the probe completely. An example of this type of experiment is shown in Figure 3-11. In addition to monitoring signal decay as a function of time, it is also possible to monitor signal stability using this mode of operation.

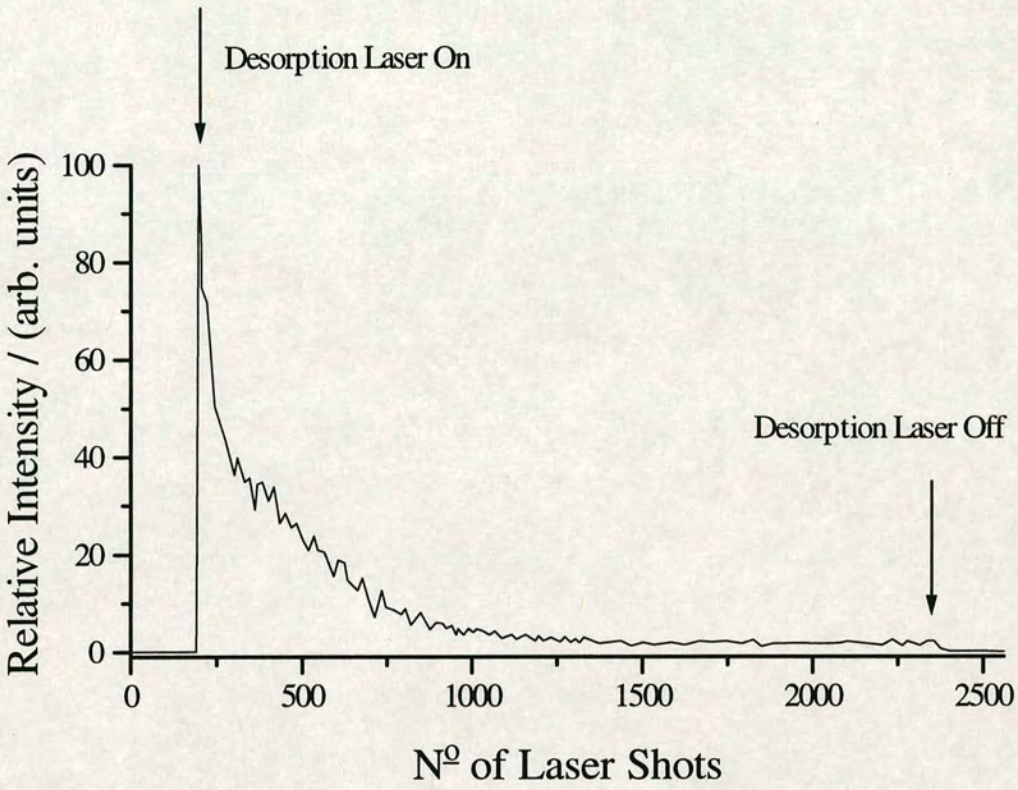

Figure 3-11: Fixed frequency scan of Parsol 1789, which demonstrates the decay of the ion signal as the sample is depleted by repeated exposure to the desorption laser. The sample has been effectively removed after approximately 2000 laser shots.

References

[1] K. F. Costello, *PhD Thesis, The University of Edinburgh*, 1991

[2] P. Voumard, Q. Zhan, R. Zenobi, *Rev, Sci. Instrum.*, **25**, 3393, (1995)

[3] M. J. Dale, *PhD Thesis, The University of Edinburgh*, 1994

[4] W. R. Gentry, C. F. Giese, *Rev. Sci. Instrum.*, **46**, 104, (1975)

[5] W. C. Wiley, I. H. Mclaren, *Rev. Sci. Instrum.*, **26**, 1150, (1955)

[6] J. L. Wiza, *Nucl. Inst. Methods*, **162**, 587, (1979) and J. L. Hellsing, L. Karrison, H. O. Andren, H. Norden, *J. Phys. E: Sci. Instrum.*, **18**, 920, (1985)

[7] G. R. Kinsel, J. Lindner, J. Grotemeyer, *J. Phys. Chem.*, **96**, 3162, (1992)

[8] C. R. Redpath, *PhD Thesis, The University of Edinburgh*, 1995

[9] D. Horelick, R. S. Larsen, *IEEE Spectrum*, **13**, 50, (1976)

[10] A. Butler, *PhD Thesis, The University of Edinburgh*, 1989

Chapter 4

L2MS of Azo Dyes and Porphyrin Pigments

4.1 Introduction

One goal of this project has been to develop the L2MS technique to a stage where it can be used routinely to image organic molecules adsorbed on a variety of substrates. It is envisaged that imaging of stains on textiles will be possible, allowing various real problems to be addressed. It should prove possible to monitor the distribution of stains on fabrics, and obtain fundamental information on the so-called "edge-effect", where stains appear different in colour at the edges. It may also be possible to directly monitor time dependent chemical changes taking place on the host substrate, such as the discolouration of blood on cotton, and the UV bleaching of dyed fabrics.

However, these problems are not trivial, and the technique is not, as yet, sufficiently developed to undertake such studies. Stains can be incredibly complex systems in their own right, and when adsorbed onto complex organic substrates, further chemistry can occur. It is therefore necessary to tackle this problem from first principles, by investigating a series of model stain systems. Azo dyes and porphyrin pigments provide good examples of model stains. For example, the porphyrin hemin is used as a model stain for blood, whereas azo dyes are extensively used as staining agents in the colourants industry. Therefore, both of these molecular classes are suitable for modelling the behaviour of molecules commonly found in complex stains.

There is an ongoing programme of research in this laboratory aimed at fully characterising the behaviour of these molecules during L2MS analysis. Information obtained on the fundamental mass spectroscopic and photochemical/photophysical

properties of the pure materials, will then be carried forward and used in the analysis of such systems adsorbed onto complex organic matrices, such as textiles.

The results presented in this chapter will illustrate the effectiveness of the two-step laser methodology for analysing such compounds. The first part of the chapter describes L2MS investigations of azo dyestuffs, and illustrates how the nature of the ionisation technique can allow wavelength dependent mass spectra to be obtained. In addition to obtaining useful photochemical information about these materials, it is also shown how important this wavelength dependence can be in the unambiguous identification of certain compound classes. In addition, it is shown that it is possible to exploit the photochemistry of these systems in order to differentiate between isomeric species, which would be difficult by other mass spectroscopic techniques. The second part of the chapter discusses the photoionisation mass spectra of porphyrin pigments. Again, it is shown that the ionisation laser wavelength has a marked effect on the appearance of the mass spectra. Once more, as well as obtaining fundamental photochemical information on such molecules, this wavelength dependence can be used for unambiguous identification.

4.2 L2MS of Azo Dyes

Azo dyes are used extensively as colourants in a wide range of industrial applications, from textiles to foodstuffs. The processes in which these dyes are used result in the discharge of ca. 15% of their volume into waste waters [1]. The reported carcinogenic behaviour of these waste products has stimulated considerable environmental interest [1]. The unambiguous determination of these dyestuffs is, therefore, an important industrial imperative.

Most azo molecules are thermally labile or involatile. They are, therefore, not readily amenable to characterisation by gas chromatography mass spectrometry (GC MS). In order to use conventional mass spectrometric analysis for thermally labile and involatile dyestuffs, it is necessary to employ indirect methodologies. Chemical derivatisation [2] has been employed in order to produce volatile neutral species for mass analysis in conventional spectrometers. Pyrolysis products have also been

examined [2]. However, in this case, the high source temperatures enhance thermal degradation and reduce molecular ion yields.

The advent of condensed phase desorption/ionisation techniques, such as FAB [3,4], plasma desorption [5] and SIMS [6], has enabled the mass spectral analysis of non-volatile species such as dyestuffs, polymers and large biomolecules. However, these techniques provide little control over the degree of fragmentation observed in the mass spectra. This may often result in little or no molecular ion signals. In addition, such ionisation techniques are inherently non-selective, thereby limiting their application to analysis of complex mixtures. Conversely, other techniques, such thermospray ionisation [7], often only provide molecular or pseudo-molecular ion signals, with limited structural information to assist in the elucidation of unknown structures. The disadvantage inherent in all of the above techniques is their inability to generate *both* molecular weight *and* structurally significant data.

The use of infrared laser desorption coupled with multiphoton ionisation (MPI) and time-of-flight mass spectrometry has been shown to be effective for the analysis of a wide range of thermally labile and involatile molecular species [8]. It is possible to generate both molecular weight and structurally significant data using this technique. This is due to the two-stage nature of the technique; temporal and spatial separation of the desorption and ionisation events allows independent optimisation of both processes. Pulsed infrared laser desorption facilitates the liberation of intact neutral gas-phase species, and variation of the ionising laser intensity can exert considerable control over the degree of fragmentation observed in the mass spectra.

In the present work, a series of azo dyes have been examined using two fixed postionisation wavelengths, 193 nm and 266 nm. The azo dyes were all used as received, without any preseparation or purification. The samples were prepared by dissolving a small amount of material in methanol and allowing the solvent to evaporate, or by mixing in glycerol to form a thin paste. The spectra obtained at these two ionisation wavelengths show marked differences in the fragmentation

Dye	Structure
4-phenylazoaniline Molecular weight = 197 u. **(paa)**	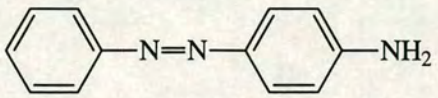
4-phenylazophenol Molecular weight = 198 u. **(pap)**	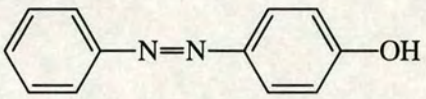
{4-[2-(amino) 4-(hydroxy) phenylazo] benzoic acid} Molecular weight = 257 u. **(ahp)**	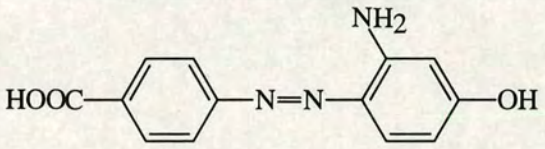
{3-[2-(hydroxy) 5-(amino) phenylazo] benzoic acid} Molecular weight = 257 u. **(hap)**	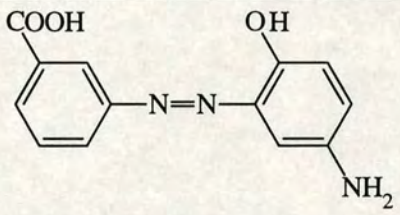
{4-[4-(dimethylamino) phenylazo] benzoic acid} Molecular weight = 269 u. **(mr1)**	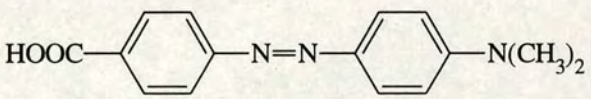
{3-[4-(dimethylamino) phenylazo] benzoic acid} Molecular weight = 269 u. **(mr2)**	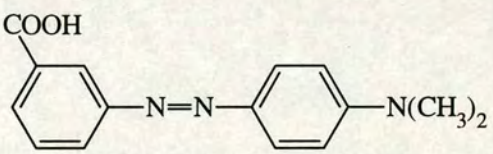
{2-[4-(dimethylamino) phenylazo] benzoic acid} Molecular weight = 269 u. **(mr3)**	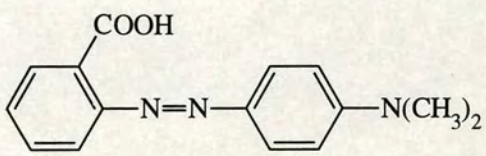

Table 4-1: Names, structures and molecular weights of azo dyes studied by L2MS.

patterns observed. In addition, significant differences in fragmentation patterns for isomeric azo dyes photoionised using 266 nm radiation have been observed.

4.2.1 L2MS of Simple Azo Dyes

Previous studies of azo dyes in this laboratory using L2MS have shown that judicious choice of the ionising laser wavelength can lead to complementary structural and molecular weight information [9,10]. For a number of compounds, photoionisation using 266 nm radiation showed no evidence of molecular ions, although characteristic fragmentation of the azo linkage was observed. Ionisation at 193 nm, however, resulted in spectra dominated by the pseudo-molecular ions $[M + H]^+$, $[M + Na]^+$ and $[M + K]^+$. Fragment ions observed at this ionising wavelength corresponded to cleavage of the C—N bonds on either side of the azo bond. These experiments were carried out using the entrainment configuration of the instrument. As discussed in Chapter 3, the instrument is inherently insensitive in this configuration.

The molecules 4-phenylazoaniline (paa) and 4-phenylazophenol (pap), shown in Table 4-1, were studied at both 193 nm and 266 nm, using the more sensitive non-entrainment configuration of the instrument. This was done in order to assess whether the gain in sensitivity would allow detection of molecular ion signals using 266 nm ionisation, which were absent in all spectra recorded using the molecular beam. Molecular ion signals, even if weak, would be very useful for unambiguously identifying these dyestuffs.

Photoionisation at 193 nm

Figure 4-1a shows the mass spectrum obtained for paa using 193 nm photoionisation. The dominant fragmentation process at this wavelength is cleavage of the C—N bond adjacent to the azo linkage; the peak at m/z = 92 corresponds to C—N cleavage to form the dehydroaniline fragment ion, with the fragment at m/z = 77 arising from cleavage of the other C—N bond to yield the phenyl ion. The likely mechanism for this C—N cleavage is for the charge to be retained by the nitrogen containing moiety, since this preserves aromaticity, followed by elimination of

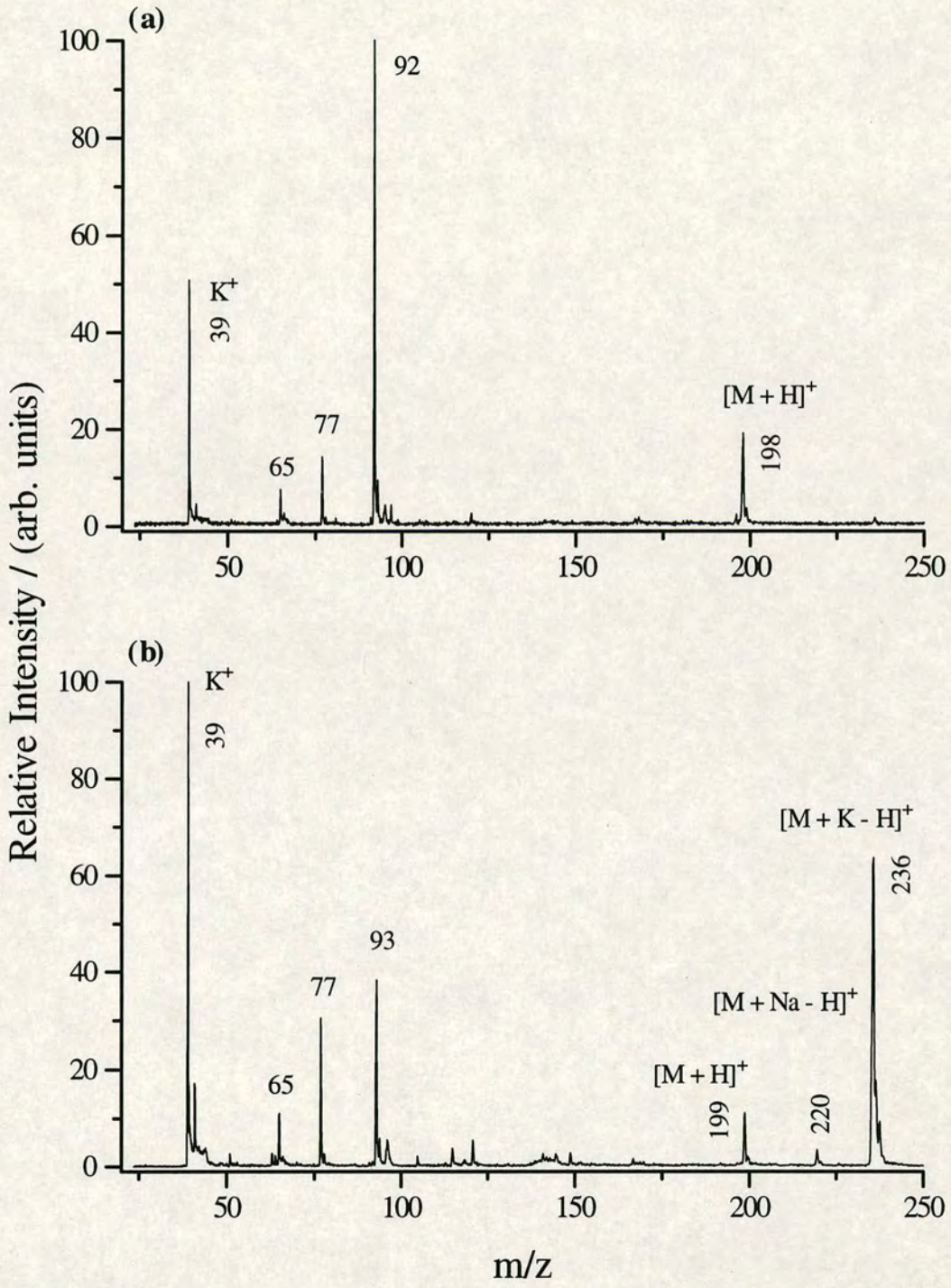

Figure 4-1: L2MS spectra of (a) 4-phenylazoaniline (paa), and (b) 4-phenylazophenol (pap), obtained using 10.6 μm laser desorption and 193 nm laser photoionisation.

molecular nitrogen to form the observed C—N cleavage product. The molecular weight of this compound can be determined from the hydrogen adduct ion, $[M + H]^+$. A summary of the proposed ionisation and fragmentation channels for 193 nm photoionisation of paa are illustrated in Figure 4-2a.

A broadly similar mass spectrum is obtained for 193 nm photoionisation of pap, as shown in Figure 4-1b. Again, C—N cleavage dominates the observed fragmentation, with the m/z = 93 fragment corresponding to the dehydrophenol ion. The m/z = 77 ion is assigned as before to the phenyl ion resulting from cleavage of the other C—N bond. The molecular weight can again be determined from the adduct ions. There is a peak at m/z = 199 corresponding to the hydrogen adduct, $[M + H]^+$. The signals at m/z = 220 and 236 seem to correspond to adducts involving sodium and potassium, respectively, as evidenced by the characteristic mass difference of 16 u . However, they do not correspond to simple $[M + \text{alkali}]^+$ ions; in each case a hydrogen seems to have been eliminated, resulting in the formation of a $[M + \text{alkali} - H]^+$ ion. A summary of the proposed fragmentation channels is illustrated in Figure 4-2b.

At present, the mechanism of this cationisation is unclear. However, it is likely that it proceeds at some stage through single photon ionisation of neutral alkali metal species. At 193 nm, photoionisation of both sodium and potassium is a single-photon process, whereas photoionisation of the azo dye is likely to require the absorption of at least two photons. One possible explanation, therefore, is that cationisation of azo dyes is able to compete effectively with photoionisation. It also appears that the way in which the alkali metal species is presented is critical to the formation of cationised azo dyes. It has been reported, for example, that the addition of large amounts of inorganic alkali metal containing salts, such as potassium bromide, does not enhance the formation of cationised species [11]. This has also been observed in this laboratory. It may be that the alkali metal containing species is present as an impurity in the azo dye, such as excess diazonium salts. Alternatively, the alkali metal species may originate as ablated material from the MACOR substrate, which is known to incorporate sodium and potassium containing materials. It is clear that the spectrum of pap in Figure 4-1b shows a far higher intensity of

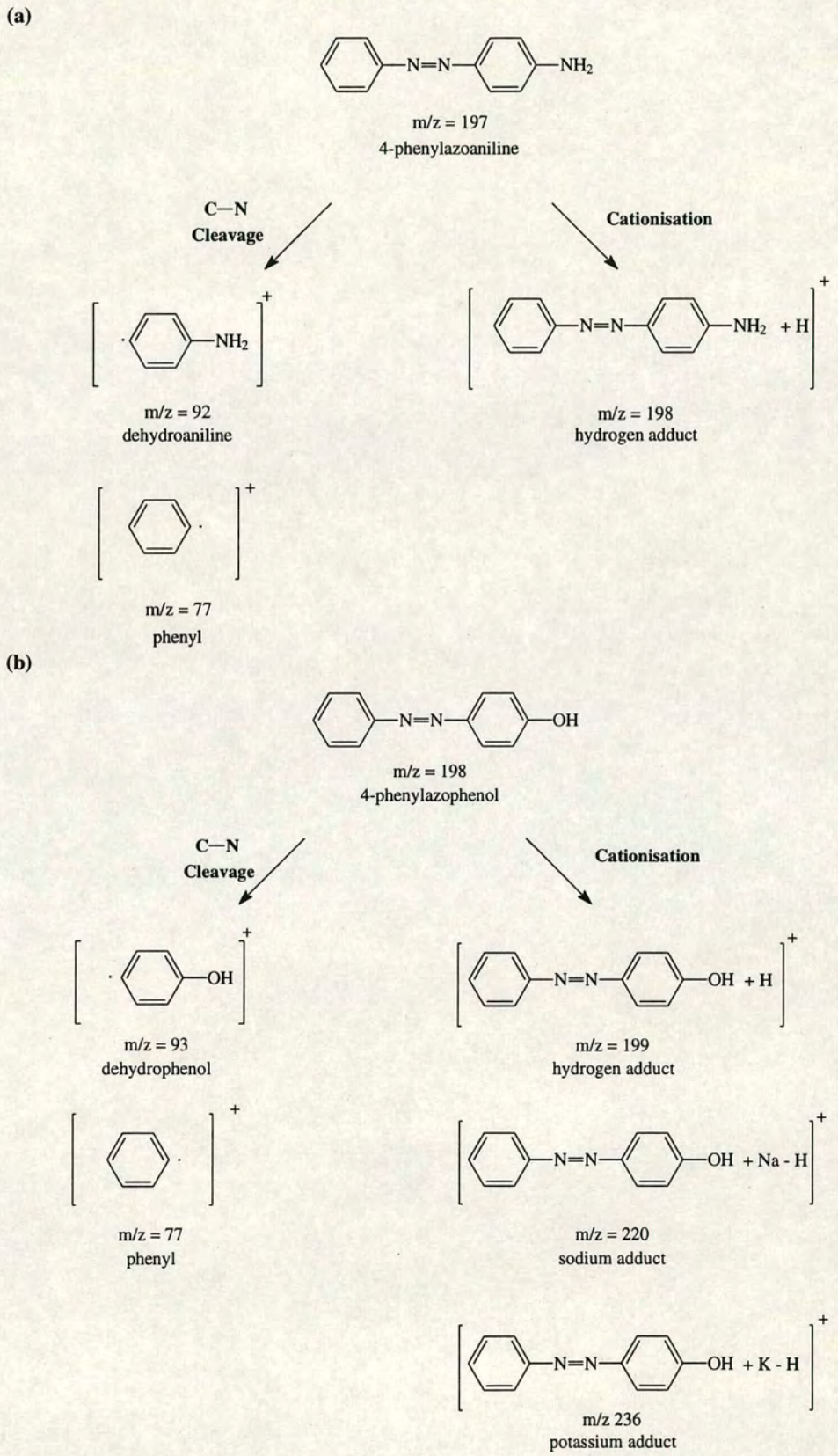

Figure 4-2: Proposed scheme of major ionisation channels for (a) paa, and (b) pap, following 193 nm photoionisation.

cationised molecular ions than is the case for paa. This would be consistent with a higher concentration of impurity, either in the sample or in that particular substrate. The higher intensity of potassium ions in Figure 4-1b also supports this explanation.

Photoionisation at 266 nm

When paa and pap were previously studied at 266 nm using the entrainment configuration [10], no molecular ion or pseudo-molecular ions were observed in the mass spectra. Although the absence of molecular ions was initially surprising, the absence of cationised molecular ions was encouraging in the light of the proposed mechanism for cationisation at 193 nm. At 266 nm, photoionisation of sodium and potassium is a two-photon process, and therefore, it is less likely that cationisation will be able to compete favourably with photoionisation. Under these conditions, the mass spectra were dominated by fragments to low mass. The base peaks were exclusively assigned to cleavage of the azo bond followed by double hydrogen transfer. Although the same general trends are observed in the mass spectra obtained using the non-entrainment configuration, other features can be extracted as a result of the increased sensitivity.

Figure 4-3a shows the mass spectrum obtained when paa is photoionised at 266 nm under soft ionisation conditions. The most significant feature is that now, a clearly identifiable molecular ion signal is observed at m/z = 197. This is an important aid in the unambiguous determination of these species for analytical purposes. However, the fragmentation observed is rather more complex than was observed using the entrainment configuration. Intense peaks at m/z = 92 and 93 are also observed. An ion at m/z = 92 has already been assigned to C—N cleavage following 193 nm ionisation of paa, to form the dehydroaniline ion. When paa was studied previously using entrainment, there was no evidence of C—N cleavage using 266 nm ionisation. The signal at m/z = 93 can be produced by azo cleavage plus double hydrogen transfer to produce the aniline fragment ion. Alternatively, this aniline fragment ion can also be formed by C—N cleavage as before, followed by single hydrogen transfer. It would, therefore, appear that using this experimental set-up, both C—N and azo cleavage are observed. Although the signals at m/z = 92 and

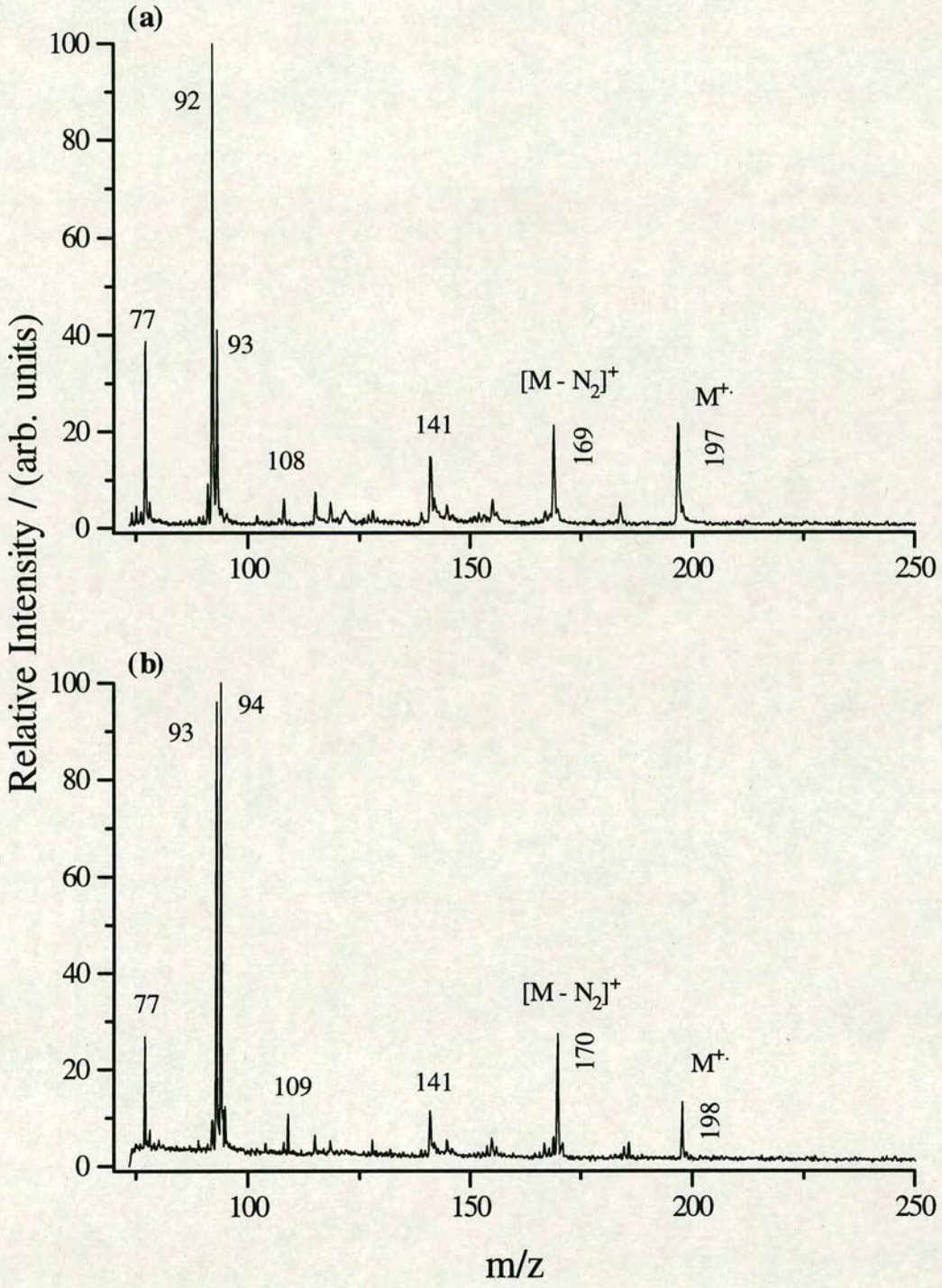

Figure 4-3: L2MS spectra of (a) paa, and (b) pap, obtained using 10.6 μm laser desorption and 266 nm photoionisation.

93 can both result from C—N cleavage, the occurrence of azo cleavage is confirmed by the presence of a signal at m/z = 108. This corresponds to azo cleavage plus double hydrogen transfer to generate the 4-aminoaniline ion. It is unclear whether azo cleavage occurs as a result of neutral photodissociation at the first excited state, followed by photoionisation of both neutral fragments, or whether the fragmentation occurs in the ion, with both sides of the molecule competing effectively to retain the charge. A peak is also obtained at m/z = 169, which can be assigned to elimination of N_2 from the molecular ion to form the substituted biphenyl species. This elimination of N_2 in azo dyes has been observed previously using other techniques [12] as well as L2MS [10]. The proposed fragmentation pathways for 266 nm ionisation of paa are illustrated in Figure 4-4a.

A similar spectrum, shown in Figure 4-3b, is obtained for 266 nm ionisation of pap. A clearly identifiable molecular ion signal can be seen at m/z = 198, along with a peak at m/z = 170 corresponding to elimination of N_2 from the molecular ion. Two fragment peaks are also observed at m/z = 93 and 94, which closely resembled those in Figure 4-2a. The fragment at m/z = 93 can be attributed to C—N cleavage to form the dehydrophenol ion. An ion of this mass may also be accounted for by an aniline fragment ion, generated by azo cleavage followed by double hydrogen transfer. An ion of m/z = 94, however, can only be formed by C—N cleavage plus single hydrogen transfer to form the phenol ion. The signal at m/z = 109 can only be rationalised in terms of cleavage of the azo bond, followed by double hydrogen transfer to form the 4-aminophenol ion. This confirms that azo cleavage followed by double hydrogen transfer occurs, and that, once again, both C—N and azo cleavage occur following 266 nm photoionisation using the non-entrainment configuration of the instrument. The proposed fragmentation channels for pap are shown in Figure 4-4b.

Rationalisation

In summary, the previous studies carried out in this laboratory on these simple azo dyes showed marked differences in their mass spectra using the two fixed ionisation laser wavelengths, 193 nm and 266 nm [9,10]. At 193 nm, molecular ion

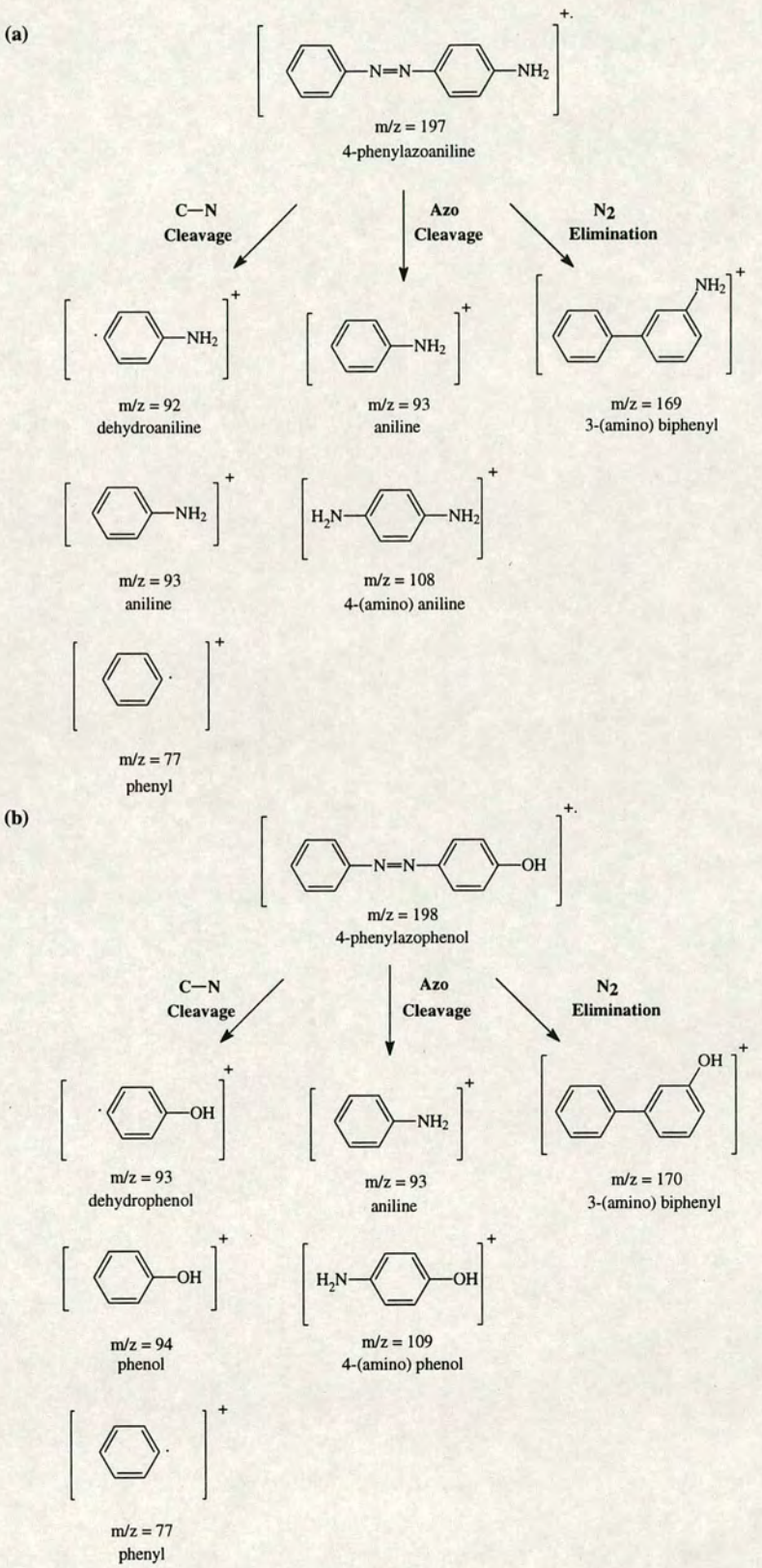

Figure 4-4: Proposed scheme of major ionisation and fragmentation pathways for (a) paa, and (b) pap, following 266 nm photoionisation.

information was available in the form of adduct ions. The only fragment ions observed at this wavelength were assigned to the products of C—N cleavage, with both aromatic moieties competing effectively for the charge. In contrast, using 266 nm photoionisation, no molecular ion or adduct signals were present in the mass spectra. At this wavelength, no C—N cleavage was observed. The dominant fragment ions detected were assigned as the products of azo bond cleavage, again with both moieties being detected. The other fragment ions observed corresponded to the products of elimination of N_2 from the azo dye. These phenomena were observed, not only for paa and pap, but also for a whole series of simple azo dyes.

The fragmentation processes observed at 193 nm were explained in terms of the conventional multiphoton fragmentation mechanism, where initially a molecular or pseudo-molecular ion is formed, which undergoes subsequent fragmentation by absorption of further photons. However, this mechanism is clearly not appropriate for explaining the entirely different fragmentation observed using 266 nm radiation.

The photodissociative ionisation observed using 266 nm was rationalised by considering the known photochemical properties of azo dyes. Azo benzenes are known to exist as *trans* and *cis* isomers. In general, the *trans* isomer is the more stable of the two species, but is known to undergo an isomerisation reaction to the *cis* form following excitation to low lying singlet electronic states [13]. Photoisomerism is believed to proceed via an excited state potential surface which exhibits a minimum at the perpendicular configuration of the torsional coordinate (i.e., midway between the *trans* and *cis* configurations) [14]. The ground state potential surface has a maximum at this point, corresponding to the barrier to rotation about the double bond. It is thought that photodissociative ionisation observed at 266 nm is linked to this photoisomerism, in that it proceeds via the same one-photon excited intermediate state [10]. The significant change in geometry between the ground electronic and intermediate states induced by *trans-cis* isomerisation results in Franck-Condon factors which favour large amounts of vibrational energy being channeled into this N-N torsional mode.

There are therefore two plausible explanations which may account for the observed azo cleavage at 266 nm. One possibility is that this vibrationally excited intermediate electronic state dissociates at the azo linkage to form two neutral fragments, which are subsequently photoionised and detected. Alternatively, if only a small change in geometry occurs between the excited state and the ion, the vibrational population of the intermediate state will be preserved in the ion. Therefore, further photon absorption by this intermediate state may lead to the production of a molecular ion which is unstable and dissociates to give an ion and a neutral fragment. In this case, the detection of both azo cleavage products suggests that there is a competition to retain the charge, which is reflected in the intensities observed in the mass spectra. This photodissociative fragmentation channel is not available at 193 nm as a result of the nature of the excited state accessed at this wavelength; it is likely that it is the phenyl moieties which absorb the 193 nm radiation, and so ionisation and fragmentation proceeds via alternative channels.

The observation of fragment ions at 266 nm corresponding to elimination of N_2 from the azo dye can also be rationalised using this argument [10]. Since N_2 is not an end group, then elimination of N_2 must be accompanied by a cyclic rearrangement to form a biphenyl fragment. In order for an azo benzene to be able to form a plausible cyclic intermediate, the molecule must be in the *cis* configuration, as illustrated in Figure 4-5. Therefore, elimination of N_2 requires the normally *trans* azobenzene to undergo a *trans-cis* photoisomerism about the azo linkage. Thus, since azo cleavage has already been linked to *trans-cis* isomerism, azo cleavage and N_2 elimination fragmentation reactions are likely to be competing fragmentation channels.

It now appears that when these molecules are studied without the use of the molecular beam, the resulting mass spectra are rather more complex, especially following ionisation at 266 nm, as shown in Figure 4-3. Ionisation at 193 nm produces similar results to those found previously, in that no molecular ions are observed, although molecular weight information is easily obtained from the adduct

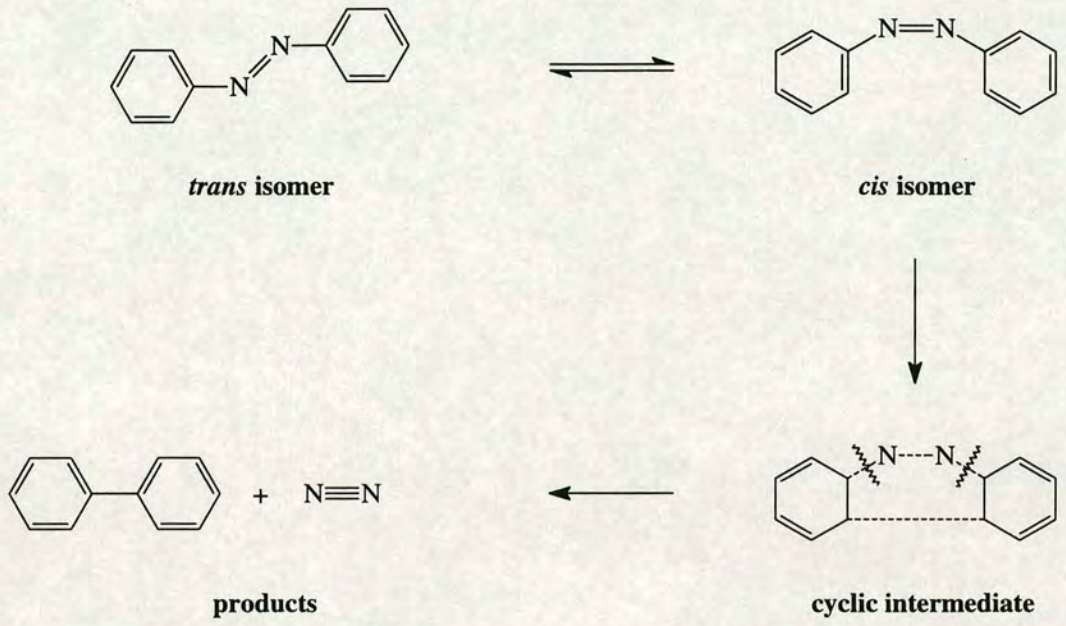

Figure 4-5: Schematic illustration of *trans-cis* isomerisation of azobenzene, and proposed cyclic intermediate required for N_2 elimination.

ions. The fragmentation products still consist exclusively of C—N cleavage products.

However, the spectra observed without the molecular beam using 266 nm photoionisation are considerably more complex. The same fragmentation behaviour is still observed in this case, in that azo cleavage definitely occurs. However, in addition, clearly identifiable molecular ions are observed along with the products of C—N cleavage. It was hoped that the increased sensitivity would lead to the detection of molecular ion species, which would provide useful molecular weight information in addition to the structural data already obtained using the molecular beam. This has clearly been achieved.

The other observations were rather more surprising and difficult to explain. It was unclear why simply dispensing with the molecular beam should result in C—N cleavage products being observed at 266 nm. An initial worry was that these species were the result of thermal decomposition during the desorption process. Although this is a distinct possibility, it is considered to be unlikely. The desorption laser power densities are significantly higher for desorption into a molecular beam, which

would be expected to result in a higher degree of thermal decomposition. However, these C—N cleavage products are entirely absent in the entrainment spectra. In addition, the molecular ion can be detected with significant intensity without the molecular beam, which is certainly a powerful argument against thermal decomposition during the desorption event

Nevertheless, the desorption process must be implicated in the formation of these C—N cleavage products. One possible means of explaining these results is to consider the internal energy of the gas-phase neutrals when they are photoionised. Following entrainment in a molecular beam, the internal energy content of the neutral dye molecules is likely to be relatively low. Therefore, most of the molecules will be excited into a narrow range of states following 266 nm excitation. The significant change in geometry between the ground and intermediate electronic states is likely to result in directed population of the N-N torsional mode, which ultimately leads to azo cleavage. As stated previously, it is, at present unclear whether this dissociation occurs in the neutral excited intermediate state or in the ion.

When a molecular beam is not used, and therefore there is no cooling of the internal degrees of freedom, it is likely that these desorbed neutrals will have significant internal energy. (Experimental proof of extensive internal excitation for the amino acid, tryptophan, and its role in the formation of fragment ions is presented in Chapter 7.) In this case, it is unlikely that all of the vibrational energy is directed into the N-N torsional mode. Excitation at 266 nm is, therefore, likely to populate a much wider range of vibronic states governed by Franck-Condon factors. Absorption of a second 266 nm photon therefore leads to the C—N cleavage products, previously observed at 193 nm, in addition to the azo cleavage products expected at this wavelength. This hypothesis needs further experimental validation, but these experimental data, together with the results presented for tryptophan in Chapter 7, suggest that the internal energy of the desorbed neutrals may have an important influence on the photoionisation fragmentation patterns.

Although the spectra obtained without the use of molecular beam entrainment appear to be more complex, there is still a clear wavelength dependence in the

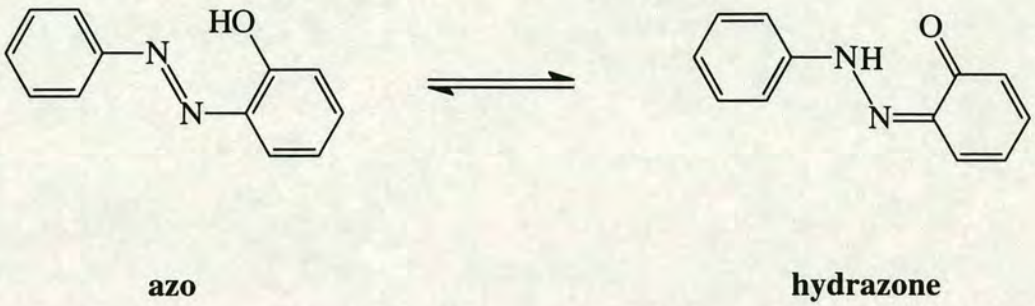

azo **hydrazone**

Figure 4-6: Schematic illustration of *azo-hydrazone* tautomerism

observed mass spectra. This, along with the increased information content resulting from the improved sensitivity makes L2MS a potentially powerful technique for the study of azo dye systems incorporated in complex matrices and mixtures.

4.2.2 L2MS of Isomeric Azo Dyes

One area in which mass spectrometry has not proved universally successful, is in the differentiation between isomeric species. However, for azo dyes, Borgerding and Hites have shown that the position of hydroxy substituent groups about the aromatic ring relative to the azo linkage can have a marked effect on the fragment ions observed in SIMS mass spectra [12]. It was found that when hydroxy groups were situated *ortho* to the azo linkage, the products of azo cleavage were increased. This increase in azo bond cleavage was linked to the ability of azo molecules of this type to undergo azo-hydrazone tautomerism. As illustrated in Figure 4-6, this leads to the hydrogen on the hydroxy group transferring to one of the nitrogen atoms forming the azo bond. The end result is that the azo bond is replaced by a single bond, which is much weaker and, therefore, more prone to fragmentation. The degree of fragmentation observed in SIMS mass spectra resulting from cleavage of the central azo bond appears to have increased as a result of this tautomerism.

Isomeric azo dyes can be different in colour, suggesting that this change in substituent position influences their photophysics. It may, therefore, be possible to exploit the differing photophysics of isomeric azo dyes using L2MS to differentiate between these isobaric species. Two isomeric azo dyes shown in Table 4-1, {4-[2-

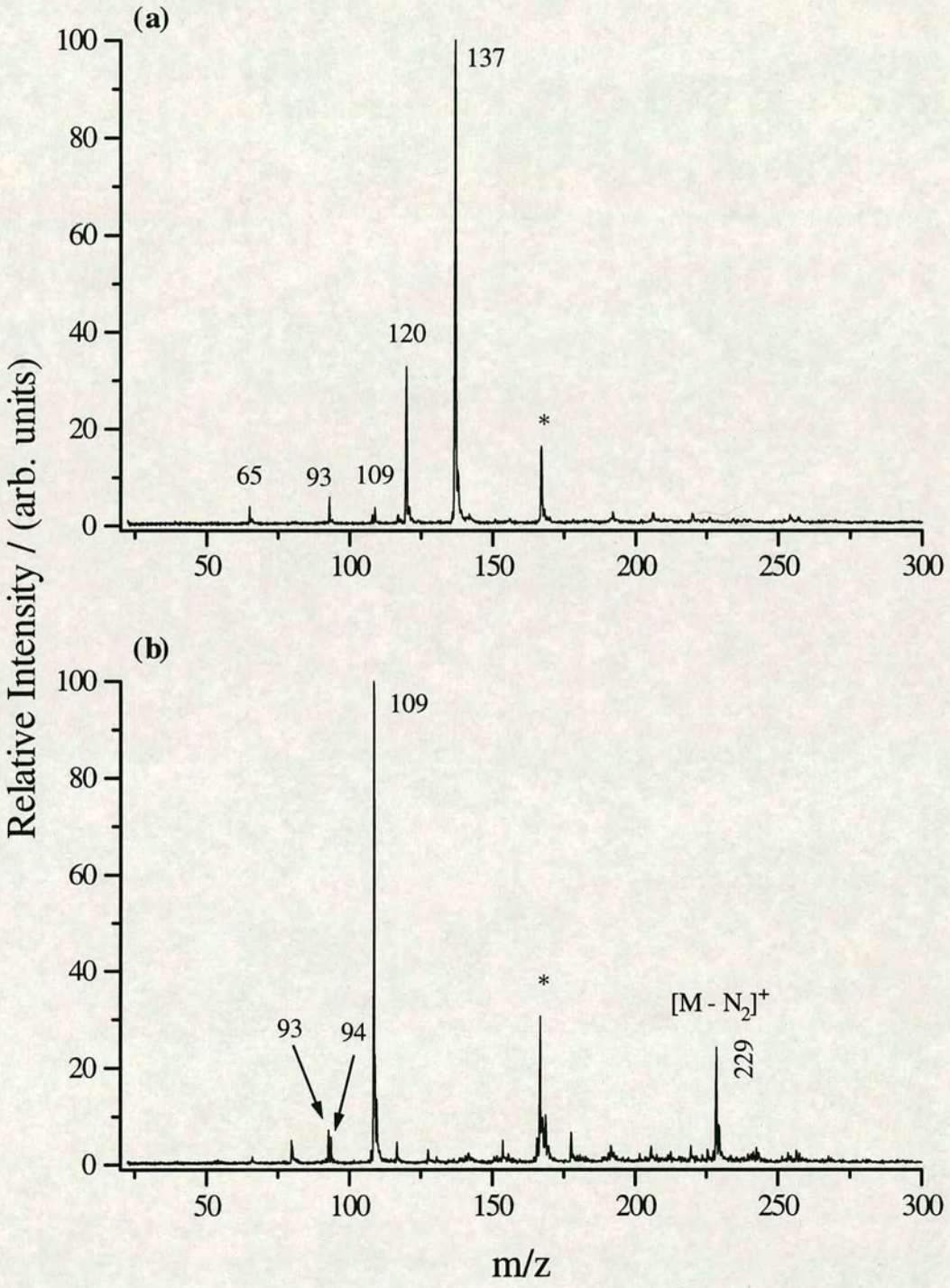

Figure 4-7: L2MS of the isomeric azo dyes (a) ahp, and (b) hap, obtained using 10.6 μm laser desorption and 266 nm laser photoionisation. The peaks denoted "*" are due to an internal mass standard, carbazole, m/z = 167.

(amino) 4-(hydroxy) phenylazo] benzoic acid} (ahp) and {3-[2-(hydroxy) 5-(amino) phenylazo] benzoic acid} (hap), were studied using 266 nm ionisation in order to test this hypothesis. The hap isomer contains a hydroxy group *ortho* to the azo linkage, and so it was expected that the degree of azo cleavage observed in the mass spectrum would differ from that observed for ahp, thereby allowing them to be distinguished.

Figure 4-7a shows the mass spectrum obtained following 266 nm photoionisation of ahp. The base peak in this spectrum is at m/z = 137, which corresponds to azo cleavage plus double hydrogen transfer to produce the 4-(amino) benzoic acid fragment ion. This is the characteristic fragmentation which was expected following 266 nm photoionisation. The signal at m/z = 120 is a fragment of this azo cleavage product, as shown by its increase in intensity relative to the signal at m/z = 137 with increasing ionising laser fluence. This fragment can be assigned to loss of OH from the azo cleavage product at m/z = 137, which is a characteristic loss for aromatic acids in electron impact studies [15]. The peak observed at m/z = 109 results from C—N cleavage followed by a single hydrogen transfer, to form the 3-(amino) phenol ion. This again illustrates that both C—N and azo cleavage can occur following 266 nm photoionisation in the absence of cooling in a molecular beam. The peak observed at m/z = 93 presumably results from fragmentation of 3-(amino) phenol as a result of subsequent 266 nm photon absorption. The proposed fragmentation pathways observed for 266 nm ionisation of ahp are illustrated in Figure 4-8a.

The spectrum obtained for the isomeric species hap, which has the hydroxy group *ortho* to the azo linkage, is entirely different, as shown in Figure 4-7b. The azo cleavage signal at m/z = 137 is completely depressed, with the base peak in the spectrum at m/z =109, resulting from C—N cleavage and hydrogen transfer to form the 4-(amino) phenol ion. The other major fragment channel at m/z = 229 arises as a result of elimination of N_2 to form a substituted biphenyl species. The proposed fragmentation channels for 266 nm ionisation of hap are shown in Figure 4-8.

From these results, it can be seen that when the hydroxy substituent is *ortho* to the azo linkage, fragmentation exclusively favours N_2 expulsion over the anticipated azo cleavage. It would, therefore, appear that the position of this hydroxy group is

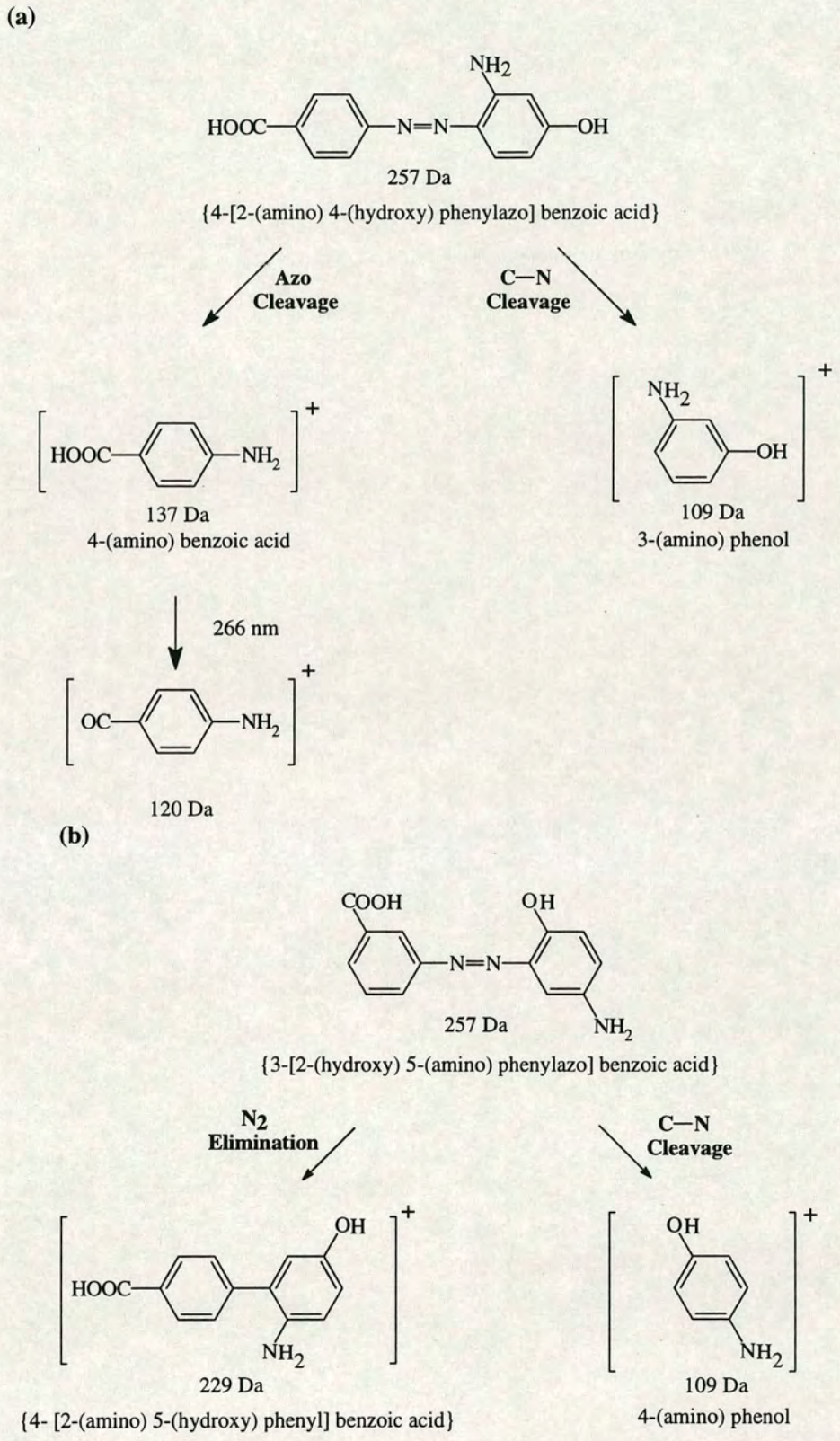

Figure 4-8: Proposed fragmentation scheme for (a) ahp, and (b) hap, following 266 nm photoionisation

directing the fragmentation. Although a difference in the relative amounts of azo cleavage observed for these two isomers was expected, these results were initially very surprising. Of the two isomers, hap was expected to undergo azo-hydrazone tautomerism, which should result in the azo bond being replaced by a single nitrogen bond. On the grounds of bond strength, therefore, it was expected that hap should show an increased tendency towards azo bond cleavage relative to ahp. However, as Figure 4-7a and 4-7b show, exactly the opposite result is obtained. In short, ahp shows predominantly azo cleavage, with hap displaying only C—N cleavage and N_2 elimination.

The reason for these experimental observations is, however, immediately apparent upon consideration of the nature of the ionisation technique. In techniques such as SIMS, large amounts of energy are deposited into the molecule. After production of a molecular ion, the excess energy is redistributed, such that the weakest bonds fragment. However, MPI is a much more subtle ionisation technique. Here, as described in detail in Chapter 2, intermediate electronic states are used as "stepping-stones" from which to ionise the molecule. In general, this results in much less energy being deposited into the system. This results in a lower degree of fragmentation from energy redistribution than is commonly observed in techniques such as SIMS. However, MPI is susceptible to photochemical/photophysical processes occurring at the excited intermediate state, which techniques such as SIMS bypass completely. The unexpected results obtained here for ahp and hap can therefore be rationalised by considering the effect of the substituents on the intermediate electronic states.

When the hydroxy substituent is *ortho* to the azo bond, as in hap, azo-hydrazone tautomerism can occur to such an extent that the compound exists almost exclusively in the hydrazone form [13]. This, therefore, has a marked effect on the nature of the intermediate state of the molecule, in that the absence of the azo bond precludes *trans-cis* photoisomerism. The criterion for azo cleavage, discussed above, stated that photoionisation proceeded via the same intermediate state as *trans-cis* photoisomerism. Absorption by this state of another 266 nm photon resulted in the

production of an unstable molecular ion, which efficiently fragmented at the azo linkage. The formation of the hydrazone tautomer has led to the removal of this barrier to rotation about the double bond such that there is no preferential population of the N-N torsional mode, with the result that the criterion for azo cleavage at 266 nm ionisation can no longer be fulfilled.

From this argument, it would also appear that if the molecule is unable to exhibit *trans-cis* photoisomerism, then the criterion for N_2 elimination can also no longer be fulfilled. It is, therefore, perhaps surprising that one of the major fragmentation channels of hap is that of N_2 elimination. However, the major criterion allowing N_2 elimination to occur was the ability of the molecule to orient itself in such a way that a cyclic intermediate could be formed. For azo molecules, where there is an N=N double bond, the only way this can be achieved is in the *cis* configuration. Since azo molecules are more stable in the *trans* configuration, the molecule must first undergo a *trans-cis* isomerism in order to orient itself in the required manner. However, if, as in the case of hap, the molecule exists predominantly in the hydrazone form, where there is no longer an N=N double bond, the molecule is free to rotate, such that it can orient itself to form the required cyclic intermediate for N_2 expulsion. Therefore, azo-hydrazone tautomerism does appear to affect azo cleavage, but not N_2 elimination.

These results show that when MPI is used for ionisation, it is not necessarily the weakest bonds in the molecule which are broken, as is often the case with techniques such as SIMS. It is possible to use the photochemistry of the system, in particular the nature of the intermediate state, to differentiate easily between isomeric species. In the case of ahp and hap, the only difference in these molecules is the position of the substituent groups about the aromatic rings, relative to the azo bond. When an amino group is situated *ortho* to the azo linkage, characteristic azo cleavage is observed. However, when a hydroxy group is in this position, the occurrence of azo-hydrazone tautomerism results in a change in the photochemistry of the system. This leads to significant changes in the fragmentation patterns observed using L2MS, allowing the two isomers to be easily distinguished.

The inference from the above discussion is that certain substituent groups can interfere with the azo bond. This results in changes in photochemistry, which can lead to different fragmentation patterns being observed. Isomer dependent fragmentation patterns are not only limited to molecules exhibiting tautomeric behaviour, however. Other isomeric azo dyes have also been examined at 266 nm ionisation, namely three isomers of the commercial dye methyl red. These azo dyes, illustrated in Table 4-1, differ only in the position of the carboxylic acid group with respect to the azo bond. These molecules were studied in order to discover whether the position of the carboxylic acid group influenced the azo bond in any way. Indeed, some differences in the fragmentation patterns were observed with respect to changes in substituent position.

The L2MS spectrum of mr1 is shown in Figure 4-9a. The azo cleavage products anticipated following 266 nm ionisation can clearly be observed, resulting in a similar mass spectrum to that observed for ahp in Figure 4-7a. The base peak in the mass spectrum corresponds to the azo cleavage product forming the 4-(amino) benzoic acid fragment ion at m/z = 137, with the signal at m/z = 120 being assigned to further loss of OH from this azo cleavage product. Figure 4-9b, c and d illustrate the behaviour of the m/z = 120 and 137 signals with increasing ionising laser power density. As is shown, the intensity of the signal at m/z = 120 increases in intensity with respect to the signal at m/z = 137 as the laser power increases, thereby supporting the proposal that the m/z = 120 species is derived from fragmentation of the 4-(amino) benzoic acid fragment. Although no appreciable molecular ion signal is observed in Figure 4-9a, the peak at m/z = 254 corresponds to the loss of a methyl radical, $\cdot CH_3$ from the molecular ion. The dominant fragmentation channels for mr1 following 266 nm ionisation are illustrated in Figure 4-10.

When the carboxylic acid group is in the *meta* position with respect to the azo bond, as in the case of mr2, ionisation using 266 nm radiation results in different fragment ions being detected, as shown in Figure 4-11a. In this case, a series of low intensity peaks towards higher mass are observed. The molecular ion at m/z = 269 is clearly evident, with the peak at m/z = 254 being attributed to the loss of a methyl

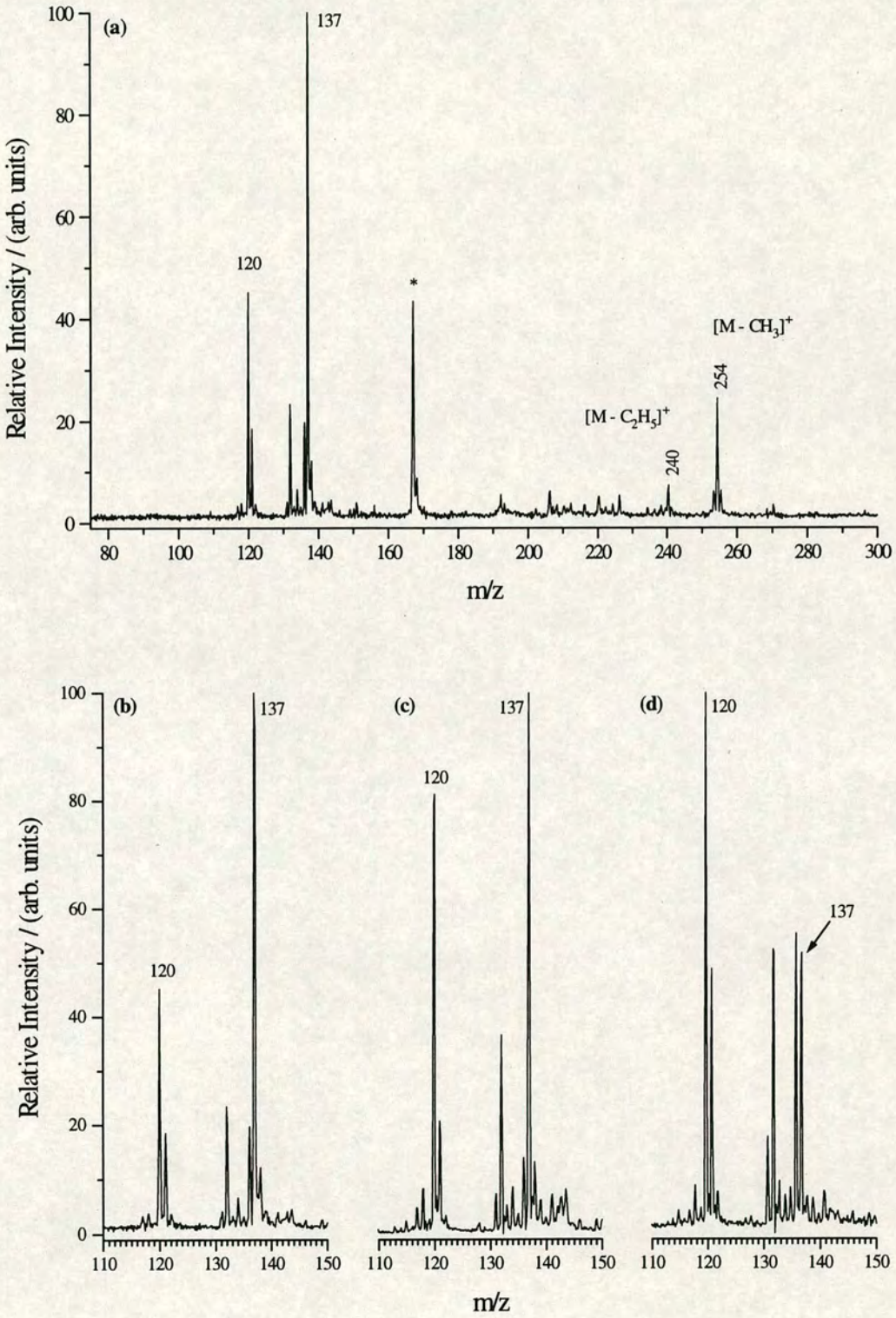

Figure 4-9: L2MS of mr1 obtained using 10.6 μm laser desorption and 266 nm laser photoionisation. Spectra (b), (c) and (d) were obtained at low, medium and high ionising laser power density, respectively, and illustrate the behaviour of the major fragmentation products with varying ionising laser power density.

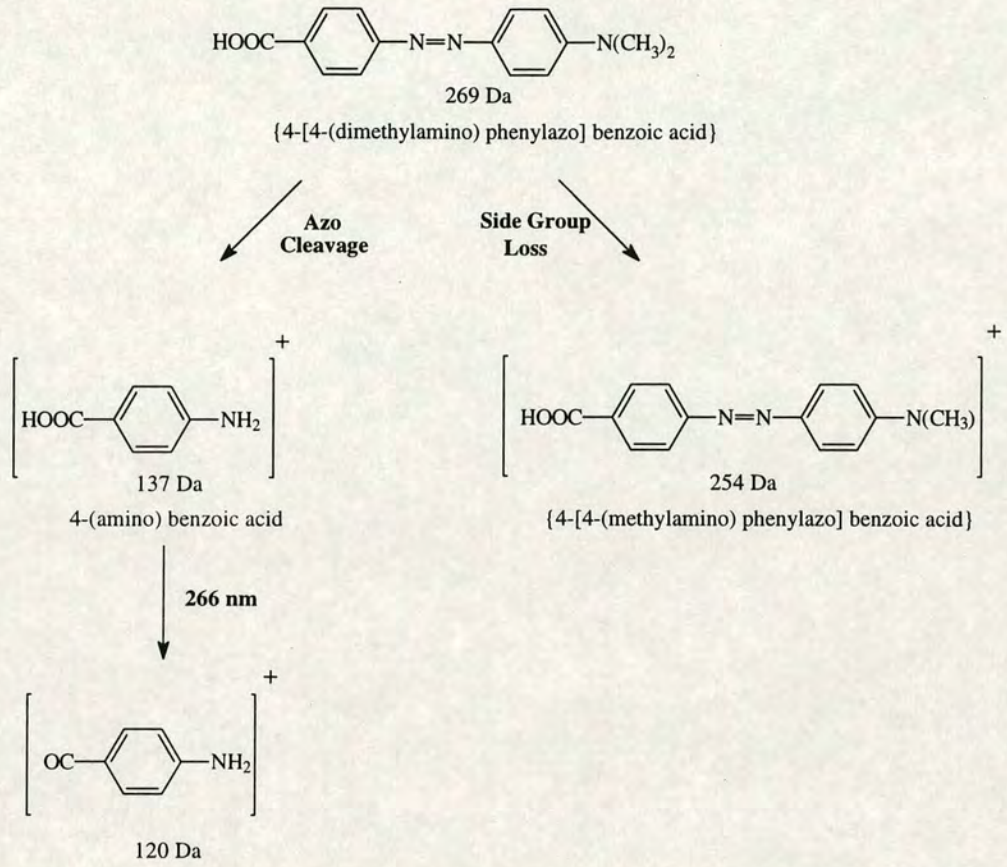

Figure 4-10: Proposed fragmentation pathways for mr1 following 266 nm photoionisation.

group from the molecular ion as before. The signal at m/z = 240 is thought to arise from further loss of a [—CH_2] group from this species, although this cannot be accomplished in a single step. It was not, however, possible to rationalise the presence of a signal at m/z = 241 by a simple side-group loss. The high intensity of this signal with respect to its neighbour at m/z = 240 obviously indicates that is not the ^{13}C isotope. However, an ion at m/z = 241 can be explained by elimination of N_2 from the molecular ion to form the substituted biphenyl species, as previously observed for other azo dye species. This, also aids in the identification of the signals observed at m/z = 226 and 212. These species could not be rationalised by further loss of side groups from the fragment at m/z = 240. They can, however, be explained by a sequential loss of methyl and —CH_2 groups from the substituted biphenyl species produced as result of N_2 elimination.

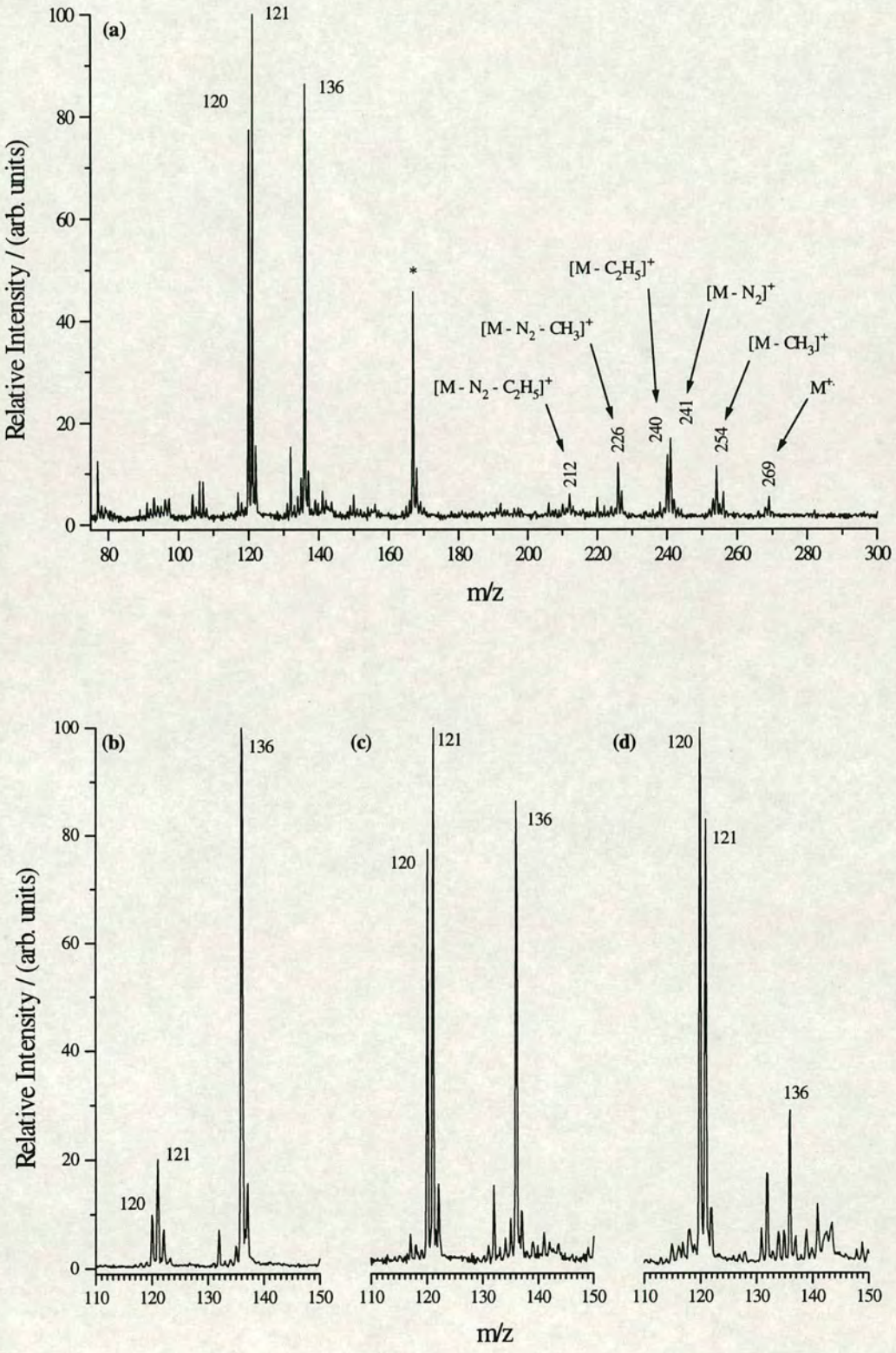

Figure 4-11: L2MS of mr2 obtained using 10.6 μm laser desorption and 266 nm laser photoionisation. Spectra (b), (c) and (d) were obtained at low, medium and high ionising laser power density, respectively, and illustrate the behaviour of the major fragmentation products with ionising laser power density.

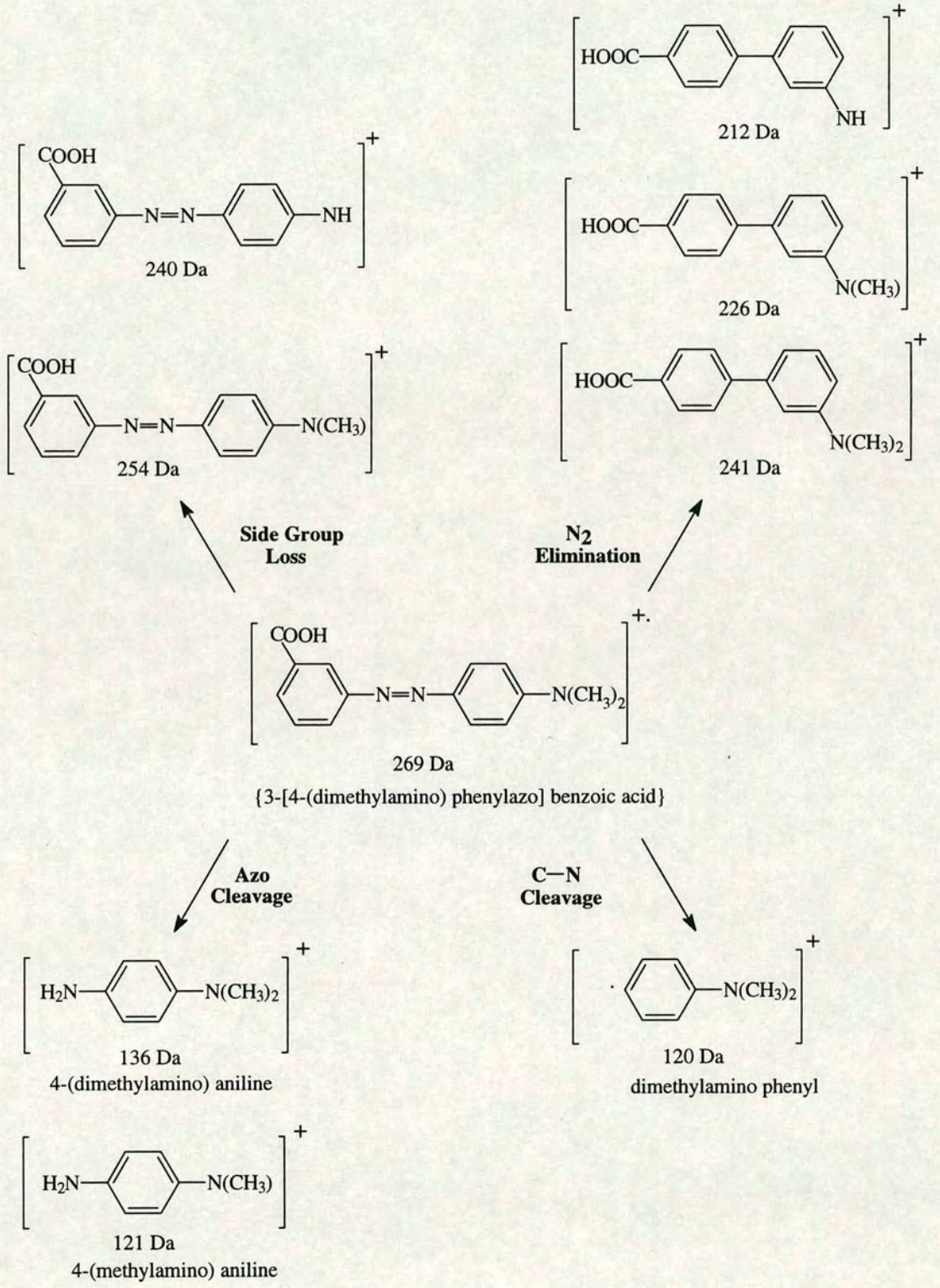

Figure 4-12: Proposed ionisation and fragmentation pathways for mr2 following 266 nm photoionisation of mr2.

No signal is observed at m/z = 137, corresponding to the 3-(amino) benzoic acid ion, similar to that observed for mr1. However, a signal is observed at m/z = 136, which would appear to be derived from azo cleavage plus double hydrogen transfer to generate the 4-(dimethylamino) aniline fragment ion. The peak at m/z = 121 can be produced by loss of a methyl group from this azo cleavage product. Alternatively, C—N cleavage to produce the benzoic acid fragment ion also results in an ion of this mass. Figure 4-11b, c and d show that when the ionising laser fluence is increased, the intensity of the m/z = 121 signal increases relative to that of the peak at m/z = 136. This suggests that the peak at m/z = 121 u is generated as a result of fragmentation from the azo cleavage product at m/z = 136. However, at these higher ionising laser fluences, it can also be seen that the signal at m/z = 120 begins to dominate over the peak at m/z = 121. This alternative fragment ion can be assigned to cleavage of the C—N bond to produce a dimethylamino phenyl fragment ion. It seems, therefore, that as the ionisation conditions become increasingly more severe, C—N cleavage begins to dominate over azo cleavage. The reasons for this are, at present, unclear. These observations may indicate that azo cleavage occurs via a neutral dissociation channel, and that as the power density of the ionising laser increases, the increased rate of up-pumping from the excited intermediate state competes effectively with the neutral dissociation leading to azo cleavage. The resulting molecular ions may then be fragmented by further photon absorption to produce the C—N cleavage products. The proposed fragmentation channels for 266 nm photoionisation of mr2 are summarised in Figure 4-12.

The 266 nm photoionisation mass spectrum for mr3, where the carboxylic acid group is in the *ortho* position, is shown in Figure 4-13a. It displays broadly similar features to those observed in the spectrum for mr2. Again, signals closely associated with the molecular ion are observed towards higher mass. However, it should be noted that they are much more intense relative to the cleavage products than was the case for mr2. The azo cleavage product, 4-(dimethylamino) aniline is again observed at m/z = 136, with its associated fragment, 4-(methylamino) aniline being observed at m/z = 121. Figure 4-13b, c and d also illustrate that these peaks behave in a similar manner with respect to increasing ionisation laser fluence. Again, the signal at m/z =

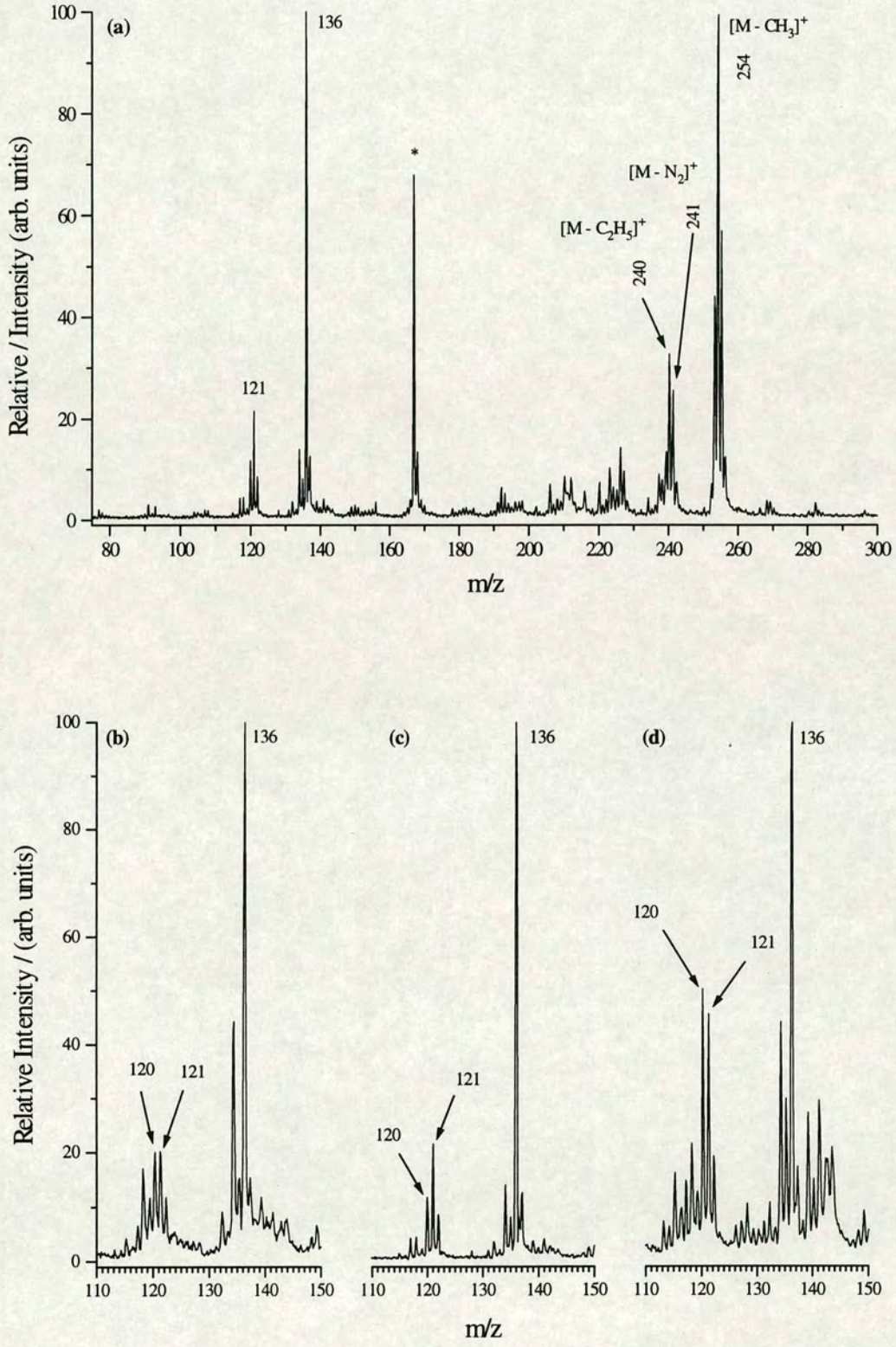

Figure 4-13: L2MS of mr3 obtained using 10.6 μm laser desorption and 266 nm laser photoionisation. Spectra (b), (c) and (d) were obtained at low, medium and high ionising laser power density, respectively, and illustrate the behaviour of the major fragmentation products with ionising laser power density.

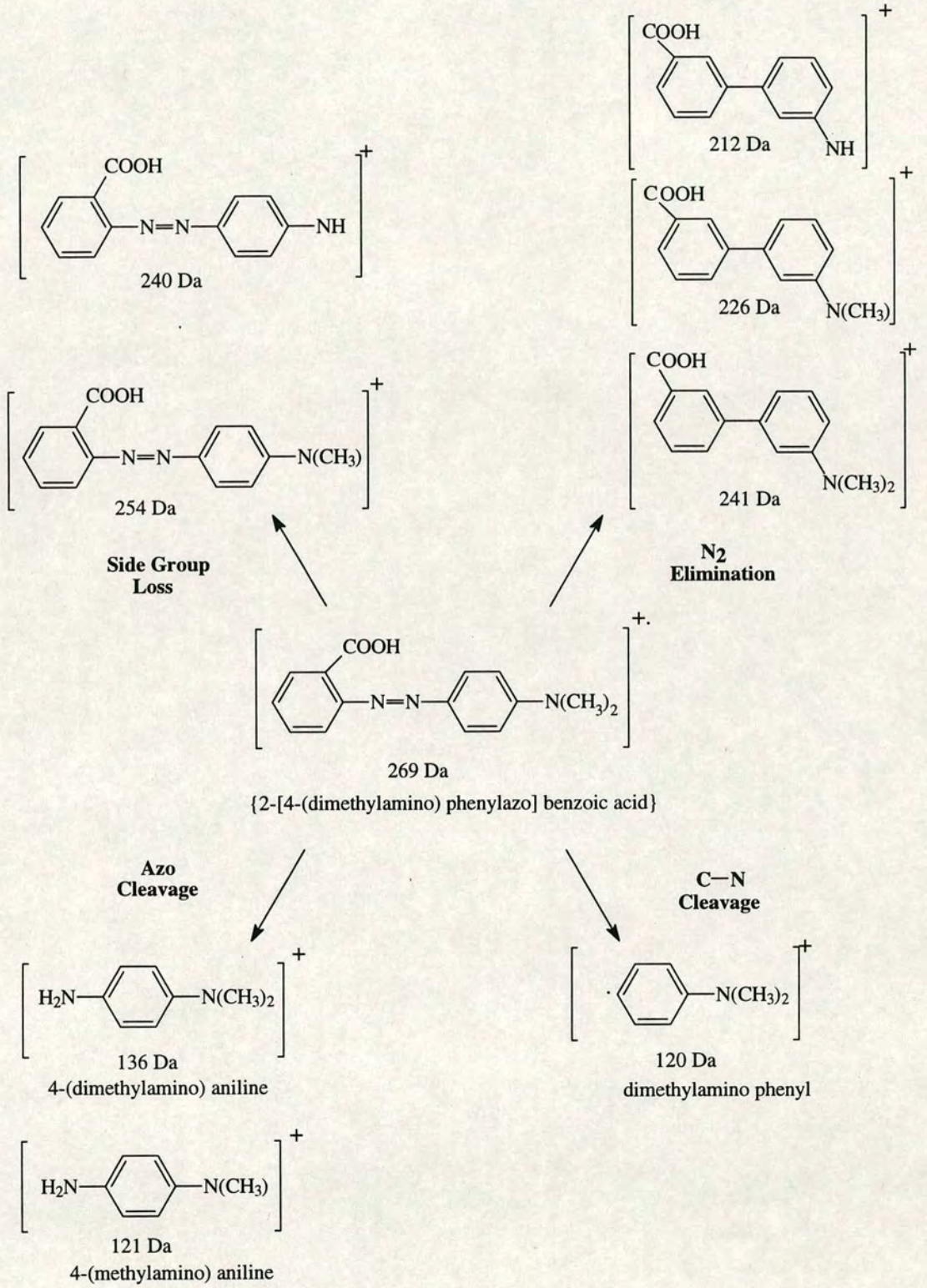

Figure 4-14: Proposed ionisation and fragmentation pathways for mr3 following 266 nm photoionisation.

121 increases relative to the ion at m/z = 136, indicating that it is formed by the loss of a methyl group from the fragment at m/z = 136. The fragment at m/z = 120, thought to result from C—N cleavage to produce the dimethyl phenyl ion, is again observed to increase in intensity relative to the other fragment ions. This once again shows that at higher ionising laser power densities, C—N cleavage begins to dominate over azo cleavage at 266 nm. The dominant fragmentation pathways for 266 nm ionisation of mr3 are illustrated in Figure 4-14.

The mass spectra obtained for these three isomers, mr1, mr2 and mr3, illustrate that the position of the carboxylic acid group in relation to the azo bond does indeed have a directing effect on the fragmentation channels observed. When the carboxylic acid group is in the *para* position, as in the case of mr1, the preferred azo cleavage product is that which produces the carboxylic acid substituted fragment ion. However, when the carboxylic acid group is in both the *ortho* and *meta* positions with respect to the azo bond, the preferred azo cleavage product is that which generates the tertiary amine substituted fragment ion. At present, it has not proved possible to directly link this isomer directed fragmentation to any chemical or physical processes, as was the case for ahp and hap. However, initial impressions are that steric factors may play some role.

In the case of mr1, the carboxylic acid group is situated as far from the azo linkage as possible, and so it can be assumed that it does not interfere with the azo bond. In this case, the azo cleavage product observed is the carboxylic acid substituted fragment, 4-(amino) benzoic acid. In mr2 and mr3, the carboxylic acid group is closer to the azo linkage, and can presumably interfere with it in some way. The result of this interference appears to be that the only azo cleavage product observed corresponds to the other side of the molecule, namely the tertiary amine substituted fragment, 4-(dimethylamino) aniline. Exactly why this interference should have such a marked effect on which products of azo cleavage are observed is, at present, unclear. However, what is clear, is that when the carboxylic acid group is close to the azo bond, the tertiary amine fragment is much more stable, whereas when the acid group is far from the azo linkage, the benzoic acid fragment is more stable.

Although not perhaps as clear cut as the case of ahp and hap, this again demonstrates that the position of substituent groups can lead to different mass spectral characteristics, and ultimately to isomer differentiation.

4.3 L2MS of Porphyrin Pigments

Porphyrins are of prime importance in a large variety of processes related to biology, biochemistry, catalysis and geology. For example, as well as occurring naturally in biological systems [16,17] and fossil fuels [18,19], porphyrins are used in tumor location and treatment [20]. The identification of porphyrin materials deposited in tissues, or excreted by organisms can aid in the identification of metabolic abnormalities [21]. Porphyrins are also very important in the oil and petrochemicals industry, occurring naturally in petroleum deposits and source rocks. Petroporphyrins found in original source materials are preserved, providing a geological history of the sample. Molecules of this type which reveal the evolution of a system over long periods of time are known as biomarkers [22]. Oil prospecting efficiency can, therefore, be enhanced by correlating these biomarkers with the source materials. Synthetic porphyrins have also been used extensively to investigate single-electron transfer reactions of natural biological processes [23], such as photosynthesis [24] and catalysis in artificial enzyme mimics [25]. Porphyrins have also been used to model stains. For example, chlorophyll a has previously been used to model grass stains, whilst hemin has been used as a model pigment for blood [9].

Mass spectrometry has proved to be an important tool for the analysis of porphyrins. This is especially true of the more volatile and robust porphyrins, which can withstand the high source temperatures required to produce gas-phase material for analysis in electron ionisation mass spectrometry (EI-MS) [26,27]. However, many biological and synthetic "biological" porphyrins are not amenable to conventional mass spectrometry. Such molecules often contain functional substituent groups which render them highly polar, involatile and thermally labile. It has, therefore, proved necessary to resort to desorption/ionisation and spraying techniques in order to characterise these materials.

The most popular techniques have been FAB [28,29] and laser desorption Fourier transform mass spectrometry (LD-FTMS) [30,31,32], although field desorption (FD) [27], ^{252}Cf-plasma desorption (PD-MS) [33], thermospray [34] and electrospray ionisation [35] have also been used to characterise a wide variety of biological, geological and synthetic porphyrin materials. However, as has been mentioned before, these techniques are all limited by the single stage nature of the volatilisation and ionisation. The desorption/ionisation techniques, such as FAB and PD-MS often suffer from extensive fragmentation, and their inherent non-selectivity precludes *in situ* analysis. The spraying techniques, on the other hand, generally only provide molecular weight information, with little fragmentation to assist in the elucidation of unknown structures. Again, the requirement for solution-phase samples precludes *in situ* analysis of real systems.

L2MS has been used previously for the analysis of porphyrin materials [9,36,37]. These studies have shown that photoionisation of laser desorbed neutral porphyrin molecules at 193 nm can produce intact molecular ions for a wide range of porphyrins. Increasing the ionisation laser power density results in the loss of substituent groups, whilst still harder ionisation leads to fragmentation of the porphyrin macrocycle. Therefore, by controlling the ionisation laser power density, both molecular weight and structural data can be obtained for porphyrin pigments. This earlier work also demonstrated that the two-step laser methodology permitted *in situ* analysis of these pigments. The porphyrin pigment, chlorophyll a, which is used to model grass stains, was detected directly from a series of organic substrates, including cotton, without recourse to extraction or pre-concentration procedures.

It was also shown by Jones et al. [36], that photoionisation of some tetraphenylporphyrins (TPPs) at 266 nm led to different mass spectra to those obtained using 193 nm. It was proposed that this wavelength dependence resulted from neutral dissociation following excitation at 266 nm. The remainder of this section will briefly discuss the results obtained by Jones et al., and describe a series of experiments which were designed in order to confirm the mechanism behind the neutral photodissociation.

4.3.1 Evidence of Class B Behaviour in MetalloTPPs

Previous studies in this laboratory on metalloTPPs showed marked differences in the mass spectra at two fixed ionisation wavelengths, 193 nm and 266 nm [36]. The molecules studied in this work were NiTPP, ZnTPP, CoTPP, CuTPP and VOTPP. In all cases, photoionisation at 193 nm resulted in the detection of the molecular ion under soft ionisation conditions. When the power density of the ionising laser was increased, typical hard ionisation mass spectra were obtained, in which the dominant fragment species were assigned as loss of one and two phenyl groups from the molecular ion, with the central metal atom being retained in the macrocycle. Loss of the phenyl groups was accompanied by loss of a number of hydrogen atoms, as has been observed previously in LD-FTMS [38] and EI-MS [39].

Photoionisation at 266 nm of CuTPP and ZnTPP produced similar spectra to those obtained using photoionisation at 193 nm. However, the behaviour of CoTPP, NiTPP and VOTPP following 266 nm photoionisation was markedly different. In each case, an intense fragment ion was observed due to the loss of the central metal from the macrocycle, with an accompanying addition of two hydrogen atoms to give the free-base TPP radical cation. This fragmentation channel was even observed at the lowest ionisation laser intensities. In fact, increasing the ionising laser power density resulted in the intensity of the molecular ion increasing relative to the free-base TPP peak.

As discussed in Chapter 2, Section 2.3.2, Gedanken et al. [40] have classified two general categories of photochemical behavior, Class A and Class B, which may be observed in multiphoton ionisation experiments. Class A describes the situation where the molecule is photoionised to form the molecular ion, which itself may then undergo further photon absorption leading to the production of fragment ions. Alternatively, a molecule is said to exhibit Class B behaviour if photodissociation occurs following absorption of the first photon, followed by photoionisation of the neutral fragment.

For all of the metalloTPPs studied, photoionisation and photofragmentation induced by 193 nm laser radiation is consistent with classic Class A behaviour.

Porphyrin Pigment	Structure
Zinc tetraphenylporphyrin **(ZnTPP)** Molecular weight = 676 u.	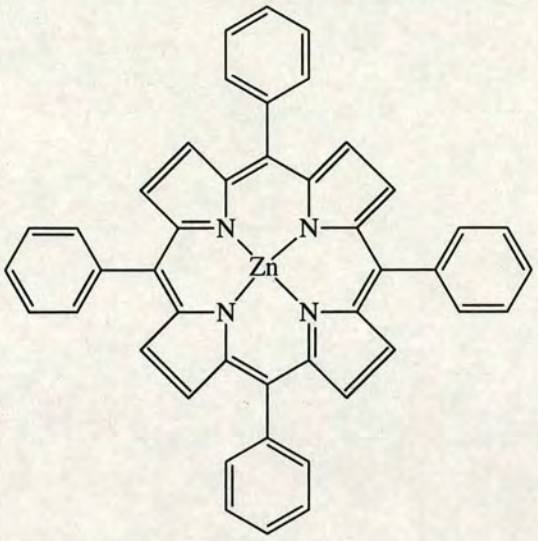
Vanadyl tetraphenylporphyrin **(VOTPP)** Molecular weight = 679 u.	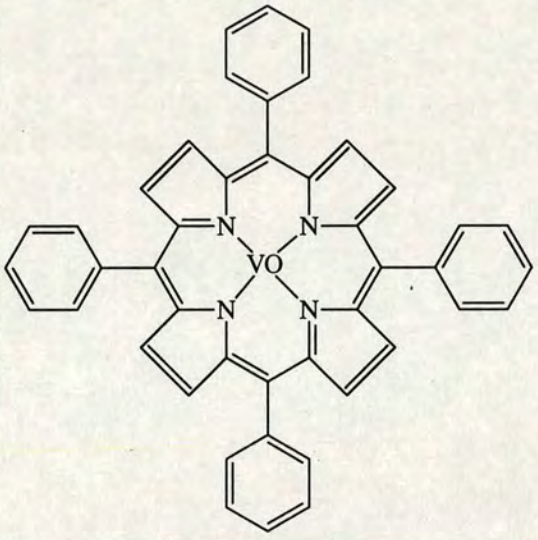

Table 4-2: Names, structures and molecular weights of the metalloTPPs studied in this work.

However, the results obtained at 266 nm were rationalised in terms of a competition between Class A and Class B behaviour. For photoionisation of CuTPP and ZnTPP at 266 nm, Class A behaviour dominates the mass spectra. However, the formation of the free-base TPP ion for CoTPP, NiTPP and VOTPP, even at very low ionising laser fluences is characteristic of Class B behaviour. At higher laser fluences, the earlier data suggested that Class A behaviour begins to compete effectively with neutral dissociation, as shown by an increase in intensity of the molecular ion. This was thought to be due to the rate of absorption of the second 266 nm photon becoming competitive with the rate of photochemical relaxation, such that both

products are observed in the mass spectra. A detailed discussion of the photochemical processes thought to be occurring for 266 nm ionisation of metalloTPPs has been given by Jones et al. [36].

4.3.2 Effect of Ionising Wavelength on Class B Behaviour

The earlier work by Jones et al. suggested that some metalloTPPs exhibited Class B behaviour following 266 nm excitation. It was therefore decided to vary the ionisation wavelength to probe for the onset of the observed neutral photodissociation. Two metalloTPPs were chosen for this study, VOTPP and ZnTPP. The structures of the molecules are shown in Table 4-2. VOTPP exhibits Class B behaviour following excitation at 266 nm, whereas ZnTPP displays conventional Class A behaviour at this wavelength. These experiments were carried out on a similar L2MS instrument at the ETH, Zürich, as part of a collaborative project with Professor Renato Zenobi. This instrument has been described in detail elsewhere [41].

Photoionisation of ZnTPP

Figure 4-15 shows a mass spectrum of ZnTPP obtained at 235 nm under partially hard ionising laser conditions. As expected, ZnTPP displayed Class A behaviour. The radical molecular cation at m/z = 676 is the base peak in the mass spectrum. There are two less intense fragment ion peaks, which are assigned as loss of one and two phenyl side groups, $[M - Ph]^+$ and $[M - 2Ph]^+$. In the earlier work of Jones et al., the relatively low resolution of the spectra obtained did not allow unit mass resolution to be achieved at this mass range. The centroids of these fragment ions in the spectra did not correspond to $[M - Ph]^+$ and $[M - Ph]^+$; rather they were assigned as $[M - Ph - 3H]^+$ and $[M - 2Ph - 2H]^+$, respectively. However, it can be seen from Figure 4-15, that even when unit mass resolution is achieved in this range, the $[M - nPh]^+$ peaks are still poorly resolved. This is indicative of metastable fragmentation, and so therefore, it is not possible to ascertain exactly how many hydrogen atoms have actually been lost during fragmentation.

In order to confirm that ZnTPP does not exhibit Class B behaviour, the photoionisation laser wavelength was varied between 240 nm and 270 nm, as shown

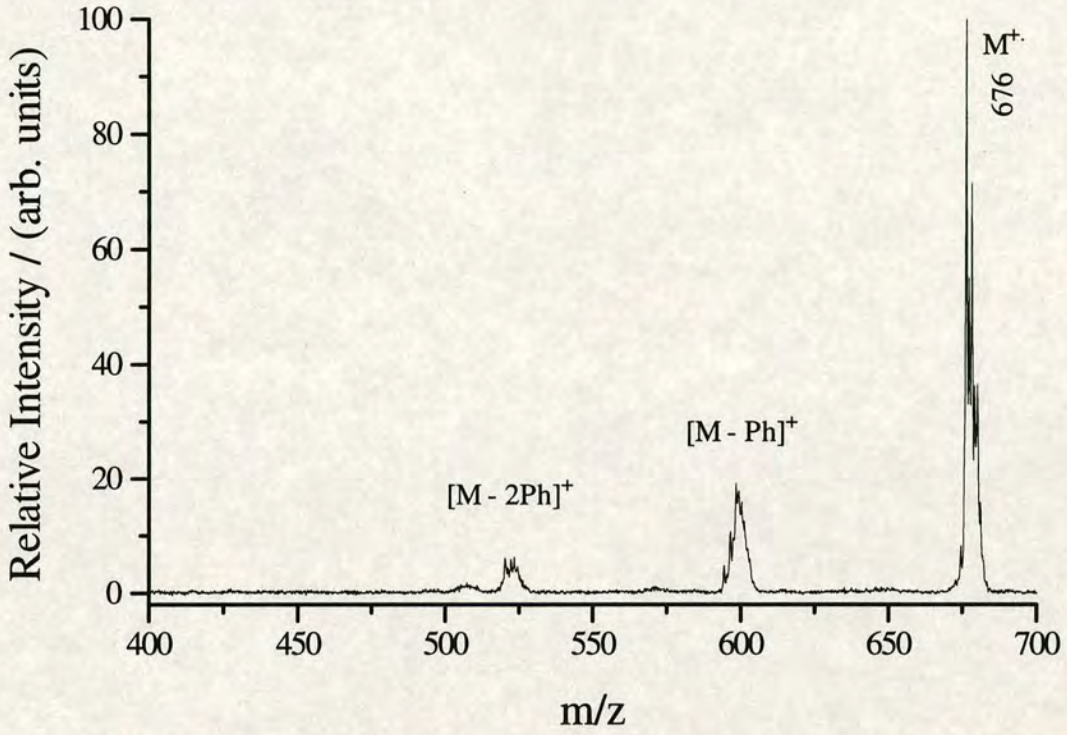

Figure 4-15: L2MS of ZnTPP obtained using 10.6 μm laser desorption and 235 nm laser photoionisation. This spectrum was obtained under partially hard ionising laser conditions in order to induce some fragmentation processes.

in Figure 4-16. Overall, it can clearly be observed that the radical molecular cation is the base peak at all of the chosen photoionisation wavelengths, with no evidence of demetallation to produce the free-base TPP. All spectra were obtained using essentially identical photoionisation laser power densities, and so the observation of an apparent increase in the observed fragmentation as the photon energy increases was initially surprising. This is probably due to the more energetic photons depositing excess energy in the molecular ion, which can be used to promote the fragmentation reactions. This type of wavelength dependent fragmentation has also been observed for other molecular classes, notably hexabenzotriazoles (Tinuvin polymer additives) and tryptophan. These will be discussed in more detail in Chapters 5 and 7, respectively. The fragments observed result from loss of the phenyl side groups, but again it is evident that the fragment peaks are very broad, and so determination of the numbers of hydrogens lost or gained is not possible. It is clearly not the mass resolving power of the instrument which is responsible for this, as demonstrated by the near unit mass resolution in the region of the molecular ion.

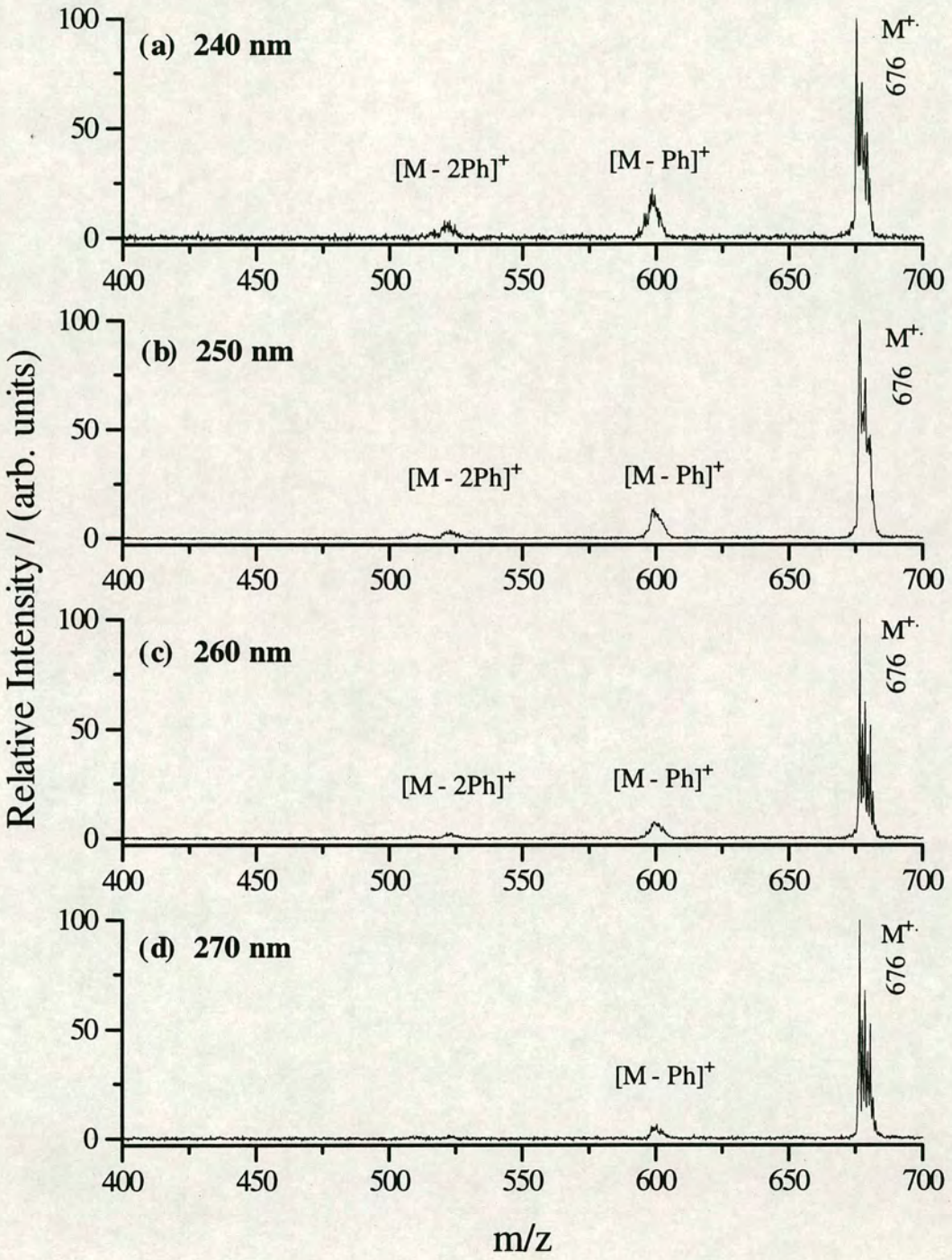

Figure 4-16: L2MS of ZnTPP obtained using 10.6 μm laser desorption and (a) 240 nm, (b) 250 nm, (c) 260 nm, and (d) 270 nm laser photoionisation. There is no evidence of demetallation of the porphyrin macrocycle at any of these ionisation wavelengths.

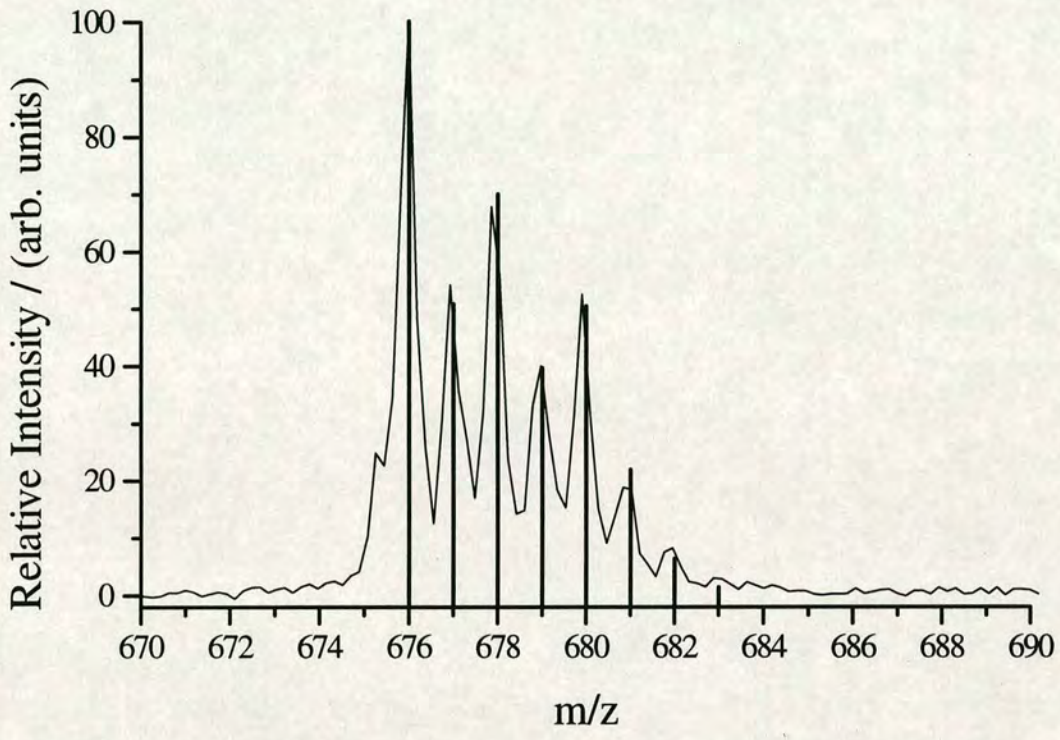

Figure 4-17: Enlargement of molecular ion region of ZnTPP, illustrating near-unit mass resolution. The solid "spiked lines" indicate the calculated isotope fingerprint of ZnTPP. This fits the experimental data very well.

Figure 4-17 shows an enlargement of the region of the molecular ion. This demonstrates that it is possible to resolve the isotope fingerprint for ZnTPP. The solid spikes show the simulated isotope fingerprint of ZnTPP, and the experimental data agrees with this very well.

Photoionisation of VOTPP

The mass spectrum of VOTPP, obtained at 250 nm under partially hard ionisation laser conditions, shown in Figure 4-18, illustrates that there is a competition between Class A and Class B behaviour. The radical molecular cation is the base peak in the mass spectrum. However, the peaks observed previously by Jones et al. as being characteristic of Class B behaviour are also observed. A signal corresponding to loss of the central "metal", VO followed by addition of two hydrogen atoms to form the free-base TPP, $[M - VO + 2H]^+$ is observed. In addition to this, a peak is also observed at m/z = 661, which can be assigned to loss of the oxygen from VO, along with a further two hydrogen atoms, giving $[M - O - 2H]^+$. However, there are also

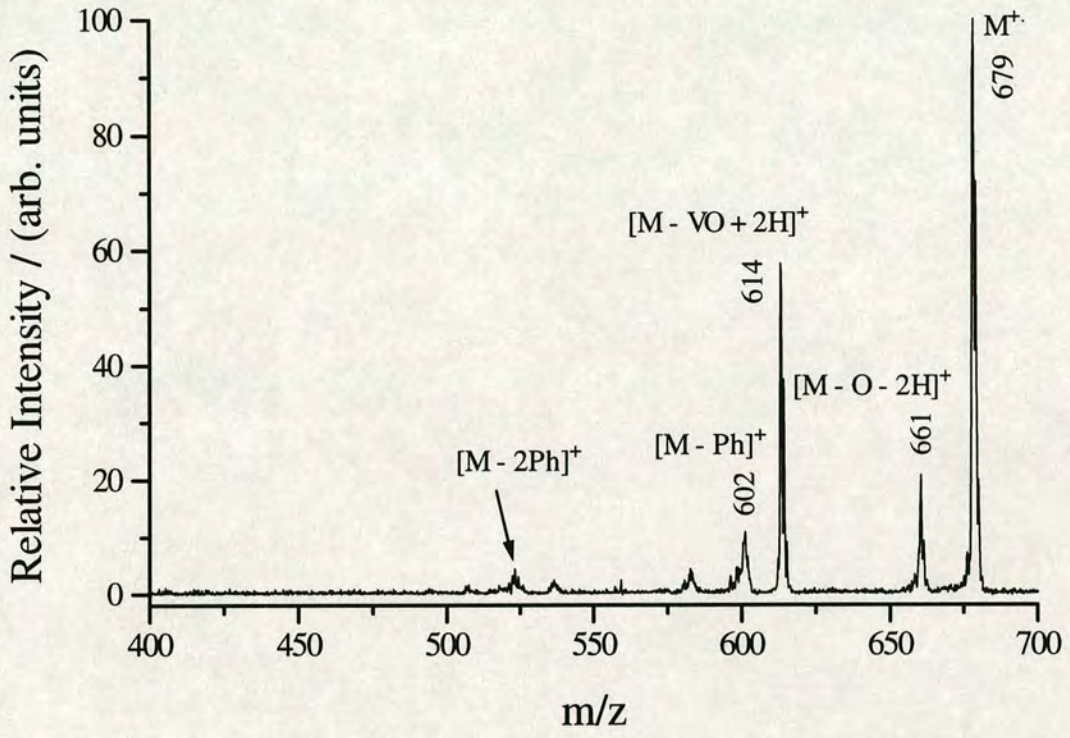

Figure 4-18: L2MS of VOTPP obtained using 10.6 μm laser desorption and 250 nm laser photoionisation. This spectrum was obtained using partially hard ionisation conditions in order to induce some fragmentation.

signals present in the mass spectrum indicative of Class A behaviour. As well as the molecular ion, signals are observed corresponding to loss of one and two phenyl groups, $[M - Ph]^+$ and $[M - 2Ph]^+$. This shows, therefore that the fragmentation channels corresponding to both Class A and Class B behaviour are in competition with each other.

A series of experiments were then carried out in which the ionising laser wavelength was varied between 235 nm and 270 nm. Figure 4-19 shows the mass spectra obtained. It can easily be observed that as the wavelength becomes longer, and the associated photon energy smaller, the intensity of the free-base TPP fragment increases. Ionisation at 235 nm, as shown in Figure 4-19a, results in a mass spectrum dominated by Class A behaviour. The molecular ion is the base peak, with the Class B fragment ions low in intensity. There is also evidence of some side group loss corresponding to $[M - Ph]^+$ and $[M - 2Ph]^+$. At the other end of the wavelength scale, Figure 4-19d shows the mass spectrum obtained when 266 nm radiation was used for

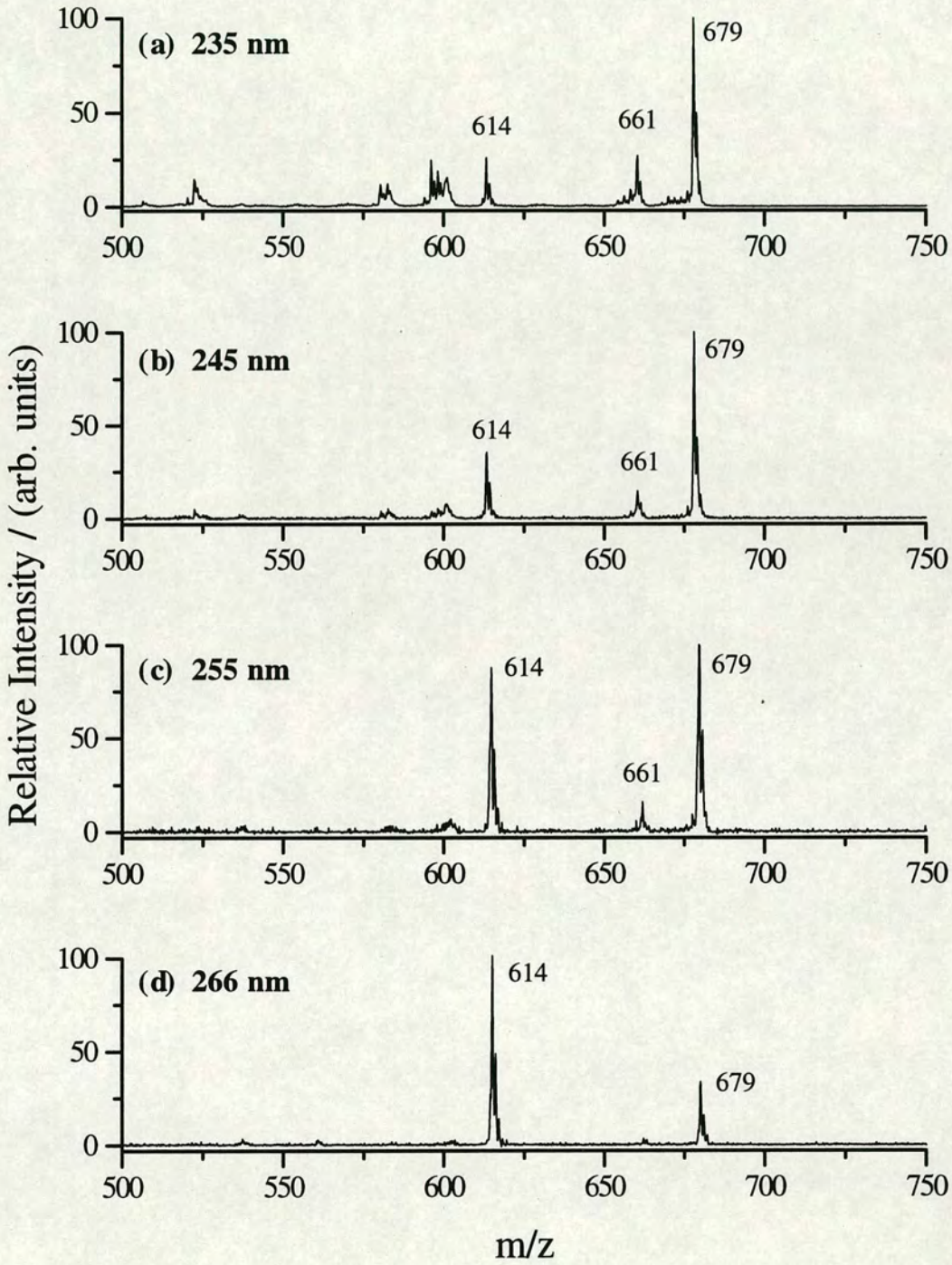

Figure 4-19: L2MS of VOTPP obtained using 10.6 μm laser desorption and (a) 235 nm, (b) 245 nm, (c) 255 nm, and (d) 266 nm laser photoionisation. It can clearly be observed that as the laser wavelength is increased, demetallation of the porphyrin macrocycle is increased.

photoionisation. In this case, Class B behaviour appears to dominate the mass spectrum, with the demetallation product, $[M - VO - 2H]^+$ constituting the base peak of the mass spectrum. In comparison, the intensity of the molecular ion is very small, and there is little evidence of the other characteristic "Class A" fragments obtained at 235 nm, $[M - Ph]^+$ and $[M - 2PH]^+$. Overall, the clear trend in using ionisation wavelengths from 235 nm to 270 nm, is for a continuous shift from Class A to Class B behaviour. This is illustrated more clearly in Figure 4-20. This shows a plot of the ratio of the molecular ion intensity to the free-base TPP intensity, $M^{+\cdot}$: $[M - VO + 2H]^+$ against photoionising laser wavelength. It can clearly be observed that as the photon energy increases, the $M^{+\cdot}$: $[M - VO + 2H]^+$ ratio increases, indicating that Class A behaviour is becoming progressively more dominant.

Discussion

The differing propensities for Class A versus Class B behaviour in these molecules following 266 nm excitation was rationalised by Jones et al. [36] by considering photophysical properties resulting from their magnetic characteristics; ZnTPP is diamagnetic, whilst VOTPP is paramagnetic. The diamagnetic ZnTPP is known to be fluorescent, with absorption of a single 266 nm photon resulting in the population of a high-lying vibronic level in the S_2 state. Intramolecular conversion of electronic to vibrational energy then occurs on the picosecond timescale, until the S_1 state is reached. This state is thought to have a lifetime of 3 ns, and is 2.17 eV above the vibrationless ground state [42]. Given that metalloTPPs typically have IPs in the region of 6.3 - 6.5 eV [43], then this state can be single-photon ionised by a 266 nm photon (4.66 eV). Further fragment ions, such as loss of phenyl side groups, are produced by subsequent photon absorption in the molecular ion.

The results obtained in this work support this argument. Since 266 nm radiation is sufficiently energetic to ionise out of the S_1 state, then the more energetic wavelengths used here, from 4.66 eV to 5.28 eV, will be able to do likewise. This may also help to rationalise the appearance of fragment ions upon photoionisation with more energetic radiation observed in Figure 4-16. The excess energy available to the molecular ion from these more energetic photons may be sufficient to populate

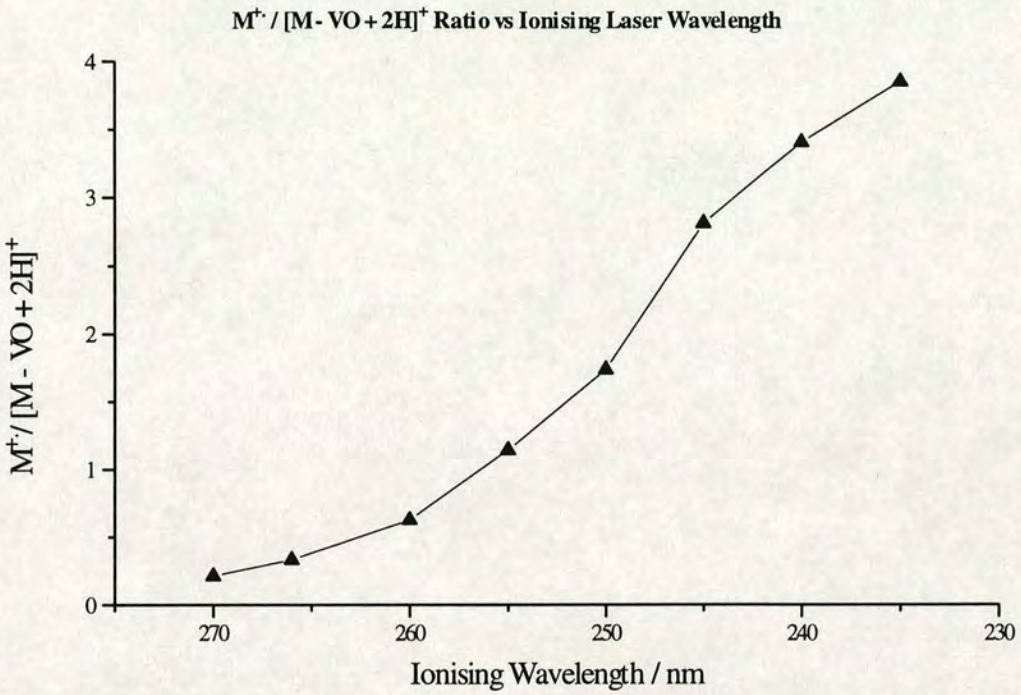

Figure 4-20: Plot of $M^{+\cdot}$:$[M-VO+2H]^+$ versus ionising laser wavelength. This clearly shows that as the laser photon energy is increased, Class A photoionisation behaviour begins to dominate over Class B behaviour.

states above the appearance potential for the formation of fragment ions. Recent work on the amino acid, tryptophan [44], has also shown that internal energy imparted to the molecule during the laser desorption process can be carried through into the molecular ion, and may used to promote fragmentation processes. This will be discussed in detail in Chapter 7.

For the paramagnetic VOTPP, the single unpaired d electron of the VO complex is coupled to the $\pi\pi^*$ states of the porphyrin macrocycle, giving rise to singdoublet (^2S), tripdoublet (^2T) and tripquartet (^4T) states [45]. Intersystem crossing from the singdoublet to the tripdoublet manifolds is spin allowed, and is thought to occur on the pico- or sub-picosecond timescale. For example, the $^2S_1$ state of CuTPP is known to decay to the tripdoublet manifold in less than 350 fs [46].

Although little is known about the photophysics of VOTPP, it is known that it is luminescent. The mechanism for the observed Class B behaviour of VOTPP at 266 nm, proposed by Jones et al. [36], suggests that the $^2T_1$ state lies within 4.66 eV of

the IP, whilst the $^4T_1$ state is more than 4.66 eV below the IP. Intersystem crossing (ISC) from the ^2S state populates the $^2T_1$ state. At low ionisation laser power densities, the rate of ISC from $^2T_1$ to $^4T_1$ is greater than the rate of absorption of the second 266 nm photon required to ionise from the $^2T_1$ state, and neutral photodissociation predominates (i.e., Class B behaviour). However, as the power density of the ionising radiation is increased, the rate of absorption by the $^2T_1$ state begins to compete with ISC to the $^4T_1$, and molecular ionisation is observed in parallel with neutral photodissociation (i.e., both Class A and Class B behaviour are observed).

The spectra in Figure 4-19 also support this hypothesis. There are two main reasons why ionisation using more energetic photons could result in a trend towards Class A behaviour. Jones et al. rationalised the Class A behaviour of VOTPP at 193 nm by proposing that the intermediate state would be a long-lived Rydberg state, which following absorption of a second 193 nm photon produced at radical molecular ion. Although it is possible that ionisation using more energetic photons, such as 235 nm (5.28 eV), as used to record the spectrum in Figure 4-19d, could populate such long-lived Rydberg states, these photons are unlikely to be sufficiently energetic.

A more likely explanation is that the more energetic photons allow photoionisation of the lower-lying $^4T_1$ state to occur. Consider the two extreme cases at 266 nm and 235 nm, illustrated in Figure 4-19. Following ISC from the $^2T_1$ state, photoionisation out of the $^4T_1$ state is not possible at 266 nm, as demonstrated by Jones et al. However, photoionisation of this state can occur at 235 nm. This suggests, therefore, that the $^4T_1$ state lies within 5.28 eV of the IP, but is more than 4.66 eV below this level.

4.4 Concluding Remarks

These experiments have illustrated the flexibility of L2MS for generating both molecular weight and structural data for azo dyes and porphyrin pigments. By

controlling the ionising laser intensity and wavelength, a considerable degree of control over the appearance of the resulting mass spectra can be exercised.

For simple azo dye molecules, where the substituents are unable to interfere with the azo linkage, complementary structural data can be obtained by photoionising using the two fixed ionisation wavelengths, 193 nm and 266 nm. At 193 nm, molecular ion information is available in the form of adduct ions, with C—N cleavage products dominating the fragmentation, whereas photoionisation using 266 nm radiation provides mass spectra with characteristic cleavage of the azo bond. This effectively demonstrates that photoionisation allows control over the fragmentation which is not possible using other mass spectrometric techniques. The data presented for these simple azo dye molecules, illustrates that the photophysiscs of the intermediate states can be exploited to selectively populate particular vibrational modes. This can lead to the fragmentation of bonds which are not the weakest bonds in the molecule. In contrast, other techniques deposit large amounts of energy in the molecule, which is redistributed statistically with the result that, in general, the weakest bonds are fragmented.

In some cases it is possible to differentiate between isomeric species by using a single photoionisation wavelength. When certain substituent groups are present *ortho* to the azo bond, the ability of these substituents to interfere with the azo linkage influences the fragment ions appearing in the mass spectrum. When hydroxy substituents are present *ortho* to the azo bond, tautomerisation may be responsible for the differences in the observed fragments, whereas for carboxylic acid substituents, steric factors are implicated in controlling which fragmentation products are formed.

In the case of porphyrin pigments, the nature of the excited intermediate state is shown to have a marked effect on the appearance on the mass spectra. At 193 nm, all TPPs studied resulted in the formation of molecular ions, exhibiting the expected Class A photoionisation behaviour. However, at longer wavelengths, some metalloTPPs showed evidence of neutral photodissociation, followed by photoionisation of the neutral fragment. The onset of this neutral photodissociation channel was probed by varying the ionisation laser wavelength. It was found that this

photodissociation channel did not open suddenly; rather the effects of Class B behaviour were found to become progressively more dominant with increasing wavelength. This work provided confirmation of the mechanism for this photo-dissociative ionisation first proposed by Jones et al [36].

In the case of both azo dyes and porphyrin pigments, it is possible to take this fundamental information, and use it to great advantage for analytical purposes. The use of different photoionisation laser wavelengths and power densities makes it possible to generate both molecular weight information and characteristic fragments ions. These data can be used to unambiguously identify the molecules under analysis, to the extent that, in some cases, isomeric species can even be distinguished. If these molecular classes are to be used as model stains for analysis from complex matrices, the highly specific signatures obtained using different ionisation laser wavelengths and intensities should prove very valuable.

References

[1] H. Zollinger, *Color Chemistry: Synthesis, Properties and Applications of Organic Dyes and Pigments*, VCH: New York, 1987, pp 321-324.

[2] V. Parameswaren, A. V. Rama Rao, K. Venkateraman, *Indian J. Chem.*, **12**, 785, (1974)

[3] J. J. Monaghan, M. Barber, R. Bordoli, R. D. Sedgewick, A. N. Tyler, *Org. Mass Spectrom.*, **17**, 529, (1982)

[4] J. J. Monaghan, M. Barber, R. Bordoli, R. D. Sedgewick, A. N. Tyler, *Org. Mass Spectrom.*, **17**, 569, (1982)

[5] L. Pannell, E. Sokoske, H. Fales, R. Tate, *Anal. Chem.*, **57**, 1060, (1985)

[6] R. G. Cooks, S. M. Scheifers, S. Veerma, *Anal. Chem.*, **55**, 2260, (1983)

[7] L. D. Betowski, T. L. Jones, J. Yinon, *Biomed. Environ. Mass Spectrom.*, **18**, 445, (1989)

[8] (a) J. Grotemeyer, K. Walter, U. Boesl, E. W. Schlag, *Org. Mass Spectrom.*, **21**, 645, (1986); (b) J. Grotemeyer, K. Walter, U. Boesl, E. W. Schlag, *Org. Mass Spectrom.*, **78**, 69, (1987); (c) F. Engelke, J. H. Hahn, W. Henke, R. N. Zare, *Anal. Chem.*, **59**, 909, (1987); (d) L. Li, D. M. Lubman, *Rev. Sci. Instrum.*, **59**, 557, (1988)

[9] M. J. Dale, *PhD Thesis, The University of Edinburgh*, 1994

[10] M. J. Dale, A. C. Jones, P. R. R. Langridge-Smith, K. F. Costello, P. G. Cummins, *Anal. Chem.*, **65**, 793, (1993)

[11] R. C. Beavis, J. Lindner, J. Grotemeyer, E. W. Schlag, *Chem. Phys. Lett.*, **146**, 310, (1988)

[12] A. J. Borgerding, R. A. Hites, *J. Am. Mass Spectrom.*, **5**, 407, (1994)

[13] J. Griffiths, *Chem. Soc. Rev.*, **481**, (1972)

[14] J. Jortner, S. A. Rice, R. M. Hochstrasser, *Advan. Photochem.*, **7**, 149, (1969)

[15] F. W. McLafferty, T. Turecek, *Interpretation of Mass Spectra, 4th Ed.*, University Science Books, California, (1993)

[16] K. M. Smith, Ed., *Porphyrins and Metalloprphyrins*, Elsevier, Amsterdam, (1975)

[17] D. Dolphin, Ed., *The Porphyrins*, Wiley, New York, Vols I-VII, (1978)

[18] E. W. Barker, J. W. Louda, in *Biological Markers in the Sedimentary Environment*, R. B. Johns, Ed., Elsevier, Amsterdam, 125, (1986)

[19] R. H. Filby, G. J. Van Berkel, in *Metal Complexes in Fossil Fuels*, R. H. Filby, J. F. Branthaver, Eds., American Chemical Society, Washington, 2, (1987)

[20] D. R. Doiron, C. J. Gomer, Eds., *Porphyrin Localisation and Treatment of Tumors,* A. R. Liss, Inc., New York, (1984)

[21] D. L. Drabkin, in *The Porphyrins*, D. Dolphin Ed., Wiley, New York, Vol I, 29, (1978)

[22] R. P. Philp, J.-N. Oung, *Anal. Chem.*, **60**, 889A, (1988)

[23] D. Gust, T. A. Moore, *Science*, **244**, 35, (1989)

[24] J. Deisenhofer, H. Michel, *Angew. Chem. Int. Ed. Engl.*, **101**, 872, (1989)

[25] J. T. Groves, R. Neumann, *J. Am. Chem. Soc.*, **111**, 2900, (1989)

[26] K. M. Smith, in *Porphyrins and Metalloporphyrins*, K. M. Smith, Ed., Elsevier, Amsterdam, 381, (1975)

[27] Budzikiewicz, in *The Porphyrins*, D. Dolphin Ed., Wiley, New York, Vol III, 395, (1978)

[28] M. Barber, R. S. Bordoli, R. D. Sedgewick, A. N. Tyler, *Biomed. Mass Spectrom.*, **8**, 491, (1981)

[29] M. Barber, R. S. Bordoli, G. J. Elliot, R. D. Sedgewick, A. N. Tyler, *Anal. Chem.*, **54**, 645A, (1982)

[30] R. S. Brown, C. L. Wilkins, *J. Am. Chem. Soc.*, **108**, 2447, (1986)

[31] R. S. Brown, C. L. Wilkins, *Anal. Chem.*, **58**, 3196, (1986)

[32] T. H. Nguyen, P. S. Clezy, G. D. Willett, G. L. Paul, J. Tann, P. J. Derrick, *Org. Mass Spectrom.*, **26**, 215, (1991)

[33] J. E. Hunt, R. D. Macfarlane, J. J. Katz, R. C. Dougherty, *J. Am. Chem. Soc.*, **103** 6775, (1981)

[34] M. A. Mabud, E. A. Prannkoch, P. J. Gill, P. A. Dreifuss, *Proceedings of the 38th ASMS Conference on Mass Spectrometry and Allied Topics*, Tuscon, AZ, 1057, (1990)

[35] G. J. Van Berkel, S. A. McLuckey, G. L. Glish, *Anal. Chem.*, **63**, 1098, (1991)

[36] A. C. Jones, M. J. Dale, G. A. Keenan, P. R. R. Langridge-Smith, *Chem. Phys. Lett.*, **219**, 174, (1994)

[37] M. J. Dale, K. F. Costello, A. C. Jones, P. R. R. Langridge-Smith, *J. Mass Spectrom.*, **31**, 590, (1996)

[38] L. M. Nuwaysair, C. L. Wilkins, *Anal. Chem.*, **61**, 689, (1991)

[39] A. D. Adler, J. H. Green, M. Mautner, *Org. Mass Spectrom.*, **3**, 955, (1970)

[40] A. Gedanken, M. B. Robin, N. A. Kuebler, *J. Phys. Chem.*, **86**, 4096, (1982)

[41] P. Voumard, Q. Zhan, R. Zenobi, *Rev. Sci. Instrum.*, **25**, 3393, (1993)

[42] U. Even, J. Magen, J. Jortner, J. Friedman, H. Levanon, *J. Chem. Phys.*, **77**, 4374, (1982)

[43] S. C. Khandelwhal, J. L. Roebber, *Chem. Phys. Lett.*, **34**, 355, (1975)

[44] Q. Zhan, S. J. Wright, R. Zenobi, *submitted to J. Am. Soc. Mass Spectrom.*, (1996)

[45] R. L. Ake, M. Gouterman, *Theoret. Chim. Acta*, **15**, 20, (1969)

[46] J. Rodriguez, C. Kirmaier, D. Holten, *J. Am. Chem. Soc.*, **111**, 6500, (1989)

Chapter 5

Analysis of Polymers and Polymer Additives Using L2MS

5.1 Introduction

Commercial polymers are, by their very nature, extremely complex systems, comprising the polymer matrix itself together with many other minor components, such as fillers, plasticisers, antioxidants, UV and thermal stabilisers as well as colouring agents. The characterisation of such commercial polymer formulations is, therefore, a challenging analytical problem. In order to fully characterise a commercial polymer formulation using mass spectrometry, it is necessary to obtain information on the molecular weight distribution, the repeat unit and terminating groups, and whether the polymer is cyclic, extensively branched or cross-linked. It is also necessary to determine the presence and nature of additives and impurities in the polymer matrix.

Previous work in this laboratory has concentrated on characterising aromatic polymers using L2MS [1]. It was shown that this technique is capable of generating useful analytical data on aromatic polymer systems with molecular weights below 4000 u. It was possible to determine both the repeat unit and the terminating groups on a number of aromatic polymer systems, including polystyrene. Oligomer distributions were also obtained. However, molecular weight averages calculated from this data were consistently lower than values quoted by the manufacturers. At present, it is not clear exactly why these polymer distributions are "shifted" to low mass, but fragmentation during the desorption process and decreasing ionisation efficiency with increasing mass are potential causes. The latter possibility is discussed in more detail in Chapter 7.

The work described in this chapter focused primarily on the problems of determining the presence of additives within commercial polymer formulations. This is a complex problem in its own right. Many polymer additives are thermally labile, whilst others are specifically designed to decompose during polymer processing. Moreover, some additives are often present in low concentrations (0.01 - 5 wt %). It is clear, therefore, that any chosen analytical technique must be sensitive, selective and must maintain the integrity of mixture composition.

Because of the complexity of polymer formulations, extraction of the additive mixture from the polymer matrix is usually required, often followed by chromatographic separation and purification. However, there are inherent difficulties in using chromatographic techniques. Gas chromatography (GC) is limited in application by the high molecular weight, thermal lability and polar nature of many additives [2]. Although HPLC is widely used, the lack of a universal detector compatible with all liquid mobile phases restricts its effectiveness in this area [3,4,5]. Supercritical fluid chromatography (SFC) has previously been successfully employed for the separation of additives in polymer extracts, and, when coupled with off-line Fourier transform infra-red detection, complementary functional group information on unknown additives has been obtained [6]. However, due to the chemical similarity of many additives, it is not always possible to identify the exact additive used.

Mass spectrometric analysis of polymer extracts has also proved challenging [7]. Electron impact (EI-MS) mass spectra are often difficult to interpret due to the high concentration of processing oils in the extracts and extensive fragmentation of the molecular ions [8]. Desorption/ionisation techniques such as field desorption (FD-MS) and fast atom bombardment (FAB-MS) have been found to be the most effective means for analysing polymer extracts [9,10]. FD-MS has proved to be a particularly useful technique, since molecular ion abundances are high, as shown in recent work on mixtures of pure polymer additives [11]. Electrospray mass spectrometry (ESI-MS and ESI-MS/MS) has also recently been used for the analysis

of polymer additive mixtures. Mechanisms and fragmentation pathways for both low and high energy CID spectra were investigated in this work [12].

There are many advantages to be gained in being able to chemically speciate additives *directly* from the polymer matrix. Extraction and separation procedures are often time consuming, rendering additive characterisation a slow and laborious process. Furthermore, there is the possibility that the extraction procedure may compromise the integrity of the additive mixture, leading to an inaccurate picture of the polymer composition. Early attempts at mass spectrometric characterisation of bulk polymer samples have centered on direct thermal desorption of additives from the bulk polymer, followed by EI-MS, chemical ionisation (CI-MS) [13] or field ionisation (FI-MS) [14]. However, this approach is limited to polymer additives which are stable or can provide meaningful fragment ions at elevated temperatures. Lattimer [15] has recently reported the use of thermal desorption and pyrolysis mass spectrometry (Py-MS) for the detection and identification of various organic additives in polypropylene polymers. Desorption/ionisation methods, such as FAB [16], laser desorption (LD) [17,18] and secondary ion mass spectrometry (SIMS) [19] have also been applied for the analysis of additives from bulk polymer samples. However, these single-step techniques suffer to varying degrees from matrix interference in the resulting mass spectra.

L2MS is a technique which has great potential for the direct analysis of molecular species from complex host matrices [20,21,22,23]. The two-step approach circumvents many of the problems, described above, that have been encountered with other techniques. A pulsed CO_2 laser is used to desorb the analyte into the gas phase as a neutral species, *directly* from the sample of interest. A second pulse from a UV laser is then used to postionise these gas phase neutral species, generally using a resonance enhanced multiphoton ionisation (REMPI) scheme. The benefits of this two-step approach lie in the spatial and temporal separation of the desorption and ionisation events, thereby enabling the independent optimisation of each process. This provides a number of advantages for the *in situ* analysis of bulk polymer samples, namely (i) desorption of neutral target molecules from the host polymer

matrix with minimal decomposition, (ii) soft ionisation of the desorbed neutral species, resulting in readily interpretable mass spectra, (iii) selective ionisation of polymer additives which have a significant one-photon absorption cross section at the chosen ionisation wavelength, and (iv) highly sensitive detection of many polymer additive species.

The L2MS technique has previously been successfully used for the analysis of polymer systems. Polystyrene samples with molecular weights up to m/z = 4000 can be characterised, as discussed above [1], and low molecular weight electro-polymerised indoles have also been readily detected [24]. Lustig and Lubman have used L2MS to selectively detect aromatic polymers in aliphatic polymer blends [25,26]. In addition, Lykke and co-workers have shown that it is possible to selectively detect aromatic polymer additives vapourised from rubber vulcanizates by careful choice of the ionisation wavelength [27].

The work presented here demonstrates the potential of L2MS for rapid generation of readily interpretable mass spectra of polymer additives directly from their host polymer matrices [28]. The polymer additives that have been studied consist of two main classes, namely antioxidants and UV stabilisers. The antioxidants are either phenolic or phosphite antioxidants, whilst the UV stabilisers all belong to the Tinuvin class of molecules (hydroxyphenylbenzotriazoles). Mass spectra were initially recorded for the pure additives, using 266 nm and 193 nm laser photoionisation. The two different ionisation laser wavelengths result in markedly different mass spectra. These mass spectral differences are a valuable aid in the unambiguous identification of the additives. The use of L2MS for *in situ* analysis of some additives directly from industrial polyoxymethylene (POM) and polypropylene (PP) formulations is also demonstrated. The spectra obtained show that not only is it possible to directly detect these additives in the polymer formulations, but also that chemical changes undergone by antioxidants, due either to processing or aging, can also be observed. The potential of L2MS for depth profiling of polymers additives from the surface into the bulk is also discussed.

Trivial Name	Chemical Name	Structure	MW/u
Irganox 1330	1,3,5,-tris(3,5-di-*tert*-butyl-4-hydroxybenzyl)-2,4,6,trimethylbenzene	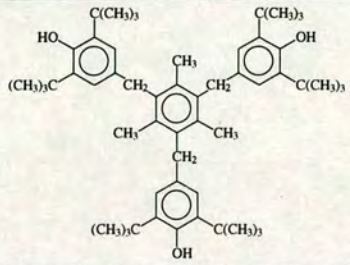	774
Irganox 1076	octadecyl-3-(3,5-di-*tert*-butyl-4-hydroxyphenyl) propionate	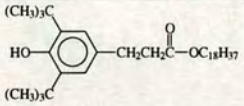	530
Irgafos 168	tris(2,4-di-*tert*-butylphenyl) phosphite	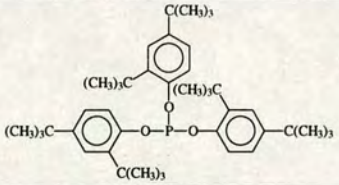	646
Santo White	4,4'-butylidene bis-6-(4-methyl-2-*tert*-butylphenol)	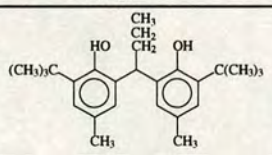	382
Tinuvin P	2-(2'-hydroxy-5'-methylphenyl)-2*H*-benzotriazole	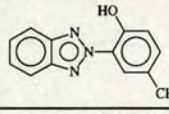	225
Tinuvin 326	2-(2'-hydroxy-3'-methyl-5'-*tert*-butylphenyl)-2*H*-5-chlorobenzotriazole	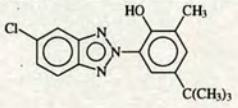	315
Tinuvin 327	2-(2'-hydroxy-3',5'-di-*tert*-butylphenyl)-2*H*-5-chlorobenzotriazole	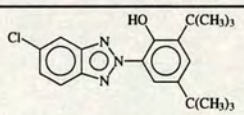	357
Tinuvin 320	2-(2'-hydroxy-3',5'-di-*tert*-butylphenyl)-2*H*-benzotriazole	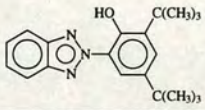	323
Tinuvin 343	2-(2'-hydroxy-3'-*tert*-butyl-5'-(1-methyl)-propylphenyl)-2*H*-benzotriazole	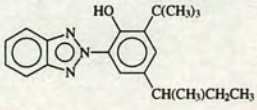	323
Tinuvin 329	2-(2'-hydroxy-5'-(1,1,3,3-di-methyl)-butylphenyl)-2*H*-benzotriazole	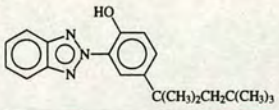	323

Table 5-1: Nomenclature and Structure of Polymer Additives

Although this work was primarily concerned with the *in situ* detection of additives directly from the polymer matrix, information on the polymer itself, such as the repeat unit and terminating groups, would also be useful. The final part of this chapter will show that there are strategies available, which allow the L2MS technique to provide useful information on the polymer matrix itself, even in cases where the polymer does not absorb UV radiation.

5.2 L2MS of Pure Polymer Additives

The ultimate aim of using L2MS for polymer additive characterisation was to provide a means for direct detection of these compounds in polymers. Prior to undertaking such experiments, L2MS spectra were first recorded for samples of the pure additives. The additives examined are shown in Table 5-1; they consist of phenolic and phosphite antioxidants, and Tinuvin UV stabilisers. All samples were deposited from solution in acetone onto a stainless steel substrate and studied using both 266 nm and 193 nm photoionisation.

5.2.1 Antioxidants

The mass spectra obtained for Irganox 1330, and Irganox 1076 using 266 nm and 193 nm photoionisation are shown in Figure 5-1. In the case of Irganox 1330, the spectra at both of these wavelengths are dominated by the molecular ion peak at m/z = 774. However, it is evident that 266 nm photoionisation results in the production of different fragment ions to those observed at 193 nm. At 266 nm, a fragment is observed at m/z = 556. This is thought to result from loss of a (3,5-di-*tert*-butyl-4-hydroxybenzyl) side group, with a concomitant hydrogen rearrangement. A weaker fragment peak at m/z = 57, due to the *tert* -butyl ion, can also be observed.

Photoionisation of Irganox 1330 at 193 nm produces fragments at m/z = 57, 219 and 569. The fragment at m/z = 569 corresponds to the loss of a (3,5-di-*tert*-butyl-4-phenol) side group via direct cleavage, without any hydrogen rearrangement. The peak at m/z = 219 is characteristic of positive ion mass spectra of dibutyl phenols and corresponds to the (3,5-di-*tert*-butyl-4-hydroxybenzyl) ion [12,29]. The peak at m/z = 57 again corresponds to the *tert*-butyl ion.

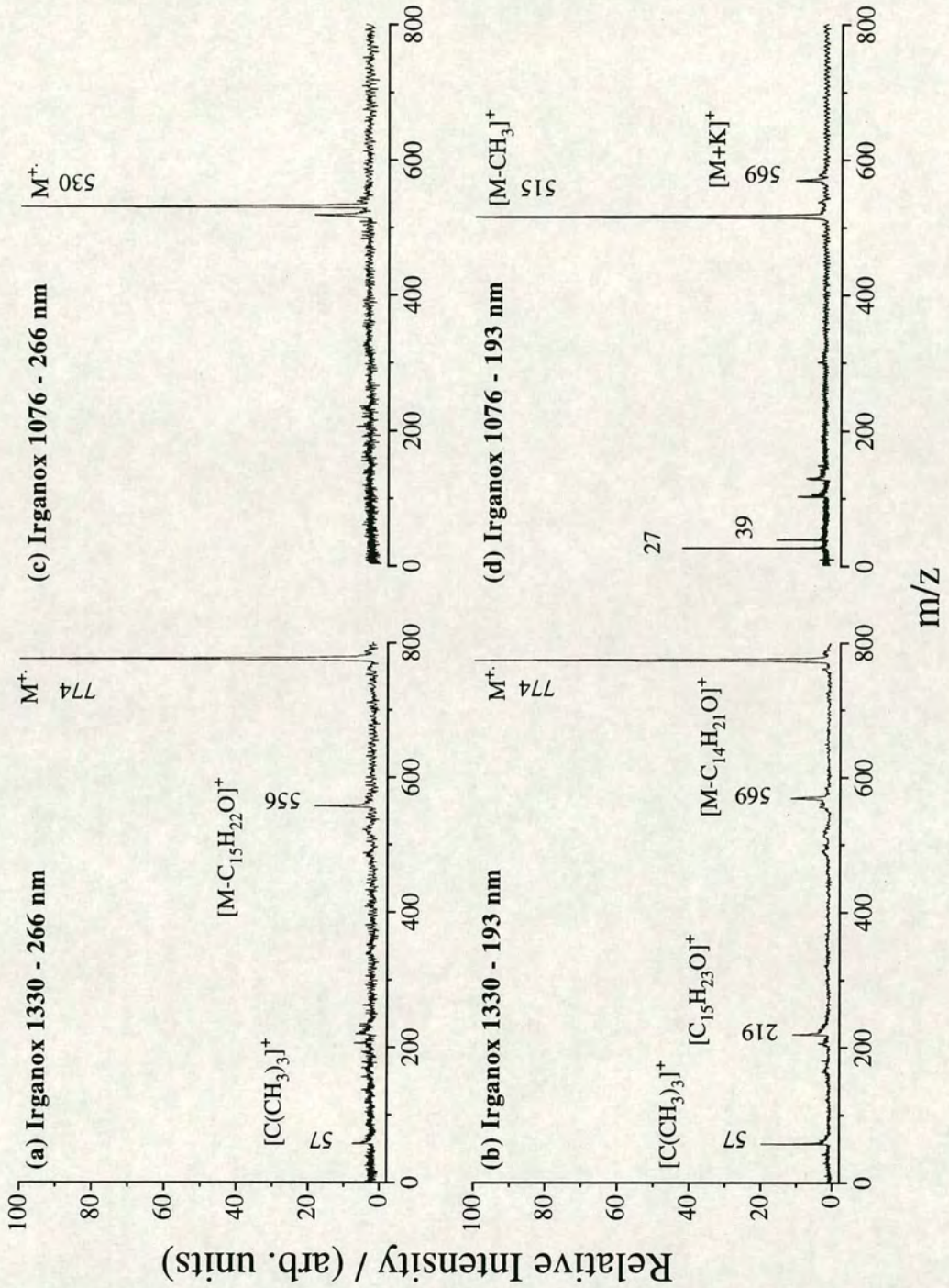

Figure 5-1: L2MS spectra of Irganox 1330 using (a) 266 nm and (b) 193 nm photoionisation; Irganox 1076 using (c) 266 nm and (d) 193 nm photoionisation.

Different mass spectra are also observed at these ionisation wavelengths for Irganox 1076, as shown in Figure 5-1c and d. When 266 nm radiation is used, the molecular ion can be clearly identified at m/z = 530. At 193 nm, however, no molecular ion peak is observed. Instead, the base peak in the mass spectrum is at m/z = 515, corresponding to the loss of a methyl radical from the molecular ion. A weak signal is also observed at m/z = 569, corresponding to the potassium adduct. Alkali metal adducts have often been observed in L2MS spectra at 193 nm, and are thought to arise from single photon ionisation of the alkali metal followed by cation attachment [30]. The low mass signals at m/z = 27 and 39 are probably due to aluminium and potassium ablated from the substrate.

The spectra obtained at 266 nm and 193 nm for Irgafos 168 and Santo White powder are shown in Figure 5-2. Irgafos 168, which is a phosphite antioxidant, once again displays a marked difference in the mass spectra obtained using these different photoionisation wavelengths. At 266 nm, the molecular ion at m/z = 646 is the base peak in the mass spectrum. A less intense fragment peak is also observed at m/z = 441, which corresponds to the loss of a (2,4-di-*tert*-butylphenyl)–O side group via direct cleavage. However, for photoionisation at 193 nm, this fragment ion is the base peak in the spectrum, and there is no signal corresponding to the molecular ion. A prominent fragment peak at m/z = 57, due to the *tert*-butyl ion, can also be observed.

Figure 5-2c shows the mass spectrum obtained for Santo White powder using 266 nm photoionisation. The molecular ion at m/z = 382 is the base peak in the spectrum, with the fragment peak at m/z = 339 corresponding to the loss of a propyl radical [$\cdot C_3H_7$] from the molecular ion. In the 193 nm photoionisation mass spectrum, shown in Figure 5-2d, no molecular ion signal is observed. The only significant peak in this mass spectrum is due to the fragment at m/z = 339, which is assigned, as before, to the loss of a propyl radical [$\cdot C_3H_7$] from the molecular ion.

In summary, for all the antioxidants studied the mass spectra obtained using photoionisation at 266 nm are dominated by molecular ion signals, with very little fragmentation. With the exception of Irganox 1330, photoionisation using 193 nm

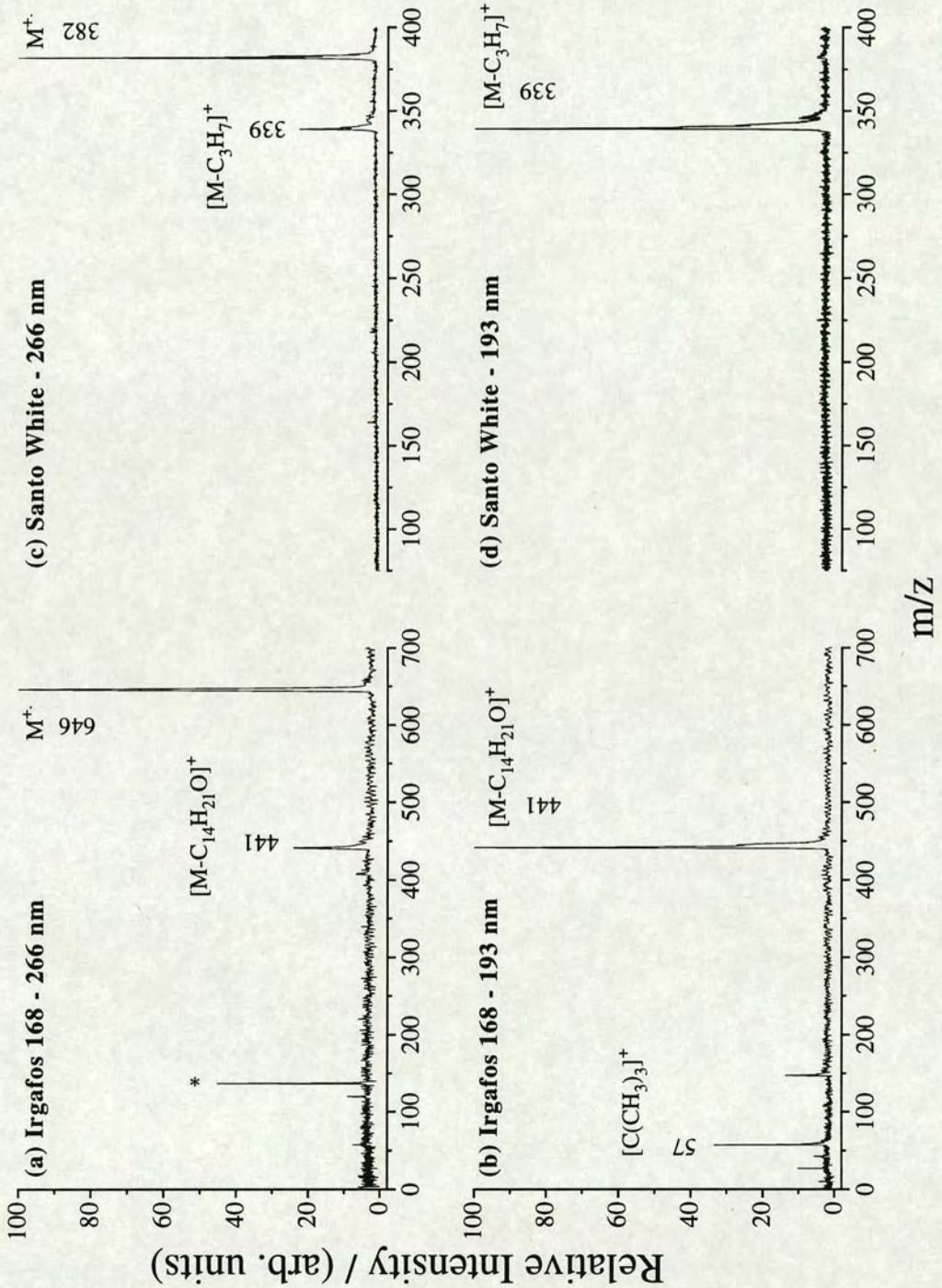

Figure 5-2: L2MS spectra of Irgafos 168 using (a) 266 nm and (b) 193 nm photoionisation; Santo White powder using (c) 266 nm and (d) 193 nm photoionisation.

radiation generated little or no molecular ion signal. There are two possible explanations for this apparent wavelength dependence. Most organic molecules have ionisation potentials (IP) in the range 7-10 eV. The energy of 266 nm photons is ca. 4.66 eV, whereas a 193 nm photon has an associated energy of 6.42 eV. In both cases, therefore, absorption of two photons is required to achieve ionisation. However, absorption of the first 193 nm photon can result in different intermediate electronic states being accessed in comparison to excitation at 266 nm, such as long-lived Rydberg states. It is possible that this may lead to different ionisation pathways being promoted, resulting in differing mass spectra at 193 nm versus 266 nm [31]. Alternatively, the wavelength dependence may simply be due to the difference in excess energy deposited initially in the molecular ion. Assuming an ionisation potential of 8 eV, photoionisation at 266 nm will produce a molecular ion with up to 1.32 eV of excess energy. This is small compared to the excess energy, of up to 4.84 eV, possible following photoionisation at 193 nm. This larger excess energy may be sufficient to exceed the appearance potential for the production of the most facile fragment ions. Therefore, at 193 nm, ionisation would be accompanied by facile fragmentation. Unfortunately, from this experimental data, it is not possible to identify which of these two mechanisms is responsible for the different fragmentation patterns observed.

5.2.2 UV Stabilisers

The 266 nm and 193 nm photoionisation mass spectra of the UV stabilisers Tinuvin P, Tinuvin 326 and Tinuvin 327 are shown in Figure 5-3. For Tinuvin P the base peak in the mass spectra at both wavelengths is due to the molecular ion, with essentially no fragmentation occurring. However, for Tinuvin 326 and Tinuvin 327, significant differences are found in the mass spectra obtained at these two photoionisation wavelengths. Figure 5-3c shows that, for photoionisation of Tinuvin 326 at 266 nm, the molecular ion is the base peak in the spectrum. Fragment ions are observed at m/z = 300 and m/z = 272, which can be attributed to the loss of a methyl radical, [$\cdot CH_3$] and [$-C_3H_7$] group, respectively, from the molecular ion. In contrast, as shown in Figure 5-3d, photoionisation at 193 nm results in the detection of no molecular ion signal. The principal peaks at m/z = 300 and m/z = 272 can be

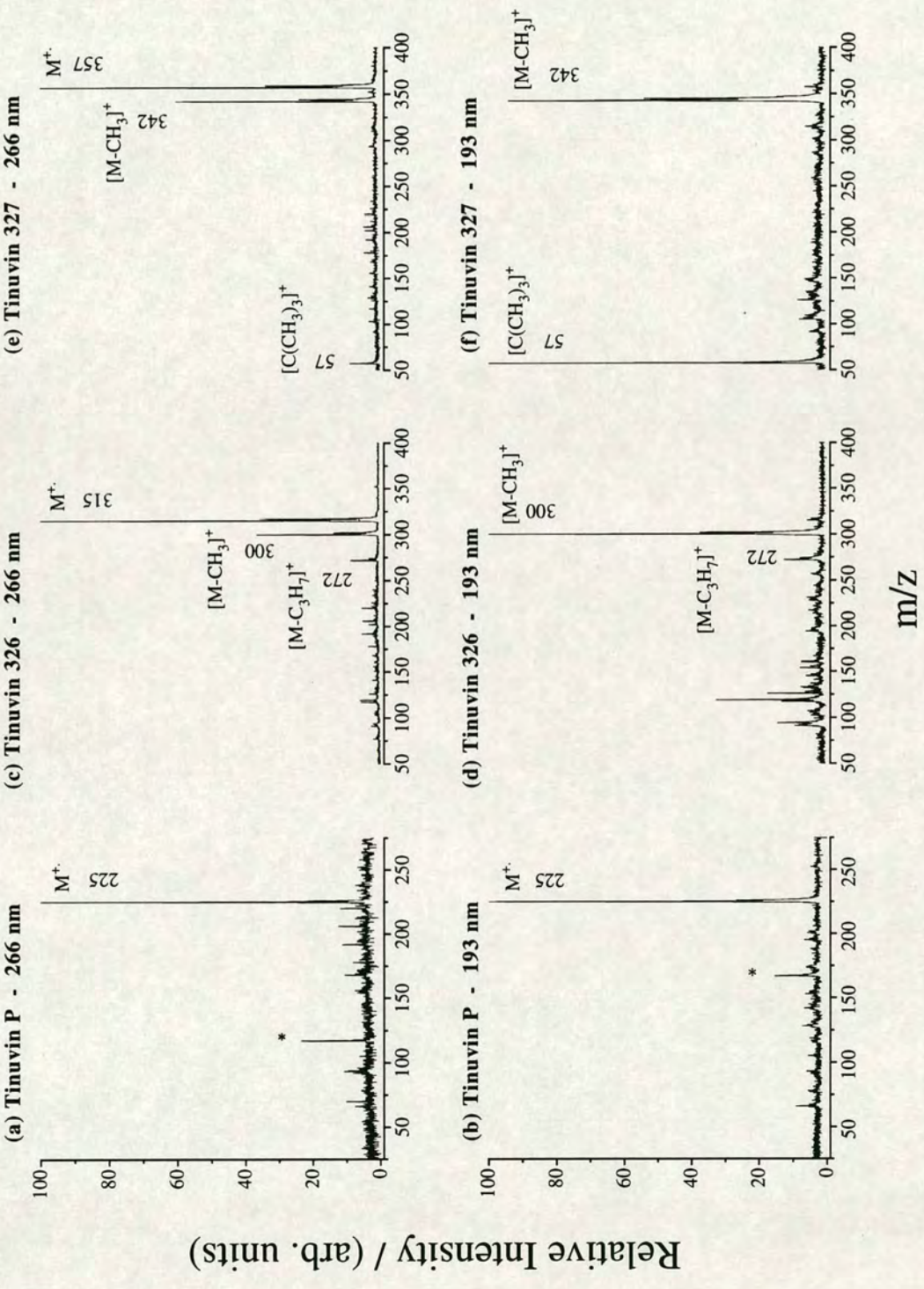

Figure 5-3: L2MS spectra of Tinuvin P using (a) 266 nm and (b) 193 nm photoionisation; Tinuvin 326 using (c) 266 nm and (d) 193 nm photoionisation; Tinuvin 327 using (e) 266 nm and (b) 193 nm photoionisation. Peaks marked with an asterisk (*) are due to the internal mass standards indole (m/z=117) and carbazole (m/z=167).

assigned to the same fragment ions as in Figure 5-3c. At both 266 nm and 193 nm, it is possible to resolve the doublets characteristic of the two naturally occurring isotopes of chlorine.

The spectra for Tinuvin 327 are similar in nature to those obtained for Tinuvin 326. At 266 nm, the molecular ion is the base peak in the spectrum, see Figure 5-3e, with a less intense fragment ion observed at m/z = 342 due to the loss of a [$\cdot CH_3$] radical from the parent molecular ion. A weaker peak at m/z = 57, due to the *tert*-butyl ion can also be observed. Figure 5-3f shows the spectrum obtained at 193 nm. Again, no molecular ion peak is observed, only a strong fragment peak due to the loss of the [$\cdot CH_3$] radical from the molecular ion, together with a very prominent fragment peak at m/z = 57 due to the *tert*-butyl ion.

In general, the photoionisation mass spectra of the Tinuvin UV stabilisers examined differ markedly at 266 nm and 193 nm. At 266 nm, the mass spectra are dominated by molecular ion signals, with very little associated fragmentation. This gives a powerful illustration of the advantage in using L2MS as a soft-ionisation technique, enabling readily interpretable mass spectra to be generated. Photoionisation at 193 nm, however, results in mass spectra in which the base peaks are fragment ions. This difference in behaviour may be due either to the difference in excess energy deposited in the molecular ion or due to excitation via different intermediate states, as discussed earlier.

5.2.3 Isomeric UV Stabilisers

The marked wavelength dependence of these photoionisation mass spectra can be exploited to aid the unambiguous identification of many polymer additives. A particularly useful application is the differentiation between isomeric additives. The mass spectra of three such isomeric species, Tinuvin 320, Tinuvin 343 and Tinuvin 329, were recorded using photoionisation at both 266 nm and 193 nm. The spectra are shown in Figure 5-4 and Figure 5-5, respectively.

The 266 nm photoionisation mass spectrum for Tinuvin 320, shown in Figure 5-4a, consists of a base peak at m/z = 323, corresponding to the molecular ion. A

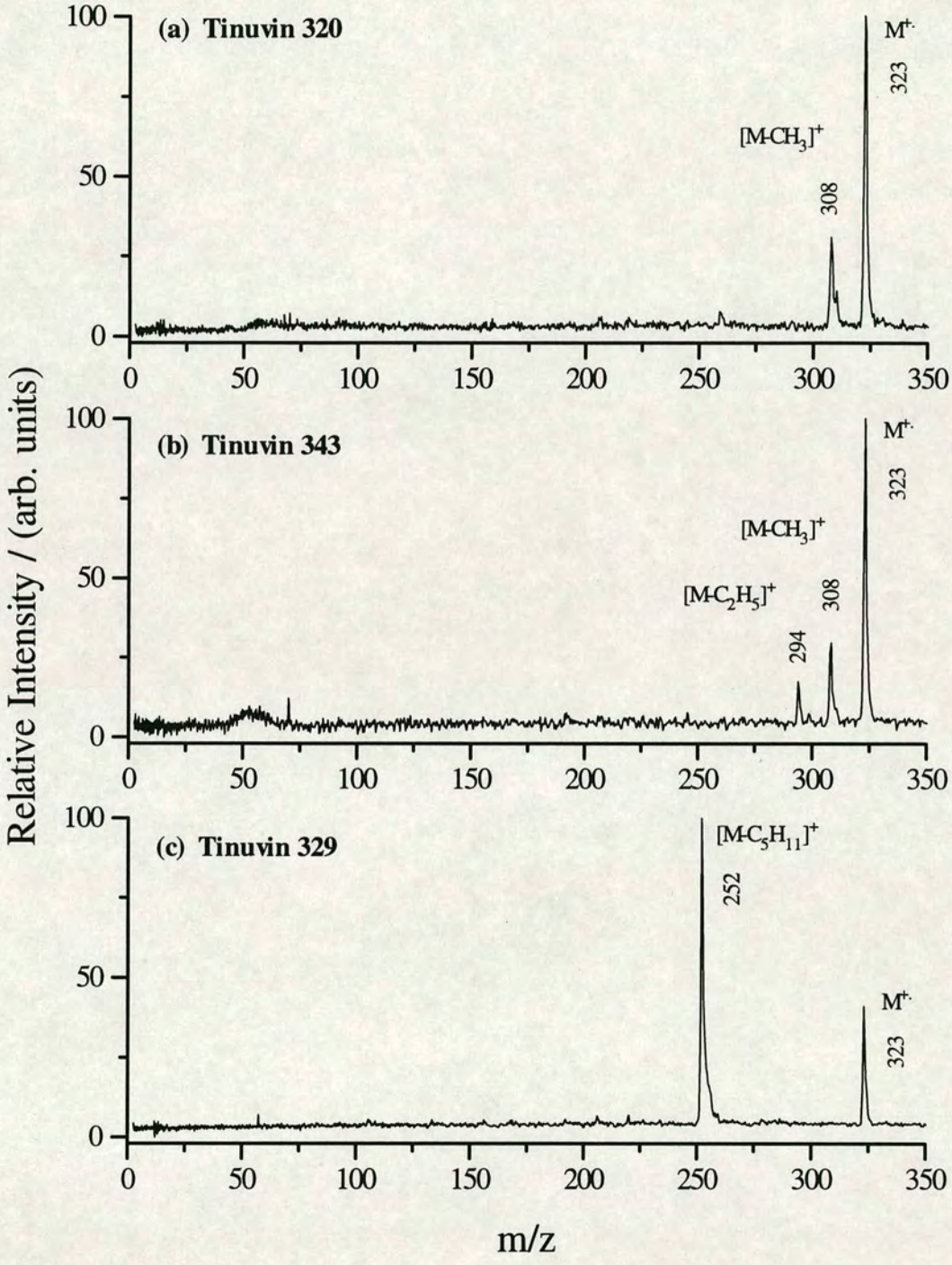

Figure 5-4: L2MS spectra obtained using 266 nm photoionisation of the isomeric UV stabilisers (a) Tinuvin 320, (b) Tinuvin 343 and (c) Tinuvin 329.

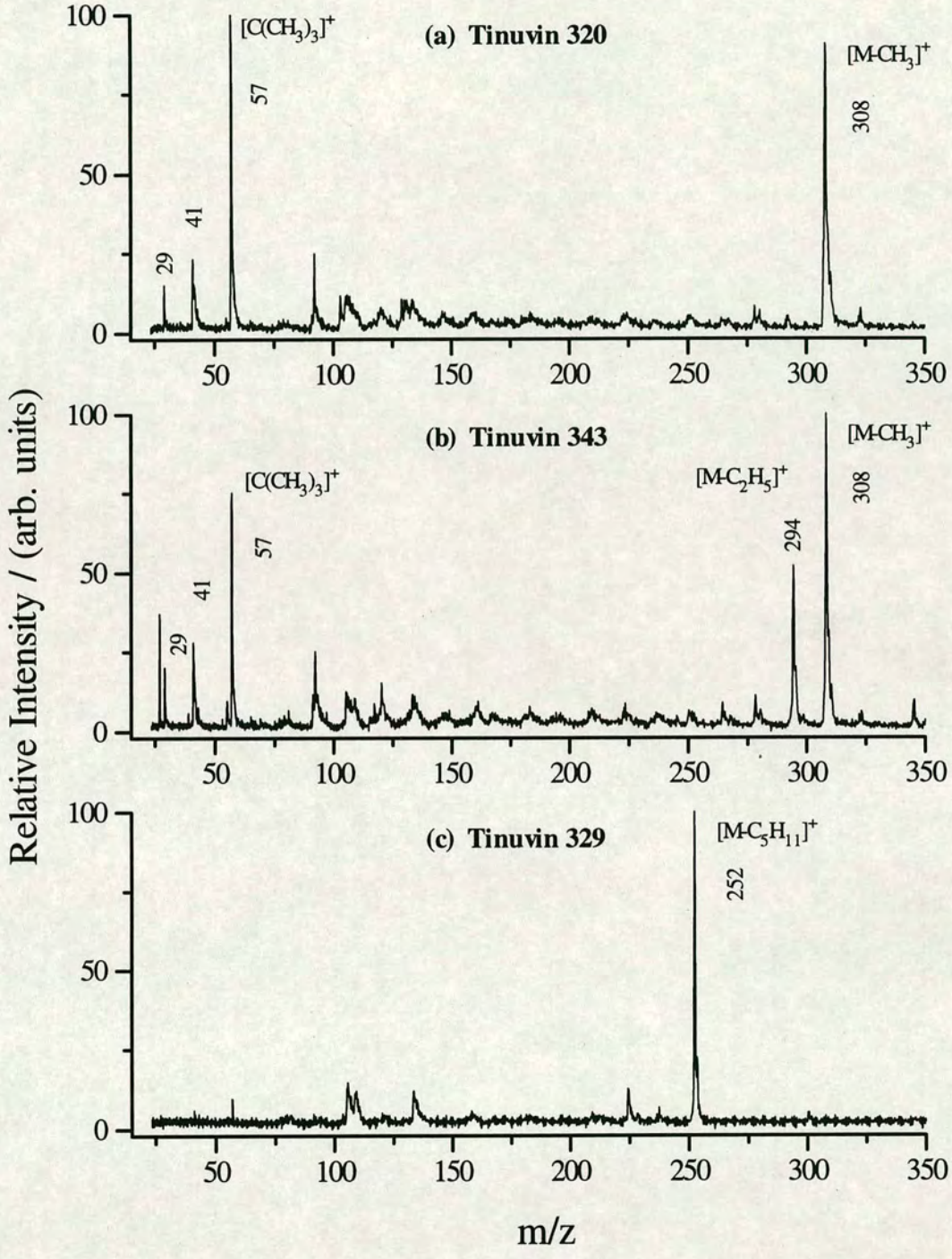

Figure 5-5: L2MS spectra obtained using 193 nm photoionisation of the isomeric UV stabilisers (a) Tinuvin 320, (b) Tinuvin 343 and (c) Tinuvin 329.

less intense fragment ion at m/z = 308, consistent with the loss of a methyl radical from the molecular ion is also observed. The mass spectrum of Tinuvin 343, shown in Figure 5-4b, also contains these two peaks. However, a further fragment peak is observed at m/z = 294, which can be assigned to the loss of an ethyl radical, [$\cdot C_2H_5$] from the molecular ion. The 266 nm photoionisation spectrum of Tinuvin 329, shown in Figure 5-4c, is markedly different, however. Whilst a peak corresponding to the molecular ion is observed, the base peak in the spectrum is at m/z = 252. This fragment ion can be attributed to the loss of a 2,2-dimethylpropyl radical, [$\cdot CH_2C(CH_3)_3$], which results from direct cleavage at the tertiary substituted carbon atom in the alkyl side chain of the molecular ion.

Photoionisation of these isomers at 193 nm produced similar mass spectra to those previously observed for the other Tinuvin UV stabilisers. For Tinuvin 320 no molecular ion is observed in the spectrum, as shown in Figure 5-5a. The base peak is at m/z = 308, which was previously attributed to loss of a methyl radical from the molecular ion. The intense fragment peak at m/z = 57 is due to the *tert*-butyl ion. The assignment of the other low mass fragment peaks at m/z = 29 and 41 is less certain, but they may correspond to $[C_2H_5]^+$ and $[C_3H_5]^+$, respectively. The weaker, and somewhat broader, peaks in the mid mass range may be due to fragmentation of the benzotriazole skeleton. The 193 nm photoionisation mass spectrum of Tinuvin 343 is shown in Figure 5-5b. Again, no molecular ion signal was detected. The fragment ions at m/z = 308 and m/z = 294 are assigned as $[M\text{-}CH_3]^+$ and $[M\text{-}C_2H_5]^+$, respectively. The peaks to low mass, and those in the mid mass range, are assigned as above. The mass spectrum of Tinuvin 329 obtained using 193 nm photoionisation is shown in Figure 5-5c. The base peak in the mass spectrum is at m/z = 252, and is again assigned to the loss of the 2,2 dimethylpropyl radical from the molecular ion. Interestingly, no prominent fragment peak at m/z = 57 for the *tert*-butyl ion is observed for this isomer.

In the case of these isomeric Tinuvin UV stabilisers, the nature of the substituent groups can affect the fragmentation and allow for differentiation between isomers. For example, Tinuvin 320 has two *tert*-butyl substituents, and so may lose a methyl

radical from either, but not both, substituent groups. This results, therefore, in a single fragment ion corresponding to $[M\text{-}CH_3]^+$, as shown in Figure 5-4a and Figure 5-5a. However, Tinuvin 343 contains only one *tert*-butyl substituent along with a [—$CH(CH_3)CH_2CH_3$] group. Again, it is possible to lose a methyl radical at the *tert*-butyl substituent, as before. However, the most stable carbocation which can be formed by a fragmentation at the other substituent corresponds to the loss of an ethyl radical, to leave the ion $[M\text{-}C_2H_5]^+$. Therefore, in this case a mass spectrum is produced which contains two high mass fragment ions, see Figure 5-4b and Figure 5-5b, which allows this molecule to be differentiated from its isomer Tinuvin 320. In the case of Tinuvin 329, there is only one alkyl substituent, and so the most stable radical which can be lost is a 2,2 dimethyl propyl radical, $\cdot CH_2C(CH_3)_3$. This results in a mass spectrum which contains the molecular ion, and a single fragment at m/z = 252, as shown in Figure 5-4c.

At each of the two photoionisation wavelengths employed, it is possible to distinguish between all three of these Tinuvin isomers. However, by comparing the spectra obtained at both of these wavelengths, one can also unambiguously identify each isomer from their fragmentation patterns, which are characteristic of the hydroxyphenylbenzotriazole compound class.

5.2.4 Discussion — Photofragmentation of UV Stabilisers

Tinuvin P displays what, at first sight, appears to be anomalous behaviour. For this molecule, both 266 nm and 193 nm photoionisation result in exclusive detection of the molecular ion, as shown in Figure 5-3a and 5-3b. This is due to the absence of tertiary substituents in Tinuvin P. All of the other Tinuvin UV stabilisers studied in this work contain tertiary substituent groups (see Table 5-1). Fragmentation is, therefore, most likely to occur at these sites, since a stable tertiary carbocation is produced as a result of resonance stabilisation. The absence of such tertiary substituents in Tinuvin P, therefore means that no such facile fragmentation process is possible, and an intact molecular ion is observed.

Apparently anomalous behaviour is also observed in the case of Tinuvin 329. In the 266 nm photoionisation mass spectrum of this compound, a fragment peak

dominates the molecular ion signal, as shown in Figure 5-4c. Reduction of the ionising laser fluence failed to enhance the molecular ion signal relative to this fragment ion. This suggests, therefore, that the observed fragmentation does not result from absorption of photons by the molecular ion. Once again, therefore, there are two possible mechanisms by which this fragment ion may be produced.

One possibility is that absorption of two 266 nm photons deposits sufficient excess energy to exceed the appearance potential of this fragment ion. However, from the earlier discussion, which assumed an approximate ionisation potential of 8 eV for these molecules, only 1.32 eV of excess energy is present in the molecular ion. Typical C—C bond dissociation energies are on the order of 350 $kJmol^{-1}$, which is equivalent to around 3.63 eV. Therefore, on energetic grounds, excess energy in the molecular ion is unlikely to be the cause of the observed fragmentation. However, recent work [32] has shown that energy imparted to the neutral molecules during the desorption process can be carried through into the molecular ion, and used to promote fragmentation. This is discussed in detail in Chapter 7.

Another possibility, as mentioned earlier, is that absorption of the first photon accesses excited electronic intermediate states, which promote ionisation pathways which do not lead exclusively to the molecular ion, favouring formation of fragment ions instead. Photoionisation of Tinuvin 329 at 193 nm produces a similar mass spectrum, see Figure 5-5c. In this case the molecular ion is not observed. Once more, it is possible that the fragmentation is caused by accessing an excited intermediate state which promotes an ionisation pathway which does not result in molecular ion production. However, without accurate ionisation potentials and more information on the excited states, it is not possible to be certain which of the two alternative explanations is correct.

Such wavelength dependent photoionisation mass spectra can enable important structural information to be obtained about the molecules under study. However, more importantly, they also be used to aid the unambiguous determination of unknown compounds directly from their host matrices.

5.3 *In situ* Analysis of Additives Directly From Polymers

Clearly, any technique which can provide chemical analysis of target analytes, at trace levels, directly from their host matrix represents an attractive and rapid methodology. L2MS has previously been used for *in situ* analysis of polycyclic aromatic hydrocarbons (PAHs) in atmospheric particulates [22,23]. The feature of the technique which allows this to be achieved, is the selectivity provided by the photoionisation process. Most organic molecules have ionisation potentials between 7-10 eV. In order to achieve ionisation, absorption of two or more UV photons is required. For efficient photoionisation a molecule must have a significant absorption cross-section at the wavelength of the ionising radiation employed. Molecules which do not possess a suitable chromophore will not be efficiently ionised. Therefore, by careful choice of the ionisation laser wavelength, the target analyte of interest may be selectively detected in preference to other components present in the mixture, including the host matrix. In the present study, it is shown that polymer additives with an appreciable absorption in the UV region of the spectrum can be selectively ionised in preference to non-UV absorbing host polymers.

Several polymer formulations were studied using this approach. A sample of polypropylene (PP) containing 0.15wt% of Irganox 1330 and 0.05wt% of Irgafos 168 was initially examined. The information already obtained on these two additives, discussed in the previous section, was used as reference data. The mass spectra obtained using 266 nm and 193 nm photoionisation following direct desorption from the PP matrix, are shown in Figure 5-6. In order to obtain an appreciable signal from this sample, it was necessary to increase the desorption laser power density fourfold, to ca. 38 $MWcm^{-2,}$ compared to the value used to desorb the pure polymer additives. The need for increased laser desorption power densities is due to the very low absorbance of the polypropylene matrix at the desorption laser wavelength of 10.6 μm [33]. In the spectrum obtained at 266 nm, shown in Figure 5-6a, the molecular ions for both Irganox 1330 (m/z = 774) and Irgafos 168 (m/z = 646) are present. For ionisation at 193 nm the molecular ion signals are very much weaker. However, a strong characteristic fragment signal at m/z = 441, anticipated from the 193 nm photoionisation mass spectrum of pure Irgafos 168, see Figure 5-2b, can be observed.

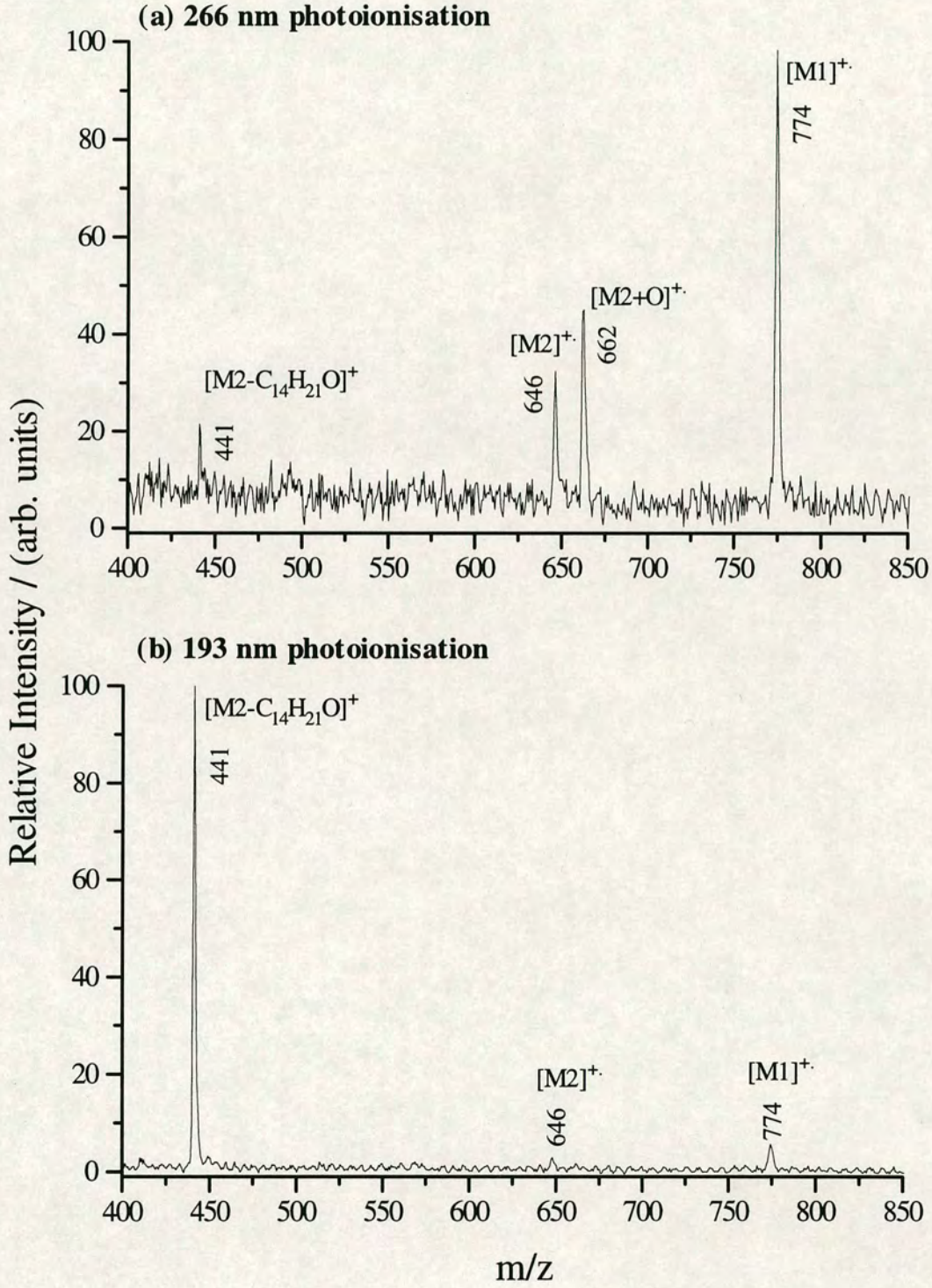

Figure 5-6: *In situ* L2MS spectra of a polypropylene (PP) sample containing Irganox 1330 (0.15wt%) and Irgafos 168 (0.05wt%). Photoionisation was carried out using (a) 266 nm and (b) 193 nm radiation. $[M1]^+$ and $[M2]^+$ denote the molecular ions of Irganox 1330 and Irgafos 168, respectively.

This peak is due to the loss of a (2,4-di-*tert*-butylphenyl)–O group from the molecular ion, as is observed in the corresponding spectrum for the pure compound. These spectra demonstrate that by use of two readily available ionisation wavelengths, and with reference to the corresponding spectra for the pure additives, it is possible to unambiguously determine the presence of Irganox 1330 and Irgafos 168 directly from the host PP matrix.

In Figure 5-6a, an apparently anomalous peak at m/z = 662 is observed using 266 nm photoionisation. This can be accounted for by considering the chemistry of Irgafos 168. This compound is a phosphite antioxidant, which is generally considered to be a secondary antioxidant. Phosphite antioxidants react with hydroperoxides, peroxy radicals, alkoxy radicals and olefinic and carbonyl moieties, thereby controlling polymer molecular weight and colour. The level of phosphite additives in polymers affects the stability of the polymer. Although it is very important to be able to determine how much additive is in the polymer, it is equally important to be able to monitor how much of the additive remains in the original phosphite form, since it is only in this form that the additive remains useful as an antioxidant. The peak at m/z = 662 in Figure 5-6a can be attributed to the oxide of Irgafos 168 (the phosphate). The ratio of phosphite to phosphate will give an indication of how resistant the polymer will be to further oxidation. Studies of this type have previously been attempted by SIMS [19] and LD-EI-FTICR [34]. The data presented here shows that it is possible, not only to determine the presence of additive species directly from the polymer, but also to monitor chemical changes caused by the polymerisation process or subsequent exposure to heat, light and other conditions which initiate polymer degradation.

The MPI efficiency of the additive under investigation is also an important factor. For example, photoionisation of pure Tinuvin 320 using 266 nm radiation produced intense signals, as shown in Figure 5-4a. However, when a sample of POM containing 0.3wt% of Tinuvin 320 was analysed using photoionisation at 266 nm, no peaks attributable to this compound were observed. This sample was supplied in the form of an injection moulded bar from which a section was cut and attached to the

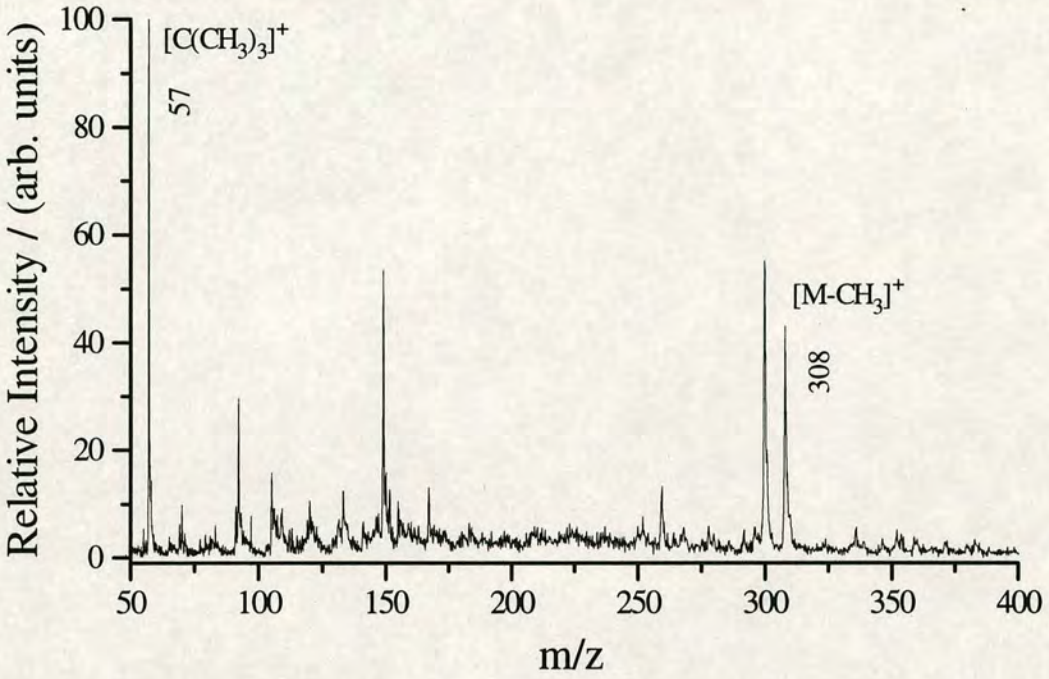

Figure 5-7: *In situ* L2MS spectrum of an injection moulded sample of polyoxymethylene (POM) containing 0.3wt% Tinuvin 320. Photoionisation was carried out using 193 nm radiation. Photoionisation using 266 nm radiation produced no signal.

sample probe. Figure 5-7 shows a mass spectrum for the same polymer sample obtained using 193 nm photoionisation. Intense signals are observed at m/z = 308 and m/z = 57, which correspond to the anticipated fragment ions for the 193 nm photoionisation of pure Tinuvin 320, as shown in Figure 5-5a. It is clear that photoionisation at 193 nm is a more efficient and sensitive detection wavelength for Tinuvin 320 than 266 nm. In this case, the desorption laser power density used was 7.7 $MWcm^{-2}$, which is similar to the value used for desorption of the pure additives from a stainless steel substrate. POM has a relatively intense absorption at 10.6 μm, and as a result, only moderate desorption powers are required for desorption of the neutral analyte species [33]. It is clear that provided sufficient material can be liberated from the polymer, the limiting factor for *in situ* detection of additives at levels typically found in real polymer formulations is the efficiency with which they can be ionised. Provided a suitable wavelength is available, the analysis of bulk polymers with additive concentrations as low as 0.01wt% should be possible using this technique.

As a further example of the utility of L2MS for analysis of real systems, another sample of POM, this time containing Santo White antioxidant, was examined using 266 nm photoionisation. This sample, also cut from an injection moulded bar of POM, contained 0.1wt% of Santo White powder. It was attached to the sample probe, such that the polished surface of the polymer was interrogated by the CO_2 laser.

Figure 5-8a shows the 266 nm photoionisation mass spectrum obtained when this finished exterior surface of the polymer sample was exposed to the CO_2 laser. In addition to the peaks at m/z = 382 and m/z = 339 observed previously from the pure sample of Santo White (shown in Figure 5-2c), a further intense peak is present at m/z = 212, together with another peak at m/z = 197. It has not proved possible to formally identify these peaks, although it is believed they may be due to a surface contaminant introduced during the finishing or injection processes. When desorption was carried out on the same location for an extended period of time, the intensity of the peaks at m/z = 212 and m/z = 197 were found to diminish relative to the peaks associated with the antioxidant. This supports the assignment of these peaks as being due to a species present on the surface of the polymer. Power density measurements suggest that the signal at m/z = 197 is actually a fragment of the m/z = 212 species. When the power density of the ionising laser was increased, the m/z = 197 signal began to grow relative to the m/z = 212 peak. It is likely, therefore, that the species producing the signal at m/z = 197 results from the loss of a methyl radical from the molecular ion at m/z = 212.

When the interior, unfinished surface, of the polymer was interrogated, these peaks were absent, as shown in Figure 5-8b. This confirms that the additional signals observed when the polished exterior surface was irradiated were derived from contaminants of some description. These results demonstrate that L2MS can be used to readily detect species from the surface of a polymer. Polymer additives are not uniformly distributed throughout a given polymer matrix. Often, the additives will migrate towards the surface, or aggregate into small clusters within the body of the polymer. Both of these effects can alter the chemical and mechanical properties of

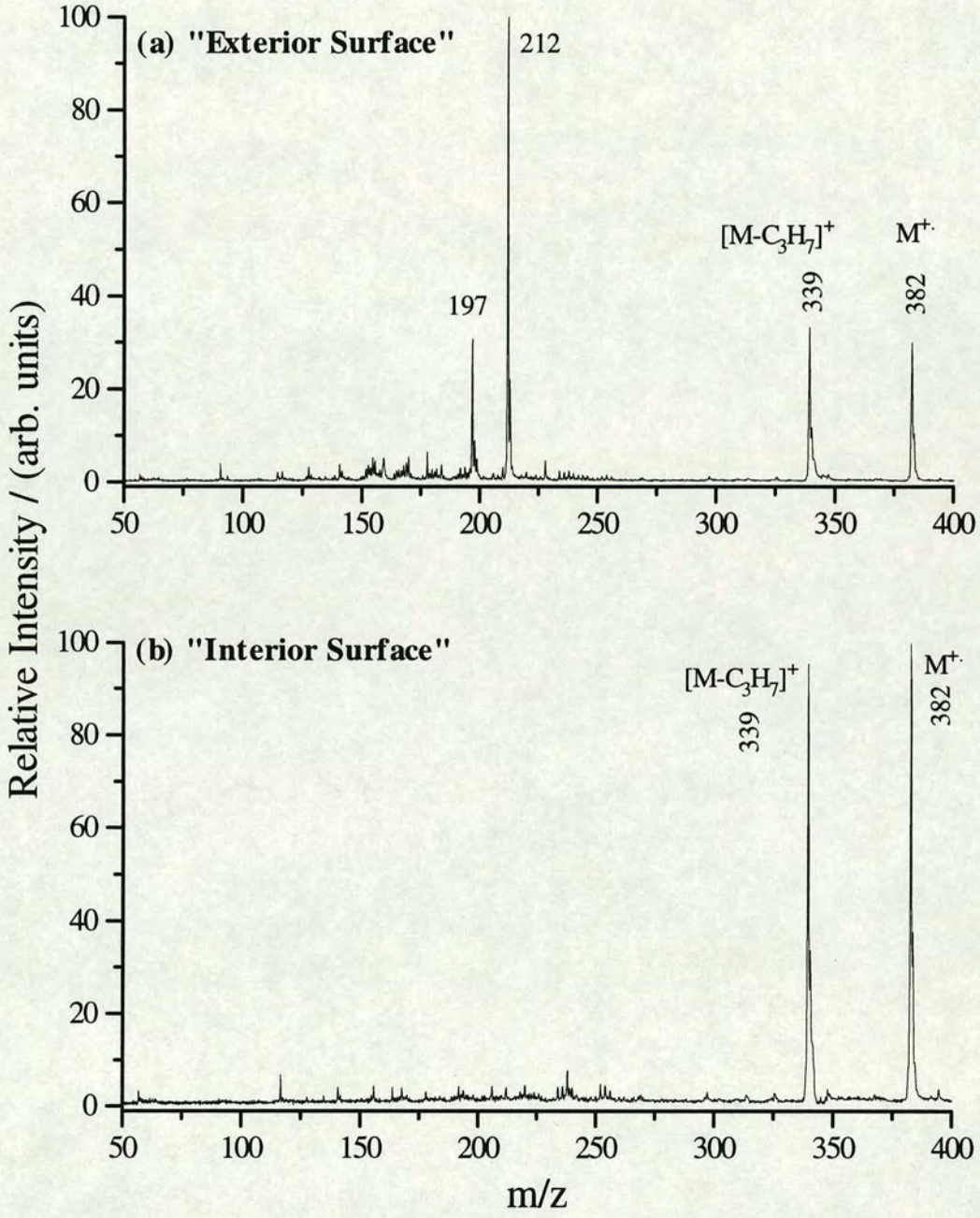

Figure 5-8: *In situ* L2MS spectra of an injection moulded POM sample containing 0.1wt% Santo White powder. The desorption laser was used interrogate (a) the finished exterior surface and (b) the unfinished interior surface.

the material. In addition, trace contaminants may be present on the surface of the polymer introduced during injection moulding and/or finishing processes.

This experiment has shown that the L2MS technique is sensitive to surface species. Therefore, it should be possible to assay for polymer additives as a function of depth within the polymer. Recent work on a POM polymer sample has shown that it is possible to monitor the concentration of Santo White antioxidant as a function of polymer depth. This will be the subject of a forthcoming publication [33]. Such studies could also be extended to include 2-dimensional imaging of additives on a polymer surface, by utilising an optical delivery system capable of achieving a desorption spot-size less than 50 μm. This would allow the investigation of inhomogeneous features on polymer surfaces, such as additive aggregation or segregation throughout a polymer formulation. It may also prove possible to monitor time-dependent phenomena, such as the extent of surface migration and segregation of additives as a function of polymer age.

5.4 L2MS of Non-Aromatic Polymers

The results in Section 5.3 show that the tremendous selectivity offered by the REMPI ionisation scheme can lead to simple readily interpretable mass spectra of minor components in real complex systems. However, although in this case the polymer additives have been easily identified, essentially no information has been obtained on the polymer matrices themselves. This is due to the fact that the polymers studied in this work did not have an appreciable absorption cross section at the ionisation wavelengths used. Previous work in this laboratory [1] has shown that aromatic polymer systems, which do strongly absorb UV radiation, can be characterised using L2MS; it is possible to obtain repeat unit and terminating group information, although any average molecular weight information obtained is rather unreliable.

Attempts to obtain similar information on non-aromatic polymer systems, has, thus far, proved to be more difficult. However, work carried out during the course of the present studies has shown that there are methodologies available, which, with

minor adjustments and modifications to the existing apparatus, enable information to be obtained which can be used to identify the polymer matrix.

5.4.1 Non-Resonant MPI

The spectra presented in Section 5.3 involved selective ionisation of the aromatic additive species in preference to the non-aromatic polymers PP and POM. Efficient multiphoton ionisation (MPI) requires that the target molecule has a significant absorption at the photoionisation wavelength. Neither polypropylene (PP) nor polyoxymethylene (POM) possess such a UV chromophore. Thus at low ionising laser fluences it is possible to effectively discriminate against material ablated or desorbed from the polymer matrix itself. It has been shown elsewhere [33] that infrared laser radiation at 10.6 μm with power densities similar to those employed here results in efficient ablation for POM, due to the relatively high absorption cross-section at this wavelength. It is unlikely, therefore, that neutral fragments associated with the polymer are not present in the gas-phase in the ionisation region. At higher ionising laser power densities it is possible to promote non-resonant MPI of non-absorbing material. At these elevated fluences, the target materials are prone to significant levels of fragmentation. Figure 5-9 shows such a spectrum for a sample of pure POM polymer, obtained using photoionisation at 193 nm. In this case the ionising laser output was focused, resulting in an increased power density of 3.4 $MWcm^{-2}$. This characteristic spectrum shows two series of low mass ions separated by units of m/z = 30, thereby providing sufficient evidence to identify the polymer as POM, with a repeat unit of $[-CH_2O-]_n$. Therefore, by simply increasing the power density of the ionising laser and promoting non-resonant MPI, the selectivity of the technique can be sacrificed in favour of sensitivity for non-aromatic species, in this case allowing positive identification of a polymer, POM, which could not otherwise have been characterised.

5.4.2 Single-Photon Ionisation (SPI)

In the previous section it was shown that polymers which did not absorb UV light strongly could be ionised by non-resonant MPI. However, at the high UV fluences required to induce ionisation in non-absorbing molecules, ionisation is often

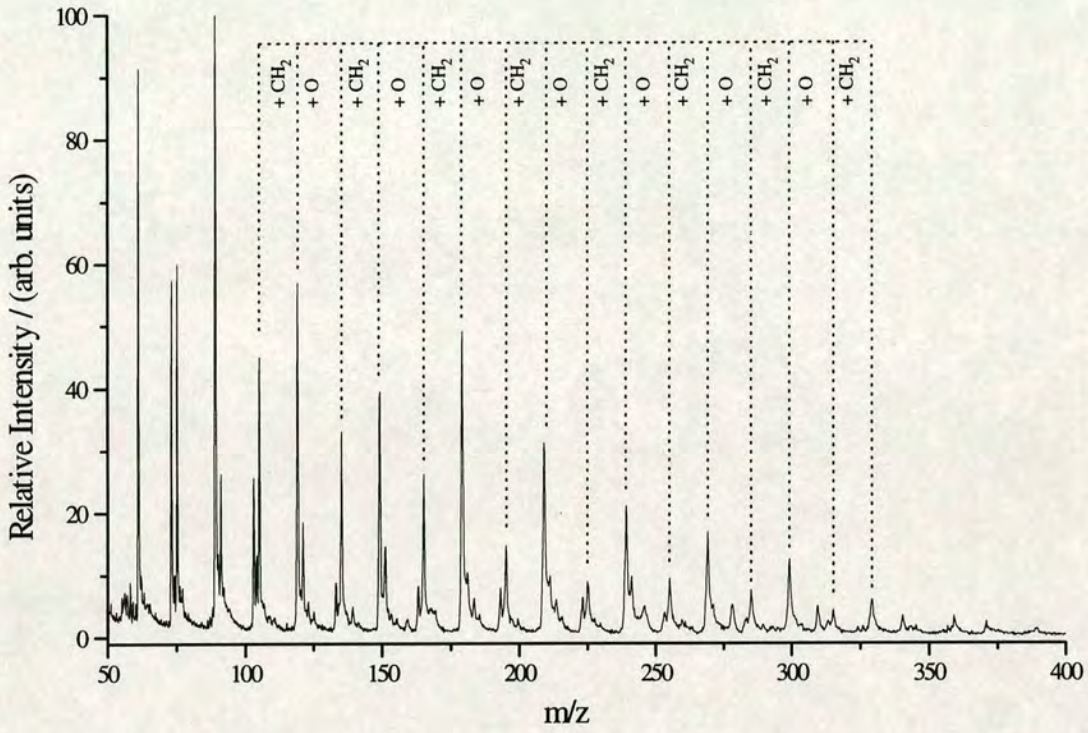

Figure 5-9: L2MS spectrum of an injection moulded sample of pure POM. The ionisation laser power density used was increased from 0.8 x 10^6Wcm^{-2} to 3.4 x 10^6Wcm^{-2} in order to promote non-resonant MPI.

accompanied by high levels of fragmentation, as shown in the spectra for POM. Another option is to access the ionisation continuum directly by using photons which are marginally greater in energy than the IP of the molecules in question, i.e., single photon ionisation (SPI). SPI can be considered to be a reasonably soft ionisation technique, since little excess energy is available to cause bond cleavage. Using SPI, only low laser fluences are required for ionisation, thereby reducing the probability of two-photon absorption. Furthermore, single-photon ionisation cross-sections are often much more uniform between molecules than the corresponding two-photon (or higher) cross-sections for MPI, yielding more quantitative detection probabilities [35]. Although ionisation using SPI obviously results in a severe degradation in selectivity, it opens a pathway for the analysis of a wide variety of molecules. Vacuum ultraviolet (VUV) radiation has previously been used to investigate a variety of aliphatic hydrocarbons, [36,37,38] laser desorbed biomolecules [39] and sputtered bulk organic polymers [40,41].

A VUV source has been designed and built in this laboratory, in which the 3rd harmonic of an Nd:YAG laser at 355 nm is frequency tripled in a gas cell of xenon to produce the 9th harmonic at 118 nm. Such radiation has an associated energy of 10.4 eV, and is sufficiently energetic to ionise most organic molecules. The apparatus used for VUV generation is described briefly in Chapter 3, Section 3.6.4. For a more detailed discussion, the reader should consult ref. [1].

In the present work, the fixed frequency VUV radiation at 118 nm was used to ionise a series of low molecular weight polydimethylsiloxanes (PDMS). These molecules do not contain a UV chromophore, and so are not amenable to analysis using MPI. These synthetic polymers are used in a wide variety of industrial applications, from additives in foodstuffs to use in biological applications. A broad overview of the current approaches to analytical chemistry of silicones can be found in ref. [42].

Low molecular weight PDMS samples have very low surface tension, so that even samples with average molecular weights of around 1000 u exist as liquids at room temperature. As the molecular weight increases up to around 4000 u, the liquids become more viscous. Therefore, in order to keep the PDMS sample on the probe, it was necessary to "bind" the viscous liquid into a thick paste with graphite powder. Graphite was chosen because it is a strong absorber of IR radiation, and so aids efficient desorption of the analyte.

Figure 5-10 shows the single-photon ionisation mass spectrum obtained for a PDMS sample of average molecular weight, M_w = 770 u. The low mass region of the mass spectrum is dominated by carbon cluster ions derived from the graphite matrix. An intense peak at m/z = 73 corresponding to the polymer end group, $[Me_3Si]^+$ can also be observed in the low mass range. The principal feature in the higher mass region is a series of intense peaks separated by 74 u (labeled n = 1-13). This separation corresponds to the mass of the PDMS repeat unit, [-O-SiMe$_2$-]. However, the peak masses do not correspond to the molecular weights of intact oligomeric species, but are 15 u below this value. It has been observed previously using electron impact mass spectrometry that appreciable molecular ion signals are only observed

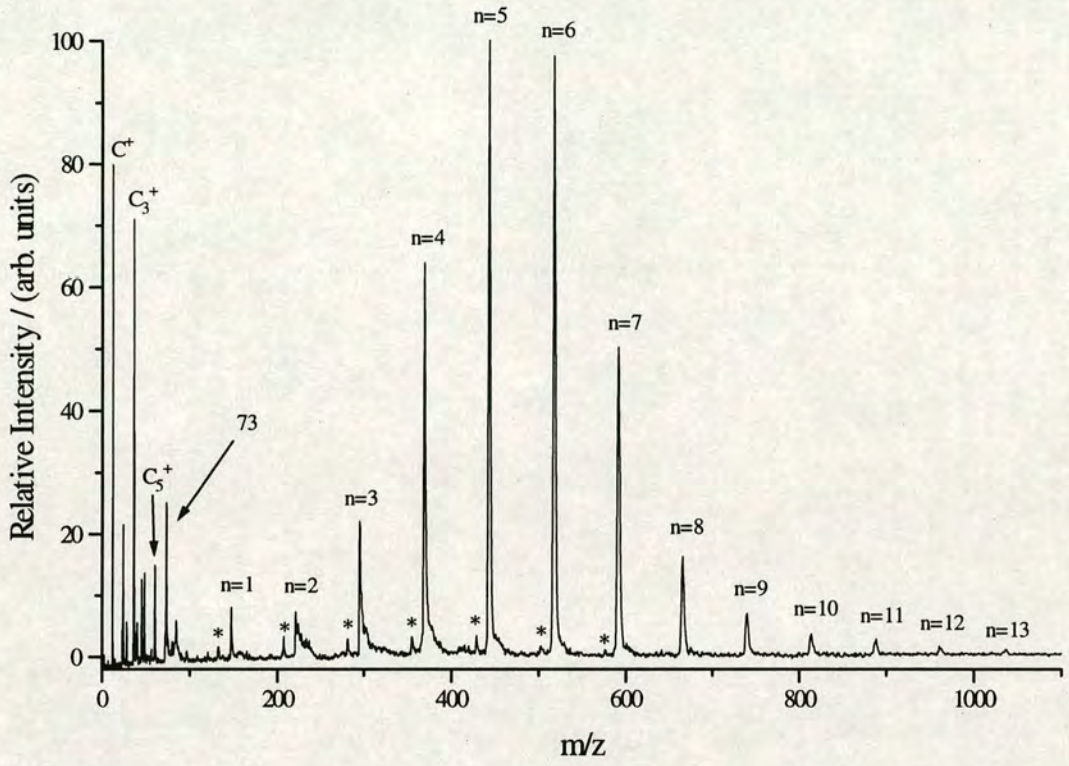

Figure 5-10: L2MS mass spectrum of a PDMS sample, M_w=770. The peaks labeled n=1-13 correspond to the siliconium series of ions, $[Me_3Si(O\text{-}SiMe_2)]^+$. The peaks labeled with an asterisk (*) correspond to the $[(O\text{-}SiMe)()\text{-}SiMe_2)_m]^+$ ion series.

when aromatic substituents are present. Therefore, EI mass spectra of PDMS are generally characterised by the even-electron ions formed by Si-C cleavage to form $[M\text{-}CH_3]^+$ ions [43]. This series of siliconium ions, has the general structure $[Me_3Si(O\text{-}SiMe_2)_n]^+$, and is observed to extend from n = 1 to 13.

A much less intense series of peaks, labelled with asterisks, can also be observed in Figure 5-10. These peaks are again separated by the repeat unit of 74 u, and can be assigned to ions with the general structure $[O\text{-}SiMe(O\text{-}SiMe_2)_m]^+$. These ions are formed by elimination of Me_4Si from the siliconium ions, $[M\text{-}Me]^+$. This has also been observed in the electron impact mass spectra (EI-MS) of low molecular weight oligomers [44]. The masses and structures of the major ionisation products are summarised in Table 5-2.

The average molecular weight for the major siliconium ion distribution in Figure 5-10 was calculated, assuming that the species in the $[Me_3Si(O\text{-}SiMe_2)_n]^+$ ion series all arise due to the loss of a methyl radical from the corresponding PDMS molecular

$[Me_3Si(O\text{-}SiMe_2)_n]^+$ series 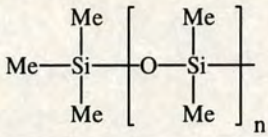		$[(O\text{-}SiMe)(O\text{-}SiMe_2)_m]^+$ series 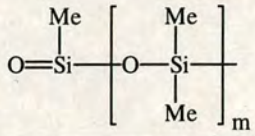	
n	**m/z**	**m**	**m/z**
1	147	1	133
2	221	2	207
3	295	3	281
4	369	4	355
5	443	5	429
6	517	6	503
7	591	7	577
8	665		
9	739		
10	813		
11	887		
12	961		
13	1036		

Table 5-2: Major ion series observed in the SPI L2MS spectra of PDMS, M_W = 770. Members of these two ion series, $[Me_3Si(O\text{-}SiMe_2)_n]^+$ and $[O\text{-}SiMe(O\text{-}SiMe_2)_m]^+$, are characteristic of PDMS samples.

ions. The calculated value of M_W = 532 is considerably lower than the value of M_W = 770 supplied by the manufacturer. This shift in the distribution to lower mass could result from rearrangements and the elimination of neutral species from higher mass oligomers. However, further work is required in order to determine why more accurate average molecular weights are not obtained.

It has also proved possible using L2MS to characterise higher molecular weight samples of PDMS. However, in order to obtain a signal, considerably higher desorption laser powers were required. The spectrum in Figure 5-11a shows the SPI mass spectrum of a PDMS sample with M_w = 3780. In this case, no evidence of a prominant oligomer distribution corresponding to the $[Me_3Si(O\text{-}SiMe_2)_n]^+$ ion series, clearly observed in the mass spectra of the lower molecular weight samples, was observed. In this case, all the peaks observed can be attributed to fragments of the PDMS oligomers. The base peak in the mass spectrum is at m/z = 73, and corresponds to the terminating group, $[Me_3Si]^+$. The signals at m/z = 147 and 221

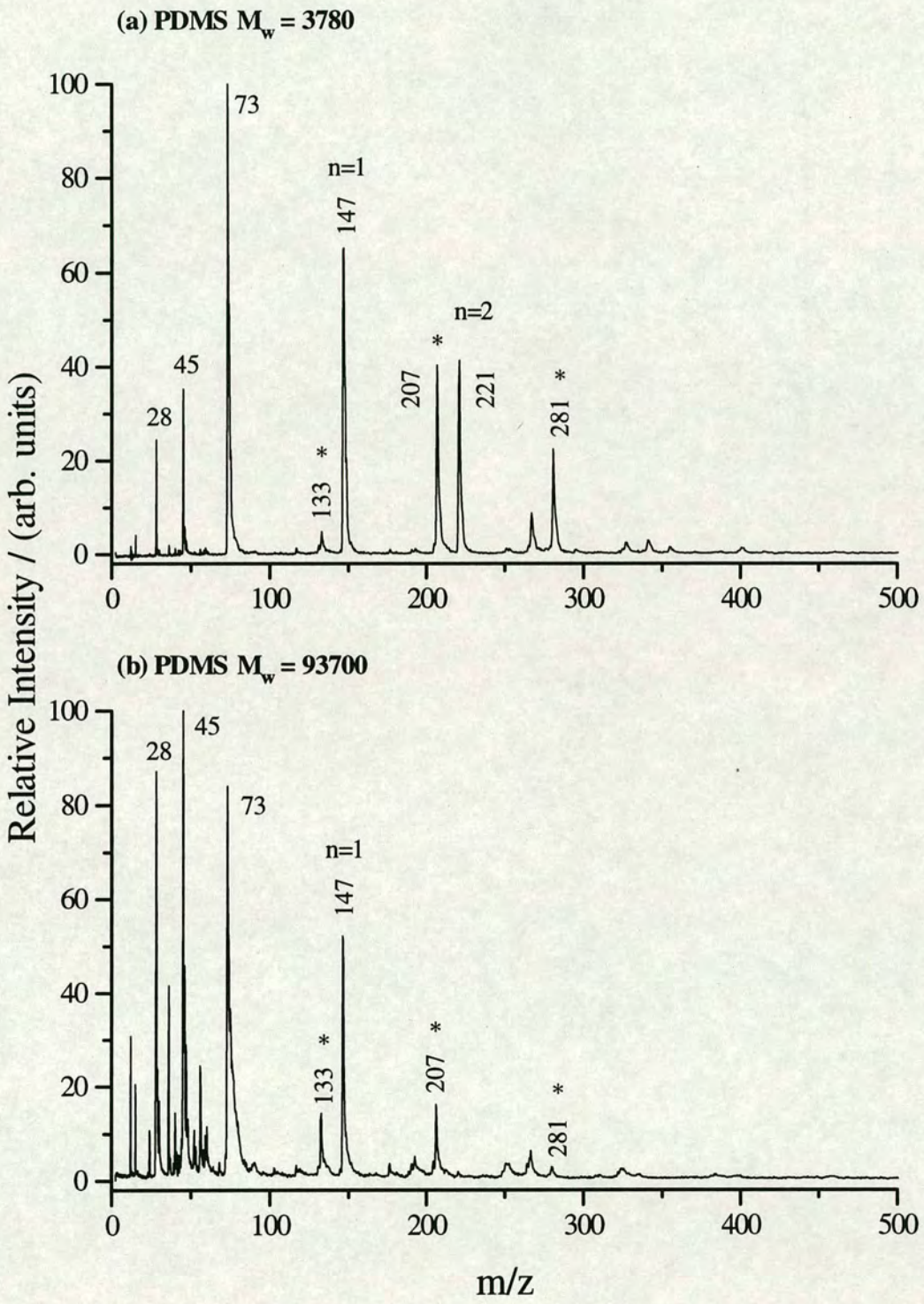

Figure 5-11: SPI L2MS spectra of higher average molecular weight PDMS samples, where (a) M_w = 3780 and (b) M_w = 93 700. Peaks denoted by an asterisk (*) are members of the $[O\text{-}SiMe(O\text{-}SiMe_2)_m]^+$ ion series, whilst the peaks marked "n" are members of the $[Me_3Si(O\text{-}SiMe_2)_n]^+$ series. These ion series are illustrated in Table 5-2.

correspond the first two members of the $[Me_3Si(O\text{-}SiMe_2)_n]^+$ series. The difference between these peaks obviously yields the repeat unit [-O-$SiMe_2$-] of 74 u. Other intense peaks corresponding to the first few members of the $[O\text{-}SiMe(O\text{-}SiMe_2)_m]^+$ ion series, m = 1-3 are labeled with asterisks. Again, the mass difference between the peaks in this series gives the repeat unit information.

The mass spectrum shown in Figure 5-11a is typical of those obtained for higher molecular weight PDMS samples. A similar mass spectrum was observed for a very high molecular weight sample of PDMS with M_w = 93 700 u, as shown in Figure 5-11b. This has many features in common with the spectrum in Figure 5-11a. Again, the mass spectrum contains no oligomeric distribution but consists of low mass fragments ions . The base peak, in this case, corresponds to the presence of the ion $[SiOH]^+$ at m/z = 45. Again, the terminating group information is available, as shown by the presence of the m/z = 73 ion. The repeat unit can also be extracted from the data. The first three members of the $[O\text{-}SiMe(O\text{-}SiMe_2)_m]^+$ ion series are present in the mass spectrum, and the mass difference between them gives the mass of the repeat unit. The higher desorption laser powers required to desorb these samples leads to mass spectra dominated by the products of fragmentations and rearrangements, and yields no information regarding the average molecular weight distribution. However, data that can be used to identify which polymer is present, and how the chain is terminated, can easily be obtained.

In summary, L2MS using SPI, instead of MPI, has been shown to be effective for producing mass spectra which allow for the identification of the polymer species present. Although average molecular weight data, even for low mass polymers, is rather unreliable, it is possible to generate information on the repeat unit and the terminating group. By using higher laser desorption power densities, it is also possible to generate such data for very high molecular weight polymers, up to at least 100 000 u.

5.4.3 Laser Induced Photoelectron Ionisation (LIPEI)

Electron ionisation (EI) is a general non-selective ionisation method, which usually leads to the formation of radical molecular cations in addition to a significant

number of fragment ions. In order to couple EI with TOF mass spectrometry, either the electron generation or the ion extraction should occur in a pulsed manner. It is possible to generate narrow pulses of electrons by slightly modifying the existing L2MS apparatus, thereby producing an EI source well suited for coupling to the TOF mass spectrometer. The approach adopted was to employ a pulsed UV laser to produce electrons from a metal target via the photoelectric effect. These photoelectrons are then be accelerated towards the gas-phase neutrals in order to effect ionisation. This technique has recently been demonstrated to be useful for the structural analysis of a wide variety of molecular classes, from non-aromatic polymers to amino acids [45,46].

Experimental Approach

The experimental set-up is illustrated schematically in Figure 5-12. The photoelectrons were produced by directing the unfocused output of the 4th harmonic (266 nm) of an Nd:YAG laser at a metal target, situated between the repeller plate and the draw-out grid of the ion extraction optics. In order to minimise the effects of spatial resolution, discussed in Chapter 2, it was necessary to construct an electron emitter which produced a narrow beam of electrons. This was done by preparing a gold plated stainless steel metal target. A small hole approximately 200 μm in diameter was ablated through the gold film, such that the stainless steel was exposed beneath. Gold has a higher work function for photoelectron generation than the energy of the 266 nm radiation (4.66 eV), and so the low-fluence UV radiation will not produce an appreciable number of photoelectrons. On the other hand, iron in the stainless steel, has a work function of 4.5 eV, and so exposure to 266 nm radiation results in efficient photoelectron production. It should be noted that increasing the fluence of the UV laser does not increase the energy of the resultant photoelectrons; the photoelectron energy is simply governed by the excess energy imparted by the photon above the work function of the metal, and the potential difference through which it is accelerated. Increasing the laser fluence simply increases the intensity of the electron beam.

(a)

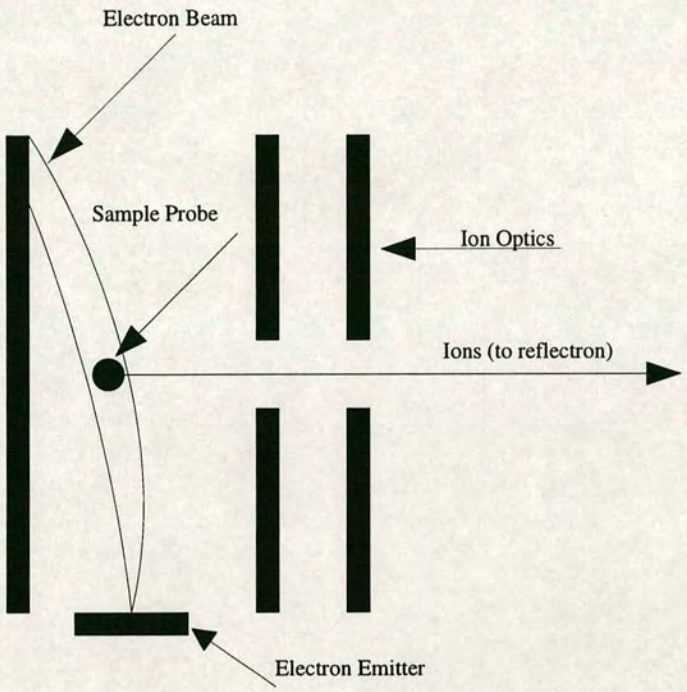

(b)

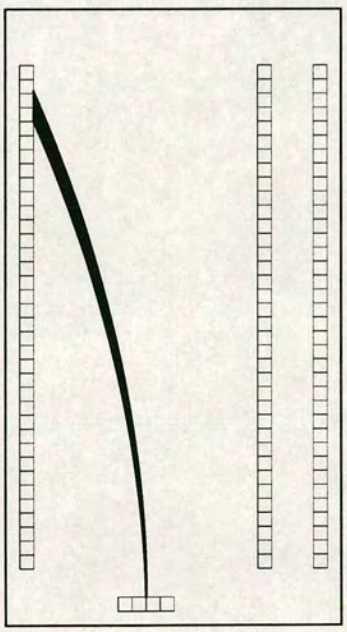

Figure 5-12: (a) Schematic illustration of the experimental arrangement for generation of laser induced photoelectrons. (b) Photoelectron trajectories as simulated by the SIMION programme, version 6.0. The electron emitter is grounded, and all other electrode potentials are at typical values as shown in Chapter 2.

The photoelectrons are accelarated into the ion extraction region, and the sample probe positioned such that the electron beam interacts with the IR laser desorbed molecules, as shown in Figure 5-12a. Figure 5-12b shows a simulation of the trajectories of the photoelectrons, obtained using SIMION version 6 [47]. From this simulation, it can be seen that there is some divergence in the electron beam as it traverses the extraction region, and that the electrons are accelerated towards the repeller. This does mean that the ions generated by this electron beam are extracted at different points, which will inevitably result in a degradation in the mass resolution. However, this can be compensated for to some extent by adjusting the ratio of the repeller and draw-out potentials. It has been demonstrated that the pulse duration of the photoelectron beam closely resembles that of the laser pulse which was used to produce it [45,46]. Typical photoelectron energies at the point of intersection with the laser desorbed neutrals have been estimated at approximately 100 eV using the SIMION program.

LIPEI of PDMS

LIPEI has been used in this laboratory to investigate a number of non-aromatic (and therefore, non-UV absorbing) polymers. One such example is the PDMS sample with M_w = 770 previously analysed using SPI, as discussed in Section 5.4.2. Figure 5-13 shows the LIPEI mass spectrum that was obtained. It can be seen that the appearance of this mass spectrum is very similar to those obtained for SPI of very high molecular weight PDMS, such as shown in Figure 5-11. The mass spectrum is dominated by the peak at m/z = 73, which is assigned, as before, to the terminating group, $[Me_3Si]^+$. The repeat unit information is again available: the peaks at m/z = 147 and 221 are assigned as the first two members of the $[Me_3Si(O\text{-}SiMe_2)_n]^+$ ion series, shown in Table 5-2. Again, these do not correspond to oligomer molecular ions, but arise from loss of a methyl radical to form the corresponding even electron species. The difference between these two peaks is 74 u, and corresponds to the repeat unit [-O-$SiMe_2$-]. Similarly, the peaks at m/z 207 and 281, denoted by an asterisk, are part of the $[O\text{-}SiMe(O\text{-}SiMe_2)_m]^+$ ion series, where m = 2 - 3. Again, the difference of 74 u is characteristic of the polymer repeat unit. This shows that with

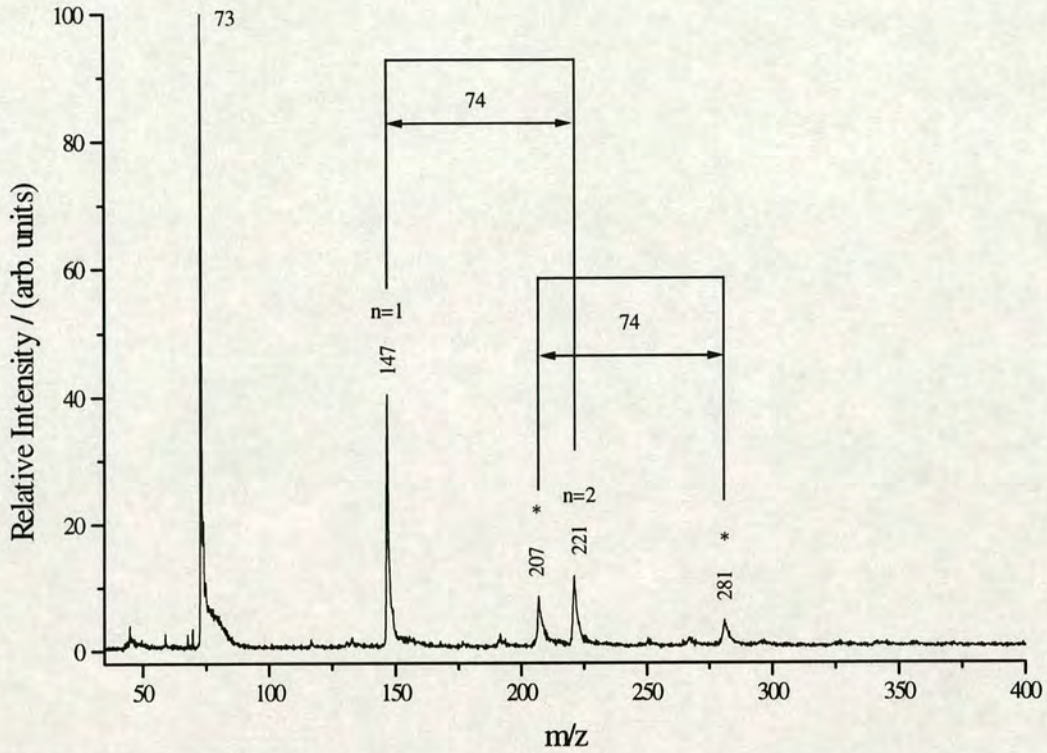

Figure 5-13: **LIPEI** L2MS spectrum of PDMS, M_w=770. The estimated photoelectron energy is approximately 100 eV. Peaks denoted by an asterisk (*) are members of the $[O\text{-}SiMe(O\text{-}SiMe_2)_m]^+$ ion series, whilst the peaks marked "n" are members of the $[Me_3Si(O\text{-}SiMe_2)_n]^+$ series. These ion series are illustrated in Table 5-2.

only minor modifications to the experimental set-up, characteristic mass spectra can be obtained which can be used to identify non-aromatic polymer systems, without the complexity associated with VUV generation required for SPI studies.

5.5 Concluding Remarks

The results shown here demonstrate that L2MS is a versatile technique for the characterisation of polymers, enabling *in situ* detection of trace levels of additives in addition to the bulk polymer. The analysis of chemical additives within bulk polymers is a complex problem. Extraction-based procedures are well established, but they are frequently time-consuming and laborious procedures. Direct analysis of additives in bulk polymers is an attractive methodology. However, traditional mass spectrometric approaches are not suitable for the analysis of such species, and other more recent techniques, such as FAB and SIMS, often suffer from considerable matrix interference. This work has shown that L2MS can generate simple, readily interpretable mass spectra for such molecules.

Photoionisation mass spectra at 266 nm and 193 nm for a series of antioxidants and UV stabilisers showed marked differences in their photofragmentation behaviour. This wavelengths dependence allows unambiguous identification of these additives, even including differentiation between isomeric species. It has also proved possible to detect these additives in polypropylene (PP) and polyoxymethylene (POM) polymers, at concentrations consistent with commercial polymer formulations. In the case of the PP polymer formulation it was possible to detect an oxidation product of the antioxidant Irgafos 168 formed either during processing or natural aging of the polymer. Such measurements could be extended to allow monitoring of additive degradation levels in aged polymer samples.

This study has also demonstrated the potential of L2MS as a surface analytical technique. It has been shown that it is possible to detect species on the surfaces of polymers, which are not present in the bulk of the sample. It should prove possible to extend this work using spatially resolved desorption to probe for additive migration and aggregation. Indeed, the use of this technique for depth profiling has recently been demonstrated [33].

It has also proved possible using L2MS to generate useful information on the polymer matrix itself, even when the polymers do not contain a UV chromophore. Non-resonant MPI, SPI and LIPEI were all shown to be effective for generating mass spectra which were characteristic of the polymer under investigation. Repeat unit and terminating group data was easily extractable from the mass spectra, although the oligomer distributions obtained were unsuitable for average molecular weight calculations. In each case, only slight modifications to the existing experimental set-up were required. Therefore, in the area of *in situ* analysis, the use of REMPI in conjunction with one of these general non-selective ionisation techniques allows both trace aromatic components (such as additives) and the polymer matrix itself to be quickly characterised.

References

[1] C. R. Redpath, *PhD Thesis, The University of Edinburgh*, 1995

[2] P. A. D. T. Vimalasiri, J.K. Haken, P. P. Burford, J. *Chromatogr.* **300**, 300, (1984).

[3] D. Munteanu, A. Isfan, C. Isfan, I. Tincul, *Chromatographia* , **23**, 7, (1987).

[4] M. A. Haney, W. A. Dark, *J. Chromatogr. Sci*, **18**, 655, (1980).

[5] F. Sevini, B. Marcato, *J. Chromatogr.*, **260**, 507, (1883).

[6] M. W. Raynor, K. D. Bartle, I. L. Davies, A. Williams, A. A. Clifford, J. M. Chalmers, B. W. Cook, *Anal. Chem.*, **60**, 427, (1988)

[7] R. P. Lattimer, R. E. Harris, *Mass Spectrom. Rev.*, **4**, 369, (1985).

[8] D. W. Carlson, M. W. Hayes, H. C. Ransaw, R. S. McFadden, A. G. Altenau, *Anal. Chem.*, **43**, 1874, (1971).

[9] R. P. Lattimer, K. R. Welch, *Rubber Chem. Technol.*, **53**, 151, (1980).

[10] R. P. Lattimer, R. E. Harris, D. B. Ross, H. E. Diem, *Rubber Chem. Technol.*, **57**, 1013, (1984).

[11] A. T. Jackson, A. Buzy, J. H. Scrivens, K. R. Jennings, *Proceedings of the 43rd ASMS Conference on Mass spectrometry and Allied Topics*, Atlanta. GA., p750, (1995).

[12] A. T. Jackson, A. Buzy, K. R. Jennings, J. H. Scrivens, *submitted to Eur. Mass Spectrom.*, (1996).

[13] P. Rudewicz, B. Munson, *Anal. Chem.*, **58**, 358, (1986).

[14] R. P. Lattimer, R. E. Harris, C. K. Rhee, H. -R. Schulten, *Anal. Chem.*, **58**, 3188, (1986).

[15] R. P. Lattimer, *J. Anal. Appl. Pyrol.*, **26**, 65, (1993).

[16] M. Barber, R. S. Bordoli, R. D. Sedgwich, A. N. Taylor, *J. Chem. Soc., Chem. Commun.*, 325, (1981).

[17] N. Furstenau, F. Hillenkamp, R. Nitsche, *Int. J. Mass Spectrom. Ion Proc.*, **31**, 85, (1979).

[18] C. L. Johlman, C. L. Wilkins, J. D. Hogan, T. L. Donovan, D. A. Laude, M. -J. Youssefi, *Anal. Chem.*, **62**, 1167, (1990).

[19] (a) M. P. Mawn, R. W. Linton, S. R. Bryan, B. Hagenhoff, U. Jürgens, A. Benninghoven, *J. Vac. Sci. Technol.*, A, **9**, 1307, (1991); (b) R. W. Linton, M. P. Mawn, A. N. Belu, J. M. Desimone, M. O. Hunt, Y. Z. Menceloglu, H. G. Cramer, A. Benninghoven, *Surf. Interf. Anal.*, **20**, 991, (1993).

[20] M. J. Dale, A. C. Jones, S. J. T. Pollard, P. R. R. Langridge-Smith, A. G. Rowley, *Environ. Sci. Technol.*, **27**, 1693, (1993).

[21] M. J. Dale, A. C. Jones, S. J. T. Pollard, P. R. R. Langridge-Smith, *Analyst*, **119**, 571, (1994).

[22] M. J. Dale, O. H. J. Downs, K. F. Costello, S. J. Wright, P. R. R. Langridge-Smith, J. N. Cape, *Environ. Pollut.*, **89**, 123, (1995).

[23] Q. Zhan, P. Voumard, R. Zenobi, *Rapid Commun. Mass Spectrom.*, **9**, 119, (1995).

[24] J. G. Mackintosh, C. R. Redpath, A. C. Jones, P. R. R. Langridge-Smith, A. R. Mount, *J. Electroanal. Chem.*, **388**, 179, (1995).

[25] D. A. Lustig, D. M. Lubman, *SPIE Laser Photoionisation and Desorption Surface Analytical Techniques*, **1208**, 170, (1990)

[26] D. A. Lustig, D. M. Lubman, *Int. J. Mass Spectrom. Ion Proc.*, **107**, 265, (1991)

[27] K. R. Lykke, D. H. Parker, P. Wurz, J. E. Hunt, M. J. Pellin, D. M. Gruen, J. C. Hemminger, *Anal. Chem.*, **64**, 2797, (1992)

[28] S. J. Wright, M. R. Dale, P. R. R. Langridge-Smith, Q. Zhan, R. Zenobi, Anal. Chem., **68**, 3585, (1996)

[29] B. Asamoto, J. R. Young, R. J. Citerin, *Anal. Chem.*, **62**, 61, (1990)

[30] M. J. Dale, A. C. Jones, P. R. R. Langridge-Smith, K. F. Costello, P. G. Cummins, *Anal. Chem.*, **65**, 793, (1993).

[31] A. C. Jones, M. J. Dale, G. A. Keenan, P. R. R. Langridge-Smith, *Chem. Phys. Lett.*, **219**, 174, (1994)

[32] Q. Zhan, S. J. Wright, R. Zenobi, *submitted to J. Am. Soc. Mass Spectrom.*, (1996).

[33] Q. Zhan, R. Zenobi, S. J. Wright, P. R. R. Langridge-Smith, *submitted to Macromolecules*, (1996).

[34] X. Xiang, J. Dahlgren, W. P. Enlow, A. G. Marshall, *Anal. Chem.*, **64**, 2862, (1992).

[35] J. H. Arps, C. H. Chen, M. P. McCann, I. Datskou, *Appl. Spectrosc.*, **43**, 1211, (1989).

[36] S. E. Van Bramer, M. V. Johnston, *J. Am. Soc. Mass Spectrom.*, **1**, 419, (1990).

[37] S. E. Van Bramer, M. V. Johnston, *Appl. Spectrosc.*, **46**, 255, (1992).

[38] R. J. J. M. Steenvorden, P. G. Kistemaker, A. E. De Vries, L. Michalak, N. M. M. Nibbering, *Int. J. Mass Spectrom. Ion Proc.*, **107**, 475, (1991).

[39] C. Köster, J. Grotemeyer, *Org. Mass Spectrom.*, **27**, 463, (1992).

[40] D. Feldmann, J. Kutzner, J. Laukemper, S. MacRobert, K. H. Welge, *Appl. Phys. B.*, **44**, 81, (1987).

[41] J. B. Pallix, U. Schühle, C. H. Becker, D. L. Huestis, *Anal. Chem.*, **61**, 805, (1989).

[42] *The Analytical Chemistry of Silicones, Chemical Analysis*, A. Lee-Smith (Ed.), vol. 112, Wiley, New York, 1991.

[43] *The Analytical Chemistry of Silicones, Chemical Analysis*, A. Lee-Smith (Ed.), vol. 112, Wiley, New York, p451, 1991.

[44] V. Orlov, *Zhur. Obshsch. Khim.*, **37**, 2300, (1967).

[45] F. Moritz, M. Dey, K. Zipper, S. Prinke, J. Grotemeyer, Org. Mass Spectrom., **28**, 1467, (1993)

[46] D. C. Schriemer, L. Li, Anal. Chem., **68**, 250, (1996)

[47] *SIMION 3D Version 6.0, Princeton Electronics*, Princeton, NJ, (1995)

Chapter 6

Further Analytical Applications of L2MS

6.1 Introduction

The work presented so far in this thesis has clearly illustrated the flexibility of the L2MS technique for the analysis of a wide variety of large polar, thermally labile and involatile molecules, some of which are difficult to analyse by other mass spectroscopic means. The separation of the desorption and ionisation events enables independent optimisation of both processes, providing facile control over the degree of fragmentation observed in the mass spectra. In addition, the two-stage nature of L2MS enables the great selectivity inherent in the photoionisation process to be exploited and permits the optimum selection of the photoionisation scheme. The results presented in Chapter 5 demonstrated that near-resonant MPI facilitates the selective detection of minor aromatic components from real complex mixtures, demonstrating effectively the potential of this technique for the investigation of real complex samples.

The results presented in this Chapter illustrate two further applications of L2MS. In the first example, it will be shown that it is possible to assay for the priority pollutants, polycyclic aromatic hydrocarbons (PAHs) directly from their host environment, in this case aerosol particulates. The second example will demonstrate the effectiveness of L2MS for studying conducting polymer films. It is believed that such conducting films, such as electrochemically polymerised indoles, may find use in a wide variety of sensor applications. It will be shown that it is possible using L2MS to characterise these polymers directly from the electrode surface.

6.2 *In Situ* Analysis of PAHs from Aerosol Particulates

6.2.1 Introduction

Polycyclic aromatic hydrocarbons (PAHs) are ubiquitous in the environment, having widespread natural and anthropogenic sources [1]. Until the beginning of the 20th century, there was a natural equilibrium between the production and degradation of PAHs. However, PAHs are also produced as a result of incomplete combustion of fossil fuels, such as coal, fuel-oil and petrol. Increasing industrial development has, therefore, disturbed this equilibrium, leading to an increase in the accumulation rates of PAHs. Early studies, in which PAHs were isolated from synthetic tars, led to the discovery of the first chemical carcinogen, dibenz[a,h]anthracene [2]. Subsequent work has since identified many other PAHs to be potent animal carcinogens [3,4]. In the light of this, PAHs have been classified as priority pollutants by the US Environmental Protection Agency (EPA).

PAHs are found in the atmosphere, both in gaseous form and adsorbed onto particulate matter. PAHs generally have low vapour pressures, and consequently readily condense onto particulates [5]. Aerosol particulates are easily transported over large distances, and can be found throughout the atmosphere, even in remote oceanic [6] and polar atmospheres [7]. In such regions, remote from pollution sources, PAHs are predominantly associated with particulate matter. Fine particulates can enter the respiratory system and be deposited in the lung. In general, chemicals administered to the lung as fine particulates in aerosol form, or orally via drinking water, are expected to be more bioavailable than chemicals administered as solid matrices [1]. Therefore, the reported carcinogenic and mutagenic properties of PAHs renders their presence in such particulate matter a potential health hazard [8]. It is, therefore, of major importance to be able to assay for PAHs in respirable fine particulate matter.

The most widely used means of investigating PAHs in such samples are based on sample extraction and chromatographic separation, using gas chromatography (GC) or high-performance liquid chromatography (HPLC), followed by some form of mass

spectrometry. Due to low volatility and high affinity for the stationary phase, the detectable mass range attainable using GC-MS for PAHs is limited to around m/z = 300. Furthermore, the low concentration of PAHs often requires that pre-concentration and purification steps are employed prior to analysis.

Extraction and separation procedures are expensive and time consuming. In addition, extraction-based methodologies cannot guarantee that the integrity of the mixture is maintained. Processes occurring during and after extraction, such as biotransformation and photodegradation, can result in an inaccurate picture of the sample composition. An alternative approach is to use desorption techniques, such as SIMS [9], FAB [10] and LD [11,12], in which ions, fast atoms or photons are used to bombard solid samples. However, these techniques are non-selective, and any mass spectral information from the analysis of complex mixtures is often obscured by matrix or fragmentation peaks.

The ability to obtain a fingerprint mass spectrum for a real environmental sample directly, without recourse to extraction, separation or pre-concentration, represents an attractive methodology. Considerable effort has been directed towards the development of techniques capable of analysing contaminants *in situ*. These include supercritical fluid extraction [13], laser-excitation fluorescence [14], thermal desorption mass spectrometry [15] and remote laser induced fluorescence [16].

In contrast to chromatographic methods, large involatile and thermally labile molecules are amenable to analysis by L2MS. Work previously carried out in this laboratory has shown that L2MS is a technique which is well suited to the analysis of environmental samples contaminated with PAHs [17,18]. It has been possible to detect PAHs, without any evidence of matrix interference, directly from a wide variety of samples, including soils, oils, coal soot and coal-tar creosote. Work carried out by other groups has shown that PAHs can also be detected directly in meteorites [19] and suspended particulates collected on quartz fibres [20]. The aim of the present study was to demonstrate the ability of L2MS to determine the polyaromatic components of cloud-water particulates, directly from the bulk particulate matter [21]. The mass spectra obtained using two different ionisation

wavelengths, 193 nm and 248 nm, are compared and contrasted. In addition, the possible application of this technique for widespread screening of condensed aerosol particulates is assessed.

6.2.2 Sample Collection and Preparation

The cloud water samples were taken from the data bank collected by the NERC Institute of Terrestrial Ecology, Penicuik, Midlothian. The samples were collected in an open area of moorland at Dunsair heights (602 m above sea level) near Peebles, Scotland. The samples were collected in a polypropylene bottle by a conical passive Harp-wire device [22] strung with a polypropylene filament, 0.55 mm in diameter, as shown in Figure 6-1. Cloud water droplets condense onto the strings and accelerate under gravity into the collection vessel. A polypropylene faced lid, 1,200 mm diameter, was supported over the collection device in order to minimise rainfall contamination. Raindrops contain a smaller concentration of particulate matter than clouds, and therefore, excessive rainfall contamination would have produced inaccurate results. The Harp-wire device excluded raindrops larger than 0.5 mm diameter at windspeeds of up to 5 ms^{-1}. An aliquot of 100 cm^3 of each sample collected was filtered through a polycarbonate membrane (Nucleopore, Costar, UK), loading the membrane with solid particles in the process. The filter was then dried over phosphorus pentoxide in a vacuum desiccator to a constant weight. Essentially, no further sample preparation was required prior to analysis.

6.2.3 Screening of Filtrates for PAHs using L2MS

Portions of each filter were attached to a MACOR sample probe, and analysed directly by L2MS using the non-entrainment configuration of the instrument, as outlined in Chapter 3. Desorption was carried out using a CO_2 laser at power densities typically around 2 x 10^6 Wcm^{-2}. The CO_2 laser output was focused to a spot-size of ~ $1mm^2$. Ionisation was carried out using either 193 nm or 248 nm radiation, using ionisation power densities which maximised the molecular ion yield whilst minimising fragmentation.

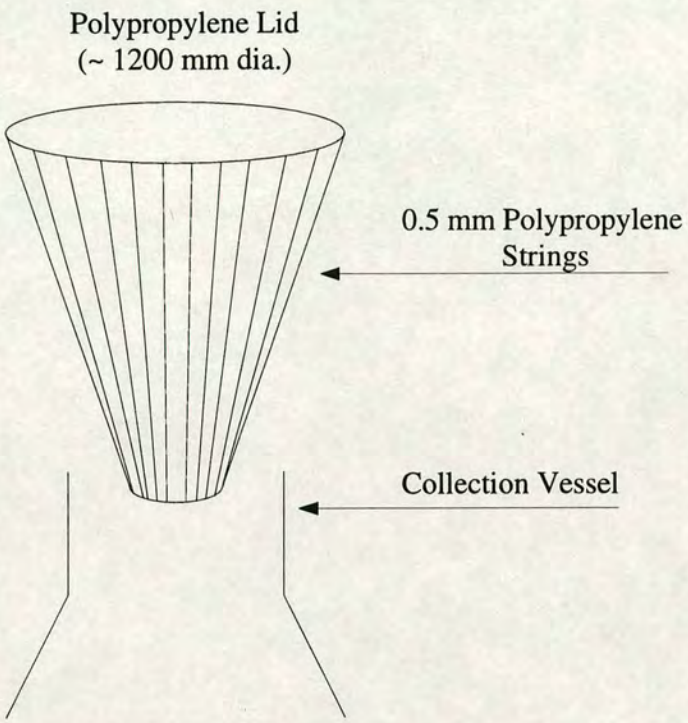

Figure 6-1: Schematic diagram of the conical passive Harp-Wire device used to collect cloud water samples.

Generally, the data collected for each sample was accumulated over 100 consecutive laser shots in order to increase the signal-to-noise ratio. The object of this series of experiments was to screen each sample for their PAH components. Therefore, a representative spectrum of the entire sample (i.e. an average) was required. For this reason, an area of approximately 3 mm^2 of the sample was interrogated in order to average out the shot-to-shot fluctuations arising from sample inhomogeneities. Although for screening applications a representative average is required, this work will be extended in future towards imaging of single particulates using spatially resolved desorption. For this type of application, averaging processes are not appropriate, since it is precisely the surface inhomogeneities of the particulate which are of interest.

The polycarbonate filters were screened for polycyclic aromatic components using 193 nm photoionisation. Initially, a relatively slow transient digitiser sampling interval of 40 ns was used. Although data collection at this sampling rate degrades

the ultimate mass resolving power of the spectrometer, it enables a larger mass window to be examined which essentially covers the whole mass range. The L2MS spectrum of a cloud water sample, collected on 25th November, 1987, is shown in Figure 6-2. There are two principal regions of interest in this mass spectrum. In the low mass region, below m/z = 100, a number of relatively intense peaks can be observed. The signals at m/z = 23, 27, 39 and 56 can be assigned to the presence of sodium, aluminium, potassium and iron in the sample. In addition to being used for molecular analysis, L2MS has previously been used to assay directly for trace levels of atomic species in complex matrices. It is possible to use REMPI to exploit atomic, species specific, intermediate electronic resonances. This is often referred to as resonance ionisation mass spectrometry (RIMS) [23]. However, in this case, no particular resonant intermediate states have been deliberately accessed. Ionisation is likely to proceed either in a non-resonant fashion (as in the case of iron), or via single photon ionisation (as in the case of sodium, potassium and aluminium). In the latter case, ionisation using 193 nm radiation is a one photon process, and so there is no requirement to access intermediate states. A number of other peaks are also present in the low mass region of the spectrum, although confident assignment of these peaks is more problematic; it is possible that these signals may result from fragmentation of the higher mass species, or may be intact unknowns in their own right.

It is the higher mass region, above m/z = 100, which is of primary interest with regard to analysis of molecular species contained in cloud-water particulates. The base peak in the spectrum is at m/z = 149. The occurrence of such a signal is generally characteristic of phthalates. Phthalates are ubiquitous impurities, found in many mass spectra, and are commonly used as plasticisers in plastics manufacture. Phthalates are known to produce characteristic mass spectra with a base peak at m/z = 149, which has previously been assigned to a protonated phthalic anhydride [24]. This ion can also lose CO_2 to produce a singly charged ion at m/z = 105. An ion of this mass is also observed in Figure 6-2, giving strong support to the assignment of this peak at m/z = 149 as being due to phthalate impurities. It was initially suspected that the presence of the phthalates resulted from leaching out of the plastic bottles in which the cloud water samples were collected. However, investigation of a blank,

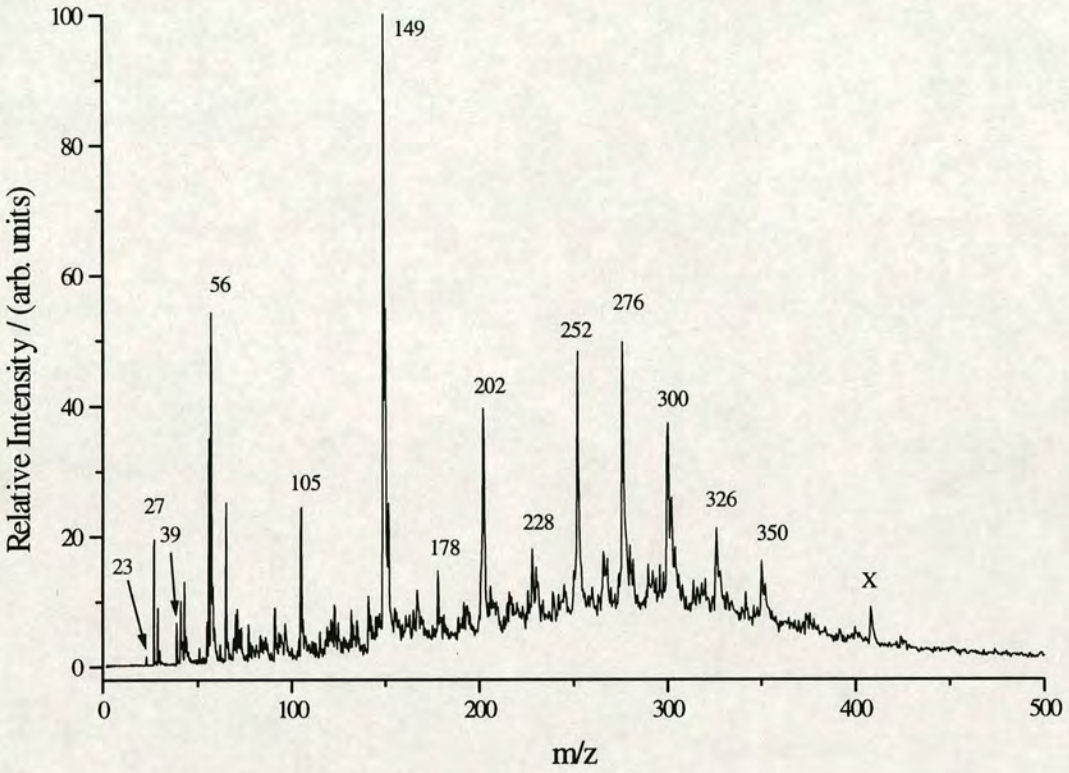

Figure 6-2: L2MS spectrum of cloud water filtrate obtained directly from the polycarbonate filter using 10.6 μm laser desorption and 193 nm photoionisation. The transient digitiser (TD) sampling interval used was 40 ns.

unused polycarbonate filter showed that a peak at m/z = 149 was again observed. This suggests that these materials are present in, or on, the polycarbonate filters themselves, and are not leached into the water sample from the plastic containers. It is unlikely that the phthalates are components of the particulate matter.

At still higher masses, all of the intense signals can be attributed to the molecular ions of parent PAH molecules. Signals are observed at m/z = 178, 202, 228, 252, 276, 300, 326 and 350, and are assigned to phenanthrene, pyrene, chrysene, benzo[a]pyrene, benzo[ghi]perylene, coronene, dibenzo[a,ghi]perylene and benzo-[a]coronene, or their isomers, respectively. The structures of these molecules are shown in Table 6-1. Additionally, a peak is also observed at m/z = 408 (denoted X). This corresponds to a known contaminant present in the diffusion pump oil used (Edwards L9). It is clear from this spectrum that rapid snapshot mass spectra can be obtained using L2MS, which provide significant information on the PAH content of cloud

PAH	m/z	Structure
Anthracene / phenanthrene	178	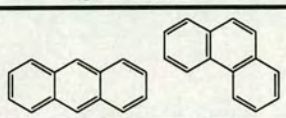
Pyrene	202	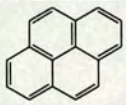
Chrysene	228	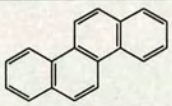
Benzo[a]pyrene	252	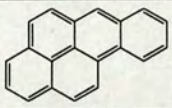
Benzo[ghi]perylene	276	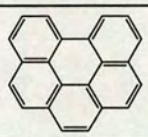
Coronene	300	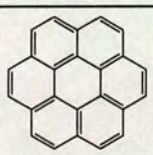
Dibenzo[a,ghi]perylene	326	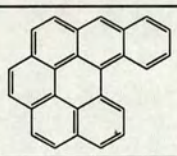
Benzo[a]coronene	350	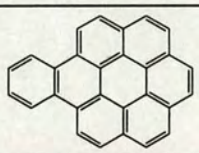
Dibenzo[a,bc]coronene	374	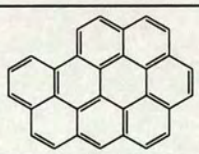
Benzonapthocoronene	424	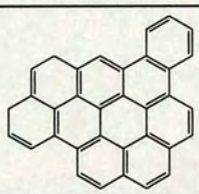
Benzo[a]ovalene	448	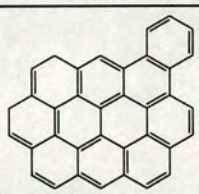

Table 6-1: Representative structures and molecular weights of PAHs detected in cloud-water particulate samples using L2MS.

water aerosol particulates. However, as can be seen in Figure 6-2, the peaks between m/z = 140 and 450 are not resolved to the baseline. It is, therefore, likely that additional information is lost as a result of this poor resolution, which is concealed beneath the "hump" in the baseline.

It is possible to improve the mass resolving power of the instrument, at the expense of the observable mass window, by sampling at a faster digitisation rate. Having carried out the experiment at the slow sampling rate, and identified the region of interest containing the PAH signals, it was possible to "zoom" in on this region (above m/z = 100) using a faster sampling interval of 20 ns. Figure 6-3a shows a mass spectrum of the same sample obtained using identical laser conditions, with 20 ns sampling. From this spectrum, it is immediately evident that more information is available. Although the PAH distribution is still not resolved to the baseline, single mass resolution is achieved even for the highest mass peak in the spectrum, at m/z = 448. Figure 6-3b shows the same spectrum, expanded into two sections in order to show the detailed information more effectively. Once again, as expected, the base peak in the mass spectrum is the phthalate impurity at m/z = 149. The associated fragment peak at m/z = 105 is also present, as is the background pump-oil contaminant (denoted with an X) as before. However, a number of other features can be extracted as a result of the improved mass resolution. In this case, the highest observable mass peak is now at m/z = 448. The additional peaks observed at m/z = 374, 424 and 448, which were obscured in Figure 6-2 as a result of the degraded mass resolution, can be assigned as benzo[a]ovalene, dibenzo[a,bc]coronene and benzonaptho-coronene, and/or their isomers, respectively. Structures for these molecules are also given in Table 6-1.

Closer examination of this mass spectrum reveals a progression of peaks, starting from prominent PAH peaks, separated by an interval of m/z = 14. Such progressions are shown for benzo[a]pyrene and coronene, (denoted with asterisks and + symbols, respectively) in Figure 6-3b. These species can be assigned to the presence of alkylated PAHs present in the cloud water particulates, and the presence of such species in airborne particulates is well documented [25].

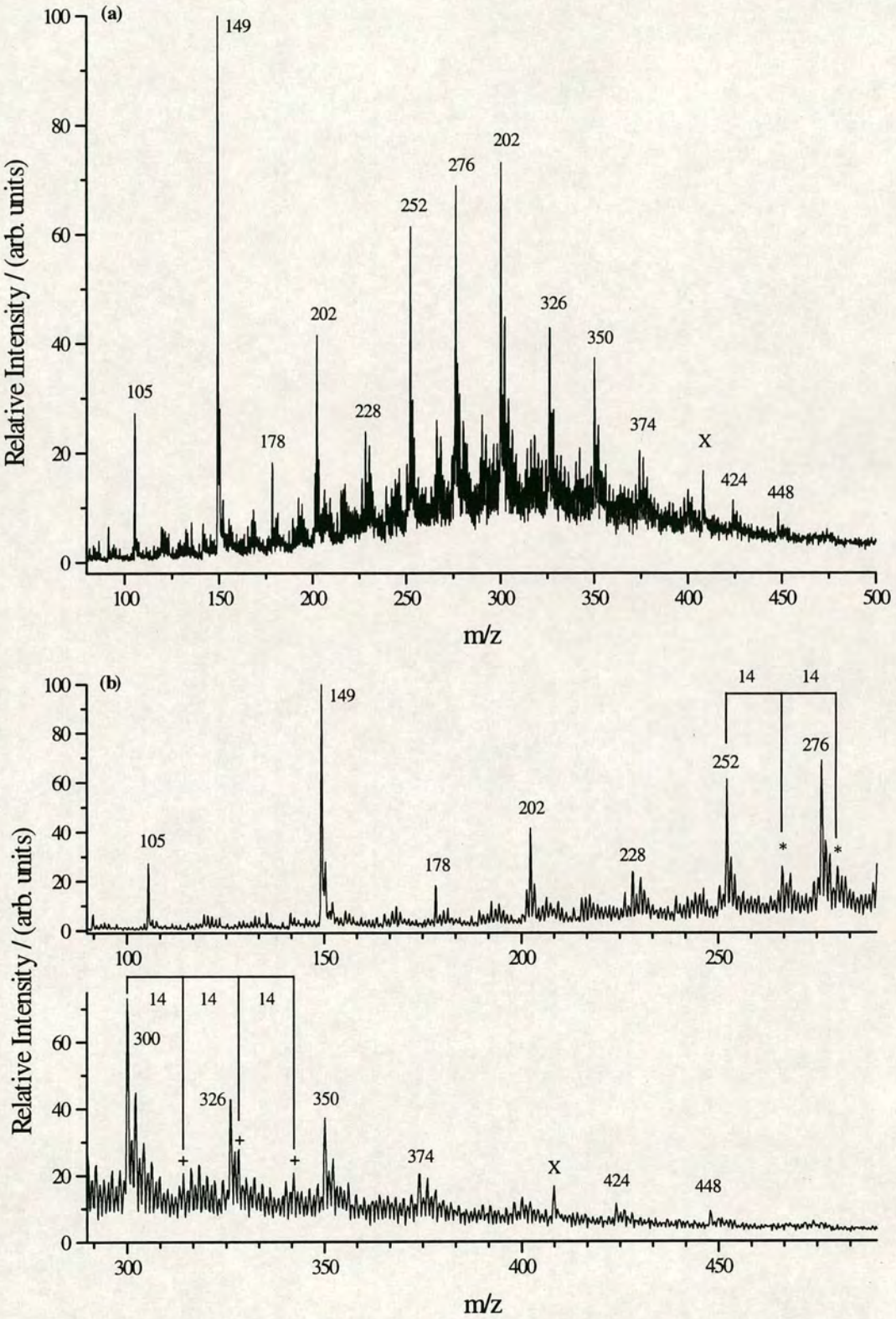

Figure 6-3: L2MS spectrum of cloud water filtrate obtained directly from the polycarbonate filter using 10.6 μm laser desorption and 193 nm photoionisation. The TD sampling interval used was 20 ns, resulting in improved mass resolution: (a) shows the full mass spectrum, whereas (b) shows the same spectrum expanded into two regions.

6.2.4 Quantitative Assessment of PAH Concentration using L2MS

The previous section demonstrated that L2MS is effective for screening PAH components directly from the bulk particulate matter. However, it would also be useful to know how much of each PAH was present in any given sample, in order to assess if the observed contamination is within specified limits. Unfortunately, parent-ion peak intensities observed in L2MS spectra are not solely proportional to the concentration of the given compound present in the mixture; the signal intensity is also dependent on the overall ionisation efficiency, along with other factors. For PAHs, the absorption of two UV photons is generally required to achieve ionisation. As this is likely to be a near-resonant process, then it can be assumed that the absorption cross-section for the second photon, σ_2 is the same for all PAHs. Therefore, the overall ionisation efficiency is primarily determined by the absorption cross-section of the first photon, σ_1. Therefore, the relative intensities observed within a single mass spectrum do not necessarily reflect the relative concentrations of analyte present in the sample mixture; rather, the observed signal intensity is a function of *both* concentration *and* the absorption cross-section, σ_1.

This effect is clearly illustrated in Figure 6-4a, which shows the mass spectrum of the same cloud-water sample, obtained instead using 248 nm photoionisation. Striking differences between this spectrum, and that obtained using 193 nm ionisation are clearly evident. The base peak in the previous spectrum at m/z = 149, is entirely absent from that in Figure 6-4a. Instead, the dominant peak in this spectrum is at m/z = 178, which corresponds to one of the isomers anthracene or phenanthrene. Although the other major signals again correspond to the same PAHs as observed previously, it appears that the higher mass components of the mixture are not detected, giving the impression that the mass spectrum has shifted to lower mass. For example, the peaks at m/z = 374, 424 and 448 observed using 193 nm ionisation are absent in this spectrum.

Differences in the relative intensities of peaks in mass spectra of the same sample, carried out using different ionisation wavelengths, can be accounted for, at least to a first approximation, by considering their molar absorption coefficients, ε, which can

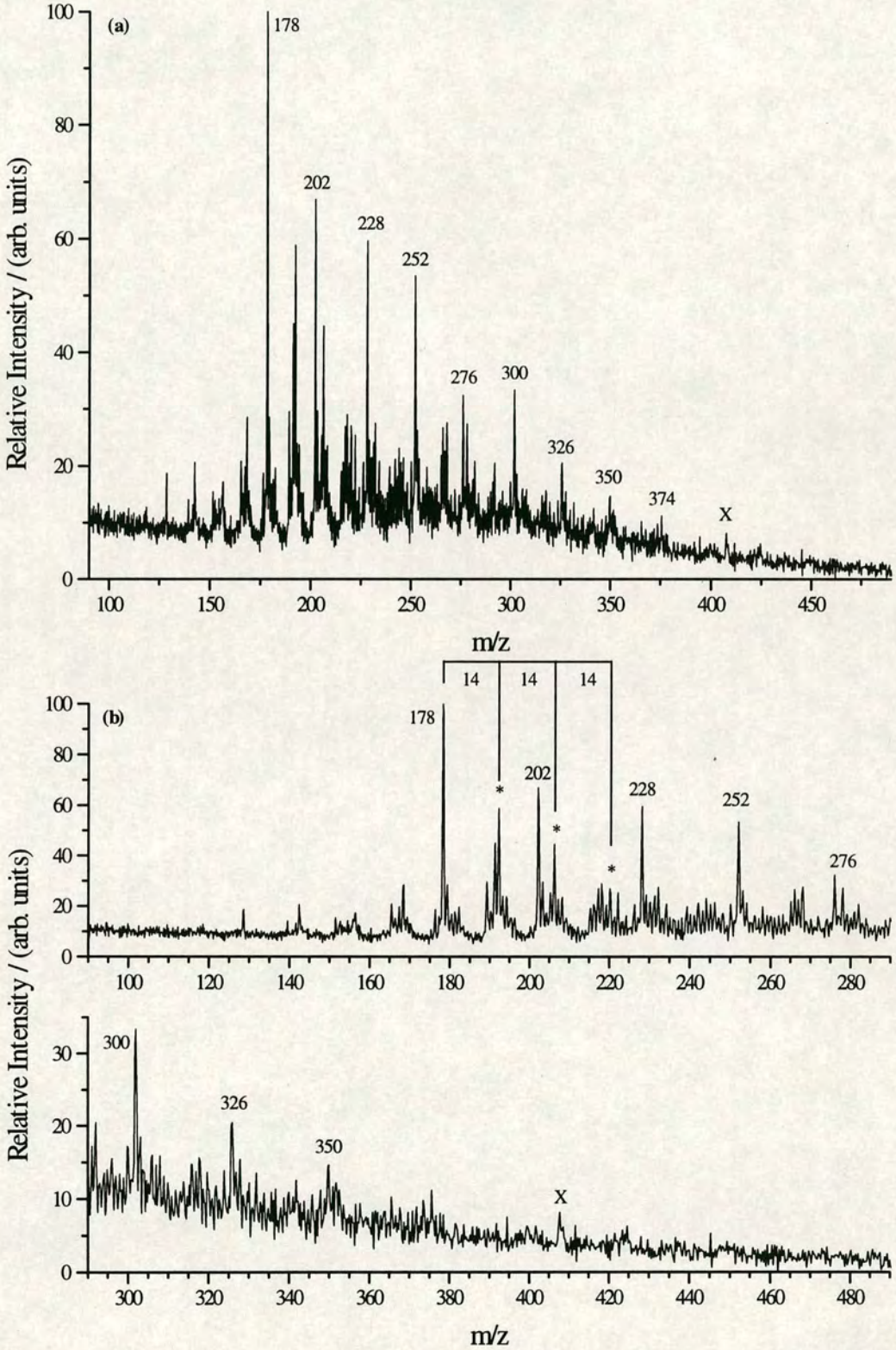

Figure 6-4: L2MS spectrum of cloud water filtrate obtained directly from the polycarbonate filter using 10.6 μm laser desorption and 248 nm photoionisation. The TD sampling interval used was 20 ns: (a) shows the full mass spectrum, whereas (b) shows the same spectrum expanded into two regions.

be related to the single-photon absorption cross-section, σ_1. The liquid-phase molar absorption coefficients provide a general indication of what the broad band gas-phase absorption coefficients will be. Solvent molecules in liquid-phase UV/VIS spectra cause broadening of the absorption bands, and induce shifts to longer wavelengths [26]. It has previously been shown that the broad band gas-phase absorption spectra exhibit similar features to UV/VIS spectra, shifted by around 3-5 nm to the blue. Given that the desorbed neutrals are not cooled in a supersonic expansion, the absorption bands are predicted to be relatively broad, and hence the approximation of gas-phase absorptions by those in solution phase seems reasonable.

Figure 6-4b shows the same L2MS spectrum expanded into two regions to display the detailed information available. Photoionisation using 248 nm radiation results in a spectrum in which the base peak is at m/z = 178, corresponding to anthracene or phenanthrene. This signal was relatively weak in the 193 nm spectrum. These results reflect the differences in the molar absorption coefficients at the two excitation/ionisation wavelengths employed. For anthracene at 252 nm, ε = 208000 $mol^{-1}cm^{-1}$, with phenanthrene having a value of ε = 64000 mol^{-1} cm^{-1} at the same wavelength. However, at the shorter wavelength of 212 nm (the closest value to 193 nm available), the corresponding values are ε = 19000 and 34800, respectively. These values of ε are clearly much lower at the shorter wavelength, with the result that the first 248 nm photon is absorbed much more readily than the corresponding 193 nm photon. This results in more efficient detection of these isomeric species at 248 nm than 193 nm.

A progression of peaks (denoted with asterisks) separated by m/z = 14 can also be observed in Figure 6-4b, starting at m/z = 178. This can also be explained by considering the strength of the absorption cross-sections of anthracene and fluoranthene at 248 nm. Given that it is primarily the π-system in the aromatic ring structure which provides the chromophore for the UV radiation, then it is reasonable to expect that the addition of alkylating substituents will not induce large shifts in the UV absorption bands. Therefore, one would expect that the methylated peaks associated with anthracene/phenanthrene will also be enhanced due to similarly large

ε values. As a result, an easily identifiable homologous series of peaks can be observed in the mass spectrum obtained at 248 nm, whereas the spectrum obtained at 193 nm is very much weaker.

It also appears that some of the higher mass PAH peaks are enhanced using 193 nm ionisation. This again fits the molar absorption data for these molecules at the wavelengths used. Benzo[ghi]perylene at m/z = 276 has a relatively low molar absorption coefficient around 248 nm (ε = 17000 mol^{-1} cm^{-1} at 254 nm), but a high molar absorption coefficient around 193 nm (ε = 59000 mol^{-1} cm^{-1} at 210 nm). Comparing this information with the relative intensities in Figure 6-4, it can be seen that the low relative intensity of ions at m/z = 276 compared to that of the peak at m/z = 178 is consistent with the lower molar absorption coefficient for benzo-[ghi]perylene at 248 nm.

It would be dangerous, however, to use the solution-phase molar absorption data to speculate as to which of two isomers is actually present. For example, consider the peak at m/z = 202 in the spectrum shown in Figure 6-3. This signal can be attributed to pyrene or its isomer fluoranthene. Inspection of the solution phase UV/VIS absorption spectra shows that fluoranthene has a much larger molar absorption coefficient than pyrene at such short UV wavelengths. It is possible that the observed mass peak at m/z = 202 is more representative of fluoranthene than pyrene. However, although the absorption cross-section of fluoranthene is larger than that of pyrene, the relative concentrations of these species will also determine their relative contribution to the total peak intensity.

In principle, it is possible to differentiate between isomeric PAHs using L2MS. Zenobi et al. [20] have shown that it is possible to distinguish between pyrene and fluoranthene isomers by measuring their UV absorption profiles using REMPI. Scanning the ionisation laser wavelength and monitoring the signal intensity of the parent ion allows the UV absorption profile to be mapped out. This is relatively straightforward for volatile PAHs, such as pyrene and fluoranthene, which have an appreciable vapour pressure at the operating pressures used. However, for the less volatile higher mass components, this is not straightforward. Inconsistencies in gas-

phase concentrations derived from the desorption process make measurements of this type very difficult.

Desorption factors will also affect the relative signal intensities in L2MS spectra. Problems regarding quantitation resulting from desorption instability are discussed in some detail in Chapter 7. Briefly, however, several factors may contribute to different relative gas-phase neutral concentrations being liberated following IR laser desorption. The adsorption and binding characteristics of PAHs to particulate matter are unlikely to be uniform. This could result in widely varying desorption efficiencies from point-to-point across a sample surface, thereby making quantitative estimates very difficult. Zare's group [19] have demonstrated that relative intensities of low and high mass peaks for a given sample at a particular ionisation laser wavelength depends upon the desorption laser power density. This suggests that the adsorbate-substrate interaction can influence the distribution of neutrals in the gas-phase, and therefore, ultimately the ion signal intensity distribution in the mass spectrum. Although this problem can be minimised for a single sample by averaging over a more extensive area of the sample, relating this to a whole series of different samples, without detailed knowledge of the analyte-matrix interactions, would prove difficult.

Quantitation of the L2MS technique is evidently very important if its full analytical potential is to be realised. Therefore, research into finding some means of extracting useful quantitative information is imperative. One method, which has been used with some success previously on contaminated soil samples, is to use standard additions. It is possible that such spiking methodologies could be used for aerosol particulates, whereby known amounts of PAHs are added to the cloud water samples prior to filtration. However, as the dopant concentration increases, the desorption characteristics are almost certain to vary, since the spiked PAHs will not necessarily adsorb directly onto the particulate, but may be trapped between the particulates upon filtering. Furthermore, some of the PAHs may well be semi-soluble in water, and so some dopant may pass through the membrane upon filtering. This methodology is likely, therefore, to produce only semi-quantitative data at best.

An alternative method of obtaining semi-quantitative information would be to dope a known amount of PAH onto the surface of the bulk filtered particulate. This approach has the advantage that the amount of dopant on the surface of the filter is accurately known. However, the disadvantage of this methodology is that the dopant will not be homogeneously distributed over the particulates, rather it will be localised in patches of varying thickness. The desorption mechanism is likely to be different at all points over such as sample, with the result that differences in the gas-phase concentrations will be obtained, making quantitative analysis extremely difficult. It is clear that further research is required in order to find appropriate methodologies for quantifying the L2MS technique. This will be discussed in more detail in Chapter 7.

6.2.5 Concluding Remarks

The experiments described in this section have illustrated the unique abilities of L2MS for rapidly screening aerosol particulates for their aromatic components, in particular PAHs. This technique can be used to assay for these involatile and non-soluble materials, whereas techniques employing chromatographic separation have met with only limited success. Most importantly, however, L2MS can provide rapid, "snaphot" mass spectra of the particulate matter *directly* from the filter surfaces on which they were collected.

The nature of polyaromatic components (PACs) in an aerosol sample can provide a useful guide to the sources of contamination. By screening samples collected at a variety of locations, and measuring the variations in concentration of PACs in the airborne particulates, the point sources contributing to the pollution at different sampling sites can be identified. One of the difficulties in such monitoring processes stems from inconsistent variations in the concentrations of PAHs and PACs in air particulate matter sampled at short time intervals, due to variations in meteorological conditions, such as rainfall and wind direction change. In order to compensate for these variations it is necessary to accumulate data over extended periods of time. Analysis of these data would then provide information concerning the temporal fluctuations in PAH concentration. For example, the levels of carcinogenic PAHs in

air can be locally elevated by periods of wood or coal burning, and by short-term increases in traffic density.

Conventional analysis of such vast quantities of samples for PAHs would be extremely time consuming and prohibitively expensive. L2MS is a methodology which can be used to rapidly screen a large number of samples and yield specific information regarding their polyaromatic content. It also enables the investigation of particulates directly from the surfaces on which they were collected, thereby removing the necessity for all chemical extraction methods. This, therefore ensures that no chemical alteration of the sample takes place, and that contamination introduced by sample handling is minimised.

Although L2MS is ideally suited to this type of sample screening, it is not, at present, a straightforward matter to extract reliable quantitative information on PAH concentrations within samples. However, it is envisaged that with further work on the fundamentals of the desorption process, standard addition methodologies will prove to be successful in generating at the very least semi-quantitative information on PAH concentrations.

A useful extension of the technique would be to utilise an optical delivery system capable of enabling a spatially resolved laser desorption point focus of less than 50 μm. Similar instruments have been developed elsewhere, and has been used to identify complex aromatic molecules in interplanetary dust particles [27]. The use of spatially resolved laser desorption should allow the study of airborne particulates as individual particles. This may permit studies of the underlying mechanisms behind particulate formation.

6.3 L2MS of Electrochemically Polymerised Indoles

6.3.1 Introduction

There has been much recent interest in the electropolymerisation of heterocyclic molecules, such as pyrroles, thiophenes and indoles due to their ability to form electrically conducting polymer films [28,29]. There are several potential

applications for these polymer films, including polymer electrodes, electro-optical display devices, battery applications and information storage devices [30]. These polymer films can probably be tailored to meet specific analytical demands by varying the functional groups on the monomer species used in the polymerisation process. For example, the current passed by poly(indole-5-carboxylic acid) has been shown to display a marked dependence on the pH of the aqueous solution. It is, therefore, possible that that this may find an application as a fast-response pH sensor.

Until recently, despite the potential importance of electroplymerised indoles, little work has appeared in the literature on the structural characterisation of these materials. Mass spectroscopic characterisation of these conducting polymer films is likely to be problematic; the high molecular weights and the ability of these polymers to adhere strongly to surfaces, requires that desorption/ionisation techniques must be used. These relatively harsh conditions are likely to induce severe fragmentation processes, thereby limiting the extraction of useful information. In addition, the lack of selectivity of these ionisation techniques means that interference from excess electrolyte may result in very complex mass spectra.

In previous work carried out in this laboratory it was shown that L2MS is capable of aiding in the structural elucidation of electrochemically polymerised indoles [31]. A series of 5-substituted indole monomers, including indole 5-carboxylic acid (ICA) and 5-cyano-indole (CI), were electropolymerised, and investigated using L2MS. The details of the electrochemistry used to produce these polymer films can be found elsewhere [32,33]. In general, two fractions are obtained following these reactions: a low molecular weight fraction which is soluble in dimethylformamide (DMF), and a high molecular weight fraction which is insoluble in DMF, but soluble in dimethylsulphoxide (DMSO). In general, L2MS mass spectra of these 5-substituted indole polymers indicated the presence of a cyclic trimer. For example, in the case of I5CA, m/z =161, the base peak in the mass spectrum was observed at m/z = 477. This is consistent with a cyclic trimer, in which three indole monomers couple by each losing two hydrogen atoms. The postulated structure of the cyclic trimer for 5-

substituted indoles is shown in Figure 6-5. This structure has subsequently been confirmed by NMR studies [34].

Analysis of the higher molecular weight, DMSO soluble fraction resulted in similar mass spectra being obtained, albeit with much reduced signal intensity. However, when this fraction was examined using TLC, no trimer band was observed. This indicates that the polymer is comprised of linked trimer units, which produce neutral fragments following IR laser desorption. UV/VIS, IR and fluorescence studies support the hypothesis that the trimer unit is the basic building block of the polymer [35]. Further evidence in support of this hypothesis is that electro-polymerisation of both 5-substituted indole monomers and the free cyclic trimers (obtained from the DMF soluble fraction) have been shown to produce conducting polymer films with identical electrochemical and spectroscopic features [32].

The previous work by Redpath [31] demonstrated that L2MS is a suitable technique for the study and characterisation of conducting polymer films. The work presented here represents an extension of this earlier study. Novel 5-substituted indole *copolymers,* which have now also been separated chromatographically, have been characterised using L2MS. Most importantly, it has proven possible to detect the products of electrochemical polymerisation reactions directly from the host electrodes.

6.3.2 L2MS of 5-Substituted Indole Copolymers

As mentioned above, electropolymerised indole films display properties which may be exploited in a variety of sensor devices. In particular, 5-substituted polyindoles have been proposed at potential candidates for fast-response potentiometric sensors [30], as well as for the direct oxidation and reduction of biomolecules such as cytochrome c [36]. Polymer films which can interact with particular target analytes can be produced by informed choice of the substituent group. If this cannot be achieved directly, the polymer film itself can be further functionalised at the substituent in order to create the required specificity. Unfortunately, the addition of functional groups which confer particular desired

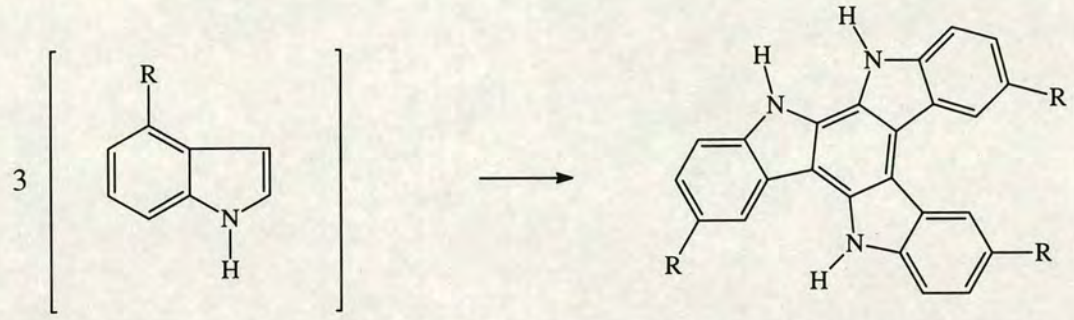

5-substituted Indole monomer **5-substituted Indole cyclic trimer**

R = -COOH, -CN, -H

Figure 6-5: Postulated structure for the cyclic trimer formed during electropolymerisation of 5-substituted indoles.

properties can, in some cases, inhibit film formation by enhancing solubility [37]. In cases where bulky substituent groups are used, film formation can be inhibited by steric factors.

An attractive methodology for fabricating these "problem" polymer films is to create copolymers with various indole monomers. This would have the effect of maintaining the desired chemical or physical property, whilst circumventing the adverse effects of enhanced solubility and steric interactions. L2MS, which has already been demonstrated to be effective in the characterisation of 5-substituted indole polymers [31], has been used in this work to investigate the copolymerisation of indole-5-carboxylic acid (ICA) and 5-cyano indole (CA) [38].

The samples investigated were produced by Mackintosh and Mount [38] at the University of Edinburgh. A 1:1 solution of ICA and CI were electropolymerised at +1.64 V with respect to the reference electrode. A detailed account of the electrochemistry used to produce these samples can be found elsewhere [38]. Once again, as was observed for the single-component 5-substituted polymerisation reactions, two fractions were obtained: a low molecular weight fraction soluble in DMF, and a higher molecular weight sample, soluble in DMSO. The DMF soluble fraction was examined by L2MS, using 266 nm photoionisation.

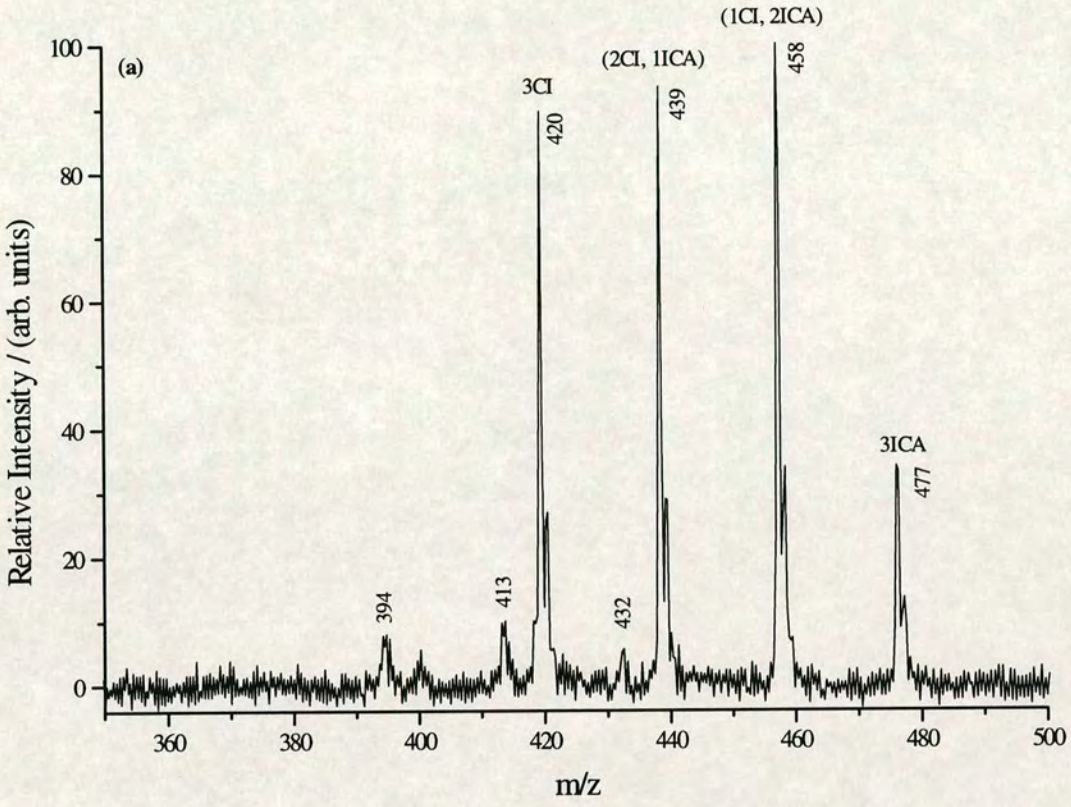

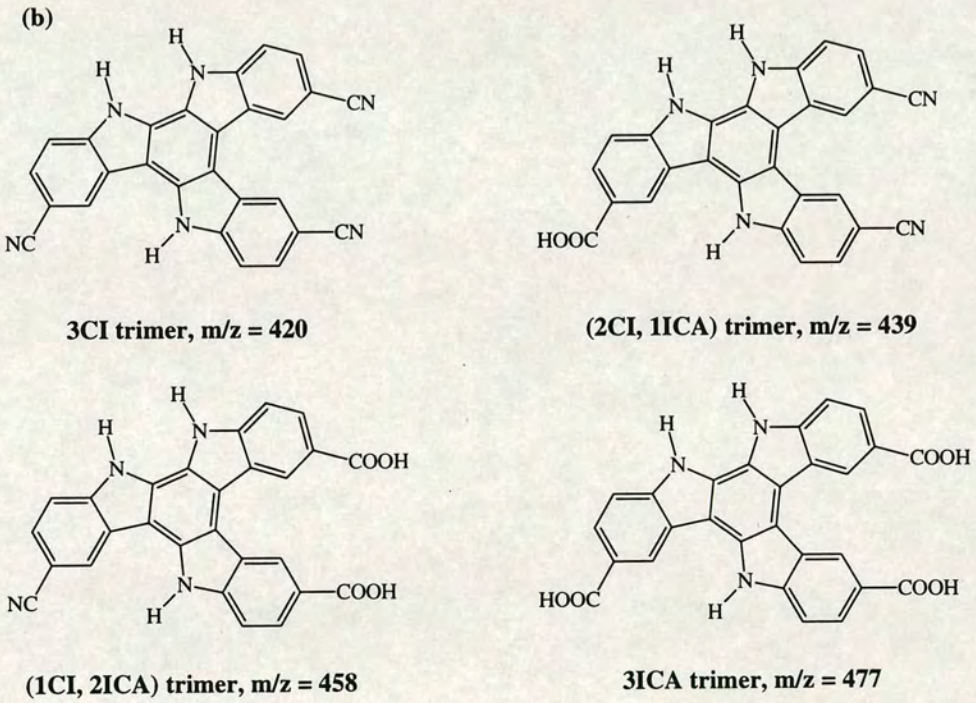

Figure 6-6: (a) L2MS spectrum of DMF soluble fraction of copolymer film produced by electroxidation of an equimolar mixture of CI and ICA, using 10.6 μm laser desorption and 266 nm photoionisation. (b) Proposed structures for asymmetric trimers and cotrimers produced by electroxidation of CI and ICA. It should be noted that each cotrimer shown is only one of three possible stuctures, since the three indole groups are not in identical environments.

A few drops of the DMF soluble fraction were placed on the sample probe, and the solvent evaporated using a heat-gun. Figure 6-6a shows the L2MS spectrum obtained following 266 nm photoionisation. Four intense molecular ion signals are observed at m/z = 420, 439, 458 and 477, corresponding to the four possible cyclic trimer products of the copolymerisation reaction. These were attributed to the CI trimer, the (2CI, 1CA) trimer, the (1CI, 2ICA) trimer and the 3ICA trimer, respectively. The structures of these species are illustrated in Figure 6-6b. The less intense peaks observed 1 u above these molecular ion signals corresponds to the ^{13}C isotope of the respective molecular ions. These mass spectra were recorded under soft-ionisation conditions, in order to minimise the observed fragmentation. However, weak fragment ions are observed at m/z = 394, 413 and 432, and correspond to loss of -COOH from each of the ICA containing trimers.

The approximately statistical 1:3:3:1 distribution of the copolymer peaks (with the exception of the 3CI trimer) suggests that there is no preference as to which of the two monomeric species are incorporated into the trimer. However, as was discussed in Section 6.2.4, the intensity of the ion signal observed for different molecules is a function, not only of concentration, but also of their relative absorption cross-sections at the ionisation wavelength employed. The absorption cross-sections were not expected to be greatly different for each of the four species present, since it is likely that excitation is via the indole chromophore. However, in order to confirm this, a 1:1 mixture of ICA and CI trimers was examined using 266 nm photoionisation. The resulting mass spectrum is shown in Figure 6-7. It is clear from this spectrum that the ionisation efficiencies of the two trimers are very similar, and that the different substituent groups do not induce any significant change in the absorption cross-sections at 266 nm. Therefore, the distribution of peaks observed in Figure 6-6a is representative of the concentration of each trimer copolymer species in the DMF soluble fraction.

It follows, therefore, that the proportion of free CI trimer in the DMF soluble fraction is significantly higher than the ICA trimer. This does not, however, necessarily mean that more CI trimer has been formed. Previous studies have shown

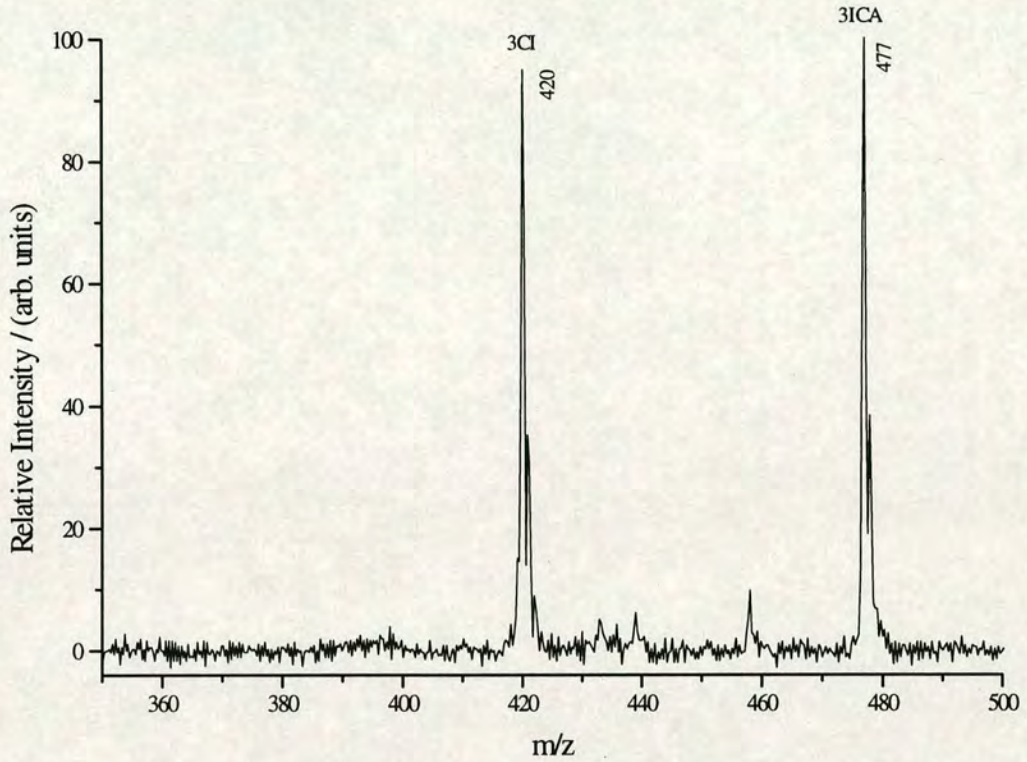

Figure 6-7: L2MS spectrum of an equimolar mixture of 3CI and 3ICA trimers obtained using 10.6 μm laser desorption and 266 nm photoionisation. This demonstrates that the different substituent groups on each of these molecules does not induce significant changes in their absorption cross-sections at 266 nm.

that the rate of linkage of free trimer to form polymer is lower for CI than for ICA [33]. This means that more free CI trimer will be present in the DMF soluble fraction. The degree of linkage of the cotrimers, (1CI, 2ICA) and (2CI, 1ICA), in the film has been found to be comparable to that for ICA trimer; assuming that the relative intensities of these cotrimer peaks also reflects their relative concentrations, it is clear that the total amount of CI trimer in the film is overestimated.

The DMF soluble fraction has also been separated by gel permeation chromatography (GPC) on a Sephadex column. Details of this can be found elsewhere [38]. Four fractions were eluted, and subsequently analysed using L2MS. Figure 6-8 shows the mass spectra obtained for the four fractions. Whilst it is clear each fraction contains more than one component, it is evident that some separation has occurred. The spectrum for the first fraction, shown in Figure 6-8a, shows predominantly CI trimer, with decreasing amounts of the other components of the mixture. The spectrum for the second fraction shows that more of the two cotrimers

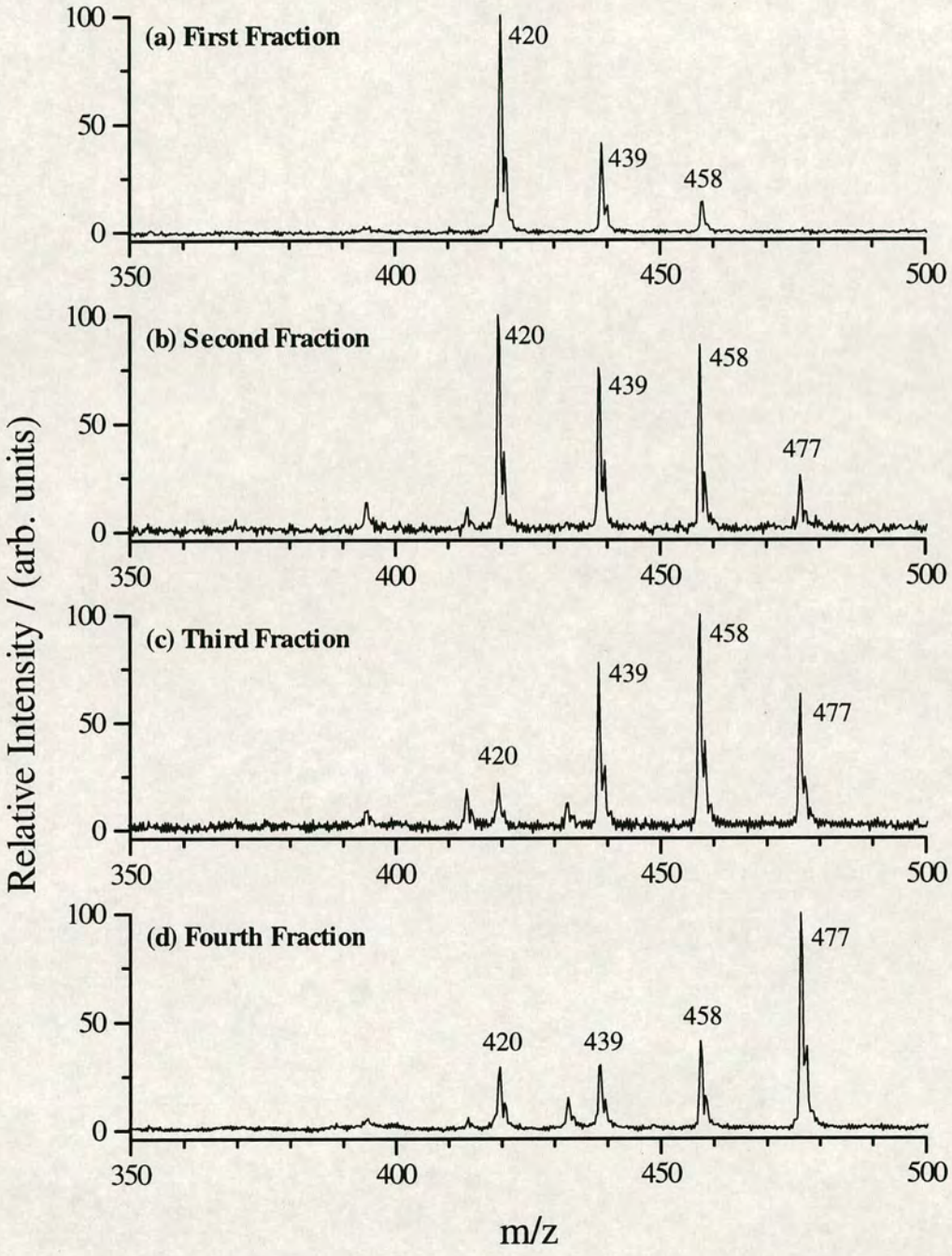

Figure 6-8: L2MS spectra of the four fractions of the original CI/ICA copolymer mixture which eluted from the Sephadex column. These spectra were obtained using 10.6 μm laser desorption and 266 nm photoionisation, and demonstrate that the individual trimer species can be partially separated.

are present in relation to the CI trimer, whilst the third fraction contains mainly the two cotrimer species. The final fraction to elute from the column is predominantly composed of ICA trimer, with only small concentrations of the other components. If more effective separation can be achieved, to the extent that each individual component can be isolated, then it is clear that polymer films with mixed functionality can be produced, which can be tailored to particular applications.

6.3.3 *In Situ* Detection of Polyindole Directly from the Electrode

L2MS is clearly a technique which is ideally suited to the analysis of conducting indole polymer films. If these materials do find application in various sensor devices, L2MS may well prove to be an acceptable technique for characterising such sensors, and monitoring their construction. In order for this to be feasible, however, the technique should be capable of providing *in situ* analysis of these materials, directly from the electrodes on which they are produced.

In order to explore this possibility, polyindole, which is deposited as a green-black film on the electrode, was chosen for study. As is the case for 5-substituted polyindoles, only part of the film is soluble in DMF, although the entire film is soluble in DMSO. However, in contrast to the 5-substituted polyindoles, TLC studies have shown that the DMSO soluble fraction consists of three components. The 5-substituted polyindoles were previously shown to consist of only two components; the free trimer and the polymer itself. Fluorescence excitation studies have also determined the presence of a third species, in addition to the cyclic trimer and polymer [39].

Previous L2MS studies by Redpath [31] confirmed the presence of a cyclic trimer species at m/z = 345 in the mass spectrum of the DMF soluble fraction. However, a relatively intense peak was also observed at m/z = 573. This was interpreted as a pentameric indole species, and is likely to be the cause of the additional bands observed in the TLC and fluorescence studies. However, the exact structure of this has yet to be determined.

Figure 6-9a shows the L2MS spectrum obtained using 266 nm ionisation for the DMF soluble fraction of polyindole which is recovered from the electrode. This is shown simply for comparison with the *in situ* spectra. This spectrum is essentially identical to that observed by Redpath using 248 nm photoionisation; the base peak at m/z = 345 can be assigned to the cyclic trimer, with the less intense peak at m/z = 573 assigned to the indole pentamer.

Figure 6-9b shows an L2MS spectrum obtained when the conducting polymer film was interrogated directly from the electrode, without any pretreatment or cleaning. The signal-to-noise is clearly much reduced from that in the spectrum above. However, this is not too surprising, since the sample studied in the top spectrum was recovered from the electrode, and applied to a stainless steel sample probe in concentrated form. The low mass signals in the lower spectrum, below m/z = 30, are thought to be due to nascent ion signals from excess electrolyte present on the polymer film. The presence of a peak at m/z = 117, indicates the presence of unreacted monomer on the polymer film. The other intense signals in this region of the mass spectrum at m/z = 142 and 162 are as yet unassigned, but could possibly result from contaminants on the gold electrode or in the electrolyte solution.

The peak corresponding to the cyclic indole trimer at m/z = 345 is easily identified. However, the pentamer species is not observed in this mass spectrum. Previous work has shown that in order for the pentamer to be observed, higher desorption laser power densities are required [31]. Attempts were made to generate a pentamer signal by increasing the desorption laser power density. However, this resulted in all signals being masked by signals to low mass, presumably resulting from nascent ion signals produced by desorption of electrolyte. It is hoped that in future work it will be possible to clean the excess electrolyte from the electrode, which will allow the desorption laser power density to be increased. In addition to possibly generating a pentamer signal, this will have the effect of increasing the overall signal-to-noise ratio. Excess indole monomer present in previous DMF soluble fractions, detected using L2MS, has been removed by washing in DMF.

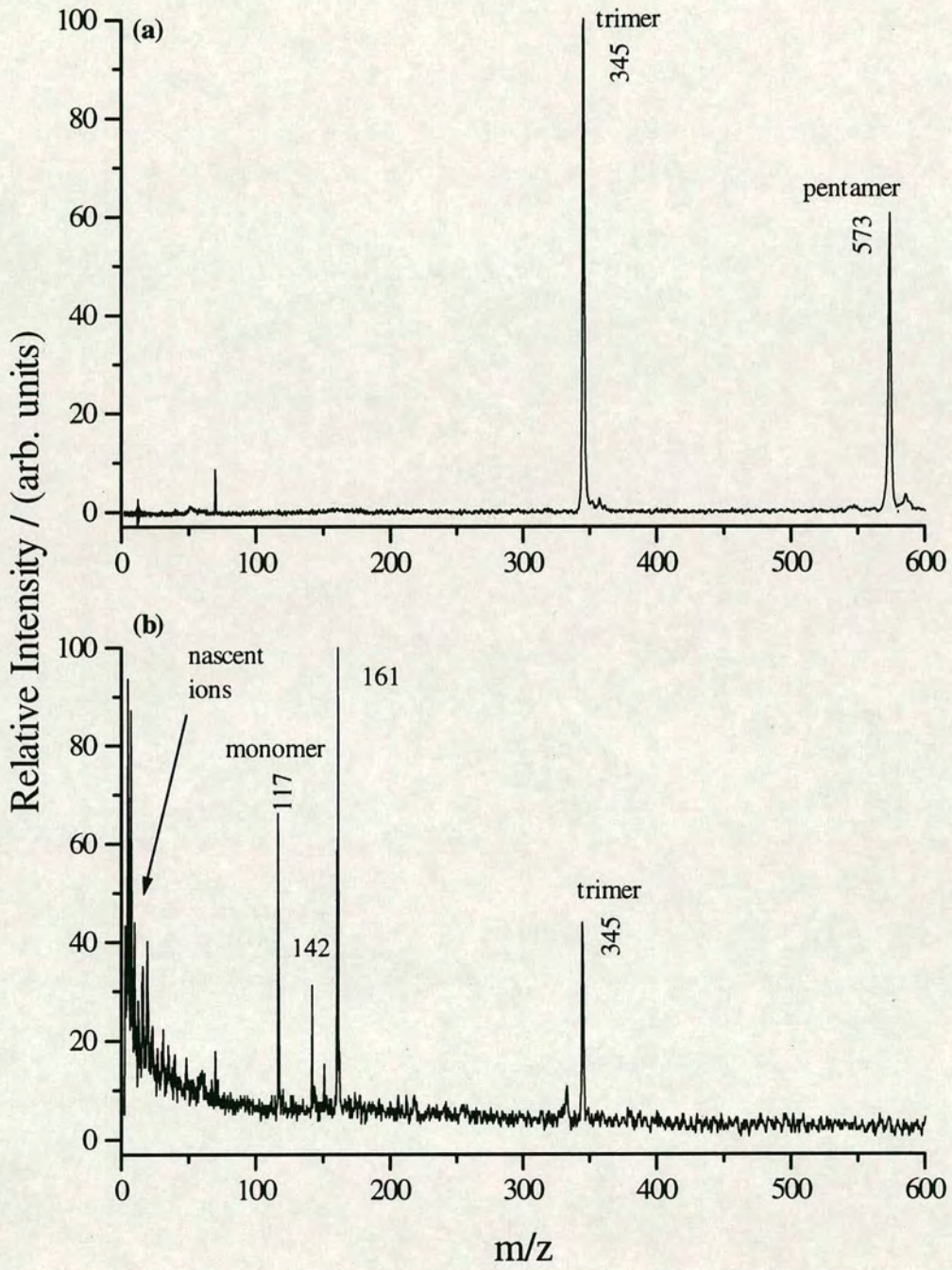

Figure 6-9: (a) L2MS spectrum of the DMF soluble fraction of a polyindole film recovered from the electrode, and applied to a stainless steel sample probe in concentrated form: (b) *in situ* L2MS spectrum of a polyindole film directly from the gold electrode. In both cases, 10.6 μm laser desorption and 266 nm photoionisation were used.

Therefore, washing the electrode should result in the indole monomer peak no longer being detected.

6.3.4 Concluding Remarks

Earlier studies in this laboratory [31] demonstrated that L2MS was a suitable technique for the characterisation of conducting polymer films. The data presented here has extended this work, and demonstrated that L2MS can be used to monitor electrochemical reactions. Copolymerisation is an attractive methodology for producing conducting polymer films with mixed functionality. This provides some control over the physical properties of the polymer film, thereby allowing films to be tailored for particular device applications. L2MS has been used to confirm that copolymerisation of indole 5-carboxylic acid and 5-cyanoindole occurs in a predominantly statistical fashion. It has also been shown that separation of these copolymers by GPC is possible, but that at this stage, the efficiency of separation is not sufficient to isolate individual copolymer components.

Perhaps more importantly it has been shown that L2MS is capable of generating characteristic data for these conducting polymer films *in situ*. Analysis of polyindole directly from an electrode surface enabled identification of the characteristic cyclic trimer, which is believed to be the basic building block of the polymer. It also showed that excess unreacted monomer was present in the film. This work has confirmed earlier expectations that L2MS is a suitable technique for characterising these materials *in situ*. Therefore, if these conducting polymer films do find applications as sensor devices, this technique would be well suited for characterising and monitoring their construction.

References

[1] C. A. Menzie, B. B. Potocki, J. Santodonato, *Environ. Sci. Technol.*, **26**, 1278, (1992)

[2] E. L. Kennaway, I. Hieger, *Br. Med. J.*, 1044, (1930)

[3] A. H. Conney, *Cancer Research*, **42**, 4875, (1982)

[4] M. Cooke, A. J. Dennis, *Polynuclear Aromatic Hydrocarbons: A decade of Progress, Battelle Press*, Columbus, 1988

[5] W. Karcher, R. J. Fordham, J. J. Dubois, P. G. J. M. Glaude, J. A. M. Ligthart Eds., *Spectral Atlas of Polycyclic Aromatic Compounds*, Joint Res. Center, Kluwer Acaqdemic Pub., Boston, USA.

[6] P. Masclet, G. Mouvier, K. Nikoloau, *Atmos. Environ.*, **20**, 439, (1986)

[7] J.-L. Jaffrezo, P. Masclet, M. P. Clain, H. Wortham, S. Beyne, H. Cachier, *Atmos. Environ.*, **27A**, 2781, (1993)

[8] G. G. Grimmer, K.-W. Naujack, G. Dettburn, *Toxicol. Lett.*, **35**, 117, (1987)

[9] R. J. Day, S. E. Unger, R. G. Cooks, *Anal. Chem.*, **52**, 557A, (1980)

[10] G. Duke, *Org. Mass Spectrom.*, **19**, 242, (1984)

[11] K. Balasanmugam, S. K. Viswanadham, D. M. Hercules, *Anal. Chem.*, **58**, 1102, (1986)

[12] T. Mauney, F. Adams, *Sci. Total, Environ.*, **36**, 215, (1984)

[13] A. Robbat Jr., T.-Y. Liu, B. M. Abraham, *Anal. Chem.*, **64**, 1477, (1992)

[14] A. Mellone, B. M. Smith, J. D. Winefordner, *Talanta*, **37**, 111, (1990)

[15] W. A. Chudyk, M. M. Carrabba, J, E. Kenny, *Anal. Chem.*, **57**, 1237, (1985)

[16] M. D. Burfoed, S. B. Hawthorne, D. J. Miller, *Anal. Chem.*, **65**, 1497, (1993)

[17] M. J. Dale, A, C. Jones, S. J. T. Pollard, P. R. R. Langridge-Smith, *Analyst*, **119**, 571, (1994)

[18] M. J. Dale, A. C. Jones, S. J. T. Pollard, P. R. R. Langridge-Smith, A. G. Rowley, *Environ. Sci. Technol.*, **27**, 1693, (1993)

[19] L. J. Kovalenko, R. R. Maechling, S. J. Clemett, J.-M. Philippoz, R. N. Zare, C. M. O'D. Alexander, *Anal. Chem.*, **64**, 682, (1992)

[20] Q. Zhan, P. Voumard, R. Zenobi, *Rapid Comm. Mass Spectrom.*, **9**, 119, (1995)

[21] M. J. Dale, O. H. J. Downs, K. F. Costello, S. J. Wright, P. R. R. Langridge-Smith, *Environ. Pollut.*, **89**, 123, (1995)

[22] A. Crossley, D. B. Wilson, R. Milne, *Environ. Pollut.*, **75**, 81, (1992)

[23] B. L. Feary, C. M. Miller, M. W. Rome, J. E. Anderson, N. S. Nogar, *Anal. Chem.*, **60**, 1786, (1988)

[24] F. W. McLafferty, R. S. Gohlke, *Anal. Chem.*, **31**, 2076, (1959)

[25] M. L. Lee, M. V. Novotny, K. D. Bartle, *Analytical Chemistry of Polycyclic Aromatic Compounds*, Academic Press, New York, USA, pp27-33, 1981

[26] L. Li, D. M. Lubman, *Anal. Chem.*, **59**, 2538, (1987)

[27] S. J. Clemett, C. R. Maechling, R. N. Zare, P. D. Swan, R. M. Walker, *Science*, **262**, 721, (1993)

[28] R. J. Waltmann J. Bargon, *Can. J. Chem.*, **64**, 76, (1986)

[29] F. Garnier, G. Tourillon, M. Gazard, J. C. Dubois, *J. Electroanal. Chem.*, **148**, 299, (1983)

[30] P. N. Bartlett, D. H. Dawson, J. Farrington, *J. Chem. Soc. Faraday Trans.*, **88**, 2685, (1992)

[31] C. R. Redpath, *PhD Thesis, The University of Edinburgh*, 1995

[32] J. G. Mackintosh, A. R. Mount, *J. Chem. Soc. Faraday Trans.*, **90**, 1121, (1994)

[33] J. G. Mackintosh, C. R. Redpath, A. C. Jones, P. R. R. Langridge-Smith, A. R. Mount, *J. Electroanal. Chem.*, **388**, 179, (1995)

[34] J. G. Mackintosh, A. R. Mount, D. Reed, *Magn. Reson. Chem.*, **32**, 559, (1994)

[35] J. G. Mackintosh, C. R. Redpath, A. C. Jones, P. R. R. Langridge-Smith, D. Reed, A. R. Mount, *J. Electroanal. Chem.*, **375**, 163, (1994)

[36] P. N. Bartlett, J. Farrington, *J. Electroanal. Chem.*, **261**, 471, (1989)

[37] R. J. Waltman, A. F. Diaz, J. Bargon, *J. Phys. Chem.*, **88**, 4343, (1984)

[38] J. G. Mackintosh, S. J. Wright, P. R. R. Langridge-Smith, A. R. Mount, *submitted to Faraday Transactions*, (1996)

[39] F. Plows, *"Fluorescence Spectroscopy of Indoles"*, Honours Project, Department of Chemistry, The University of Edinburgh, 1994

Chapter 7

Current Limitation of L2MS as an Analytical Technique

7.1 Introduction

The previous chapters have illustrated how effective two-step laser mass spectrometry is for analysis of involatile, thermally labile molecules. Such molecules, which have proved difficult to analyse by many other mass spectrometric methods, can be detected directly from their native environments as well as in pure form. However, it would be misleading to proclaim L2MS as a routine analytical tool, capable of being used as an analytical "black box" by non-experts. There are aspects of the technique that still pose problems. The aim of this chapter is to identify the key factors which limit the widespread use of L2MS.

There are three main areas of concern. Firstly, as was discussed in Chapter 2, the desorption process is not fully understood. Strange effects are observed in some cases, presumably resulting from non-linear absorption processes during desorption, which cannot be fully explained by current theories. Secondly, there is an apparent limit to the size of molecule which can be photoionised. It is unclear why photoionisation of species over m/z = 2000 proves to be so difficult. This obviously places a severe limit on the type of systems which can be studied. Finally, and perhaps most importantly, in order for L2MS to be widely accepted as a viable analytical technique, it must be able to provide some quantitative information on the concentration of material present in a given sample. At present, quantitation is probably the most challenging issue.

Several attempts have been made to address these problems, and unfortunately, it has been found that they cannot be considered in isolation. There is considerable experimental evidence that desorption can influence the ionisation process, especially as mass increases [1,2,3,4]. Since both the amount of material liberated into the gas-phase and the absorption cross-section at the ionising wavelength used affect the signal intensity, then the ability to quantitate must be intimately linked to both processes. Therefore, in order to answer the most pressing question of "how do we quantify?", it is necessary to take a step backwards in order to address the more fundamental problems concerning the desorption and the ionisation processes. Hopefully, careful consideration of these more fundamental issues will lead towards more reliable quantitation using the technique.

The first part of this chapter will present data illustrating some of the current difficulties experienced with the desorption process. An attempt was made to rationalise these difficulties in terms of the current theories, and to shed some light on their shortcomings. It is then shown that although the desorption and ionisation events are both temporally and spatially separated, the desorption process can, and does, influence the ionisation process and the ultimate appearance of the mass spectrum. The next section focuses on the factors which affect the ability to photoionise high mass molecules. Again, current theories explaining why there is a "ceiling" to the maximum measurable mass using this technique are discussed. Possible experiments to investigate this issue are proposed, and the likely outcomes discussed. In the final section of this chapter, the manner in which these desorption and ionisation issues affect the use of L2MS for *in situ* analysis of real complex systems is discussed, with special emphasis on the contentious issue of quantitation.

7.2 Desorption Issues

It is generally accepted that laser desorption of solid involatile material is a very complex process. It is widely believed that, in fact, several mechanisms may be operative at any one time. However, what cannot be denied, is that using laser desorption one can generate intact gas-phase neutrals of these difficult species, amenable to postionisation by some appropriate means. Chapter 2 presented a

lengthy discussion on some of the current desorption mechanism theories which attempt to explain some of the experimental observations. The recurring theme in these theories is that the most efficient and controllable means of volatilising a sample is by rapid heating of some mediator, be it a substrate or a matrix, which indirectly transfers its energy into a suitable form to enable desorption of the analyte to occur.

For infrared laser desorption of neutral species, the most commonly referred to model is the so-called bottleneck model of Zare and Levine [5]. As discussed in Section 2.2.1, a molecule physisorbed on a surface is bound by a weak van der Waals (vdw) type bond. In comparison to the stronger chemical bonds within the molecule, this bond has a very low vibrational frequency. Rapid heating of the substrate surface excites the surface phonons, which can readily pump this weak vdw bond. Due to the frequency mismatch between this bond and the intramolecular chemical bonds, a bottleneck in the energy flow is established. This results in the vdw bond rupturing, resulting in the desorption of an intact, internally lukewarm molecule. This model is obviously only strictly applicable for sub-monolayer coverages, and it is therefore an over-simplification to treat systems of several hundred monolayers in this way. However, in some cases it does seem to explain the experimental observations, and also gives a very useful visual illustration of what may be going on during desorption.

This model was proposed to rationalise the experimental observation that neutral molecules ejected into the gas-phase following irradiation by a pulsed IR laser are internally cool, and do not decompose, either prior to, or after ionisation. However, at the time that this model was proposed, most workers in the field were desorbing material into a pulsed supersonic expansion. This has the effect of cooling the internal degrees of freedom of the desorbed species, and so it is therefore difficult to know how internally excited the molecules are immediately after desorption. In general, it is assumed that the molecules are not highly vibrationally excited. In the following section some unexpected results which shed doubt on the current theories

are presented and illustrate the effects desorption laser power density and sample morphology can have on the appearance of the mass spectra.

7.2.1 Unexpected Experimental Observations

After using the L2MS technique in this laboratory for several years with the molecular beam capability and entrainment configuration of the instrument, it became increasingly apparent that the analysis of "real world" systems was being limited by relatively poor sensitivity. This was a direct result of the inherently inefficient entrainment step. It was therefore decided to dispense with this step, and to postionise the desorbed species directly above the sample. As demonstrated in Chapter 3, this did indeed result in the expected increase in sensitivity, allowing effective analysis of a number of real systems, hitherto undetectable using this instrument.

Whilst using the entrainment configuration of the instrument, the appearance of the mass spectrum, in terms of the fragmentation observed, appeared to be effectively independent of the desorption laser fluence. Attenuation of the laser power was only required in order to optimise the amount of material picked up by the supersonic expansion; if too high a laser fluence was used, the desorbed material was not effectively entrained [6]. Relative intensities of the molecular and fragment ions did not appear to be affected. This is exactly what would be predicted if the bottleneck model of desorption was found to prevail, even though in this case several hundred monolayers of sample were placed on the probe. The criterion defined by Zare and Levine for the desorption of internally cool molecules, the so called adiabaticity parameter, ε, is related only to the vibrational frequencies of the vdw bond and the chemical bonds in the molecule [5]. Therefore, providing these frequencies are sufficiently different, a bottleneck should be established, irrespective of the laser fluence, and intact desorption should still occur with minimal internal excitation. In fact, at high power densities, an increase in the heating rate would be expected, and so it would be reasonable to expect the bottleneck to be established more quickly, resulting in *less* internal excitation.

On dispensing with the molecular beam, some early results showed that the appearance of the mass spectrum was indeed affected by the desorption laser power density. Figure 7-1 shows photoionisation mass spectra, under different desorption conditions, of Parsol 1789, a material used in commercial sunscreen products. From previous experience using the molecular beam set-up, it was expected that an increase in the laser desorption power density would serve only to increase the intensity of the detected photoion signal. However, as can be seen from Figure 7-1, a dramatic increase in the degree of fragmentation is observed with increasing desorption power density. Since the ionisation conditions were kept constant during these experiments, this increase in fragmentation must therefore be derived from the desorption process.

Other surprising results, which again can only be rationalised in terms of variations in the desorption conditions, quickly became apparent. Figure 7-2 shows two fixed frequency scans (described in Chapter 3, Section 3.8.3) of the azo dye 4-phenylazoaniline (PAA). The photoionisation mass spectra of this material were discussed in Chapter 4, Section 4.2.1. A small amount of PAA was dissolved into a thin paste in glycerol, and applied to the sample probe. The sample was desorbed using 10.6 μm radiation, and photoionised at 266 nm.

Two scans were carried out on different locations of the same sample. The three major peaks in the mass spectra were monitored: the molecular ion, $M^{+\cdot}$ (m/z = 197), $[M - N_2]^+$ (m/z = 169) and the product of azo cleavage at m/z = 93. It can be clearly seen that the monitored signals behave differently for each scan. However, *identical* experimental parameters were used for each scan. It was somewhat surprising, therefore, that such different results could be obtained simply by desorbing at different locations on the sample.

Rationalisation of Apparent Experimental Anomalies

These experimental observations illustrate that the currently accepted bottleneck theory of desorption from surfaces is invalid under the experimental conditions used for many of the experiments described in this thesis. The observation of increased levels of fragmentation in Parsol 1789 resulting from an increase in the laser

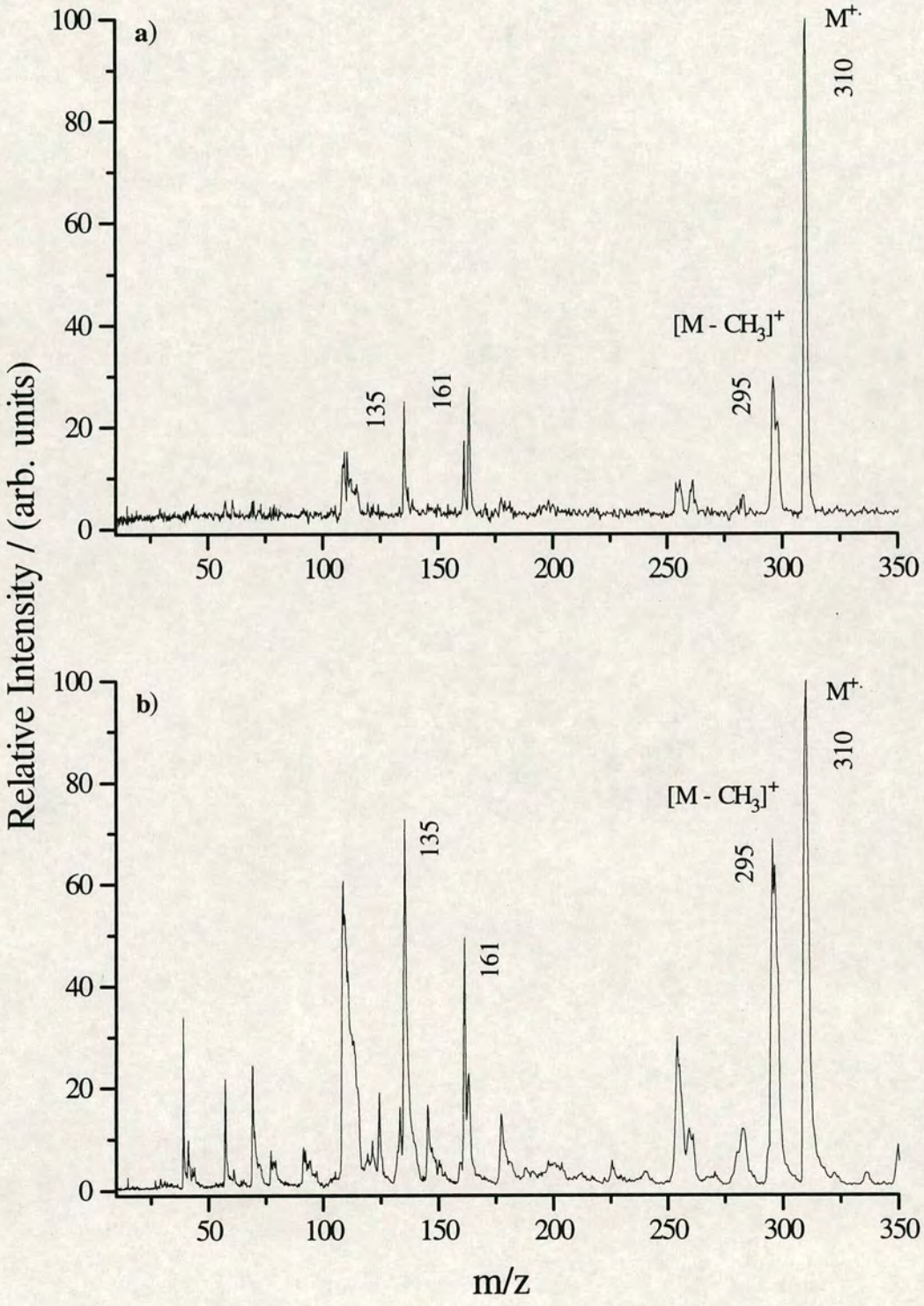

Figure 7-1: Time-of-flight mass spectra of Parsol 1789 using 10.6 mm laser desorption and 193 nm photoionisation; (a) with a low desorption power density of 7 x 10^6 Wcm^{-2}, and (b) with a higher desorption power density of 12 x 10^6 Wcm^{-2}.

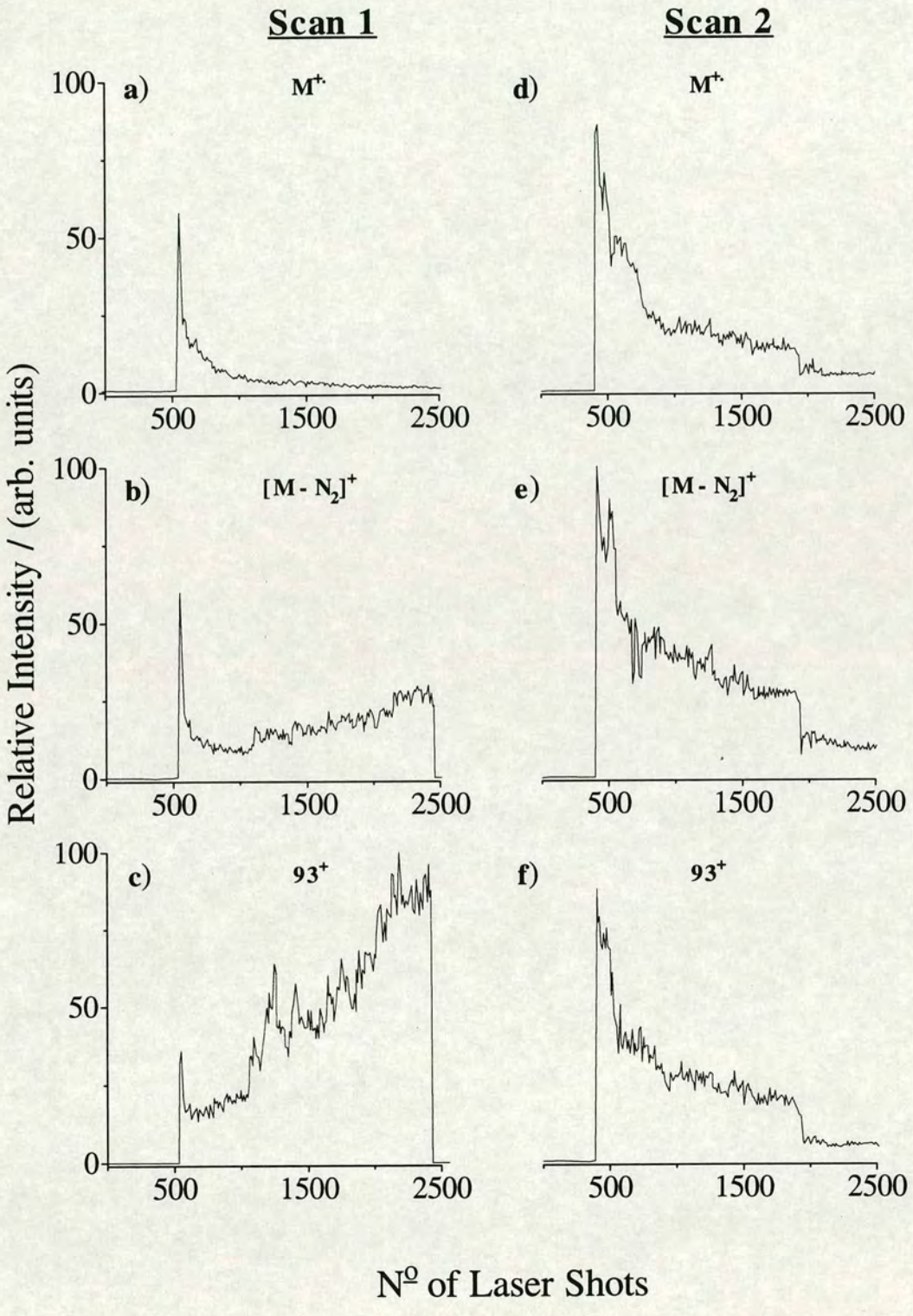

Figure 7-2: Fixed frequency scans of the three major ion peaks of 4-phenylazoaniline. Scans 1 and 2 were obtained using identical laser conditions, but at different locations on the sample. The three major ion peaks correspond to the molecular ion, (a) and (d), elimination of N_2 from the molecular ion, (b) and (e), and the aniline fragment ion, (c) and (f).

desorption power density was somewhat surprising (see Figure 7-1). Since the ionisation conditions were held constant, it would therefore appear that there are two possible mechanisms by which these molecules can fragment.

One fragmentation process which would be consistent with the IR laser power dependence, is that of laser induced thermal dissociation. For this to occur, the desorption laser would have to cause the molecule to dissociate into a series of neutral fragments, which are subsequently postionised and detected.

There are several reasons as to why this is unlikely. Firstly, the laser power density used to record the spectrum of Parsol 1789 shown in Figure 7-1b, where considerable fragmentation was observed, was 12 x 10^6 Wcm^{-2}. However, when this molecule was studied using the entrainment configuration, where Parsol 1789 was laser desorbed into a supersonic expansion of helium, the desorption power density was 20 x 10^6 Wcm^{-2}, which is almost a factor of 2 higher. As shown in Figure 7-3, this resulted in a mass spectrum in which very little fragmentation was observed, even though a much higher laser desorption power density was used. Therefore, if thermally induced dissociation to neutral fragment species did occur during desorption, it should be observed both with and without the molecular beam. Indeed, laser induced thermal dissociation would be even more likely for the case of entrainment if this argument were true. It is clear from this spectrum that this is not the case.

Moreover, the fragments which are observed as a result of increasing the desorption laser power density are essentially identical to those observed when the ionising laser intensity was increased at constant desorption laser conditions. Figure 7-4a and 7-4b show soft and hard ionisation mass spectra of Parsol 1789, respectively. The increased fragmentation observed in Figure 7-4b is likely to be caused by the well known ladder-switching mechanism [7]. Comparison of Figure 7-1b and Figure 7-4b shows that they are almost identical in appearance, yet they are generated by varying different laser parameters. It is unlikely that neutral fragmentation channels opened by the increased desorption power will be identical to

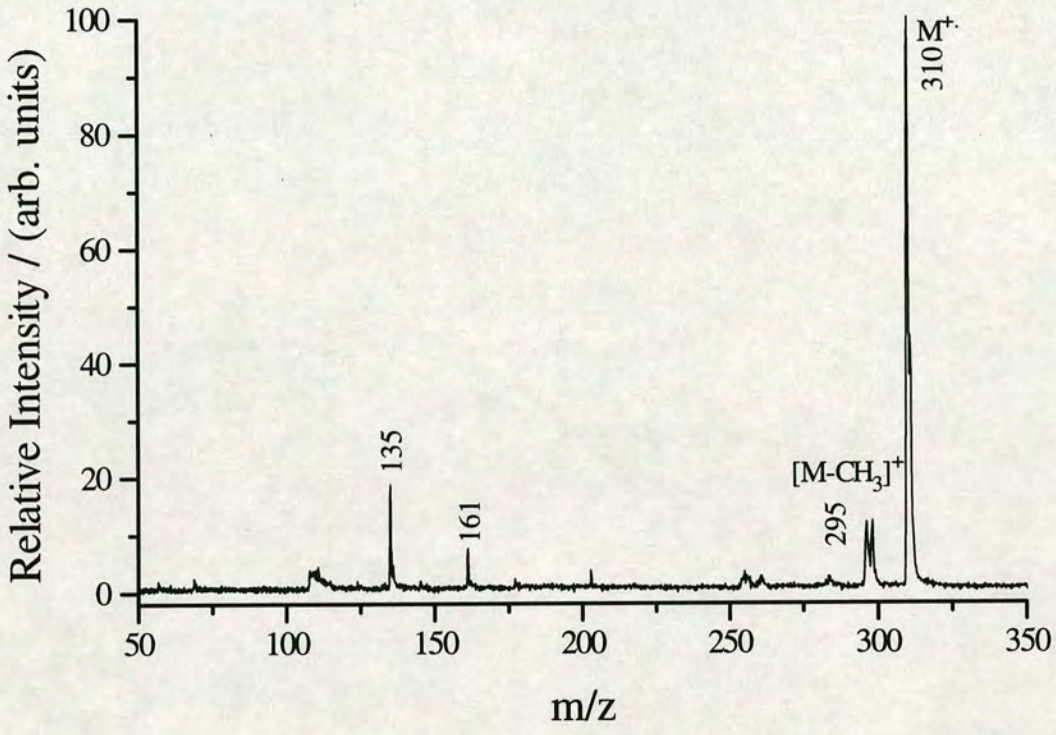

Figure 7-3: Time of flight mass spectrum of Parsol 1789 using 10.6 μm laser desorption, with entrainment of the desorbed neutrals in a supersonic molecular beam of helium. Photoionisation was carried out at 193 nm radiation.

the ionic fragmentation channels generated by ladder switching. This again makes neutral decomposition immediately following desorption an unlikely scenario.

The evidence thus far points to an alternative mechanism for this desorption driven fragmentation. The most likely alternative is that these molecules are desorbed with considerable internal energy, which is carried through into the ion by the photoionisation process. These vibrationally excited molecular ions must have sufficient energy to exceed the appearance potential for facile fragmentation reactions. From this, it would appear that the fragmentation is caused by there being excess energy in the molecular ion. Further experimental evidence corroborating this hypothesis has been obtained for the amino acid tryptophan, and will be discussed in Section 7.2.2.

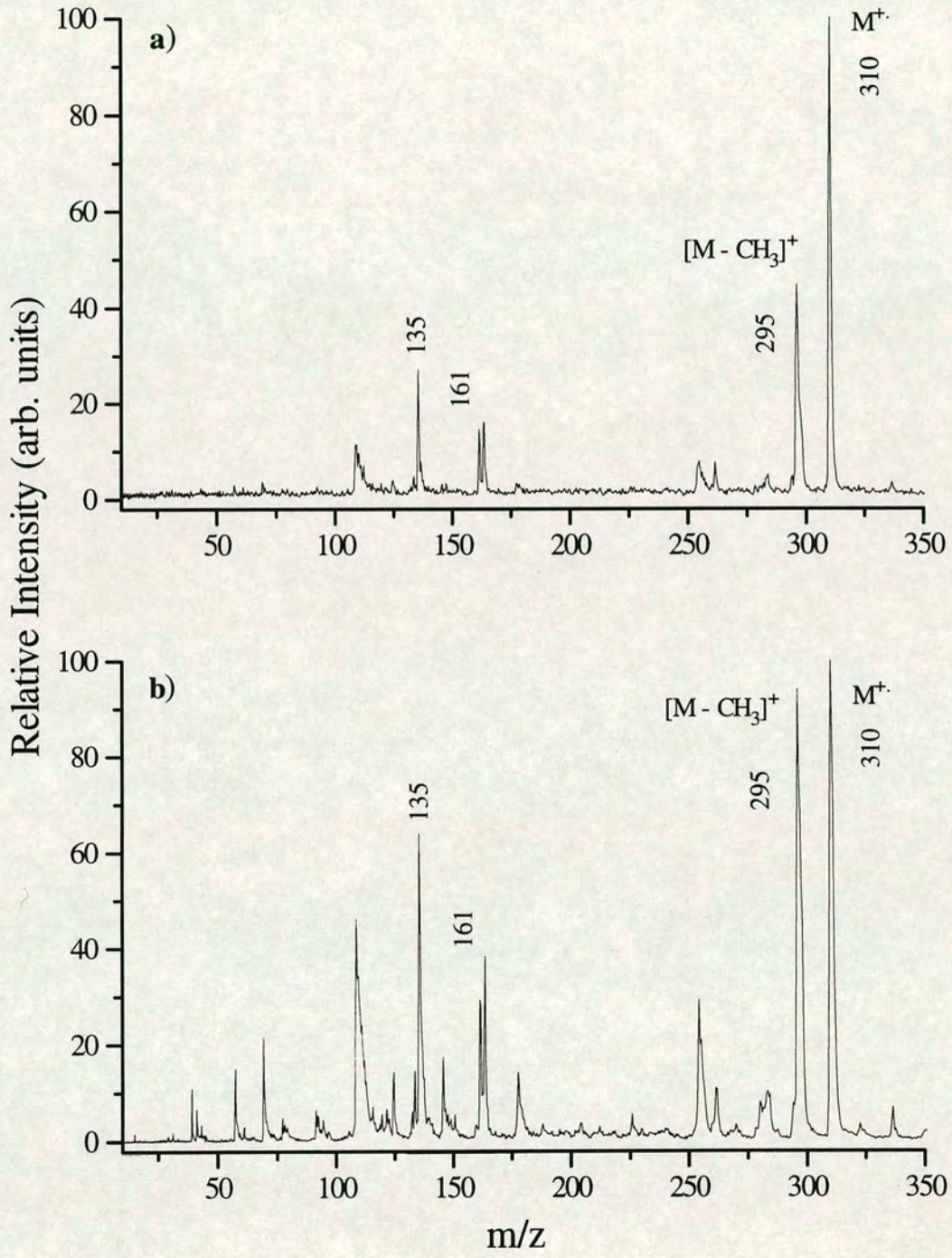

Figure 7-4: Time-of-flight mass spectra of Parsol 1789 using 10.6 μm laser desorption and 193 nm photoionisation; (a) using a low ionising laser power density, and (b) a high ionising laser power density.

The other unexpected result, shown in Figure 7-2, where the location of the desorption laser on the sample probe affected the behaviour of signals monitored in the fixed frequency scans upon exposure to repeated laser shots, illustrates that the morphology of the sample surface is the controlling factor. The initial reasoning behind using 10.6 μm radiation for the desorption was that most organic molecules are optically transparent at this wavelength region, and as such the desorption process should occur via thermal heating of the substrate, very much as suggested by the bottleneck model. Also, the low photon energy means that the likelihood of photochemical/photophysical processes occurring during desorption, which may alter the sample in some way, is reduced. However, the results shown in Figure 7-2 demonstrate that for certain sample morphologies, some heating of the sample must occur during the desorption.

During the course of these experiments, it had previously been noted that the intensity of the fragment ions often increased relative to the molecular ion when the CO_2 laser was incident on the same spot for an extended period of time. This, therefore, suggested that prolonged heating of the sample, either directly via the laser radiation or indirectly via the substrate, was contributing to thermal decompostion of the sample. Therefore, as described above, a "fixed frequency scan" was carried out in order to monitor the behaviour of the three major ion peaks as the CO_2 laser irradiated the sample.

The variation in signal intensity with increasing number of laser shots observed for the $M^{+\cdot}$ and $[M - N_2]^+$ ions, along with the fragment ion at m/z = 93, is shown in Figure 7-2 for two such frequency scans. A simplified "bar" mass spectrum for the initial and final laser shots in both frequency scans is shown in Figure 7-5. In Scan 1, the first laser shot produced intense $M^{+\cdot}$ and $[M - N_2]^+$ peaks. In comparison, the signal due to the ion at m/z = 93 was somewhat smaller. As the same location was repeatedly irradiated, the intensities of the $M^{+\cdot}$ and $[M - N_2]^+$ signals decreased. However, simultaneously, the intensity of the m/z = 93 fragment was observed to increase, as shown in Figure 7-2 and 7-5. This, therefore, suggests that the azo dye is being thermally decomposed as it is further exposed to the IR radiation. At then end of the scan, the dominant ion signal is due to the m/z = 93. fragment ion,

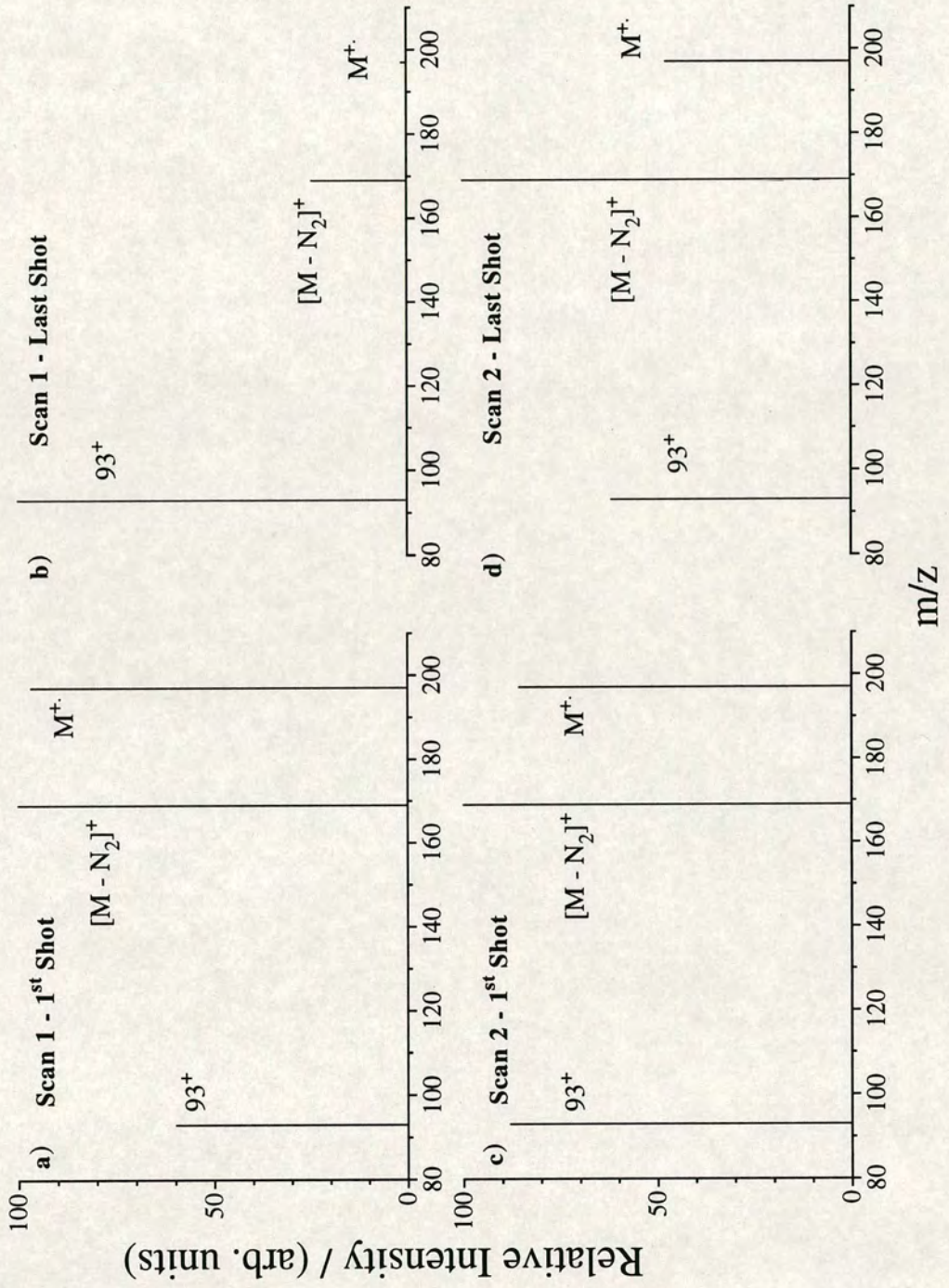

Figure 7-5: Simple "bar" mass spectra of 4-phenylazoaniline. Spectra (a) and (b) correspond to the first and laser shots of Scan 1, respectively. Spectra (c) and (d) correspond to the first and laser shots of Scan 2, respectively.

with only a minor contribution from the $M^{+\cdot}$ and $[M - N_2]^+$ ions.

Scan 2 was recorded using identical laser powers on the same sample, but at a point far enough removed to be unaffected by the previous experiment. A completely different result was obtained at this sample location, as shown in Figure 7-2. For each signal monitored, the intensity of the ion signal was observed to decrease relatively smoothly as it was exposed to more laser shots. This is consistent with the concentration of material available for desorption decreasing with each laser shot, as would be expected. The simple bar spectra for the first and last laser shots of this scan are shown in Figure 7-5c and 7-5d. In contrast to the spectra in Figure 7-5a and 7-5b, these are broadly similar, with appreciable intensity from all of the monitored signals. The differences in signal intensity in this case are presumably due to shot-to-shot variations, and would probably even out with averaging.

It is clear from the above results that the sample morphology can significantly affect the observed result. There was no means by which to view the sample during the experiment, and so it was not possible to ascertain whether this type of difference could be attributed to visual aspects of the sample morphology. However, a reasonable assumption would be that for very thin layers, desorption would tend toward the scenario suggested by the bottleneck model. Here, as the desorption continued for a prolonged period of time, the amount of material would be depleted, resulting in a decrease in the observed intensity of all ions. This is what was observed in Scan 2 (Figure 7-2d, e and f). This would result in similar mass spectra for each successive laser shot, although the absolute signal intensity would decrease over time (Figure 7-5c and d). Thicker layers, on the other hand, would be more likely to undergo non-linear absorption processes during desorption, which may result in significant sample heating. This is consistent with the behaviour of the ion peaks in Scan 1 (Figure 7-2a, b and c). In this case, it may be that the molecules are thermally decomposed upon continuous irradiation such that fragment ion intensities increase, whilst ions associated with the molecular diminish. This would result in mass spectra for the first and last laser shots similar to Figure 7-5a and b being observed.

It is clear, therefore, that even if the desorption and ionisation laser conditions are held constant, different desorption mechanisms are operative at different points over the sample. Therefore, if fundamental studies are to be carried out, only one desorption regime should be employed, i.e., uniform sample coverage is essential, such that reproducible desorption conditions can be achieved. This will be discussed more fully in Section 7.3.3.

7.2.2 Tryptophan as a Chemical Thermometer

From the above discussion, it is clear that for the sample preparations used for much of this work, molecules are not desorbed internally cold; in some cases, considerable fragmentation is observed in the mass spectrum. A number of experiments have been carried out to use this molecular fragmentation as a crude "chemical thermometer", capable of giving a rudimentary estimate of the internal energy content of gas-phase molecules immediately following desorption, and to show that this energy imparted during desorption could lead to fragmentation of the molecular ion. The amino acid, L-tryptophan, was chosen as a suitable candidate for this purpose, since it displays a single characteristic facile fragment ion at m/z = 130, the dehydroindole ion. This ion arises from cleavage of the C_α — C_β bond of the amino acid side group [3]. Tryptophan has been the subject of study by several groups, and the observation that the desorption process is implicated in controlling the degree of fragmentation observed in the mass spectrum is well documented [2,3,4,8].

In early work by Benninghoven [9], using 2.25 keV Ar^+ static SIMS on thin layers of tryptophan deposited on silver foil, very weak $[M + H]^+$ and $[M - H]^-$ signals in positive and negative ion mode were observed. Similarly, 10 keV Ar^+ bombardment of tryptophan in a frozen aqueous matrix failed to produce the molecular ion at m/z = 204 [10]. Several attempts to produce molecular ions, by decoupling the desorption and ionisation events, have employed laser postionisation of the neutral species produced by ion bombardment [10,11,12]. Although the expected increase in signal intensity was observed, in all cases, irrespective of the postionisation wavelength and sample preparation, the dehydroindole ion at m/z = 130 dominated the mass spectra.

Rizzo et al. [13] have used thermal desorption to inject gas-phase tryptophan molecules into a supersonic molecular beam of helium or argon. Resonant photoionisation with 290 nm photons produced mass spectra dominated by the radical molecular cation at m/z = 204, although the dehydroindole fragment was also observed. Grotemeyer et al. [14] used a CO_2 laser to desorb tryptophan into a molecular beam, followed by postionisation at 266 nm, which resulted in a mass spectrum dominated by the dehydroindole fragment ion. However, the molecular ion was also observed with an abundance of ~ 40 % of the base peak intensity.

A systematic study of how various desorption processes affected the fragmentation of tryptophan has been carried out by Ayre et al. [2]. A series of different desorption techniques, including static SIMS, postionised SIMS and LD, as well as both laser desorption and thermal desorption with laser postionisation, were used. They found that thermal desorption and laser desorption followed by laser ionisation produced at least some molecular ion signal, whilst the SIMS and postionised spectra SIMS showed only fragment ions. The conclusions from this study were that *both* the desorption *and* ionisation processes were implicated in controlling the degree of fragmentation observed in the mass spectra.

Previous work in this laboratory by Costello [3] has shown that IR laser desorption of tryptophan into a supersonic expansion, followed by photoionisation at 289.96 nm, (which is close to the $S_1 \leftarrow S_0$ band origin of 286.75 nm, as measured by Levy et al. [13]) results in a mass spectrum containing only the molecular ion at m/z = 204. However, when a more energetic wavelength, 266 nm, was chosen for photoionisation, the dehydroindole fragment ion at m/z = 130 was observed with significant intensity. Costello postulated that there were three possible mechanisms which could account for this observed fragmentation at 266 nm:

- the molecules could have dissociated during the desorption event, after which they were photoionised by MPI.

- Neutral photodissociation may have occurred at the first excited intermediate state, which preceded ionisation. This is known as Class B behaviour as classified by Gedanken et al [16].

- Efficient molecular ion dissociation may have occurred after ionisation, even at ionisation laser power densities insufficient to induce ladder switching.

It is unlikely that the fragmentation occurred during the desorption event. If the m/z = 130 fragment had been produced as a neutral species during sample desorption, then it would almost certainly absorb strongly enough at 286.96 nm for an ion signal to be detected. This is because dehydroindole, like tryptophan itself, contains the indole chromophoric group. Such a neutral fragment species would absorb strongly enough at this wavelength to be ionised because the supersonic expansion was not optimised for maximum cooling; it was simply used as a pick-up source to transport the neutral species into the ionisation chamber. Dey et al. [15] also considered the possibility of neutral dissociation during desorption, and concluded that low desorption laser powers in conjunction with molecular beam entrainment made any such process unlikely.

The available experimental data does not allow the possibility that tryptophan may exhibit Class B behaviour [16] at the first excited intermediate state to be ruled out. However, a more plausible explanation is that at 266 nm, the absorption of the two photons required for ionisation excites the molecule to an energy that exceeds the appearance potential for the dehydroindole ion. At the longer, less energetic wavelength of 286.96 nm, the two-photon energy is sufficient to ionise the molecule, but not enough to promote fragmentation to the dehydroindole ion. It appears likely, therefore, that the observed fragmentation in the L2MS spectrum at 266 nm is due to the MPI process. It seems from this earlier work that the fragmentation observed in the mass spectrum is related to the amount of excess energy deposited in the molecular ion due to the absorption of the second photon. However, it should also be noted that when Grotemeyer et al. [14] used 266 nm radiation to ionise tryptophan entrained in a molecular beam, the base peak in the spectrum was due to the dehydroindole ion, with the molecular ion appearing less intense. This increased

fragmentation observed by Grotemeyer compared to that seen by Costello at the same ionising laser wavelength, suggests that perhaps another factor, such as energy imparted during desorption and carried through into the ion, also contributed to the observed fragmentation.

A similar experiment to that carried out by Costello was carried out during the course of this work. Here, 532 nm radiation from an Nd:YAG laser was used to desorb tryptophan into the gas-phase. It might be expected that more decomposition would be observed as a result of photochemical processes induced by desorption using the more energetic 532 nm radiation. However, as Figure 7-6 shows, photoionisation at 286.5 nm of tryptophan, desorbed into a jet expansion of helium using 532 nm radiation, results only in the detection of the molecular ion. It would therefore appear that the desorption wavelength does not affect the fragmentation. If there is any additional internal excitation as a result of the alternative desorption wavelength, this is evidently removed by the entrainment process.

A series of experiments were subsequently carried out on tryptophan without the use of molecular beam entrainment. This was carried out as part of a collaborative project with Professor Renato Zenobi at the ETH in Zürich [8]. The instrument on which these experiments were carried out has been described in detail elsewhere [17]. Briefly, the output from a CO_2 laser was directed onto the sample surface at an angle of 45°. The sample probe formed part of the accelerating plate of the ion extraction optics. One advantage of this configuration over the arrangement on the instrument used in Edinburgh is that it is possible to move the sample continuously using a stepper motor. This allowed fresh material to be exposed to each laser shot. A second UV laser was introduced perpendicular to the axis of extraction, and the resulting photoions extracted into a reflectron time-of-flight mass analyser.

A wavelength close to the $S_1 \leftarrow S_0$ origin (290 nm) was initially chosen for photoionisation. The resulting mass spectrum is shown in Figure 7-7. Extensive fragmentation is observed, with the base peak corresponding to that of the dehydroindole fragment ion, F^+, at m/z = 130. Given the discussion above, a mass

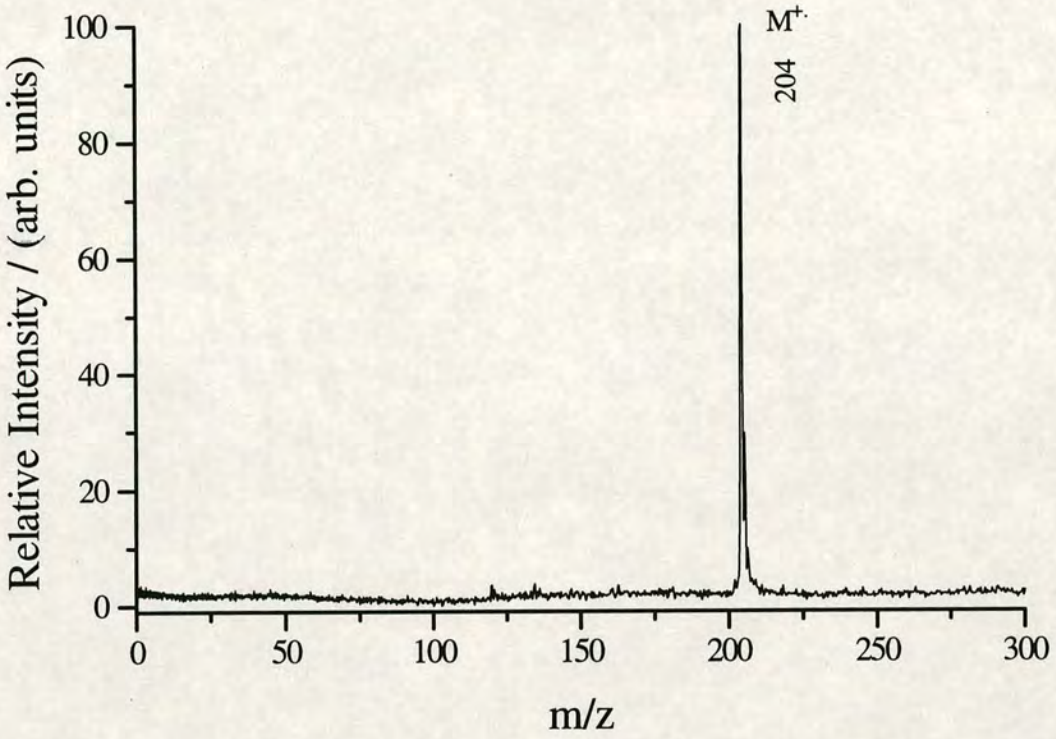

Figure 7-6: Time-of-flight mass spectrum of tryptophan obtained using 532 nm laser desorption in conjunction with a supersonic expansion. Photionisation was carried out at 286.5 nm.

spectrum dominated by the molecular ion, with no contribution from F^+ would be expected following photoionisation at this wavelength. Therefore, this increase in the degree of fragmentation must be linked in some way to the change in desorption conditions, caused by the removal of the molecular beam. As before, there can only be three physical processes which can account for this fragmentation.

The first reason, that the molecules fragment during sample desorption, can be confidently eliminated. In the case of the entrainment experiment, the desorption laser power density was higher than in the corresponding non-entrainment experiment. If the observed fragmentation resulted from laser induced thermal decompostion, then the fragmentation would be even more likely to occur with no molecular beam. In the entrainment experiment, the molecular beam was not optimised for maximal cooling, and so given the high density of populated states, it is likely that any such fragments would be photoionised at 290 nm. It can therefore be concluded with some confidence that decomposition to neutral fragments during

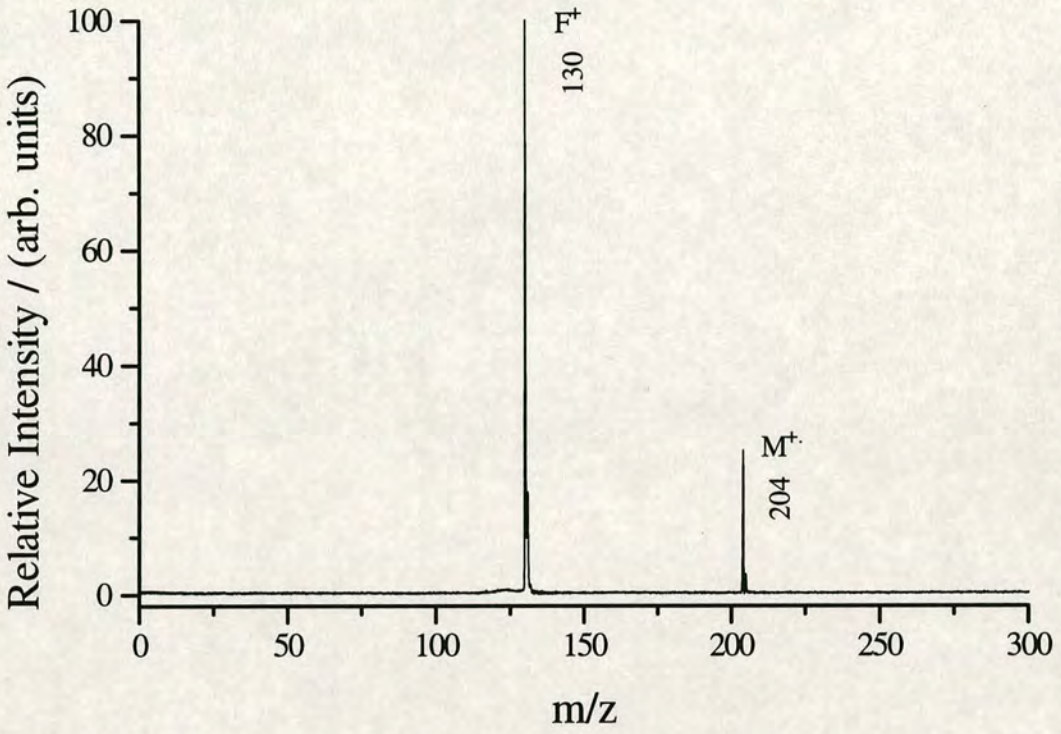

Figure 7-7: Time-of-flight mass spectrum of tryptophan obtained using 10.6 μm laser desorption and 290 nm photoionisation, without the use of molecular beam entrainment.

desorption, followed by photoionisation, does not contribute significant signal intensity to the mass spectrum.

The second possibility, that tryptophan exhibits Class B behaviour following excitation to the S_1 state, also seems unlikely. In both cases, similar ionising wavelengths, (286.5 and 290 nm) were used, and so if neutral dissociation occurred after absorption of one 290 nm photon in the case of non-entrainment, it would be reasonable to expect excitation at 286.5 nm photon to produce a similar result (especially since the molecular beam was not optimised for cooling). This is clearly not the case.

There are two experimental tests which can be carried out in order to assess the contribution to the fragment ion intensity as a result of neutral dissociation at the intermediate state. The first, is that the photoionisation laser power density can be increased. Instead of inducing further fragmentation, it would be expected that the higher photon density will increase the probability of the second photon being

absorbed before the excited state decomposes to neutral fragments. This would lead to an increase in the intensity of the molecular ion relative to the F^+ ion. This effect has previously been observed for porphyrins [18]. This was attempted for tryptophan at a series of different wavelengths. It was found that there was no consistent trend, and that inconsistencies in the desorption signal during the course of these experiments had a more significant effect on the relative intensities observed.

A second experimental test would be to use femtosecond (fs) laser excitation. This has been carried out for tryptophan by Aicher et al. [19] At threshold ionisation conditions, it was shown that fs excitation exhibited a much higher degree of fragmentation. This is contrary to what would be expected if Class B behaviour were prevalent in the ionisation of tryptophan. If fs laser pulses were used for (1 + 1) REMPI of tryptophan, it would be expected that excitation out of the S_1 state and into the ion would occur on a timescale much faster than dissociation to two neutral fragments. This would again result in an increase in the molecular ion intensity relative to the fragment ion. Therefore, since a higher degree of fragmentation was observed, it can be assumed that the fragmentation does not occur as a result of Class B behaviour.

The third, and final, explanation seems to be the most likely: efficient molecular ion dissociation may occur after ionisation, even at low ionisation power densities. However, although the likely cause of the fragmentation has been identified, it remains somewhat unclear why so much more fragmentation should occur without entrainment at an ionisation wavelength so close to the $S_1 \leftarrow S_0$ origin. Therefore, a series of experiments were carried out in order to establish whether the previously observed ionising wavelength effect was still in effect. Figure 7-8 shows photoionisation mass spectra of tryptophan at ionising laser wavelengths between 250 and 340 nm. All spectra are normalised to the F^+ ion at m/z = 130. The wavelength dependence of the dominant fragmentation channel can clearly be observed here. As the wavelength increases, and hence the photon energy decreases, the degree of fragmentation in the mass spectrum is observed to diminish. From this information, and given that the other fragmentation mechanisms have been

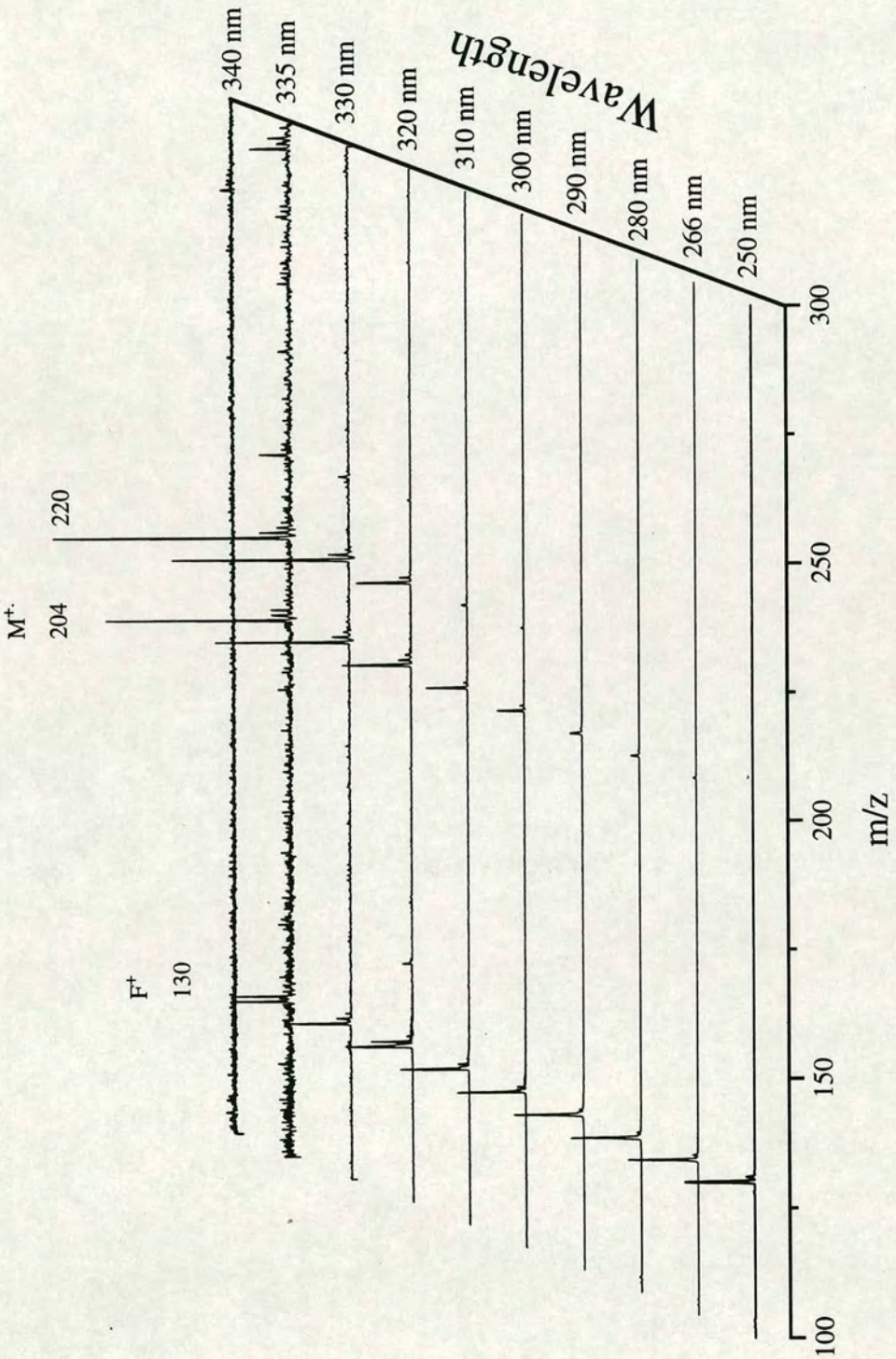

Figure 7-8: Time-of-flight mass spectra of tryptophan obtained using 10.6 μm laser desorption. The photoionisation wavelength is varied between 250 nm and 340 nm. All spectra are normalised relative to the dehydroindole ion. The peak at m/z = 220 corresponds to an oxide of tryptophan, produced in the solution phase.

discounted, it can be concluded that fragmentation must arise as a result of the excess energy present in the molecular ion.

Consider the two extreme cases, at 250 and 335 nm photoionisation. At 335 nm, the absorption of two photons leads to the formation of a molecular ion, with only a very small amount of fragmentation observed. This suggests that there is sufficient energy to effect ionisation, but not to exceed the appearance potential of the fragment ion. Conversely, at 250 nm, no molecular ion is observed. Clearly, at this ionisation wavelength, sufficient excess energy is present in the molecular ion to exceed the appearance potential for the production of the dehydroindole ion, such that it is formed exclusively.

Although this shows that fragmentation is linked to the amount of excess energy deposited in the molecular ion, does this offer any clues as to why there is more fragmentation observed with non-entrained molecules, for constant ionisation conditions? On the basis of the results so far, it suggests that energy imparted to molecules during desorption is "carried through" into the molecular ion such that the appearance potential for the fragment ion is exceeded. In order to corroborate this hypothesis, a series of experiments were conducted in which only the desorption conditions were altered.

Figure 7-9 shows four photoionisation spectra of tryptophan recorded using 300 nm photoionisation at a constant power density. Figure 7-9a shows the spectrum obtained when a thin layer of tryptophan, drop coated from aqueous solution onto a glass surface, was irradiated by the output of the CO_2 laser just above threshold conditions for desorption. It is clear that F^+ is the dominant peak in the mass spectrum, with the molecular ion much less intense. The next spectrum, Figure 7-9b, shows the spectrum obtained when identical laser conditions were used, but the tryptophan was this time dissolved in a solution of poly(ethylene) glycol (PEG). It is clear that desorption of tryptophan from this PEG matrix results in a greatly enhanced molecular ion peak. It is believed that this reduction in fragmentation may be linked to cooling of the internal degrees of freedom of the tryptophan molecules, arising from collisions with PEG molecules expanding into the vacuum.

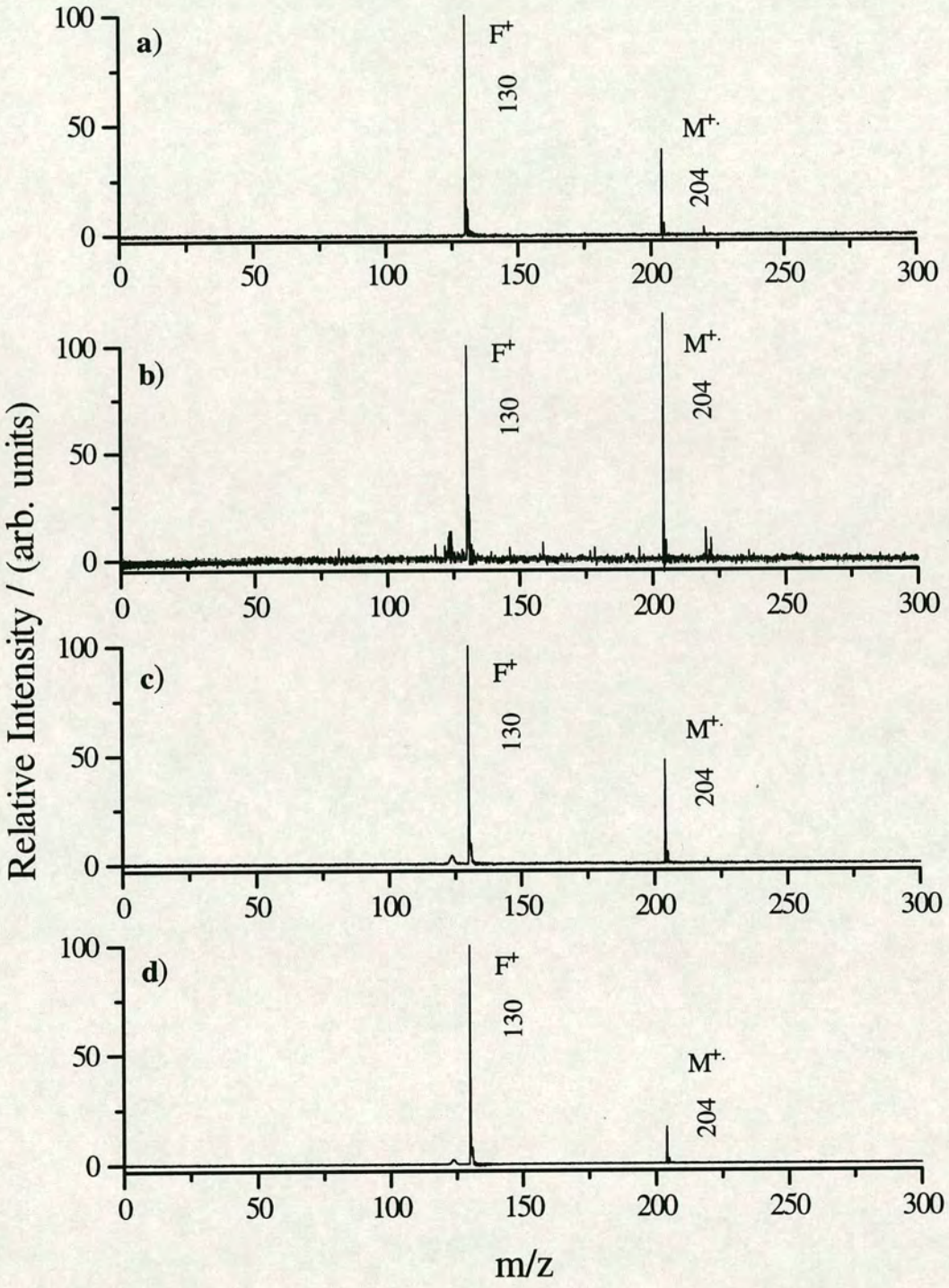

Figure 7-9: Time-of-flight mass spectra of tryptophan obtained using 10.6 μm laser desorption and 300 nm photoionisation; (a) desorption of a thin layer of tryptophan from a glass substrate; (b), (c) and (d) desorption of tryptophan dispersed in a PEG matrix. The desorption power density is systematically increased from spectra (b) to (d).

Similar effects have also been observed by Reilly et al [4]. In their experiments, a solution of tryptophan, rhodamine B and glycerol was desorbed by 532 nm radiation and photoionised at 266 nm. The glycerol was used in order to improve shot-to-shot stability, by continuously replenishing the sample, in much the same way as is commonly done in FAB; rhodamine B was used as a chromophore for the 532 nm radiation to assist in laser desorption. These authors state that, without the use of a supersonic jet for cooling, photoionisation mass spectra at 266 nm containing the tryptophan molecular ion are rarely found. However, by desorbing using this matrix, they were able to generate significant amounts of molecular ion. They also demonstrated that the molecular ion:fragment ion ratio increased as the desorption laser power density was increased. At first sight, this seems to be counter-intuitive. However, Reilly et al. [4] have rationalised these findings, proposing that collisions above the surface play an important role in keeping tryptophan intact. Increased energy deposition in the matrix (by using higher desorption powers) leads to a more explosive desorption event, which in turn leads to faster evaporative cooling and a higher collision rate in the gas-phase above the point of desorption. These higher collision and cooling rates remove internal energy from excited neutral molecules, and clearly help to keep the tryptophan molecular ion intact. Although this explanation is consistent with their reported results, they do not state what happens at still higher desorption power densities.

The present studies, as shown in Figure 7-9c and d, as the desorption laser power density is increased, the contribution from F^+ again increases. This seems to be contrary to the findings of Reilly et al. [4]. However, it is difficult to directly compare results, since different matrices were used, and the power densities may in fact be in entirely different regimes. The results presented in Figure 7-9 can be explained as follows: with no matrix, relatively hot molecules are desorbed into the gas-phase, which upon photoionisation, fragment readily to produce more dehydroindole ions than molecular ions. However, dispersion in a PEG matrix results in desorption of tryptophan molecules which are cooled via collisions with PEG molecules in the expansion from the surface. Postionisation of these internally cooler molecules leads to less vibrationally excited ions, which do not dissociate as

efficiently. However, further increasing the desorption laser power density, as shown in Figure 7-9c and d, results again in desorption of hotter molecules. This may be due to direct heating of the tryptophan molecules by the CO_2 laser. It is possible that this effect may be reduced by using a larger matrix:analyte ratio. It is possible that the effects observed by Reilly et al. may then be reproduced with this matrix. This has not, as yet, been tested experimentally, but is planned for the future.

The present experiments have shown that at almost identical photoionisation wavelengths, 286.5 and 290 nm, completely different degrees of fragmentation are observed as a result of a variation in the desorption conditions, as shown in Figure 7-6 and Figure 7-7. It is, therefore, evident that excess energy is imparted to the molecules during sample desorption, and that with entrainment in a molecular beam, even when not optimised for ultimate cooling, this internal energy is substantially removed. Figure 7-10 schematically illustrates energy level diagrams describing photoionisation of tryptophan molecules with varying degrees of internal excitation. Photoionisation mass spectra corresponding to each scenario are shown in Figure 7-11. In the case of entrainment, a vibrationally cold ground state molecule is therefore excited into a vibrationally cold S_1 state using 286.5 nm radiation, whereupon it is further excited to a vibrationally cool ionic state, as shown in Figure 7-10a. Here, only the molecular ion is observed, as observed in Figure 7-11a. When a molecular beam entrainment is not used, the neutrals in the vibrationally excited ground state (S_0^*) retain this energy over the period of time it takes to interact with the ionising radiation. As a result of the Franck-Condon principle, following irradiation at 290 nm, the molecule will undergo a transition to an upper electronic state which most closely resembles the ground state from which it came, i.e., it will be excited into a vibrationally hot singlet state, S_1^*. Similarly, absorption of the second 290 nm photon will result in production of an ion which is vibrationally excited. This is illustrated in Figure 7-10b. It must be, therefore, that this excess vibrational energy, which has been carried through from the desorbed neutral molecule into the ion, is sufficient to exceed the appearance potential for the facile fragmentation to the dehydroindole ion.

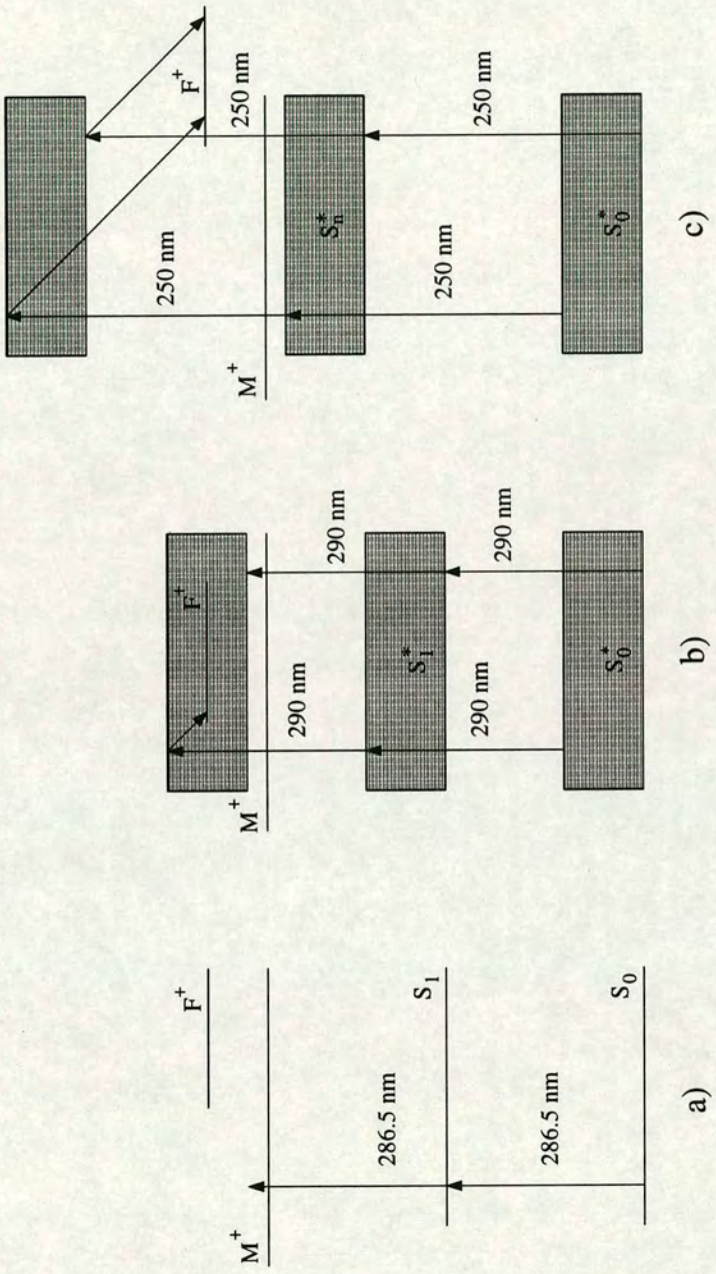

Figure 7-10: Energy level diagram for the photoionisation of tryptophan under three different experimental conditions: (a) photoionisation at 286.5 nm of internally cool neutral molecules, as would be expected with the use of molecular beam entrainment. (b) photoionisation at 290 nm of vibrationally excited neutral molecules. (c) photoionisation using 250 nm of vibrationally excited neutral molecules.

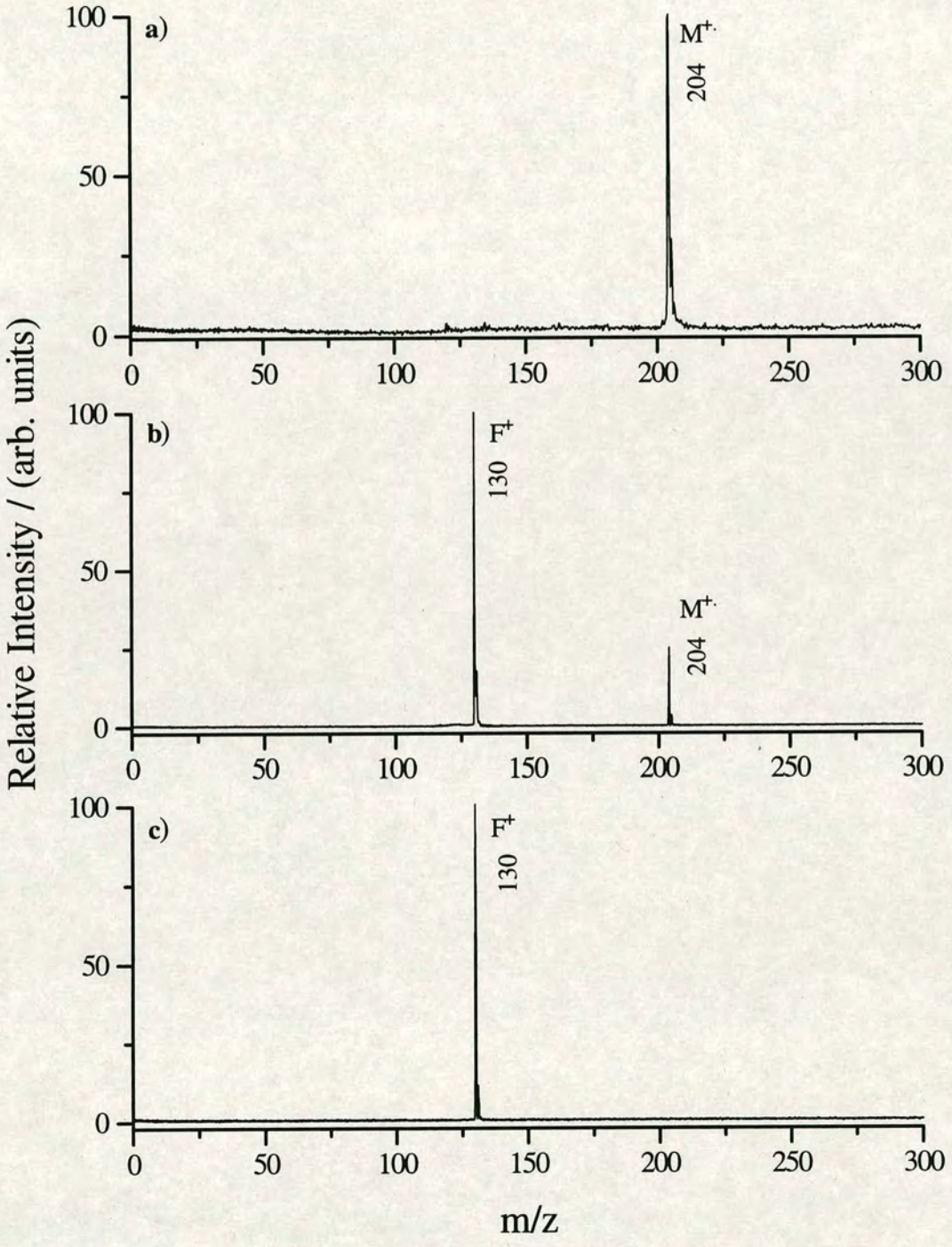

Figure 7-11: Time-of-flight mass spectra of tryptophan obtained under three different experimental conditions. This Figure should be read in conjunction with Figure 7-10: (a) shows 286.5 nm photoionisation of tryptophan desorbed into a molecular beam. (b) shows photoionisation of tryptophan at 290 nm without seeding in a molecular beam. (c) shows photoionisation at 250 nm, without seeding in a molecular beam.

It can also be observed from Figure 7-8 that the degree of fragmentation observed increases with the excess energy imparted due to more energetic photoionising radiation. Figure 7-10c illustrates the extreme case where complete fragmentation is observed following 250 nm photoionisation. Vibrationally excited neutral species are excited from the ground electronic state into a higher lying singlet state, S_n^* than is accessed by 290 nm excitation. This then results in population of higher electronic states in the ion, which are again vibrationally excited, due to Franck-Condon factors. In this case, all of the ionised species have energies above the appearance potential for the fragment ion, F^+, and so no molecular ions are detected. This means that in this case, the excess energy imparted due to the highly energetic 250 nm photons results even in vibrationally cold neutral species being photoionised to produce fragment ions. This results in mass spectra containing only F^+, as shown in Figure 7-11c.

In the case of vibrationally excited neutrals photoionised with 290 nm radiation, as shown in Figure 7-11b, the neutrals with the lowest level of internal excitation do not posses sufficient energy to overcome the appearance potential of the fragment ion, and so are detected as molecular ions. The final result of this is that mass spectrum contains contributions from both the molecular ion and F^+.

These results show that the degree of fragmentation observed in the photoionisation mass spectra of tryptophan, assuming no other photophysical processes occur such as neutral decomposition, neutral dissociation or ladder switching, is dependent only on the amount of energy deposited in the molecular ion, and that this excess energy can be influenced by *both* the desorption (in terms of vibrational excitation) *and* by the ionisation (in terms of excess photon energy). Therefore, in principle, if the IP of the molecule and the appearance potential above the IP of the facile fragment ion are known, it is possible to use this molecule as a rudimentary chemical thermometer for monitoring the amount of internal energy deposited in the neutral during the desorption process.

Tryptophan has an IP of ~ 7.2 eV. From Figure 7-8, it is clear that the ionisation threshold must be between the equivalent two-photon energy of 335 nm and 340 nm

photons. If it is assumed, for the sake of argument, that to longer wavelength than 335 nm only the molecular ion is formed and that no fragment ion is observed, then the (1 + 1) REMPI process at 335 nm deposits a total energy of 7.4 eV in the molecule. Now, if this were a cold ground state molecule, this would mean that the appearance potential for the fragment ion was 0.2 eV. However, it is known that with cooling in a molecular beam, REMPI at 287 nm leads to exclusive molecular ion production. This, therefore, is a better approximation of a cool gas-phase tryptophan molecule. The combined total energy here is 8.64 eV, which means that the appearance potential of the dehydroindole ion is at least 1.44 eV above the IP, provided excitation slightly to the blue of 287 nm signaled the onset of the fragment ion.

Dey et al. [15] have investigated the fragmentation of tryptophan in some detail using 270 nm photoionisation, and investigated the behaviour of the fragment ions as a function of ionising laser intensity. A double-logarithmic plot of laser intensity versus signal intensity showed that absorption of three 270 nm photons was required to produce the dehydroindole fragment, whereas only two photons were required to produce the molecular ion. This, therefore provided a window for the appearance potential for F^+ of between 9.2 and 13.8 eV from the vibrationless electronic ground state. This translates into an excess energy of between 2.0 and 6.6 eV above the IP, compared to the estimate above of 1.44 eV

It is not presently known exactly what the appearance potential for the dehydroindole is. However, if this quantity were measured, by tuning the ionisation wavelength to progressively longer wavelengths, until only molecular ion was observed, it would be possible to determine a lower limit on the internal excitation introduced during the desorption process. Then, tryptophan could be used as a crude chemical thermometer for the desorption process.

7.3 Ionisation of High Mass Molecules

The advent of desorption/ionisation techniques has revolutionised mass spectrometry of large molecular systems. In particular, the development of photon-

induced ionisation techniques has opened new pathways for the mass spectroscopic investigation of large polar, thermally labile and involatile molecules. There has been considerable interest in such species recently, especially in the area of peptide and protein analysis. MALDI has perhaps produced the most spectacular data on high molecular weight biopolymers, extending to a mass range in excess of 250 000 u [20]. However, the disadvantage of MALDI, is that in general, only adduct ions are formed.

On the other hand, multiphoton ionisation (MPI) and single-photon ionisation (SPI) of laser desorbed thermally labile molecules has been shown to successfully produce radical molecular cations. However, it has consistently proved difficult to produce such species for masses in excess of 2000 u. In fact, this inability to generate radical molecular cations of 5000 u and above is not limited only to photoionisation. It seems that other techniques, such as electron impact, also encounter this high mass ceiling [21].

There are two obvious possible explanations for this inability to produce high mass photoions:

- a decrease in neutral desorption efficiency as a function of mass.
- a reduction in the efficiency of the ionisation process with increasing mass.

There is a formidable body of evidence available in the literature to discount the first of these two suggestions [1,19,22]. Most strikingly, there is the reported observation of peptide species using MALDI at masses in excess of 250 000 u [20]. Even though it is the protonated adduct ion that is generally observed in MALDI spectra, the molecule still has to be desorbed intact. Also, Aicher et al. [19] have investigated the relationship between mass and photoion intensity for a series of tryptophan-containing peptides. It was found that by recovering the sample after desorption, and carrying out HPLC separation and quantitation, the desorption process was not responsible for the decreasing ion signals. They concluded that the desorption process has no major influence on the decreasing ion yield. In order to prove that even larger molecules can be desorbed intact following CO_2 laser

irradiation, cytochrome c was recovered after desorption and subsequently ionised by "any other ionisation method" to give a characteristic mass spectrum. Photoionisation of cytochrome c, however, produced no observable signal. Although the authors do not report what ionisation techniques were used, similar findings were obtained by Reilly et al.[21].

Therefore, it is reasonable to assume that the laser desorption process is not directly responsible for preventing the detection of radical molecular ions, and that intact neutrals are available for postionisation. However, although it is generally accepted that the inability to detect high mass ions is linked to processes occurring during, or after, ionisation, and not as a result of sample desorption, the reasons for this are still highly contentious.

At present, there are two main schools of thought. Schlag et al. [22] have proposed that in large molecules, ionisation occurs through intermediate formation of geminate charge-pairs which can ionise in a unimolecular fashion due to energy fluctuations. They argue that it is much more probable for the charge pair to recombine, with the result that the excess energy is thermalised and no longer available to eject the electron. The second hypothesis, is that the inability to observe large radical photoions is linked to efficient photofragmentation. It is believed that this fragmentation is influenced by large amounts of internal energy imparted to molecules during the laser desorption process. These theories will be discussed below.

7.3.1 Geminate Charge-Pair Formation and Ionisation

The basic argument behind this model is that in large molecules, close to the ionisation threshold, there is a rapid increase in the density of states [22]. If the energy of the exciting photon was able to populate all isoenergetic states with equal probability, then ionisation would be extremely improbable. It is only Franck-Condon factors that prevent population of most of these states. It is then proposed that only electrons whose binding energy is within the range of probable energy fluctuations in the system can be ionised. The authors argue that the use of more energetic photons and shorter laser pulses will extend the observable mass range.

More energetic photons should result in the population of higher lying states, leading to less strongly bound electrons, whilst it is believed that shorter, femtosecond, light pulses will result in a faster perturbation to the molecule, which will overcome the randomisation of the energy of the initially created charge-pairs. Although some of the predictions of this model have been experimentally verified, these findings can also be rationalised in other ways.

For example, the increase in the ion yield predicted by the charge-pair model was observed upon reducing the photoionisation laser pulse width from the nanosecond to femtosecond regime. However, this increased ionisation efficiency can also be rationalised simply by considering the behaviour of the system at the first excited state [19].

In the nanosecond domain, molecules in the intermediate state can either absorb the next photon, which should lead to photoionisation, or undergo singlet-triplet intersystem crossing to a long lived triplet state. Additionally, this intermediate state can radiatively decay, via fluorescence, back to the ground state. In many molecules, this fluorescent decay occurs over nanosecond timescales. In the femtosecond time domain, it is possible that both of these deactivation channels are bypassed, in that subsequent photon absorption by the first excited state occurs before any deactivation. This, therefore, is an alternative plausible explanation of the observed increasing ionisation efficiency upon femtosecond excitation.

In addition to the geminate charge-pair model, Weinkauf et al. [23] have proposed that vanishingly small Franck-Condon factors may account for the observed decrease in ionisation efficiency at higher mass. In larger molecules, it is argued that the molecular structure in the ion may be considerably different from the neutral ground state, and that even for two-photon ionisation, the Franck-Condon factors will be small enough to make ionisation unlikely. This is why it is thought that higher excitation energy would improve the situation, because the higher excited state would be likely to have a structure more in keeping with the molecular ion, and hence have larger Franck-Condon factors. One suggestion is that the use of femtosecond lasers

could induce resonant (1+1+1) three-photon ionisation, for which the Franck-Condon factors would be larger, and so the ionisation probability may rise.

7.3.2 Efficient Photofragmentation as a Result of Internal Energy

The formation of geminate charge-pairs precluding ionisation of large molecular systems has been challenged by other workers. Becker et al. [1] have proposed that the inability to observe large radical photoions is related to efficient photofragmentation of the radical cation formed. They suggest that the difficulty experienced in generating radical photoions of these large molecules is due to their increasing internal energy per bond. It is argued that, in many cases, this internal energy is not efficiently cooled, even by a supersonic expansion, and that this coupled with the lower stability of the radical cations compared to the corresponding even electron species, results in efficient bond cleavage. These workers present considerable experimental evidence, obtained both by them and other workers, supporting their hypothesis.

When Becker et al. investigated a series of decapeptides, signals were only observed for the cyclic molecule, Gramacidin S. No signal was observed for the linear Gramacidin D. However, other workers [24,25] using supersonic molecular beams to cool the internal energy of the laser desorbed neutrals, have detected photoion signals for linear peptides up to 2000 u. Although the photoionisation wavelengths were different in each case, a plausible conclusion is that internal energy removed by the molecular beam allows intact molecular ions to be detected.

Therefore, the inability to observe signals for linear peptides, in Becker's case, could be due to the greater internal energy per bond of the laser desorbed neutrals resulting from the absence of cooling which would be achieved with molecular beam entrainment. It could also be that the non-detection of peptide molecular ions of over 2000 u reported by Dey et al. [24] and Frey et al. [25] could result again from excess internal energy. In this case, even the use of a supersonic expansion was not sufficient to remove this excess energy.

Another confusing result in the literature is the observation by Anex et al. [26] of radical molecular ions of perfluorinated polyethers up to molecular weights of 7000 u, following laser desorption into a supersonic expansion and two-photon ionisation. This sheds some doubt on the geminate charge-pair model, in that if model is valid, why should the observable mass range of perfluorinated polyethers be so much higher than that of peptide systems? Becker accounts for these observations by considering the polar nature of peptides in comparison with polyethers.

Perfluorinated polyethers are fairly non-polar, and as such, have no sites whereby efficient hydrogen-bonding can occur. Peptides, on the other hand, are very polar in character, and have several sites where hydrogen-bonding can occur. Therefore, the binding energy of peptides to polar surfaces, such as glass, will be very much higher than for polyethers, and so desorption will, therefore, occur for a considerably lower energy input for a given molecular weight. It is therefore likely that the internal energy of polyethers for any given molecular weight, will be much lower than that for peptide molecules or oligonucleotides. This may translate to a greater stability for polyethers of a given molecular weight, or alternatively, a higher detectable molecular weight range. Another way of thinking about this, which is visually useful, it to consider the bottleneck mechanism described earlier. Strong hydrogen-bonds between peptides and the substrate surface will be more close matched in frequency to the intramolecular bonds of the molecule than would be the case for the weak physisorption bond present in the case of polyethers. Therefore, it will be more difficult to establish the bottleneck which effects sample desorption, with the result that more energy will flow into the peptide than the polyether. Consequently, for species of the same size, peptides will contain more internal energy per bond, leading to more efficient photofragmentation and hence a lower radical molecular ion detection efficiency.

In any case, it seems that the degree of internal energy affects the photoionisation of high mass molecules. Becker concludes that large molecules can photoionise efficiently, but that the limiting factor for the detection of radical molecular cations is

fragmentation. It is thought that this is greatly enhanced by the considerable internal energy content associated with the desorption process.

In the experiments on tryptophan described in the previous section, it was shown that the internal energy imparted during desorption could be carried through into the ion and used to promote fragmentation reactions. One possibility for the non-detection of high mass ions, is that for very large molecules, there may be a very high internal energy content. This energy can then be used to induce fragmentation following photoionisation. However, in such a large molecular system, there may be many isoenergetic (and Franck-Condon allowed) dissociation channels, which are essentially indistinguishable. This would perhaps result in the detectable signal being distributed over a large number of channels, resulting in the loss of viable signal to noise.

The issue of photoionisation efficiencies of large molecules remains contentious. Some workers are still sold on the idea of geminate charge-pair formation, whilst others identify more readily with the idea that the effects of internal energy with increasing mass adversely affect the ionisation yield.

7.3.3 Experimental Tests

A series of experiments were carried out in attempt to shed some additional light on this issue. In Becker's paper [1], it was shown that the highly polar nature of peptides was implicated in the lower detectable mass range of these materials in comparison to the apolar perfluorinated polyethers. This, therefore, suggests that the interaction between the substrate and the adsorbate can influence the internal energy content of laser desorbed species.

The idea behind these experiments was to alter the degree of interaction of some suitable analyte with the substrate, and to monitor the internal energy content and fragmentation characteristics of the laser desorbed species as a result. The molecule chosen for these experiments was again the amino acid, tryptophan. As discussed in Section 7.2, it is believed that this molecule can be used as a chemical thermometer for internal energy.

It is possible to alter the degree of interaction between the adsorbate and substrate by using chemical derivatisation of the substrate. The best choice of substrate for this study is simple glass. In its untreated form, the surface of glass basically consists of hydroxyl groups, which should form significant amounts of hydrogen bonds with the polar side groups in tryptophan. Therefore, in this case the tryptophan molecules will be relatively strongly bound to the surface, with the result that a significant amount of internal energy will be transferred to the molecular ion upon photoionisation. This energy, as shown earlier, should result in fragmentation being promoted.

It is possible to remove the surface hydroxyl groups on glass by a simple chemical reaction: mixing with a silylating agent, such as hexamethyldisilazane (HMDS), results in replacement of these surface hydroxyl groups with silyl groups [27]. These groups are very apolar, and so the interaction with the adsorbate should be of the weak physisorption type. It is expected that this should result in more facile desorption, with less transfer of internal energy to the tryptophan molecules. Therefore, the degree of fragmentation in the mass spectrum, for identical desorption and ionisation conditions, should be considerably lower.

Obviously, for this experiment to work, very thin, uniform and reproducible layers of tryptophan must be laid down on the glass surface. It is likely that adsorbate-substrate interaction effects will be relatively subtle, and that these will be eclipsed by layers consisting of several hundred monolayers (ML) or more. Therefore, simply drop coating tryptophan onto glass substrates from solution is clearly going to be inappropriate for observing these subtle effects: the layer thickness will be different at all points on the sample probe and only a tiny proportion of the molecules will be able to interact with the substrate. Clearly, other methods of preparing thin layers (10-20 ML) are required in order to carry out this type of study. Various methods of doing this are currently being investigated, including the use of electrospray, an airbrush and a nebuliser.

Recent results, obtained during the ongoing collaboration with the Zürich group during the writing of this thesis [8], have shown that indeed the internal energy of

laser desorbed material does appear to be affected by the adsorbate-substrate interaction. Thin 10-20 ML layers of tryptophan on derivatised and non-deravitised glass substrates showed significant differences in the degree of fragmentation observed in the mass spectra. For constant ionisation and desorption conditions, the non-derivatised substrate resulted in the desorption of neutrals which were more prone to fragmentation than those desorbed from derivatised glass. By tuning the ionising radiation to progressively longer wavelengths, it was possible to determine lower limits for the internal energy content of tryptophan, laser desorbed from glass. The internal energy was observed to diminish from 0.62 eV to 0.19 eV upon treatment of the glass to remove polar surface species.

These results show that the internal energy content of laser desorbed neutrals is affected by the interaction with the substrate, that this energy can be high and, in some cases, prevent detection of intact parent radical molecular cations. This, therefore, lends credence to the argument of Becker et al. [1], that internal energy imparted during desorption can aid efficient photofragmentation following photoionisation. Also, going back to the geminate charge-pair argument, the authors claimed that this model predicts that ionisation of internally excited (or hot) molecules will be more efficient. By ionisation, they meant the production of radical molecular cations. The work of Becker [1] and Anex [26], as well as the work discussed here on tryptophan, all suggest that internally hot molecules are more prone to fragmentation. This is, therefore, in direct contrast to the suggestion of Schlag et al [22].

In conclusion, in order to increase the mass range of the L2MS technique, it is evident that the internal energy content of desorbed species must be minimised, whether by using a molecular beam, non-interacting substrates, or both. Also, the use of ultra-short ionisation laser pulses may be required in order to increase the ionisation efficiency, most probably as a result of defeating decay and intersystems crossing processes at the first excited intermediate state. Although the formation of geminate charge-pairs cannot be ruled out, none of the experimental evidence accumulated to date directly supports or offers any validation of the theory.

7.4 Limitations on *in Situ* Analysis

In the previous two sections, it has been shown that there are fundamental issues, concerning both the desorption and ionisation processes, which are more complex than were previously thought. It is evident, therefore, that these effects will also be prevalent in real complex systems, as well as in the relatively well controlled laboratory sample preparations. There are two main areas of concern. The first is the desorption issues raised in Section 7.2. If the desorption mechanism varies from point to point across a sample surface, then the appearance of the mass spectrum may, in certain cases, also change dramatically, as was observed in the case of the azo dyes. However, at present, the second area of concern, quantitation of the technique, is more pressing.

The most important advantage of the two-step approach to mass spectrometric analysis of complex systems containing large thermally labile molecules, is the high selectivity which can, if desired, be achieved using photoionisation. This allows for the discrimination against unwanted matrix and contaminant species, simply by judicious choice of the ionising laser wavelength. However, for obtaining quantitative information on the concentration of target species in the mixture, this renders quantitative measurements very difficult, particularly if a strongly resonant (1+1) photoionisation scheme is employed.

Consider a simple mixture of two aromatic compounds, A and B. At the ionisation wavelength used, the base peak in the mass spectrum corresponds to compound A, whilst the less intense signal is due to compound B. However, it is not necessarily true that compound A constitutes the major component of the mixture. This is a result of the (1+1) photoionisation process commonly used. It is possible that the major component of a mixture can produce a peak in the mass spectrum which is orders of magnitude less intense than that corresponding to the minor component. This is because it does not absorb the ionisation radiation strongly, making absorption of the second photon leading to ionisation less likely. This is the first problem with quantification using L2MS employing REMPI.

Previously, it has always been assumed that it would be possible to generate calibration curves for each species at a particular ionisation wavelength. In other words, by measuring the intensity of ion peaks obtained from known amounts of sample, it should be possible to read the intensity of an unknown concentration and arrive at an accurate estimate of the concentration of that species. However, the results presented in Section 7.2, show that such relative comparisons can sometimes be very misleading.

The problem with the above assumption is that it relies on the desorption process producing a gas-phase concentration of target material which is representative of the amount present in the bulk sample. This is obviously difficult enough for simple single component systems, as shown in Section 7.2, but the level of difficulty considerably greater for inhomogeneous complex mixtures. The main problem here is that the desorption mechanism can change from point to point over the sample surface, which may lead to different amounts of gas-phase material being liberated at different locations over the sample, *even if* the mixture composition is relatively homogeneous.

For example, consider the desorption of polymer additives from their host polymers as described in Chapter 5. When the laser wavelength was well coupled to an absorption in the bulk polymer, as was the case with poly(oxymethylene) (POM), efficient desorption occurred, in which sufficient gas-phase additive was liberated to be easily detected. However, in the case of polypropylene (PP), which does not absorb strongly at the desorption laser wavelength, the polymer was simply melted, with little or no additive signal being detected. Consider a situation, therefore, where two samples with differing infrared absorption cross-sections at 10.6 μm are intimately mixed, and the total concentration of a certain polymer additive present in both polymers is required. At one location, the desorption laser may hit the more strongly absorbing polymer, desorbing a large amount of material including the polymer additive, and it would be concluded that there was a high concentration of additive. However, at another location on the sample, the laser may hit an area containing the other polymer, and perhaps no additive would be detected. From this

location, it would be concluded that the additive was not present. Therefore, it can easily be seen how in a sample matrix which is very complex in its construction, different amounts of target material may be liberated into the gas-phase at different points, even if the concentration of that material within the matrix is relatively uniform.

Another situation in which the desorption mechanism could vary over the sample was illustrated by the fixed frequency scans, shown in Section 7.2. Here, different desorption mechanisms were seen to operate at different points across the sample, depending presumably on the thickness of the target material. In cases where the target species are located in localised pockets within the matrix, the relative thickness of these particulates may have a significant bearing on the amount of material liberated, and ultimately detected. This is likely to be a significant problem when standard addition procedures are carried out in the construction of calibration curves.

Overall, therefore, it can be seen that it will be very difficult to obtain constant gas-phase concentrations upon desorption from complex mixtures. In order to overcome this problem, a greater understanding of the desorption process is required, so that it is possible to predict how inhomogeneous samples will behave upon irradiation with high powered lasers. Alternatively, some means of averaging out these effects will be required, for example, using large desorption laser spot sizes. However, this obviously limits the technique in terms of the spatial resolution attainable, and limits its use as an imaging tool.

7.5 Concluding Remarks

The work presented in this chapter has illustrated some of the shortcomings of the L2MS technique. Firstly, as previously suspected, it has demonstrated that our understanding of the IR laser desorption process is not adequate. The commonly accepted bottleneck mechanism, while it does manage to rationalise the experimental data produced by desorption of thin layers (10 - 20 ML), is not able to explain the experimental data obtained from thicker and more inhomogeneous sample layers.

The data presented in Section 7.2, shows that in the absence cooling by a supersonic molecular beam, considerable internal energy can be imparted to the neutral species. This energy can be carried through into the molecular ion, inducing fragmentation. The work carried out on Parsol 1789, showed that internally hot molecules were more prone to fragmentation than molecules cooled in a molecular beam. It was also established that different desorption mechanisms could operate, under identical laser conditions, at different locations on the sample probe. None of these observations were expected in the light of the bottleneck model.

The work on tryptophan presented in Section 7.2, corroborated the hypothesis that the internal energy imparted during desorption could be used to cause fragmentation in the molecular ion. It was also shown that changes in the desorption conditions could greatly affect the degree of fragmentation. Dispersion of tryptophan in a matrix of PEG, or entrainment within a molecular beam, both led to cooling of the internal degrees of freedom, such that the observed fragmentation was reduced.

It still appears that the issue of why ionisation efficiency decreases with increasing mass is rather contentious. The model proposed by Schlag et al. [22] has been shown to be very difficult to prove experimentally. Some of the predictions of this model, such as increased ionisation efficiency using shorter ionising laser pulses, can be explained equally well by other means. Other predictions of the model, such as hotter neutral molecules producing radical photoions more efficiently, are found not to be true experimentally.

It seems that this issue cannot be considered in isolation. Experimental evidence obtained by Becker et al. [1] and Anex et al. [26], as well as work carried out here, show that the desorption process can have a considerable influence on the observed mass spectrum. Therefore, it has been proposed that the ionisation of high mass molecules is not limited by the photoionisation process, but by efficient photofragmentation aided by large amounts of internal energy arising from the desorption process.

It seems, therefore, that there are still several fundamental issues that must be resolved before L2MS can truly be accepted as a viable analytical technique. Greater

emphasis must be placed on quantitation using the technique. However, in order to do this, these fundamental issues, especially those concerning desorption, need to be addressed. More work is also required to identify why there is still a high mass ceiling for the detection of radical photoions. An increase in the mass range of the technique would allow the potentially lucrative area of peptide analysis and sequencing to be investigated by L2MS. At present, it seems that the maximum observable masses can be observed by using short pulsed laser systems and by minimising the internal energy of the desorbed neutrals. This is best achieved by using supersonic expansions or non-polar substrates and matrices.

References

[1] C. H. Becker, K. J. Wu, *J. Am. Soc. Mass Spectrom.*, **6**, 882, (1995)

[2] C. R. Ayre, L. Moro, C. H. Becker, *Anal. Chem.*, **66**, 1610, (1994)

[3] K. F. Costello, *PhD Thesis, The University of Edinburgh*, 1991

[4] P. T. A. Reilly, J. P. Reilly, *Rapid Comm. Mass Spectrom.*, **8**, 731, (1994)

[5] R. N. Zare, R. D. Levine, *Chem. Phys. Lett.*, **136**, 593, (1987)

[6] M. J. Dale, *PhD Thesis, The University of Edinburgh*, 1994

[7] R. N. Zare, R. D. Levine, *Chem. Phys. Lett.*, **136**, 593, (1987)

[8] Q. Zhan, S. J. Wright, R. Zenobi, *Submitted to J. Am. Soc. Mass Spectrom.*, 1996

[9] A. Benninghoven, W. K. Sichtermann, *Anal. Chem.*, **50**, 1180, (1978)

[10] M. H. Ervin, M. C. Wood, N. Winograd, *Anal. Chem.*, **65**, 417, (1993)

[11] D. M. Hrubowchack, M. H. Ervin, M. C. Wood, N. Winograd, *Anal. Chem.*, **63**, 1947, (1991)

[12] R. Möllers, M. Terhorst, E. Neihuis, A. Benninghoven, *Surf. Mass Spectrom.*, **27**, 1393, (1992)

[13] T. R. Rizzo, Y. D. Park, L. A. Peteanu, D. H. Levy, *J. Chem. Phys.*, **84**, 2534, (1986)

[14] J. Grotemeyer, K. Walter, U. Boesl, E. W. Schlag, *Int. J. Mass Spectrom. Ion Phys.*, **78**, 69, (1987)

[15] M. Dey, J. Grotemeyer, *Org. Mass Spectrom.*, **29**, 659, (1994)

[16] A. Gedanken, M. B. Robin, N. A. Kuebler, *J. Phys. Chem.*, **86**, 4096, (1982)

[17] P. Voumard, Q. Zhan, R. Zenobi, *Rev. Sci. Instrum.*, **25**, 3393, (1995)

[18] A. C. Jones, M. J. Dale, G. A. Keenan, P. R. R. Langridge-Smith, *Chem. Phys. Lett.*, **219**, 174, (1994)

[19] K. P. Aicher, U. Wihelm, J. Grotemeyer, *J. Am. Soc. Mass Spectrom.*, **6**, 1059, (1995)

[20] F. Hillenkamp, M. Karas, R. Beavis, B. Chait, *Anal. Chem.*, **63**, 1193, (1991)

[21] P. T. A. Reilly, J. P. Reilly, *Proceedings of the 42nd Annual Conference on Mass Spectrometry and Allied Topics*, Chicago, p 954, 1994

[22] E. W. Schlag, J. Grotemeyer, R. D. Levine, *Chem. Phys. Lett.*, **190**, 521, (1992)

[23] R. Weinkauf, P. Aicher, G. Wesley, J. Grotemeyer, E. W. Schlag, *J. Phys. Chem.*, **98**, 8381, (1994)

[24] M. Dey, W. Böhm, S. Prinke, J. Grotemeyer, *Proceedings of the 40th Annual Conference on Mass Spectrometry and Allied Topics*, p 332, 1992

[25] R. Frey, A. Holle, F. J. Mayer, R. Schäfer, *Proceedings of the 40th Annual Conference on Mass Spectrometry and Allied Topics*, p 334, 1992

[26] D. S. Anex, M. S. De Vries, A. Knebelkamp, J. Bargon, H. R. Wendt, H. E. Hunziker, *Int. J. Mass Spectrom. Ion Proc.*, **131**, 319, (1994)

[27] D. W. Sindorf, G. E. Maciel, *J. Phys. Chem.*, **86**, 5208, (1982)

Chapter 8

L2MS – Concluding Remarks

8.1 Thesis Summary

This thesis has described the application of laser desorption laser photoionisation time-of-flight mass spectrometry (L2MS) for the analysis of a wide variety of large organic molecules, both as pure compounds and directly from a number of matrices or native environments. Chapter 1 provides an introduction to L2MS, with an outline of where this technique succeeds over conventional mass spectrometric approaches for the study of large thermally labile molecules. Chapter 2 contains a discussion of the underlying principles behind the three main elements of the technique, and why laser desorption and laser photoionisation are ideally suited to being coupled with TOF mass spectrometry. Chapter 3 provides a detailed description of the experimental apparatus and procedures used to generate L2MS spectra. The main body of the thesis, Chapters 4 to 7, contain detailed accounts of how L2MS can be applied to several diverse applications. It is shown that the technique can be used for both fundamental studies and as an analytical tool for investigating real systems.

The work presented in Chapter 4 demonstrates the ability of L2MS to probe the photophysics and photochemistry of azo dyes and porphyrin pigments. Mass spectra of simple azo dyes obtained using 193 nm and 266 nm photoionisation display markedly different ionisation and fragmentation channels. At 193 nm, molecular ion information is available in the form of adduct ions, with fragmentation being dominated by C—N cleavage. Photoionisation using 266 nm radiation, on the other hand, results in mass spectra dominated by the products of photoreductive cleavage of the azo bond. Previous work by Dale et al. [1] proposed that this photodissociative fragmentation at 266 nm was directly related to photoisomerism, in

that it proceeds via the same one-photon excited intermediate state. The experiments carried out in this thesis have shown that the presence of certain substituents *ortho* to the azo linkage can alter the nature of this excited intermediate state, with the result that azo cleavage, characteristic of simple azo dyes, no longer occurs. This has allowed isomeric azo dyes to be easily distinguished. When hydroxy groups are in the *ortho* position, tautomerism is thought to be responsible for the unexpected fragmentation products, whereas for carboxylic acid substituents, steric factors are implicated in controlling which fragment ions are observed.

For porphyrin pigments, the nature of the excited state is again shown to have a marked affect on the appearance of the mass spectra. All tetraphenylporphyrins (TPPs) studied using 193 nm photoionisation resulted in the production of radical molecular cations. However, for ionisation using less energetic radiation, some metallo TPPs, including VOTPP, display neutral dissociation at the first excited intermediate state. For both of these molecular classes, it has been shown that fundamental photophysical and photochemical properties can be investigated in large, polar and involatile molecules using L2MS. These compounds are considered to be useful model stains, and so the fundamental data gained from these studies may be used to aid the analysis of such systems adsorbed onto a variety of complex matrices.

The analytical power of L2MS was demonstrated for the characterisation of polymer systems in Chapter 5. The selectivity inherent in the REMPI process was exploited, effectively discriminating against the non-UV absorbing polymer matrix in favour of the aromatic additives present. Photoionisation spectra for pure antioxidants and UV stabilisers show marked wavelength dependence in their fragmentation channels. This wavelength dependence permits unambiguous identification of these materials, even between isomeric species. It was also shown that L2MS has potential as a surface analytical technique. The presence of aromatic surface contaminants, not present in the sample bulk, were detected. It is envisaged that this work can be extended, using spatially resolved desorption, to probe for

additive migration and aggregation. Indeed, the use of L2MS for depth profiling has recently been demonstrated [2].

In Chapter 5 it was shown that general, non-selective ionisation techniques can be successfully coupled with IR laser desorption and TOF mass spectrometry. Non-resonant MPI, single photon ionisation (SPI) and laser induced photoelectron ionisation (LIPEI) have been used to ionise gas-phase neutrals produced by laser desorption. This has allowed the characterisation of non-UV absorbing polymer matrices, not previously possible using REMPI. Therefore, this two-step approach can be used to characterise both the aromatic additives (REMPI) and the non-UV absorbing polymer matrix (non-resonant MPI, SPI and LIPEI) by judicious choice of ionisation technique.

In Chapter 6 two further examples are presented in which L2MS has been used to address analytical problems. In the first of these examples, the technique was used to assay for PAHs, a class of priority pollutants, *directly* from their host environment, in this case, aerosol particulate matter. It was shown that L2MS could deliver rapid fingerprint mass spectra of PAHs adsorbed onto these particulates, without recourse to extraction, separation or pre-concentration procedures. Environmental monitoring of such contaminants requires the collection large amounts of samples in order to correlate short-term pollution effects, such as coal/wood burning and increases in traffic density. Conventional extraction and separation procedures for such high volumes of material will be prohibitively expensive and time consuming. L2MS, although not quantitatively rigorous, can therefore be used as a rapid screening tool, thereby reducing the volume of samples requiring analysis by conventional methods.

The second example discussed, presented in Chapter 6, demonstrates that L2MS is a suitable technique for the characterisation of conducting polymer films. Most importantly, it has been shown that these films can be detected directly from the electrode surface on which they were produced. Therefore, if these conducting polymer films find applications as sensor devices, then L2MS would be an ideal technique for their characterisation, and for monitoring device construction.

Finally, in Chapter 7, some of the current limitations of the L2MS technique are discussed. It is suggested that many of the problems currently experienced with the technique are inextricably linked to the laser desorption process. Current models describing IR laser desorption work well in specific cases, but are not universally applicable to all systems. It was shown that the desorption mechanism can vary from point to point over a surface, sometimes resulting in large variations in the gas-phase concentration of laser desorbed neutrals. This places severe restrictions on the ability to extract quantitative information. Experiments carried out on the amino acid tryptophan further demonstrate that current desorption theories, such as the "bottleneck model" [3], inadequately described the experimental observations; it was shown that internal energy imparted during laser desorption can be carried through to the ion and used to promote fragmentation. In addition, changes in the desorption conditions, such as dispersion of the analyte in a matrix, or seeding into a supersonic expansion, are shown to affect the internal energy, and ultimately, the degree of fragmentation observed. Internal energy imparted during the desorption event has also been implicated as a potential cause of the inability to observe radical molecular cations at m/z > 2000. This issue remains contentious, but a significant body of evidence [4,5,6] suggests that the observable mass range is limited, not only by the photoionisation process, but also by efficient photofragmentation, aided by large amounts of internal excitation derived from the laser desorption process.

8.2 Future Outlook

The experiments carried out during the course of this thesis have been primarily concerned with developing the L2MS technique towards spatially resolved *in situ* analysis of real, complex molecular systems. The results obtained clearly demonstrate that L2MS provides not only a viable approach to the analysis of such complex systems, but that it can also be employed to obtain fundamental information on the photochemistry and photoionisation dynamics of laser desorbed molecules. It is envisaged, therefore, that the L2MS technique can be used to good effect in two principal areas in the future; for fundamental studies and as an analytical tool for the study of complex systems. Interestingly, it appears that the realisation of the main

goals in both of these areas is hindered, at present, by a poor understanding of the laser desorption process.

The use of supersonic jets in conjunction with L2MS enables the generation of dramatically simplified optical spectra for relatively large involatile molecules, which allows fundamental studies of the photochemical and photophysical properties of these molecules to be carried out. There are significant advantages to be gained in using this approach to L2MS. The low temperatures which can be achieved in supersonic molecular beams allows spectroscopic investigation of intermediate electronic states to be undertaken. The excellent selectivity attainable can be used to determine particular components in complex mixtures, even to the extent of differentiating between isomeric and isotopic species from their differing absorption spectra. The development of this optically selective aspect of L2MS has been the goal of several research groups [7,8,9]. The major difficulty experienced in all cases has been the inability to generate constant gas-phase concentrations of laser desorbed material in order to allow reproducible wavelength-scanned spectra to be recorded. Several attempts have been made to address this issue by using ever more elaborate sample preparations, which have met with varying degrees of success. These have included dispersion of the target analyte in polymers [10], silver containing polymer matrices [11], slurry matrices [12] and glycerol [13]. It is clear, provided stable desorption signals can be achieved, that L2MS used in conjunction with supersonic molecular beams is a powerful technique for spectroscopic investigations of large molecular systems. However, the widespread use of L2MS in conjunction with molecular beam entrainment for the analysis of real complex samples is likely to be limited in the future as a result of the relatively poor sensitivity rendered by the inefficient entrainment process. In order to analyse such systems, in which the concentration of target analytes is low, some of the selectivity must be sacrificed in favour of the sensitivity gained by removing the molecular beam.

In Chapters 5 and 6, the analytical power of L2MS for generating readily interpretable mass spectra of target species in complex mixtures, without the use of a molecular beam was illustrated. Although the selectivity is somewhat compromised

by the absence of jet-cooling, L2MS is shown to be enable rapid determination of the presence of trace quantities of aromatic materials in complex systems, such as additives in polymers and PAHs in particulate matter. However, if the technique is to successfully replace conventional (and time-consuming) extraction and separation procedures, it must be capable of providing reliable quantitative information on the concentration of these target analytes. Quantitation has, however, thus far, proved difficult to achieve in practice. The principal cause of the difficulties experienced in extracting quantitative data, is that the signal intensity observed in the mass spectrum is a function of both the analyte concentration and the absorption cross-section at the ionising wavelength.

The generation of quantitative information would be relatively straightforward if the absorption cross-sections of the target molecules at the ionisation wavelength used were accurately known. However, in general, this is not the case. The obvious means of circumventing this problem is to use standard additions, as discussed in Chapter 6, to generate a series of calibration curves from which the concentration in unknown mixtures can be determined. However, once more, instability in the gas-phase concentration of neutral molecules following laser desorption means that absolute signal intensities are unreliable.

Therefore, it would appear that *both* quantitative analysis of materials in complex mixtures *and* fundamental spectroscopic studies using molecular beams would benefit from a more complete understanding of the desorption process. A more detailed appreciation of why the gas-phase concentration of laser desorbed neutrals varies so dramatically for apparently homogeneous samples, will undoubtedly aid in the pursuit of these goals; a better understanding of how the sample must be presented in order to generate stable desorption signals for periods of time long enough to record meaningful optical spectra may be obtained. This may ultimately allow the determination of absorption cross-sections, which will solve the problem of quantitation. Alternatively, more detailed knowledge of the desorption process may allow more effective spiking methodologies to be developed, which would extend the usefulness of the standard addition approach to quantitation.

The inhomogeneity of many samples has proved to be a significant problem for quantitative analysis of materials in real, complex mixtures using L2MS. However, L2MS can be used in a configuration which is specifically designed to study these inhomogeneities. It has been shown in the present work that dispensing with the entrainment stage, in which laser desorbed molecules are seeded into a molecular beam and transported into the ion source, results in a marked improvement in the sensitivity of the instrument. For spatially resolved analysis, in which the desorption laser is tightly focused (1- 50 μm spot-size), only very small quantities of material are desorbed, and so the increased sensitivity achieved by dispensing with the entrainment step is crucial to the success of such experiments. Three groups have developed instrumentation capable of achieving spatially resolved desorption in this regime [14,15,16]. It is envisaged that spatially resolved desorption on this scale will enable the investigation of many different surface phenomena. The preliminary data obtained on polymer systems presented in Chapter 5 showed that L2MS is capable of generating surface specific information. Recent work has also shown that depth profiling of the additive concentration in commercial polymer formulations is possible [2]. A natural extension of this, therefore, is to utilise spatially resolved desorption to generate 2-dimensional images of polymer surfaces. Additive migration and aggregation are known to adversely affect the physical and mechanical properties of polymer systems. Spatially resolved analysis using L2MS may, therefore, be used to monitor these phenomena as a function of polymer age, and provide useful data which can be used to minimise the negative effects of these processes. Other potential mapping applications could include the investigation of heterogeneous stains on organic fibres, detergents on hair, oils on clean surfaces, PAHs on individual aerosol particulates and biomolecules in plant tissue. Following the successful characterisation of several real complex systems in this, and previous, work a new specialist instrument based on the same principles has been developed in this laboratory, and dedicated to this type of analysis. An optical delivery system, capable delivering an IR laser desorption spot of < 50 μm has been designed and built, in tandem with an XYZ translatable sample stage with 2.5 μm resolution. This will allow features on the 100 μm scale to be imaged.

In this laboratory, work in the immediate future will be concerned with developing the new instrumentation to undertake point and feature analysis on a number of complex systems. Ultimately, it is hoped that this research will lead to the generation of 2-D images for a wide variety of systems. A concerted effort to more fully understand the desorption process is also planned. Attempts will be made to generate reproducible homogeneous samples; research into the preparation of thin layers of material onto a variety of different substrate materials using electrospray and aerosol techniques is currently underway. It is hoped that, providing reproducible samples can be generated, various film thicknesses between one and several thousand monolayers can be created for model systems. It has already been shown for many systems that the layer thickness affects the appearance of the mass spectrum; by closely monitoring film thickness and fragmentation products, a better understanding of the role of internal energy transfer during desorption may be achieved. Also, the effects of different substrates, and laser desorption wavelengths and pulse durations on the internal energy content of desorbed neutrals will be investigated. It is hoped that a more complete fundamental understanding of the desorption process will result from such studies, which may then be put to constructive use towards solving some of the problems experienced in the application of L2MS to real complex.

Overall, therefore, L2MS has been shown to be a powerful technique for the analysis of involatile and thermally labile molecules, both as pure materials and directly from various complex matrices. It is clear that it is possible to rapidly generate significant amounts of data on samples which are problematic using many other techniques. Although, at present, reliable quantitative information is difficult to obtain using this technique, there is currently a concerted effort directed towards overcoming these difficulties. The analytical power of L2MS is, however, unquestioned. Spatially resolved analysis of complex samples using the main principles of this technique is clearly feasible, and demonstrates the most exciting future use of the technique.

References

[1] M. J. Dale, A. C. Jones, P. R. R. Langridge-Smith, K. F. Costello, P. G. Cummins, *Anal. Chem.*, **65**, 793, (1993)

[2] Q. Zhan, R. Zenobi, S. J. Wright, P. R. R. Langridge-Smith, *submitted to Macromol.*, (1996)

[3] R. N. Zare, R. D. Levine, *Chem. Phys. Lett.*, **136**, 593, (1987)

[4] C. H. Becker, K. J. Wu, *J. Am. Soc. Mass Spectrom.*, **6**, 882, (1995)

[5] D. S. Anex, M. S. De Vries, A. Knebelkamp, J. Bargon, H. R. Wendt, H. E. Hunziker, *Int. J. Mass Spectrom. Ion Proc.*, **131**, 319, (1994)

[6] Q. Zhan, S. J. Wright, R. Zenobi, *submitted to J. Am. Soc. Mass Spectrom.*, (1996)

[7] G. Meijer, M. S. de Vries, H. E. Hunziker, H. R. Wendt, *J. Phys. Chem.*, **94**, 4394, (1990)

[8] J. R. Cable, M. J. Tubergen, D. H. Levy, *J. Am. Chem. Soc.*, **111**, 9032, (1989)

[9] L. Li, D. M. Lubman, *Applied Spectrosc.*, **43**, 543, (1989)

[10] J. R. Cable, M. J. Tubergen, D. H. Levy, *Faraday Discuss. Chem. Soc.*, **86**, 143, (1988)

[11] R. T. T. Karaiste, I. M. Atkinson, J. A. Shorter, A. E. Knight, F. R. Keene, *Anal. Chem.*, **65**, 2776, (1993)

[12] R. C. Beavis, J. Lindner, J. Grotemeyer, I. M. Atkinson, F. R. Keene, A. E. Knight, *J. Am. Chem. Soc.*, **110**, 9534, (1988)

[13] L. Li, D. M. Lubman, *Applied Spectrosc.*, **42**, 418, (1988)

[14] M. S. de Vries, D. J. Elloway, H. R. Wendt, H. E. Hunziker, *Rev. Sci. Instrum.*, **63**, 3321, (1992)

[15] L. J. Kovalenko, C. R. Maechling, S. J. Clemett, J.-M. Philippoz, R. N. Zare, C. M. O'D. Alexander, *Anal. Chem.*, **64**, 682, (1992)

[16] P. Voumard, Q. Zhan, R. Zenobi, *Rev. Sci. Instrum.*, **64**, 2215, (1993)

Appendix A

Courses and Conferences Attended

In accordance with the regulations of the Department of Chemistry, University of Edinburgh, I have attended the following courses during my period of study:

1. Laser Physics
2. Inelastic and Reactive Scattering Theory
3. Unix 1
4. Unix 2
5. C Programming
6. Infrared Spectroscopy: Practise and Theory
7. Numerical Data Handling
8. Chemometrics
9. Maximum Entropy

In addition, I have also attended Laser Chemistry Research Group meetings and Physical Chemistry Section Seminars over my three years study.

I have also attended the following conferences:

1. Thirteenth International Mass Spectrometry Conference, Budapest, (1994) — poster presentation entitled "*Direct In Situ Analysis of Molecular Adsorbates Using Laser Desorption Laser Photoionisation Time-of-Flight Mass Spectrometry*".

2. Royal Society of Chemistry, Annual Congress, Edinburgh, (1995) — poster presentation entitled "*Structural Determination of Azo Dyes by Photoionisation Mass Spectrometry*".

3. 43rd ASMS Conference on Mass Spectrometry, Atlanta, (1995) — poster presentations entitled "*Structural Determination of Azo Dyes by Photoionisation Mass Spectrometry*" and "*Two-Step Laser Mass Spectrometry of Copolymerised Indole Derivatives*".

4. 21st Annual Meeting of the British Mass Spectrometry Society, Manchester, (1995) — oral presentation entitled "*Characterisation of Laser Desorbed Polymers Using Multi-Photon and Single-Photon Ionisation*".

5. 22nd Annual Meeting of the British Mass Spectrometry Society, Swansea, (1996) — oral presentation entitled "*Two-Step Laser Mass Spectrometry: The Role of Internal Energy in Fragmentatation Processes*".

Appendix B

Publications and Official Reports

M. J. Dale, O. H. J. Downs, K. F. Costello, C. R. Redpath, S. J. Wright, P. R. R. Langridge-Smith, "Laser Photoionisation Time-of-Flight Mass Spectrometry of Laser Desorbed Polycyclic Aromatic Hydrocarbons from Cloud Water Aerosol Filtrates", RAL-94-042, 197, (1994)

M. J. Dale, O. H. J. Downs, K. F. Costello, S. J. Wright, P. R. R. Langridge-Smith, "Direct *In Situ* Analysis of Polycyclic Aromatic Hydrocarbons in Cloud Water Aerosol Filtrates Using Laser Desorption Mass Spectrometry", *Environmental Pollution*, **89**, 123, (1995)

S. J. Wright, M. J. Dale, P. R. R. Langridge-Smith, Q. Zhan, R. Zenobi, "Selective *In Situ* Detection of Polymer Additives Using Laser Mass Spectrometry", *Analytical Chemistry*, **68**, 3585, (1996)

J. G. Mackintosh, S. J. Wright, P. R. R. Langridge-Smith, A. R. Mount, "The Electrochemical Copolymerisation of 5-Substituted Indoles", *accepted for publication in Faraday Transactions*, (1996)

Q. Zhan, R. Zenobi, S. J. Wright, P. R. R. Langridge-Smith, "Spatially Resolved *in-situ* Analysis of Polymer Additives by Two-Step Laser Mass Spectrometry", *Macromolecules*, 29, 7865, (1996)

ELSEVIER

0269-7491(94)00065-4

Environmental Pollution, Vol. 89, No. 2, pp.123–129, 1995

0269-7491/95 $09.50+0.00

DIRECT ANALYSIS OF POLYCYCLIC AROMATIC HYDROCARBONS IN CLOUD-WATER AEROSOL FILTRATES USING LASER DESORPTION MASS SPECTROMETRY

M. J. Dale, O. H. J. Downs, K. F. Costello, S. J. Wright, P. R. R. Langridge-Smith*

Department of Chemistry, The University of Edinburgh, West Mains Road, Edinburgh, UK, EH9 3JJ

&

J. N. Cape

NERC Institute of Terrestrial Ecology, Bush Estate, Penicuik, Midlothian, UK, EH26 0QB

(Received 1 June 1994; accepted 22 August 1994)

Abstract

A novel technique for the rapid screening of polyaromatic hydrocarbons (PAHs) in atmospheric particulates is presented. Two-step laser desorption laser photoionisation time-of-flight mass spectrometry was used to assay for PAHs in cloud-water particulates collected near Peebles in southern Scotland. The particulates were examined in situ on their host filters removing the requirement for time-consuming sample extraction and separation. The mass spectra obtained from a single filter are shown. The principal components of these are assigned to PAH contaminants and phthalate contaminants. A distribution of PAHs was observed using 193 nm laser photoionisation. The mass spectrum obtained on using 248 nm laser photoionisation exhibits a different intensity distribution demonstrating an ionisation wavelength dependence. The utility of the technique for rapid screening of PAHs and other polyaromatic species is discussed.

Keywords: Aerosols, polyaromatic hydrocarbons, laser desorption, mass spectrometry.

INTRODUCTION

Polycyclic aromatic hydrocarbons (PAHs) make up a significant fraction of the atmospheric aerosols of anthropogenic origin. These compounds arise from the combustion of fossil fuels (fuel-oil, coal, petrol etc.) and can be found in the atmosphere in gaseous form or adsorbed onto particulates. The PAHs generally have low vapour pressures (Karcher, 1988), and therefore, they can readily condense onto particulate matter. As a consequence there is considerable interest in the abundances of PAHs in aerosols derived from urban environments (Masclet *et al.*, 1986). Aerosol materials can be translated over very long distances and are found throughout the atmosphere in remote oceanic (Masclet *et al.*, 1988) and polar atmospheres (Jaffrezo *et al.*, 1993). In such regions, remote from pollution sources, PAHs are mainly associated with particulate matter. As the PAHs are mutagenic or carcinogenic, their presence in such particulates represents a potential environmental health hazard (Grimmer, 1987). Fine particulates can enter the respiratory system and be deposited in the lung. In general, chemicals administered to the lung as fine particulates in aerosol form, or orally via drinking water, are expected to be more bioavailable than chemicals administered in solid matrices such as food or soil (Menzie *et al.*, 1992). It is, therefore, of major importance to be able to assay respirable fine particulates for their polyaromatic components.

In order to characterise an atmospheric particulate sample, a variety of specific analytical techniques are required. Techniques have been developed for this purpose, including: bulk elemental analyses, microscopy for size and morphology and electron probe microanalysis for elemental analysis of individual particles. The most widely used analytical methods for the determination of PAHs are based on sample extraction and chromatographic separation followed by mass spectrometry (for example, Grimmer *et al.* (1987) and McClennen *et al.* (1990)). However, due to the low volatility of the PAHs, the detectable mass range using GC/MS is limited to around 300 amu. Furthermore, the low concentration of PAHs often requires that pre-concentration and purification steps are employed prior to analysis. Along with solubility problems, the combination of all these procedures means that each complete analysis can take from hours to days to complete.

The technique of laser desorption laser photoionisation time-of-flight mass spectrometry (L^2TOFMS) has previously been shown to circumvent many of the difficulties inherent in the analysis of PAHs directly from environmental matrices (Dale *et al.*, 1993, 1994). A pulsed CO_2 laser is used to desorb the material under investigation as intact neutral species. A pulsed ultraviolet laser is then used to ionise these gas-phase species.

* To whom correspondence should be addressed.

Photoionisation is achieved via a resonance enhanced multiphoton ionisation (REMPI) process. PAHs are a class of compounds which can be efficiently ionised using REMPI and show virtually no fragmentation at low incident laser influences (Dale *et al.*, 1993, 1994; Zhan *et al.*, 1995).

The advantages of the technique are (i) laser desorption of the target molecules directly from their environmental matrices (in-situ analysis), (ii) soft ionisation of the desorbed species leading to mass spectral simplification, (iii) semi-selective ionisation of target molecules possessing a significant absorption cross-section at the chosen ionisation wavelength, and (iv) highly sensitive detection for PAHs. Therefore, the technique offers the unique potential to analyse directly trace quantities of target PAHs, contained in complex mixtures, without requiring recourse to time-consuming and expensive sample extraction, separation or preconcentration steps. Several L^2TOFMS instruments have been constructed by various groups around the world (Lubman, 1988; de Vries *et al.*, 1992; Kovalenko *et al.*, 1992). Most recently, Zhan *et al.* (1995) have demonstrated the application of their instrument to the determination of organic adsorbates on suspended particulates collected on quartz-fibre filters.

In the present work, the results of an investigation into the analysis of PAHs associated with the particulates contained in cloud-water aerosols are reported. The purpose of the investigation was to demonstrate the ability of L^2TOFMS to determine the polyaromatic components of cloud water particulates directly from the bulk particulate matter. The mass spectra obtained using two different ionising wavelengths, 193 nm and 248 nm, are compared. In addition, the possible application of this technique for the widespread screening of condensed aerosol particulates is assessed.

EXPERIMENTAL

Collection and preparation of cloud-water samples

The cloud-water samples were taken from the data bank collected by the NERC Institute of Terrestrial Ecology, Penicuik, Midlothian. The sample examined in the work presented here was collected at Dunslair Heights (602 m above sea level) near Peebles, southern Scotland, over a period of several weeks in October and November 1987. The cloud water collector consisted of a conical passive Harp-wire device strung with polypropylene filament (0·55 mm diameter) and draining to a polypropylene bottle (Crossley *et al.*, 1992). A polypropylene faced lid, 1200 mm in diameter, was supported over the cloud collector to reduce rainfall contamination of the cloud-water sample; this excluded raindrops larger than 0·5 mm in diameter at wind speeds up to approximately 0·5 ms^{-1}. The collector was situated in an open area of moorland between an established mixed conifer forest and a young Sitka spruce plantation. A 100 ml sub-sample of the cloud-water sample was filtered through a polycarbonate membrane (Nucleopore, Costar, UK). The membrane, loaded with solid particles, was dried to a constant weight at room temperature in a vacuum desiccator over phosphorus pentoxide. They were then placed individually in small polystyrene petri dishes and stored in the dark at room temperature. It is unlikely that there has been any significant loss of the nonvolatile PAHs during storage as the samples were never subjected to heat.

Mass spectrometric analysis of particulate material

The L^2TOFMS instrument used in the experiments described here consists of two differentially pumped vacuum chambers: the desorption/ionisation chamber and the reflection time-of-flight mass spectrometer. A schematic of the instrument is shown in Fig. 1.

The sample filter was attached to a Macor sample probe in the desorption/ionisation chamber. This probe was connected to an externally mounted *XYZ* vacuum compatible manipulator to enable various locations on the sample filter to be interrogated. Sample desorption was carried out using a pulsed TEA CO_2 laser (Alltec 854MS). This was focussed to *ca* 1 mm^2 using a 30 cm focal length NaCl lens. Typical desorption power densities were *ca* 2 MW cm^{-2}. The desorbed neutral molecules were photoionised directly above the surface of the sample. The sample probe–ionisation laser separation was typically 5 mm. Photoionisation was performed using both 193 nm and 248 nm laser radiation. These laser wavelengths were generated using the ArF and KrF lines of a Lumonics TE-860T excimer laser. Typical ionising laser power densities were *ca* 2 MW cm^{-2} at 193 nm and *ca* 7·2 MW cm^{-2} at 248 nm. These power densities were selected as they maximised the molecular ion intensities whilst minimising laser induced fragmentation of the molecular ions.

The photoions were mass analysed using a reflectron time-of-flight mass spectrometer. The ions were detected using a tandem microchannel plate detector,

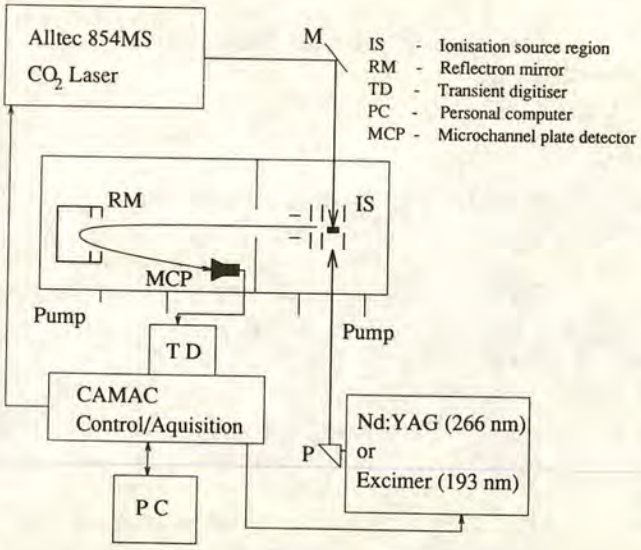

Fig. 1. Schematic diagram of the L^2TOFMS mass spectrometer used in this work. Ionisation of the desorbed material occurs directly above the sample probe in the ionisation source region.

the output of which was fed to a Joerger 200 MHz transient digitiser (TD). Under normal working conditions the resolution of the mass spectrometer is limited by the sampling speed of the transient digitiser. For example, when a 40 ns sampling interval was used the mass resolution was degraded to *ca* 230, whilst a sampling interval of 20 ns allowed mass spectra to be obtained with a mass resolution of *ca* 600. Experimental control and data aquisition were performed using a CAMAC-based system and interfaced to a Dell system 325 personal computer with in-house custom software. The experiment was performed at a repetition rate of 5 Hz. Typically, data from 100 consecutive laser shots were accumulated in order to increase the signal to noise ratio. During the collection of these data an area of *ca* 3 mm^2 was interrogated in an attempt to average out inconsistencies resulting from the inhomogeneous nature of the particulates deposited on the polycarbonate filter. Under these experimental conditions the time taken to prepare the sample and obtain a snapshot mass spectrum is *ca* 10 min.

RESULTS AND DISCUSSION

The polycarbonate filters were examined using 193 nm laser photoionisation and a 40 ns sampling interval in order to screen them for their major polycyclic aromatic components. Although data collection at this sampling frequency degrades the ultimate mass resolution of the spectrometer, it enables a larger mass window to be examined in a single experiment. The L^2TOF mass spectrum obtained for a sample collected on the 25th November 1987 is shown in Fig. 2. There are two principal regions of interest in the mass spectrum. At the low mass end, below 100 amu, there are a number of relatively intense peaks which correspond in mass to a number of metal cations. For example, the peaks at 23, 27, 39 and 56 amu can be attributed to the presence of sodium, aluminium, potassium and iron in the sample. There are a number of other peaks present in this region of the mass spectrum. It is difficult to interpret these peaks with confidence. They may be fragments resulting from the disintegration of higher mass species, or may be intact unknowns in their own right. The L^2TOFMS technique can, however, be used to assay for trace quantities of specific metal target species in complex matrices by taking advantage of atomic, species specific, intermediate electronic resonances, and employing resonance ionisation mass spectrometry (RIMS) (Fearey *et al.*, 1988).

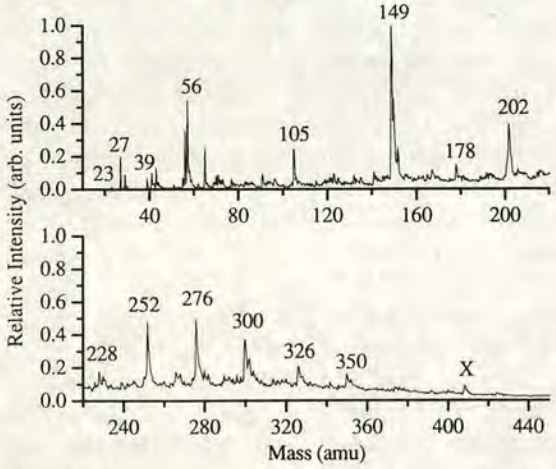

Fig. 2. L^2TOF mass spectrum obtained from a cloud-water particulate sample collected on 25 November 1987, using infrared laser desorption (CO^2 laser power = 2 MW cm^{-2}) followed by 193 nm laser photoionisation (UV laser power = 2·2 MW cm^{-2}).

It is the higher mass region in Fig. 2 which is of most interest with regard to the organic analysis of the cloud-water particulates. The base peak of the mass spectrum is at 149 amu. This can be assigned to the presence of phthalates. The same peak is observed in a mass spectrum obtained on examining an unused polycarbonate filter and is therefore not a principal component of the cloud-water particulates. Phthalates are ubiquitous impurities found in mass spectra, since they are common components of plasticisers used in plastics manufacture. These materials are known to give mass spectra with a base peak at 149 amu, postulated to be a protonated phthalic anhydride (McLafferty & Gohlke, 1959). Furthermore, it is plausible that the ion of mass 105 amu is a product of the fragmentation, by loss of CO_2, of the protonated phthalic anhydride. Above mass 160 amu, all the notably intense mass peaks can be attributed to the molecular ions of parent PAH molecules. The signals at 178, 202, 228, 252, 276, 300, 326 and 350 amu can be assigned to phenanthrene, pyrene, chrysene, benzo[a]pyrene, benzo[ghi]perylene, coronene, dibenzo[a,ghi]perylene, and benzo[a]coronene, or their isomers, respectively. The structures and masses of these species and other representative PAHs, determined to be present in the cloud-water particulates, are given in Table 1. The peak marked with an X is a background signal derived from diffusion pump oil (Edwards, L9). Clearly, using L^2TOFMS rapid 'snapshot' mass spectra can be obtained which yield significant information concerning the nature of the PAHs contained in a cloud-water particulate sample. The principal PAH containing region, observed in Fig. 2 between 140 and 400 amu, is not resolved to the mass spectral baseline. This suggests that there is unresolved information present in the mass spectrum.

Figure 3 shows the mass spectrum obtained using a 20 ns sampling interval for the examination of the same sample discussed above. The use of this faster sampling speed produces a spectrum with improved mass resolution. Again background peaks are labelled with an X. The spectrum is expanded into four sections to show the more detailed information it contains. As in Fig. 2, the base peak is at 149 amu and the more intense mass peaks correspond to molecular ions of the PAHs. There are, however, a number of notable differences. In Fig. 3, mass peaks are observed up to *ca* 490 amu. In Fig. 2, on the other hand, the highest identifiable peak is that marked with an X, at *ca* 408 amu. The higher mass peaks in Fig. 3, at 374, 424 and 448 amu, can be

Table 1. Representative structures and molecular weights of PAHs observed to be present in cloud-water particulate samples using L^2TOFMS

PAH	Mass (amu)	Structure
Anthracene/phenanthrene	178	
Pyrene/fluoranthene	202	
Chrysene	228	
Benzo[a]pyrene	252	
Benzo[ghi]perylene	276	
Coronene	300	
Dibenzo[a,ghi]perylene	326	
Benzo[a]coronene	350	
Dibenzo[a,bc]coronene	374	
Benzonapthocoronene	424	
Benzo[a]ovalene	448	

assigned to benzo[a]ovalene, dibenzo[a,bc]coronene and benzonapthocoronene, and/or their isomers, respectively. These molecules are shown in Table 1. The peak at 202 amu can again be attributed to pyrene or its isomer fluoranthene. Inspection of the solution-phase UV/VIS absorption spectra shows that fluoranthene has a much stronger molar absorption coefficient at

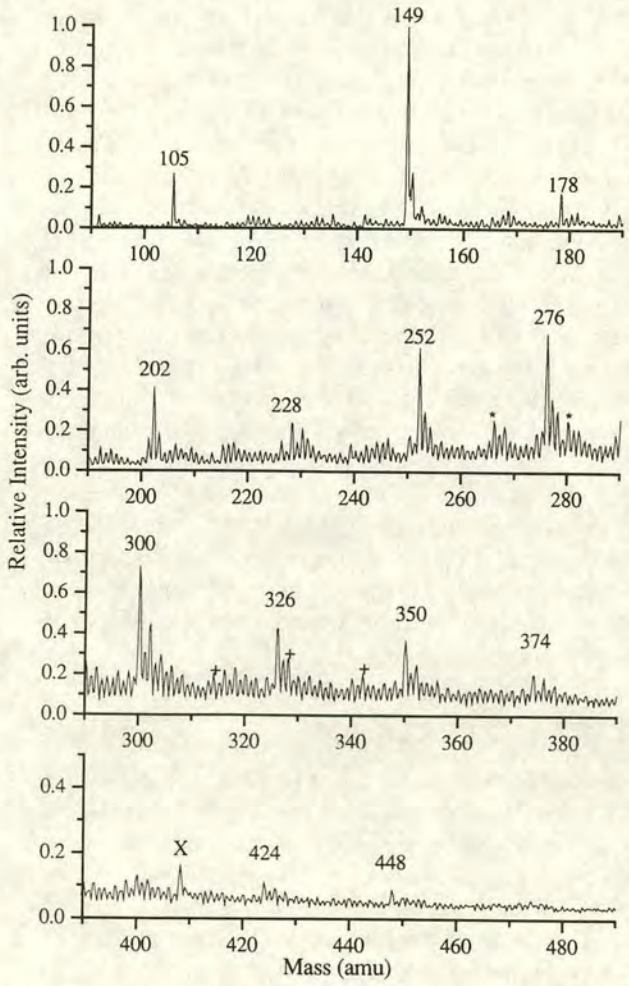

Fig. 3. L^2TOF mass spectrum obtained from a cloud-water particulate sample collected on 25 November 1987, using infrared laser desorption (CO^2 laser power = 2 MW cm^{-2}) followed by 193 nm laser photoionisation (UV laser power = 2·2 MW cm^{-2}).

193 nm than pyrene. Thus, it is possible that the observed mass peak at 202 amu is more representative of fluoranthene than pyrene. Qualitative statements of this kind are, however, often misleading. Although the absorption cross-section for fluoranthene is larger than that for pyrene, the relative concentrations of these species will have the most significant impact on their relative contribution to total peak intensity. Furthermore, the adsorption or binding characteristics and, therefore, the desorption efficiencies may also have some influence with regards to their relative gas-phase concentrations.

A closer examination of the mass spectrum reveals that there are a series of peaks, starting from the prominent parent PAH peaks, which are separated by a mass interval of 14 amu. These peaks are labelled on the spectrum in Fig. 3 for the distributions stemming from signals at 252 amu (indicated with asterisks) and 300 amu (indicated with + symbols). It would appear likely that these species can be assigned to multiply alkylated PAHs present in the cloud-water particulates. The presence of such species in airborne particulates is

well known (Lee *et al.*, 1981). It is also reasonable to expect their presence in the mass spectrum obtained at this wavelength as alkyl substituents do not induce large shifts in the UV absorption bands.

A typical operating pressure for the desorption/ionisation vacuum chamber is 10^{-5} mbar. At this low pressure any volatile species not firmly bound to the particulates will be pumped away and lost from the sample. This will affect the observed distribution of PAHs. This phenomenon will be negligible for the higher mass PAHs, however, as these have extremely low vapour pressures and remain in the sample until they are laser desorbed. Thus, as the volatiles will predominantly consist of the low mass components, it is possible that the distribution of PAHs observed will be skewed in favour of the higher mass species. Figures 4(a) and 4(b) show the L²TOF mass spectra obtained without using a desorption laser, but with a filter, containing cloud-water particulates, present in the evacuated chamber. These mass spectra represent the composition of the volatiles which are being released from the sample and are present in the gas-phase. The two mass spectra are shown on the same relative intensity scale to enable direct comparison. The spectrum in Fig. 4(a) was obtained after *ca* 10 min of pumping. At this point the pressure had not fallen to its lowest value, suggesting that volatiles were still coming off the sample. It is clear that there is a considerable amount of gas-phase material present in the ionisation chamber at this time. The peaks marked with an X are again background signals associated with the diffusion pump oil (Edwards, L9). As in the spectra shown in Figs 2 and 3, the base peak of the mass spectrum is at mass 149 amu. The spectrum obtained in Fig. 4(b) was obtained after exposing the sample to the high vacuum for *ca* 40 min. Clearly the concentration of volatiles has diminished considerably. The only signals of significant intensity in this mass spectrum are those at 149 amu and 202 amu.

It is important to note that the parent ion peak intensities are not only proportional to the concentration of the compound in the sample but also depend on the overall ionisation efficiency which is largely determined by the single-photon absorption cross-section for that compound at the laser wavelength employed. Therefore, the relative peak intensities within a specific mass spectrum do not necessarily directly reflect the relative concentration of the different PAHs in the sample. This point is illustrated by the mass spectrum shown in Fig. 5. This spectrum was obtained using 248 nm laser ionisation rather than 193 nm. The resulting mass spectrum is clearly very different to that shown in Fig. 3. The dominant peaks again correspond in mass to the

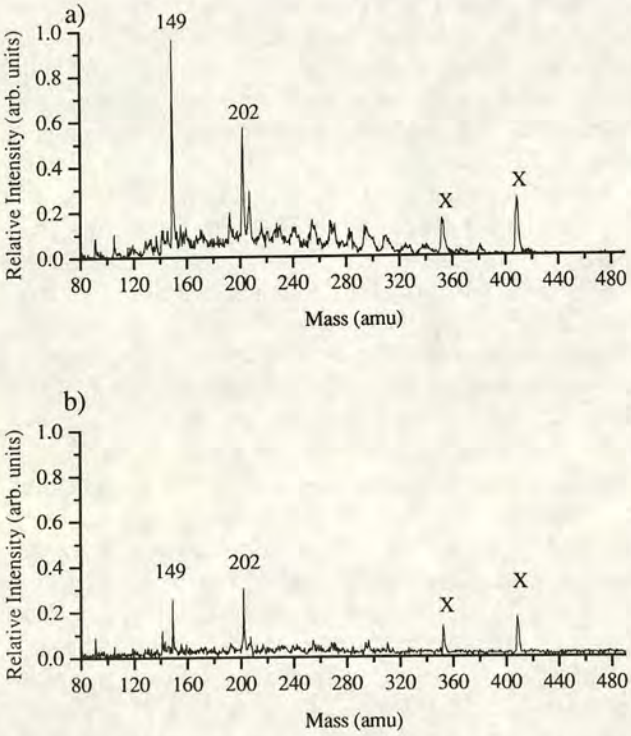

Fig. 4. L²TOF mass spectra of gas-phase headspace organics originating from a cloud-water particulate sample and obtained using 193 nm laser photoionisation. (a) Spectrum recorded after 10 min pump down; (b) spectrum recorded after 40 min pump down.

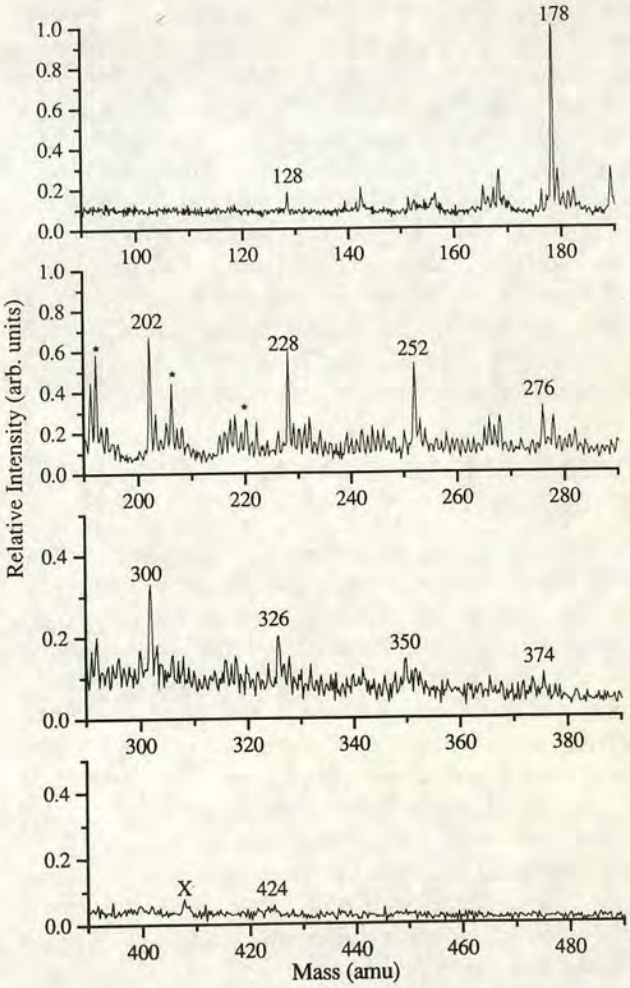

Fig. 5. L²TOF mass spectrum obtained from a cloud-water particulate sample collected on 25 November 1987, using infrared laser desorption (CO^2 laser power = 2 MW cm^{-2}) followed by 248 nm laser photoionisation (UV laser power = 7·2 MW cm^{-2}).

PAHs. Signals at 178, 202, 228, 252, 276, 300, 326, 350, 374 and 424 amu are once again present in this mass spectrum. However, the relative intensities of these peaks has altered considerably. In Fig. 3, the base peak occurs at 149 amu, whilst the most intense of the PAH signals is that at 300 amu. In contrast, the base peak in the spectrum in Fig. 5 occurs at 178 amu (corresponding to anthracene and phenanthrene) and the peak intensity of the PAHs diminishes to higher mass. This reflects the large molar absorption coefficient for phenanthrene and anthracene at 248 nm (ϵ = 208 000 mol^{-1} cm^{-1} for anthracene at 252 nm, 64 000 mol^{-1} cm^{-1} for phenanthrene at 252 nm (Karcher, 1988)). Similarly, the peaks in Fig. 5, at 192, 206 and 220 amu (labelled with asterisks), assigned to methylated anthracene or phenanthrene, are also more intense in relation to the spectrum obtained at 193 nm.

Conversely, benzo[ghi]perylene (276 amu), has a lower molar absorption coefficient near 248 nm (ϵ = 17 000 mol^{-1} cm^{-1} at 254 nm) compared to that around 193 nm (ϵ = 59 000 mol^{-1} cm^{-1} at 210 nm). Consequently the photoion yield of this species (276 amu) relative to the mass 178 amu peak, is much lower when using 248 nm laser photoionisation. However, the most dramatic illustration of the dependence of ion yield on photoionisation wavelength is the notable absence of the mass peaks at 149 amu and 105 amu which were observed to be prominant in Fig. 3.

The mass spectra discussed above demonstrate that the photoionisation wavelength is an important experimental parameter, and can influence not only the relative intensity of peaks but can also discriminate against non-absorbing species. Although this can make spectral interpretation problematic it does add a further dimension to the technique. For example, it is now possible to select ionising wavelengths in order to assay for chosen target compounds in a mixture.

L²TOFMS FOR THE ANALYSIS OF AIRBORNE PARTICULATES

It is clear from the mass spectra presented here that L²TOFMS has unique potential as a technique for screening aerosol particulates for their aromatic components, in particular the PAHs. It has proved capable of analysing nonsoluble and nonvolatile materials which are not readily amenable to chromatographic separation techniques. Most importantly, it can deliver rapid, 'snapshot' mass spectra of the particulate samples directly from their collection surfaces.

Typical studies of cloud-water particulates have often concentrated on the determination of total suspended particulates and total suspended particulate carbon (including organic carbon). Using L²TOFMS it is possible to extend the amount of information that can be readily obtained to include a detailed analysis of the PAH components. In the investigation described here, the analysis revealed primarily homocyclic aromatic components. However, the wider class of polycyclic aromatic compounds (PAC) includes nitrogen, oxygen and sulphur containing heterocyclic species. Over the last decade, the search for major genotoxic compounds has evolved from the investigation of the parent PAHs (National Academy of Science, 1983) to the study of the wider group of PACs (Schuetzle *et al.*, 1982). The emphasis evolving from the basic PAHs to heterocyclic PACs is a result of the observation that homocyclic aromatic compounds cannot account for all the biological activities encountered in many environmental and biological samples. For example, it is clear that the PAH class itself is responsible for only a small fraction of the mutagenic activity of ambient airborne particulate matter (Vo-Dinh, 1989). L²TOFMS is capable of determining the presence of such heterocyclic aromatic species directly from their host matrices. For example, nitrogen-containing heterocyclic PACs can be readily identified from their presence as odd mass peaks in a mass spectrum (Zhan *et al.*, 1995).

The nature of the polyaromatic components in an aerosol sample can provide a useful guide to the sources of the contamination. By screening samples collected at a variety of locations and measuring the variation in the concentrations of PAC in the airborne particulates, the point sources contributing to the pollution at different sampling sites can be identified. One of the difficulties in such monitoring stems from inconsistent variations in the concentrations of PAHs/PACs in air particulate matter sampled over short periods of time. This is a result of variations in metereological conditions, such as rainfall and wind direction change. In order to compensate for these variations it is necessary to accumulate data over extended periods of time. Analysis of these data would then provide information concerning the temporal fluctuations in PAH concentration. For example, the levels of carcinogenic PAHs in air can be locally elevated by periods of wood or coal burning and by short-term increases in traffic density.

Conventional analysis of such vast quantities of sample materials for PAHs would be extremely time-consuming and, therefore, prohibitively expensive. L²TOFMS is a methodology which can rapidly screen a large number of samples and yield specific information regarding their polyaromatic content. It also enables the investigation of the particulates directly from their collection surfaces, thus avoiding all chemical extraction methods which could alter the sample or introduce sample-handling contamination. L²TOFMS is therefore ideally suited to this type of sample screening.

At present the L²TOFMS methodology is difficult to utilise as a quantitative technique. The principal difficulty arises from the intensity variations encountered as a result of sample inhomogeneity on the filter surface. This problem could be overcome by averaging signal over a more extensive area of the sample. In previous work (Dale *et al.*, 1993) we have demonstrated that quantitative information, concerning the level of PAHs in contaminated soil samples, can be obtained using a series of standard additions. A similar spiking technique could be employed in the case of cloud-water

particulates either by adsorbing known quantities of pollutants onto the filter prior to filtration of the cloud water or by doping known quantities onto the filtered material itself. Future investigations will be concerned with the development of suitable approaches to address the problem of quantitation.

A useful extension of the technique would be to utilise an optical delivery system capable of enabling a spatially resolved laser desorption point focus of less than 50 μm. Similar instrumentation has been developed elsewhere and applied to the identification of complex aromatic molecules in interplanatery dust particles (Clemett *et al.*, 1993). Using spatially resolved laser desorption it should be possible in the future to study airborne particulates as individual particles. In this way it may be possible to investigate the mechanism of particulate formation and their individual source history.

In conclusion, therefore, L^2TOFMS has been shown to be a powerful analytical tool for the screening of PAHs associated with cloud-water particulates. The high resolution mass spectra show peaks which correspond to the intact parent ion of a component of the heterogeneous samples. Compared to chromatographic techniques, the L^2TOFMS methodology is faster, generates more direct information and does not require time-consuming extraction and pre-separation procedures to be employed prior to analysis.

ACKNOWLEDGEMENTS

The authors are grateful to Unilever plc for financial support and for the award of a post-doctoral fellowship to M. J. Dale.

REFERENCES

Clemett, S. J., Maechling, C. R., Zare, R. N., Swan, P. D. & Walker, R. M. (1993). Identification of complex aromatic molecules in individual interplanatery dust particles. *Science*, **262**, 721–5.

Crossley, A., Wilson, D. B. & Milne, R. (1992). Pollution in the upland environment. *Environ. Pollut.*, **75**, 81–7.

Dale, M. J., Jones, A. C., Pollard, S. J. T., Langridge-Smith, P. R. R. & Rowley, A. G. (1993). Application of two-step laser mass spectrometry to the analysis of polynuclear aromatic hydrocarbons in contaminated soils. *Environ. Sci. Technol.*, **27**, 1693–5.

Dale, M. J., Jones, A. C., Pollard, S. J. T. & Langridge-Smith P. R. R. (1994). Direct determination of polynuclear aromatic hydrocarbons in environmental matrices using laser desorption laser photoionisation time-of-flight mass spectrometry. *Analyst*, **119**, 571–8.

de Vries, M. S., Elloway, D. J., Wendt, R. & Hunziker, H. E. (1992). Photoionisation mass spectrometer with a microscope laser desorption. *Rev. Sci. Instrum.*, **63**, 3321–5.

Deutshwenel, R. P., Brune, H., Grimmer, G., Dettborn, G. & Misfeld, J. (1983). Experimental studies in rat lungs on the carcinogenicity and dose-response relationships of 8 frequently occuring environmental polycyclic aromatic hydrocarbons. *J. Nat. Cancer Inst.*, **71**, 539–44.

Fearey, B. L., Miller, C. M., Rome, M. W., Anderson, J. E. & Nogar, N. S. (1988). Pulsed laser resonance ionisation mass spectrometry for elementally selective detection of lead and bismuth mixtures. *Anal. Chem.*, **60**, 1786–91.

Grimmer, G. G., Naujack, K.-W. & Dettburn, G. (1987). Gas-chromatographic determination of polycyclic aromatic hydrocarbons, azaarenes, aromatic amines in the particle and vapour phase of mainstream and sidestream smoke of cigarettes. *Toxicol. Lett.*, **35**, 117–24.

Jaffrezo, J.-L., Masclet, P., Clain, M. P., Wortham, H., Beyne, S. & Cachier, H. (1993). Transfer function of polycyclic aromatic hydrocarbons from the atmosphere to the polar ice — I. Determination of atmospheric concentration at Dye 3, Greenland. *Atmos. Environ.*, **27A**, 2781–5.

Karcher, W. (1988). *Spectral Atlas Polycyclic Aromatic Hydrocarbons.* Joint Res. Center, Kluwer Academic Pub., Boston, USA.

Kovalenko, L. J., Maechling, C. R., Clemett, S. J., Philippoz, J.-M. & Zare, R. N. (1992). Microscopic organic analysis using two-step laser mass spectrometry: Application to meteoritic acid residues. *Anal. Chem.*, **64**, 682–90.

Lee, M. L., Novotny, M. V. & Bartle, K. D. (1981). *Analytical Chemistry of Polycyclic Aromatic Compounds.* Academic Press, New York, USA, pp. 27–33.

Lubman, D. M. (1988). Analytical multiphoton ionisation mass spectrometry. Part I. Theory and instrumentation. *Mass Spectr. Rev.*, **7**, 535–54.

Masclet, P., Mouvier, G. & Nikolaou, K. (1986). Relative decay index and sources of polycyclic aromatic hydrocarbons. *Atmos. Environ.*, **20**, 439–46.

Masclet, P., Pistikopoulos, P., Beyne, S. & Mouvier, G. (1988). Long range transport of gas/particle distributions of polycyclic aromatic hydrocarbons at a remote site in the mediterranean sea. *Atmos. Environ.*, **4**, 639–50.

McLafferty, F. W. & Gohlke, R. S. (1959). Mass spectrometric analysis; aromatic acids and esters. *Anal. Chem.*, **31**, 2076–82.

Menzie, C. A., Potock, B. B. & Santodonato, J. (1992). Exposure to carcinogenic PAHs in the environment. *Environ. Sci. Technol.*, **26**, 1278–84.

McClennen, W. H., Arnold, W. S., Roberts, K. A., Meuzelaar, H. L. C., Lightly, J. S. & Lindgren, E. R. (1990). Fast, repetitive GC/MS analysis of thermally desorbed polycyclic aromatic hydrocarbons from contaminated soils. *Combust. Sci. Technol.*, **74**, 297–309.

National Academy of Science. (1983). *Polycyclic Aromatic Hydrocarbons: Evaluations of Sources and Effects*, Washington, D.C., USA.

Schuetzle, D., Riley, T., Prater, T. J., Harvey, T. M. & Hunt, D. F. (1982). Analysis of nitrated polycyclic aromatic hydrocarbons in diesel particulates. *Anal. Chem.*, **54**, 265–71.

Vo-Dinh, T., (1989). Significance of chemical analysis of polycyclic aromatic compounds and related biological systems. In *Chemical Analysis of Polycyclic Aromatic Compounds*, Vol. 101, ed. T. Vo-Dinh. Wiley Interscience, NY, USA, pp. 1–30.

Zhan, Q., Voumard, P. & Zenobi, R. (1995). Application of two-step laser mass spectrometry to the chemical analysis of aerosol particle surfaces. *Rap. Comm. Mass Spectr.*, **9**, 119–27.

Spatially Resolved in-Situ Analysis of Polymer Additives by Two-Step Laser Mass Spectrometry

Qiao Zhan, Renato Zenobi, Scott J. Wright, and Patrick R. R. Langridge-Smith

Department of Chemistry, Swiss Federal Institute of Technology (ETH), 8092 Zürich, Switzerland, and Department of Chemistry, King's Buildings, West Mains Road, The University of Edinburgh, Edinburgh EH9 3JJ, U.K.

Macromolecules®

Reprinted from
Volume 29, Number 24, Pages 7865–7871

Spatially Resolved in-Situ Analysis of Polymer Additives by Two-Step Laser Mass Spectrometry

Qiao Zhan,[†] Renato Zenobi,*[,†] Scott J. Wright,[‡] and Patrick R. R. Langridge-Smith[‡]

Department of Chemistry, Swiss Federal Institute of Technology (ETH), 8092 Zürich, Switzerland, and Department of Chemistry, King's Buildings, West Mains Road, The University of Edinburgh, Edinburgh EH9 3JJ, U.K.

Received April 12, 1996; Revised Manuscript Received August 16, 1996[⊗]

ABSTRACT: Two-step laser mass spectrometry has been employed for the direct in-situ analysis of a variety of additives in different polymers. Because of the high sensitivity and optical selectivity of this approach, mass spectra can be obtained directly from the polymer material. The effects of CO_2 laser irradiation (λ = 10.6 μm) on samples of poly(oxymethylene) (POM), poly(vinyl chloride) (PVC), polypropylene (PP), and poly(ethylene terephthalate) (PET) and the mechanism of additive desorption have been examined. Several hydroxyphenylbenzotriazole (Tinuvin) UV stabilizers as well as a phenolic antioxidant (Santo White) were successfully detected in typical industrial polymers. The detection limit for Santo White antioxidant in POM was found to be as low as 28 ppm. Finally, depth profiling by stepwise CO_2 laser ablation was carried out for a POM injection bar containing 0.1 wt % antioxidant. These spatially resolved measurements established that the near surface concentration of antioxidant was 40% lower than in the bulk.

Introduction

Polymers are among the most important materials used in today's world. Virtually all polymeric materials, both of synthetic and natural origin, undergo reactions with oxygen or degradation under sunlight. Oxidation can manifest itself in every stage of the life cycle of a polymer, e.g. during manufacturing and storage of the material or during processing and use. The UV component of sunlight, in the 290−400 nm wavelength range, leads to photochemical reactions in many polymers, which result in changes in their optical and mechanical properties. To improve their stability, additives protecting them against oxidation, UV radiation, weathering, etc. are widely used.[1,2]

Throughout the lifetime of the polymer, the additives will be depleted by photochemical reactions or by diffusion out of the host material, which can greatly influence the material properties. Normally, many different additives are used in a polymer formulation. UV stabilizers and antioxidants may be present in the polymer matrix at a level of only 1 wt % or less. Due to this low concentration and complex environment, sensitive and selective methods of chemical analysis are necessary to identify additives in a typical commercial polymer.

Because of the polarity and nonvolatilty of many UV stabilizers and antioxidants, gas chromatography is not commonly employed as an analysis method. However, other spectroscopic and liquid chromatographic methods are very powerful in identifying ingredients in compounded polymeric materials. High-pressure liquid chromatography (HPLC) or its combination with mass spectrometric detection (HPLC−MS) has been used for the analysis of additives in polymers.[3,4] Approximately 1 g of the polymer is necessary for extraction with solvents, typically acetone or acetonitrile, which may take 12 h or longer. Supercritical fluid extraction (SFE) offers a faster alternative for polymer extraction and SFE coupled with subsequent chromatographic separation is also employed for analysis of polymer additives.[5,6] However, in extraction-based analytical techniques, all information on the additive's spatial distribution within the polymer is lost.

As an alternative to extraction-based analytical methods, Lattimer and co-workers advocated the use mass spectrometric methods (FAB-MS, field ionization MS, pyrolysis−MS) for direct analysis of nonvolatile agents in polymer matrices.[7−10] Organic secondary ion mass spectrometry (SIMS) with[11,12] or without postionization[13] can be used for direct analysis of polymer surfaces. The drawbacks of FAB and SIMS are that they provide no selectivity for the detection of minor sample components. Also, these techniques deposit large amounts of energy at the sample surface and typically generate predominantly fragment ions of the polymer itself. Laser desorption (LD) and laser desorption/Fourier-transform ion cyclotron resonance (LD-FTICR) mass spectrometry have also been applied with considerable success to the detection of many classes of nonvolatile compounds including organic polymers.[14−19] Johlman et al. demonstrated that LD-FTICR could be used to identify polymer additives in polyethylene extracts. The spectra were found to contain intense quasimolecular ions (Na^+ and K^+ adducts) as well as fragments.[16−19]

Since its introduction by Hillenkamp[20,21] and Tanaka,[22] matrix-assisted laser desorption/ionization (MALDI) mass spectrometry has been widely used as a soft ionization technique that allows desorption and ionization of very large molecules, for example polymers.[22,23] However, this technique is employed neither as an *in-situ* analytical method nor as a selective method for detecting minor polymer constituents. This is due to the requirement that in MALDI the analyte must be well mixed with the matrix *prior* to analysis. Furthermore, the molecular weights of typical UV stabilizers and antioxidants are normally a few hundred mass units, a range that is often obscured by intense matrix peaks present in MALDI mass spectra.

* To whom correspondence should be addressed at: Analytical Chemistry Group, Department of Chemistry, ETH-Zentrum, Universitätstrasse 16, CH-8092 Zürich, Switzerland. Tel: +41-1-632-4376. Fax: +41-1-632-1292. E-mail: ZENOBI@org.chem.ethz.ch.
† Swiss Federal Institute of Technology.
‡ University of Edinburgh.
⊗ Abstract published in *Advance ACS Abstracts,* October 15, 1996.

S0024-9297(96)00547-5 CCC: $12.00

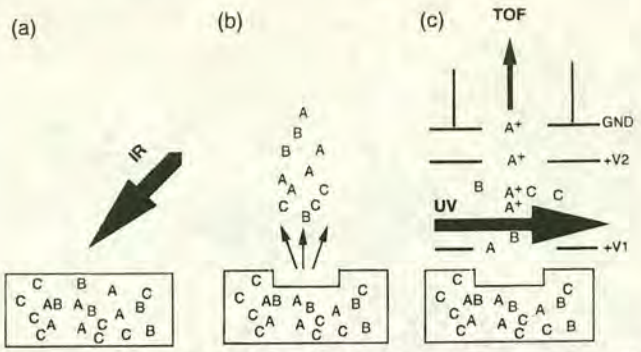

Figure 1. Principle of L2MS. A, B, and C are different additives. The polymer is irradiated by an IR laser pulse (a) and decomposes and is ejected from the bulk together with intact additives (b). Selective ionization is carried out by a UV laser with resonant two-photon ionization (c). Finally, the ions are mass-separated and recorded in a time-of-flight mass spectrometer.

Direct laser desorption/ionization mass spectrometry (LDMS) has proven to be quite useful for direct in-situ analyses,[24-26] but it suffers from ionization matrix effects. To circumvent this problem, a postionization step can be used. Lykke et al.[27,28] have used this approach to analyze vulcanizates in rubber and rubber extracts. They demonstrated that the use of different wavelengths for the postionization step provides important additional information about the chemical composition of the samples.

In the present study we have applied two-step laser mass spectrometry (L2MS) to the direct chemical analysis of additives in a range of polymers. It has been previously demonstrated that L2MS is a highly sensitive and optically selective method[29] which can serve as a very powerful tool for the direct detection of selected compounds in complex sample mixtures. This methodology decouples the desorption and the ionization step, allowing each process to be independently optimized. In brief, an infrared laser is used to irradiate the polymer and cause ablation, probably by a pyrolysis mechanism[30] (Figure 1a). During this ablation step the polymer is thermally decomposed and ejected from the bulk material, together with intact additives (Figure 1b). After a suitable time delay, the liberated molecules are intercepted by a pulse from a UV laser. This leads to soft ionization of the liberated species via a resonance-enhanced multiphoton ionization (REMPI) process. For common UV laser wavelengths, two photons are necessary to overcome the ionization potentials of the substances investigated here. If the first photon is resonantly absorbed by the molecule under study, a greatly enhanced ionization efficiency is found, providing a high degree of optical selectivity. The second photon then raises the energy of the excited molecules above the ionization threshold. Finally, a reflectron time-of-flight (TOF) mass spectrometer is used for mass separation of the ions produced (Figure 1c).

In order to analyze additives in a polymer sample with L2MS, it is necessary to desorb neutral species from bulk material. It was first reported in 1982 that with pulsed UV laser radiation, the surface of an organic polymer can be ablated to a depth ranging from 0.1 μm to several micrometers.[31] Nearly all organic polymers can be ablated by UV laser photodecomposition.[32-34] However, ionization of the ejected material often occurs simultaneously, which complicates mass spectrometric analysis of minority species such as additives. Infrared laser radiation, in contrast, excites vibrational states and can induce pyrolysis of polymers. Dyer et al. examined the irradiation of poly(ethylene terephthalate) (PET) films by radiation from a TEA CO_2 laser tuned to the 9R42 line ($\approx$9.2 μm).[35] They found that the PET film could be successfully ablated with 9.2 μm laser radiation. The major volatile ablation products found were carbon monoxide, carbon dioxide, methane, ethyne, ethene, benzene, ethanal, similar to products found in the purely thermal pyrolysis of PET.[30] In contrast, ablation of poly(ether ether ketone) (PEEK) with 9.2 μm laser light was found to be difficult.[30]

In this work, several complementary methods have been used to improve L2MS analysis of polymers and polymer additives. In preliminary studies, we found that for many polymers, no signals of polymer additives (dyes, antioxidants, UV stabilizers) could be detected by L2MS, although large craters were generated by IR laser irradiation of the polymer surface. We therefore studied the behavior of different polymers under 10.6 μm laser irradiation using IR spectroscopy and electron microscopy. We found that either laser-induced ablation or laser melting occurred for different polymers, depending on their IR absorption cross section. Information about the spatial resolution of IR laser ablation was also obtained from the electron microscopy studies. Direct in-situ detection of polymer additives as well as measurements of mass spectra for the pure additives were then carried out. Finally, stepwise CO_2 laser ablation was used to study the spatial distribution of an antioxidant in an injection-molded bar of poly(oxymethylene) (POM).

Experimental Section

Materials. Several different polymers were used in this study, most of them commercial polymers (PVC and PET sheets and a POM injection bar), although some samples did not contain additives and had to be mixed with UV stabilizers or antioxidants in the laboratory (e.g., POM powder, PP film). Pure POM powder, antioxidants, and a POM injection bar stabilized with $\approx$0.1 wt % of an antioxidant were obtained from DuPont (Geneva, Switzerland). A 100 μm thick PP film as well as the Tinuvin UV stabilizers were obtained from Ciba-Geigy (Marly, Switzerland). PVC and PET sheets were obtained from Notz Plastics A.G. (Brügg bei Biel, Switzerland). Little is known about the additives present in these two commercial polymers. The structures of the polymers and additives used in this study are shown in Table 1. Pyrene and coronene were used as internal mass standards for mass calibration and were obtained from Socochim SA (Lausanne, Switzerland).

Sample Preparation. Pure additives were dissolved in acetone and dosed onto a glass plate for L2MS experiments. Commercial polymers that contained the additives were used as received; the POM injection bars containing Santo White powder antioxidant were further machined into 1 mm thick sheets for depth profile experiments. Tinuvin UV stabilizers were added to several polymer samples in the laboratory using two different procedures: (i) POM powder was mixed with the UV stabilizer (0.1–0.3 wt %) and pressed under 400 atm into a 12 mm diameter by 4 mm thick pellet. This is a quick and easy sample preparation method, although it is not used in standard polymer processing. (ii) For the PVC and PET sheets and the PP film, pure UV stabilizers were spread onto the polymer surface and covered with an aluminum foil to form a sandwich. This sandwich was fixed between two aluminum plates and then kept in an oven at 100 °C in a nitrogen atmosphere for 12 h, allowing the UV stabilizer to diffuse into the polymer samples. The residual UV stabilizer was then washed away from the polymer surface with acetone, a simple and effective cleaning process also used by other researchers.[36] Due to their high solubility, the residual amount of additives on the surface was negligible.

Table 1. Structure of Polymers and Polymer Additives

Name	Structure	Name	Structure
Polyoxymethylene	$-[OCH_2]_n-$	Polyvinylchloride	$-[CH_2CH(Cl)]_n-$
Polypropylene	$-[CH_2CH(CH_3)]_n-$	Polyethylene terephthalate	$-[OCOC_6H_4COOC_2H_4]_n-$
Tinuvin™ PS (m/z = 267)	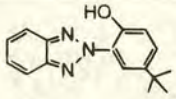	Tinuvin™ 327 (m/z = 357)	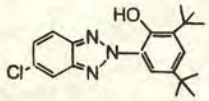
Tinuvin™ 234 (m/z = 447)	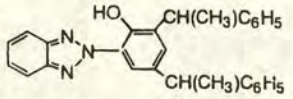	Tinuvin™ 328 (m/z = 351)	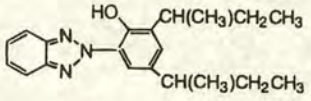
Tinuvin™ 320 (m/z = 323)	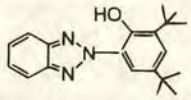	Tinuvin™ 329 (m/z = 323)	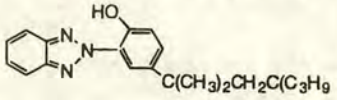
Tinuvin™ 326 (m/z = 315)	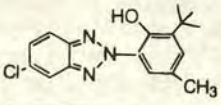	Tinuvin™ 343 (m/z = 323)	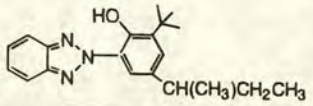
Lowinox 22 (m/z = 340)	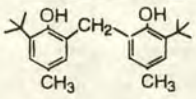	Santo white powder (m/z = 382)	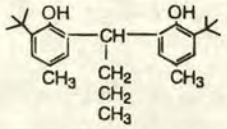

IR Spectroscopy. PP and POM were also studied by IR spectroscopy. The 100 μm thick PP film was used directly, whereas 7 mg of POM powder were mixed with 159 mg of KBr and pressed into a pellet. The effective thickness of the POM was 40 μm, as calculated from the amount of material used to make the KBr pellet. The spectra were taken on a 5SXC FT-IR spectrometer (Nicolet Instrument Corp., Madison, WI).

Electron Microscopy. To study the surface appearance of the polymers after infrared laser irradiation, scanning electron microscopy was carried out using a S-700 electron microscope (Hitachi, Japan). The samples were vacuum coated with a 20 nm layer of Au–Pt alloy. The microscope was operated with 25 kV acceleration voltage, about 70 V emission voltage, and a current ≤ 1 μA. A standard copper photoresist stripe was used to calibrate the length scale.

L2MS System. For mass spectrometric analysis, a home-built L2MS system was used.[29] The polymer samples were cut to size, mounted onto the tip of the sample holder and directly introduced into the vacuum chamber through a rapid vacuum interlock. No extraction, purification, or preconcentration steps are required for the L2MS experiment. The beam of the CO_2 laser used for ablation (Alltech model 853 MS, Lübeck, Germany) was directed into the system by a set of mirrors and a ZnSe lens. The power density was regulated to ca. 6×10^6 W/cm^2, by two irises and by the size of the laser focus. The infrared laser (10.6 μm wavelength, $\leq$100 ns pulse width) was operated at 4 Hz repetition rate to avoid cumulative heating of the polymers. The ionization laser wavelength was 266 nm (fourth harmonic of a Nd: YAG laser, model Surelite II, Continuum). The UV laser power density was ca. 6×10^7 W/cm^2, and this UV laser pulse was delayed with respect to the CO_2 laser pulse by about 20 μs. Mass spectrometric analysis was achieved using a reflectron time-of-flight instrument (R. M. Jordan Co.) with a mass resolution of $\approx$1500 at $m/z = 300$. The total acceleration potential in the ion source of the time-of-flight mass spectrometer was about 5 kV. Ions were detected by a pair of microchannel plates in a Chevron configuration, and the data were collected with an acquisition rate of 100 MS/s on a digital oscilloscope (model 9350, Le Croy, Geneva, Switzerland). The spectra were then transferred to a PC for further data processing. Only positive ion spectra were acquired in these experiments. A two-point mass calibration was performed using pyrene ($m/z = 202$) and coronene ($m/z = 300$). For CO_2 laser depth profiling experiments, care was taken to keep all experimental conditions constant for successive experiments.

Results and Discussion

CO_2 Laser Ablation of Polymers. In the present study CO_2 laser ablation of POM, PVC, PP, and PET was carried out at a wavelength of 10.6 μm. The IR spectra of all polymers used in this study can be found in the literature or in handbooks.[37–40] As a result of different polymerization processes (e.g. isotactic and syndiotactic PP), the spectra of specific polymer formulations may appear quite different. We found that polymers absorbing strongly at 10.6 μm showed good laser ablation characteristics whereas weakly absorbing materials exhibited poor ablation. In order to illustrate this, infrared spectra for PP and POM are shown in Figure 2. The absorbance scales were normalized to a sample thickness of 100 μm, so that these two spectra are directly comparable. POM absorbs well at 10.6 μm, whereas PP has almost no absorption at this wavelength. The IR spectra of PVC and PET, obtained from the literature,[40] show strong IR absorption for PVC at 10.6 μm and weak absorption of PET at this wavelength.

Figure 3a,b shows electron micrographs of ablation craters in the POM and PVC samples at a laser radiant exposure of 7.6 J/cm^2. The elliptical shapes are due to the 45° angle of incidence of the focused desorption laser

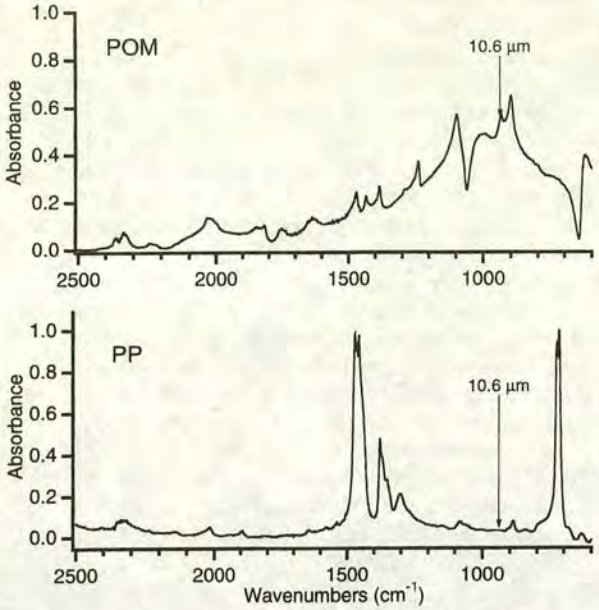

Figure 2. Infrared spectra of POM (top) and PP (bottom). The PP sample was a 100 μm thick film; the POM powder was pressed into a pellet with KBr. The spectra were normalized to an effective sample thickness of 100 μm. As shown in the picture, POM has a relatively strong absorption band at 10.6 μm while PP has almost no absorption.

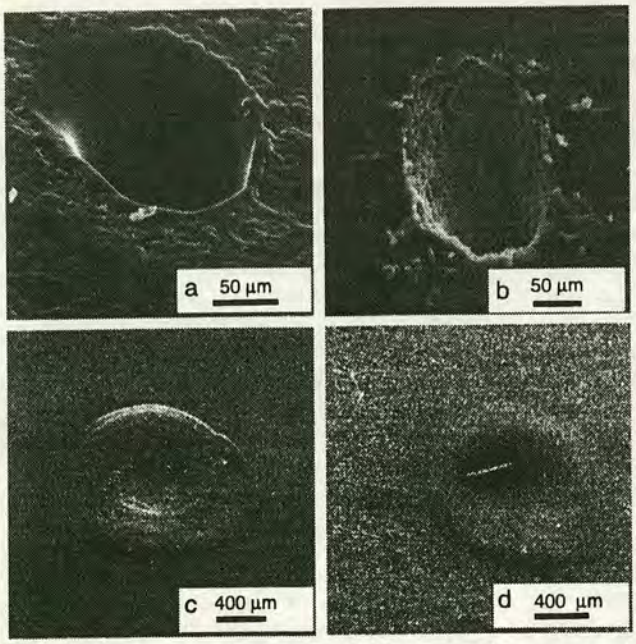

Figure 3. Electron micrographs of different polymer surfaces after irradiation with 10 shots from a pulsed CO_2 laser at 10.6 μm. POM (a) and PVC (b) show efficient ablation; PP (c) and PET (d) show only laser melting.

beam. Since POM and PVC strongly absorb the 10.6 μm laser light, efficient ablation is observed. The edges and the crater walls are well-defined. By optimizing the laser beam focus and the laser power density, a spatial resolution of 40 μm in diameter can be obtained, close to the theoretical diffraction limit for our IR optical system. The crater depth was not measured but is estimated to be several tens of micrometers in Figures 3a,b. During ablation the polymer is pyrolytically decomposed and fragments are ejected with high velocity within a short time after the laser pulse. Comparatively little energy will be directly deposited in the additives at 10.6 μm. We propose that, by analogy with

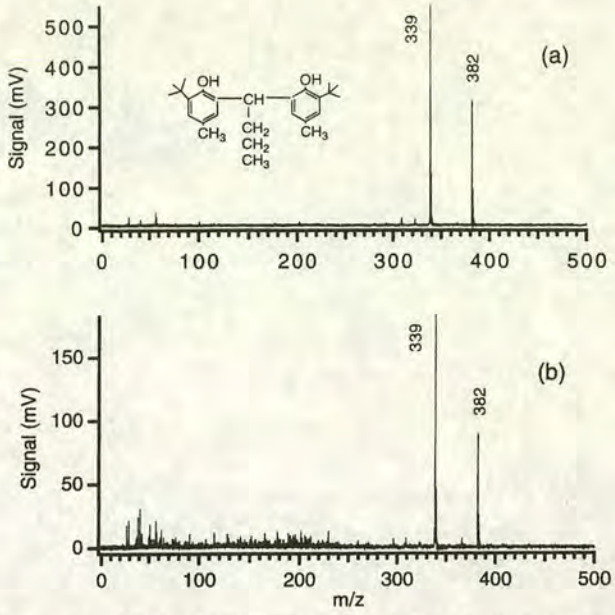

Figure 4. L2MS spectra of (a) a pure antioxidant, Santo White powder, and (b) in-situ L2MS spectrum of Santo White powder in a POM injection bar (40 shot average). 266 nm was used as a postionization wavelength.

the MALDI process, the laser only heats up the host polymer directly, whereas the guest molecules are still close to their initial temperature at the maximum desorption rate.[41] In addition, collisions in the plume can assist in the relaxation of the desorbed molecules, so that intact neutral additive molecules are obtained.

If the laser radiation is only weakly absorbed by the polymer, as in the case of PP and PET, there is a large penetration depth, and the energy spreads over a large volume. Ablation is difficult and the laser power required is 5 times higher than that needed for ablation of POM and PVC. These polymers showed extensive melt flow when irradiated by the IR laser. Figure 3c,d shows the surfaces of PP and PET after 10.6 μm laser irradiation. Melted material seems to have flowed over from the exposed to the unexposed region. The foamlike region around the center hole on PP is probably due to internal vapor production. The 200 μm bright streak in the center in Figure 3d is probably a dust particle on the PET surface. Under our normal L2MS experimental conditions it proved difficult to observe additives directly from the PP and PET samples. However, the use of higher desorption laser power along with a considerable enlargement of the desorption spot can lead to some desorption of additives. In this way, it was possible to obtain L2MS data for additives in PP beads, although at lower spatial resolution.[42]

L2MS Studies of Polymer Additives. Table 1 shows the structures of all additives we investigated. Figure 4 shows the positive ion L2MS spectra of (a) pure Santo White antioxidant, and (b) of an antioxidant-stabilized POM injection bar. Signals characteristic of Santo White powder at m/z = 382 and 339 are very intense in both spectra, although the additive concentration in the polymer was only 0.1 wt %. The peak at m/z = 382 is the parent ion, while the m/z = 339 fragment $[M - 43]^+$ results from the loss of the C_3H_7 side chain, resulting in a planar fragment ion that is resonance stabilized. The spectrum in Figure 4b which was obtained from a freshly exposed interior surface of the injection bar is virtually identical to the spectrum for the pure additive. Neither greater fragmentation

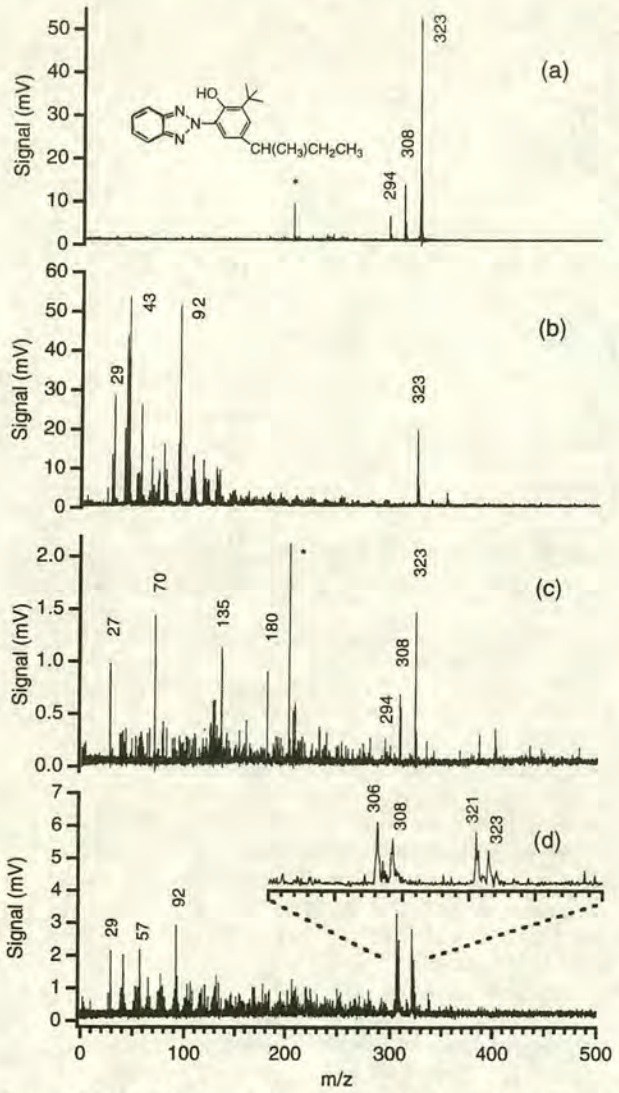

Figure 5. (a) L2MS spectrum of a pure UV stabilizer, Tinuvin 343, deposited onto a glass substrate from an acetone solution. (b) in-situ L2MS spectrum of Tinuvin 343 in a POM pellet (concentration 0.1 wt %). (c) in-situ L2MS spectrum of Tinuvin 343 diffused into a commercial PVC sheet. (d) L2MS analysis after CO_2 laser transfer from a 100 μm PP film to a glass backing plate. Peak assignments are given in the text.

nor significant contamination is observed; the weak signals in the low mass range are not related to Santo White antioxidant. The additive signals at m/z = 382 and 339 persisted with every shot. Given a known additive concentration in the polymer, and by measuring the ablated polymer volume, we calculate a detection limit of 28 ppm (S/N = 3, 40 shot average) for the Santo White antioxidant in this POM injection bar.

Figure 5 shows L2MS spectra of Tinuvin 343, obtained from the pure compound deposited on a glass plate (Figure 5a), and from different polymers (Figures 5 b–d). Pure Tinuvin 343 was deposited on a glass substrate and mass spectra were averaged over 40 shots (Figure 5a). The spectrum was very clean, dominated by an intense molecular ion peak at m/z = 323. The peaks at m/z = 308 and 294 are fragments resulting from the loss of CH_3 and CH_2CH_3 groups, and that at m/z = 202 is a mass standard, pyrene (asterisk), which is sometimes still present in the background gas of the chamber after calibration measurements.

The L2MS spectra of a number of other Tinuvin UV stabilizers as well as Lowinox 22 antioxidant were also recorded (spectra not shown, refer to Table1). We observed that fragmentation of the Tinuvin UV stabilizers always occurred on the aliphatic side chains, mostly by loss of methyl or ethyl radicals. Although the ionization potentials (IPs) for these compounds are unknown, they can be estimated by comparison with model compounds such as indole, 2,4-dimethylphenol, or 4-ethylphenol which have IPs of 7.76, 8, and 7.8 eV, respectively.[43] Hydroxyphenylbenzotriazole has a more extensive conjugated π-electron system and we therefore assume that its IP is less than 8 eV. The two-photon energy at λ = 266 nm is 9.32 eV. This yields ions with more than 1.32 eV excess energy, which, combined with some internal excitation (from laser desorption) should lead to fragmentation. At λ = 193 nm, the excess energy is over 4.8 eV and more extensive fragmentation was observed.[42] It is interesting to note that although Tinuvin 320, Tinuvin 329, and Tinuvin 343 have the same molecular weight (see Table 1), it was possible to distinguish between them by the fragmentation pattern observed in the L2MS spectra.[42]

Figure 5b shows an in-situ L2MS spectrum of Tinuvin 343 obtained directly from a POM pellet. The concentration of Tinuvin 343 was about 0.15 wt %. For a signal-to-noise ratio of 3, we estimate the detection limit to lie in the 10–100 ppm range. The uncertainty is due to the sample preparation process which does not allow control over the spatial distribution of the UV stabilizer in the POM pellet.

No signal was obtained with either the desorption laser or the ionization laser blocked, confirming that laser ablation liberates neutral additive species only. Quasimolecular ions which are typically obtained in MALDI (e.g. Na, K cationized or protonated species) are not observed in the L2MS spectra, facilitating spectral interpretation.

The molecular ion at m/z = 323 is clearly seen in Figure 5b but the M − CH_3 and M − CH_2CH_3 fragments are not observed. We believe that in the case of efficient polymer ablation, the additive molecules were collisionally cooled in the plume, reducing fragmentation induced by the UV ionization laser. The fragments in the low mass range, however, appear to be fundamentally different from those seen in Figure 5a. Since the repeating unit of POM is [OCH_2], these peaks are not derived from the polymer itself. We interpret these signals as degradation products of the Tinuvin 343 (or fragments thereof) produced during preparation of the POM pellet. For example, the peak at m/z = 92 is interpreted as a fragment peak (either C_6H_4O or C_7H_8) based on a phenyl ring permitting REMPI detection; other aromatic and alkane fragments originating from such degradation products (C_2H_5, C_3H_7, and C_4H_9 at m/z = 29, 43, and 57) are also detected. From visual inspection of the sample surface, we speculate that during preparation of the POM pellet under 400 atm pressure, the sample melted. The temperature at that moment must be several hundred degrees Celsius, which might have induced some thermal degradation of the additives.[44]

Figure 5c shows a L2MS spectrum of Tinuvin 343 diffused into a commercial PVC sheet.[36] No other UV stabilizers had been added to this PVC sample by the manufacturer. Again, the molecular ion and the M − CH_3 and M − CH_2CH_3 fragments were observed. This sample of commercial PVC sheet was filler reinforced, and several new peaks of unknown origin were observed in the lower mass range (m/z = 27, 70, 135, 180). As

shown in the electron micrograph in Figure 3b, the PVC sheet has a foamlike morphology, and the apparent polymer density is low. Laser ablation from this sample was less efficient than from POM, resulting in a lower detection sensitivity for the Tinuvin 343. Another possible reason for the lower detection sensitivity for Tinuvin 343 from PVC is the sample itself, prepared by additive diffusion into the PVC film rather than by pressing as in the case of POM.

As mentioned above, irradiation of PP and PET did not lead to any ablation, only laser melting was observed. It was very difficult to liberate additives by pulsed CO_2 laser irradiation ($\lambda = 10.6$ μm) of these materials.[40] Therefore, a "laser transfer" experiment was carried out.[45] The PP film, stretched over a clean glass substrate, was attached to the tip of the sample holder. The sample holder was then exposed in vacuum to the CO_2 laser operated at a slightly elevated power density. This resulted in melting of the PP film and partial transfer of the material to the glass substrate. The sample holder was then retracted from the mass spectrometer and the polymer film removed, revealing the transferred material on the glass substrate. Finally, the glass plate was reintroduced into the mass spectrometer for L2MS analysis.

Using this approach, the additive signal could be detected with regular CO_2 laser desorption from glass. Figure 5d shows the result of such a laser transfer experiment for Tinuvin 343 diffused into a 100 μm PP film. Besides the molecular ion peak and the known fragments, low mass peaks similar to the data in Figure 5b were found. Additionally, peaks at $m/z = 306$ and 321 were observed (insert in Figure 5d). These peaks are two mass units below the molecular ion and M − CH_3 fragment signals. They are interpreted as the result of dehydrogenation of the isobutyl side chain of Tinuvin 343. A fairly stable structure could result from conjugation with the aromatic rings of Tinuvin 343. This dehydrogenation pathway seems to open up in conjunction with the laser transfer process, where a high temperature might persist for a relatively long time, facilitating dehydrogenation.[46] In spite of these added complications, the data in Figure 5d show that laser transfer makes additives from the host polymer available for regular L2MS detection by accumulating them, probably together with some polymer, on the backing plate. Although this method is only applicable to thin samples such as films and the spatial information is partially lost, the selective nature of the ionization process removes the requirement for any wet chemical separation procedures to be performed prior to mass spectral analysis. Furthermore, laser transfer might be an interesting option for detection of the transferred species with other analytical methods, for example optical spectroscopy.

Spatially Resolved L2MS by Stepwise Ablation. Depth profiling experiments have also been carried out to study the additive distribution perpendicular to the sample surface. The sample used was the POM injection bar containing Santo White powder. In this sample the antioxidant was well mixed and distributed in the polymer matrix. However, polymer processing such as injection and molding can change the additive distribution and result in concentration gradients, especially near the surface. Similarly, diffusion of the additive into the ambient air can lead to a depletion in the near-surface region.

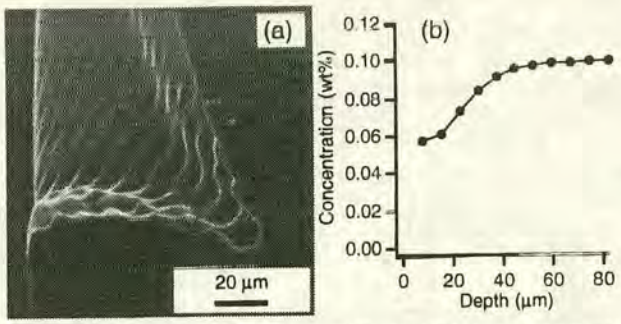

Figure 6. Spatial distribution of Santo White powder antioxidant in a POM injection bar near the surface. The concentration near the surface is 40% lower than in the bulk.

The depth profiling experiment was carried out in a stepwise fashion: 200 laser shots (using <1 J/cm^2 of laser energy density) were fired at the sample, and L2MS spectra were recorded simultaneously. After 200 laser shots, the experiment was paused and the L2MS data (200 shot average) were stored. Then the next 200 shots were accumulated, and so on. Figure 6a shows an electron micrograph of a cross section of the resulting ablation crater. During 200 shots the polymer was ablated by about 7 μm, as judged from the staircase-like structure. Since the desorption laser beam was focused at a 45° angle with respect to the sample surface, the resulting ablation crater assumes a tilted shape. Because the laser focus was located behind the surface of the polymer piece under study, the volume sampled in each profiling step was not constant. A calibration experiment was therefore carried out. The interior of the injection bar was analyzed in the same fashion after removing a layer of about 1 mm thick from the surface. Assuming that the additive concentration at any depth is homogeneous in the interior and equals 0.1 wt %, the resulting peak areas can be taken as a measure of the volume sampled.

The combined peak areas of the M and M − C_3H_7 signals in each L2MS spectrum were used as a measure of the additive concentration. The normalized additive signal versus depth was plotted to show the spatial distribution of the additive in the near-surface region of the injection bar (Figure 6b). Since the exterior surface turned out to be contaminated, the first point is omitted in the figure. We found that the additive concentration near the surface is 40% lower than that in the bulk. This may be a result of the polymer injection process: the melting points of POM and the antioxidant are 175 and 209 °C, respectively, whereas the mold temperature was only 90 °C. Therefore, during injection, the POM would have solidified first, and the additive concentration near the surface is expected to be lower than bulk. Furthermore, the sample was exposed to air for more than 1 year, so depletion of the antioxidant near the surface by diffusion processes is also possible.

Conclusions

The analysis of UV stabilizers and antioxidants both as pure compounds and in a variety of polymers has been successfully carried out using L2MS. This method shows considerable potential for direct in-situ chemical analysis of small concentrations of additives in a range of polymers. The effects of far infrared laser irradiation of the polymers and the desorption mechanism of additives from the host polymer have been studied. It was found that for strongly absorbing polymers, such

as POM and PVC, laser-induced pyroablation decomposes the host matrix but liberates intact neutral additives. Hydroxyphenylbenzotriazole UV stabilizers and phenolic antioxidants were efficiently and selectively postionized with a UV laser pulse by two photon REMPI. The detection limit for Santo White powder antioxidant in a POM injection bar was found to be as low as 28 ppm.

Weakly absorbing polymers, such as PP and PET, showed only laser melting. Additives in these polymers are not easily detectable by L2MS. For this case detection of the additives after laser transfer from a polymer film to a substrate has been demonstrated, although thermal decomposition has been found to occur concomitantly. Depth profiling L2MS experiments were carried out for the first time and enabled the spatial distribution of an antioxidant within an injection-molded bar of POM to be determined with micrometer resolution. In this sample, the near-surface concentration of the antioxidant was found to be about 40% lower than that in the bulk.

Acknowledgment. We gratefully acknowledge financial support for this work by the Swiss National Science Foundation. We thank Dr. V. Dudler (Ciba-Geigy, Marly) Dr. J.-M. Philippoz (DuPont, Geneva), and Dr. M. J. Dale (University of Edinburgh) for providing samples and/or for helpful discussions. This collaborative study was made possible through a CIBA-ACE award and through a J. Beynon studentship award to S.J.W. P.R.R.L.S. would also like to thank CIBA for the award of a Senior Research Fellowship.

References and Notes

(1) Gächter, R., Müller, H., Eds. *Plastics Additives Handbook*; Hanser/Gardner Publications, Inc.: Cincinnati, OH, 1993.
(2) Rabek, J. F. *Photostabilization of Polymers, Principles and Applications*; Elsevier: London, 1990.
(3) Haney, M. A.; Dark, W. A. *J. Chromatogr. Sci.* **1980,** *18*, 655.
(4) Vargo, J. D.; Olson, K. L. *Anal. Chem.* **1985,** *57*, 672.
(5) Hawthorne, S. B. *Anal. Chem.* **1990,** *62*, 633A.
(6) Knowels, D. E.; Hoge, T. K. In *Applications of supercritical fluids in industrial analysis*; Dean, J. R., Ed.; Blackie: Glasgow, 1993; p 104.
(7) Lattimer, R. P.; Harris, R. E.; Rhee, C. K. *Anal. Chem.* **1986,** *58*, 3188.
(8) Lattimer, R. P.; Harris, R. E. *Rubber Chem. Technol.* **1989,** *62*, 548–567.
(9) Lattimer, R. *J. Anal. Appl. Pyrol.* **1993,** *26*, 65.
(10) Riley, T. L.; Prater, T. J.; Gerlock, J. L.; de Vries, J. E.; Schuetzle, D. *Anal. Chem.* **1984,** *56*, 2145.
(11) Schühle, U.; Pallis, J. B.; Becker, C. H. *J. Vac. Sci. Technol. A* **1988,** *6*, 936.
(12) Ervin, M. H.; Winograd, N. *Surf. Interface Anal.* **1994,** *21*, 298.
(13) Benninghoven, A. *Surf. Sci.* **1994,** *299/300*, 246.
(14) Hogan, J. D.; Laude, D. A., Jr. *Anal. Chem.* **1992,** *64*, 763.
(15) O'Malley, R. M.; Randazzo, M. E.; Weinzierl, J. E.; Fernandez, J. E.; Nuwaysir, L. M.; Castoro, J. A.; Wilkins, C. L. *Macromolecules* **1994,** *27*, 5107.
(16) Asamoto, B.; Young, J. R.; Citerin, R. J. *Anal. Chem.* **1990,** *62*, 61.
(17) Johlman, C. L.; Wilkins, C. L.; Hogan, J. D.; Donovan, T. L.; Laude, D. A. Jr.; Youssefi, M.-J. *Anal. Chem.* **1990,** *62*, 1167.
(18) Nuwaysir, L. M.; Willkins, C. L. *Anal. Chem.* **1988,** *60*, 279.
(19) Brown, R. S.; Wilkins, C. S. *Anal. Chem.* **1986,** *58*, 3396.
(20) Karas, M.; Hillenkamp, F. *Anal. Chem.* **1988,** *60*, 2299.
(21) Hillenkamp, F.; Karas, M.; Beavis, R. C.; Chait, B. T. *Anal. Chem.* **1991,** *63*, 1193A.
(22) Tanaka, K.; Waki, H.; Ido, Y.; Akita, S.; Yoshida, Y.; Yoshida, T. *Rapid Commun. Mass Spectrom.* **1988,** *2*, 151.
(23) Cotter, R. J.; Honovich, J. P.; Olthoff, J. K.; Lattimer, R. P. *Macromolecules* **1986,** *19*, 2996.
(24) Lattimer, R. P.; Harris, R. E. *Mass Spectrom. Rev.* **1985,** *4*, 369.
(25) Holm, R.; Karas, M.; Vogt, H. *Anal. Chem.* **1987,** *59*, 371.
(26) Blease, T. G.; Scrivens, J. H.; Monaghan, J. J.; Weil, D. *Proceedings of the 36th ASMS Conference on Mass Spectrometry and Allied Topics*, San Francisco; 1988; p 357.
(27) Lykke, K. R.; Parker, D. H.; Wurz, P.; Hunt, J. E.; Pellin, M.; Gruen, D. M.; Hemminger, J. C. *Anal. Chem.* **1992,** *64*, 2797.
(28) Lykke, K. R.; Wurz, P.; Parker, D. H.; Pellin, M. J. *Appl. Opt.* **1993,** *32*, 857.
(29) Voumard, P.; Zhan, Q.; Zenobi, R. *Rev. Sci. Instrum.* **1993,** *25*, 3393.
(30) Kelly, J. M., McArdle, C. B., de F. Maunder, M. J., Eds. *Photochemistry and Polymeric Systems*; Royal Society of Chemistry: Cambridge, U.K., 1993; p 54.
(31) Srinivasan, R.; Mayne-Banton, V. *Appl. Phys. Lett.* **1982,** *41*, 576.
(32) Srinivasan, R.; Baren, B. *Chem. Rev.* **1989,** *89*, 1303.
(33) Srinivasan, R.; Braren, B.; Casey, K. G. *J. Appl. Phys.* **1990,** *68*, 1842.
(34) Dickinson, J. T. J.; Shin, J.; Jiang, W.; Norton, M. G. *J. Appl. Phys.* **1993,** *74*, 4729.
(35) Dyer, P. E.; Oldershaw, G. A.; Sidhu, J. *Appl. Phys.* **1989,** *B 48*, 489–493.
(36) Dudler, V.; Muinos, C. In *Polymer Durability: Degradation, Stabilization, and Lifetime Prediction*; Clugh, R. L., Billingham, N. C., Gillen, K. T., Eds.; American Chemical Society: Washington, DC, 1996; p 441.
(37) Mucha, M. *Colloid Polym. Sci.* **1984,** *262*, 841.
(38) Haslam, J.; Willis, H. A.; Squirres, D. C. M. *Identification and analysis of plastics*, 2nd ed.; Heyden: London, 1980.
(39) Crompton, T. R. *The analysis of plastics*; Pergamon Press: Oxford, U.K., 1984.
(40) Hummel, D. O., Ed. *Atlas der Polymer und Kunststoffanalyse*; Carl Hanser Verlag: München, 1978.
(41) Vertes, A., Gijbels, R., Adams, F., Eds. *Laser Ionization Mass Analysis*; John Wiley & Sons: New York, 1993.
(42) Wright, S. J.; Dale, M. J.; Langridge-Smith, P. R. R.; Zhan, Q.; Zenobi, R. *Anal. Chem.*, in press.
(43) Lias, S. G., Bartmess, J. E., Liebmen, J. F., Holmes, J. L., Levin, R. D., Mallard, W. G., Eds. *Gas-phase Ion and Neutral Thermochemistry*; American Chemical Society: Washington, DC, 1988.
(44) A thermogravimetry experiment (Perkin-Elmer Sereis 7 thermal analysis system, 20 °C/min, ~8 mg sample) showed that thermal decomposition for Tinuvin 343 starts at 250 °C and is complete at 335 °C.
(45) Dale, M. J.; Zhan, Q.; Zenobi, R.; Costello, K.; Langridge-Smith, P. R. R. *Anal. Methods Instrum.* **1994,** *2*, 101.
(46) Chauvel, A.; Lefebvre, G. *Petrochemical Processes - Technical and Economic Characteristics*; Editions Technip: Paris, 1989.

MA960547R

Selective in Situ Detection of Polymer Additives Using Laser Mass Spectrometry

Scott J. Wright, Michael J. Dale, Patrick R. R. Langridge-Smith, Qiao Zhan, and Renato Zenobi

Department of Chemistry, The University of Edinburgh, King's Buildings, West Mains Road, Edinburgh EH9 3JJ, United Kingdom, and Analytical Chemistry Group, Department of Chemistry, Swiss Federal Institute of Technology (ETH), 8092 Zürich, Switzerland

ANALYTICAL® CHEMISTRY

Reprinted from
Volume 68, Number 20, Pages 3585–3594

Anal. Chem. **1996**, *68*, 3585–3594

Selective in Situ Detection of Polymer Additives Using Laser Mass Spectrometry

Scott J. Wright,[†] Michael J. Dale,[†,§] Patrick R. R. Langridge-Smith,*[,†] Qiao Zhan,[‡] and Renato Zenobi[‡]

Department of Chemistry, The University of Edinburgh, King's Buildings, West Mains Road, Edinburgh EH9 3JJ, United Kingdom, and Analytical Chemistry Group, Department of Chemistry, Swiss Federal Institute of Technology (ETH), 8092 Zürich, Switzerland

A series of polymer additives, including phenolic antioxidants and UV (Tinuvin) stabilizers, have been analyzed using two-step laser desorption/laser photoionization time-of-flight mass spectrometry (L2MS). A pulsed CO_2 laser was used to desorb the additives as neutral species into the gas phase, where they were postionized using a second UV laser operating at either 266 or 193 nm. For all the antioxidants studied, the 266 nm photoionization mass spectra are dominated by the molecular ion peak; very little fragmentation is observed. In contrast, at 193 nm, the molecular ion peak is usually absent from the photoionization mass spectra. Similar behavior is exhibited by the UV (Tinuvin) stabilizers in their photoionization mass spectra. This wavelength-dependent fragmentation can be exploited for unambiguous identification of many polymer additives. For example, it is shown that the isomeric UV stabilizers Tinuvin 320, Tinuvin 343, and Tinuvin 329 can be differentiated on the basis of the extent or nature of the observed fragmentation in their photoionization mass spectra. Several commercial polymer formulations containing these types of additives have also been analyzed using this experimental approach: the samples were interrogated directly without any pretreatment or extraction. It is shown that UV laser postionization enables selective detection of the additives in preference to the polymer, providing unambiguous in situ identification. The potential of this technique for surface analysis and depth profiling is also discussed.

The characterization of chemical additives in commercial polymer formulations is a challenging analytical problem. By their very nature, commercial polymers are complex systems, comprising the polymer matrix itself together with many other minor components, such as fillers, plasticizers, antioxidants, and UV and thermal stabilizers, as well as coloring agents. Many polymer additives are thermally labile, while others are specifically designed to decompose during polymer processing. Moreover, some additives are often present in low concentrations (0.01–5 wt %). It is clear, therefore, that any chosen analytical technique must be sensitive and selective and must maintain the integrity of the mixture composition.

Because of the complexity of polymer formulations, extraction of the additive mixture from the polymer matrix is usually required, often followed by chromatographic separation and purification. However, there are inherent difficulties in using chromatographic techniques. Gas chromatography (GC) is limited in application by the high molecular weight, thermal lability, and polar nature of many additives.[1] Although HPLC is widely used, the lack of a universal detector compatible with all liquid mobile phases restricts its effectiveness in this area.[2–4] Supercritical fluid chromatography (SFC) has previously been successfully employed for the separation of additives in polymer extracts, and, when SFC has been coupled with off-line Fourier transform infrared detection, complementary functional group information on unknown additives has been obtained.[5] However, due to the chemical similarity of many additives, it is not always possible to identify the exact additive used.

Analysis of polymer extracts by mass spectrometry has also proved challenging.[6] Electron impact (EI-MS) mass spectra are often difficult to interpret due to the high concentration of processing oils in the extracts and extensive fragmentation of the molecular ions.[7] Desorption/ionization techniques such as field desorption (FD-MS) and fast atom bombardment (FAB-MS) have been found to be the most effective means for analyzing polymer extracts.[8,9] FD-MS has proved to be a particularly useful technique, since molecular ion abundances are high with respect to fragmentation, as shown in recent work on mixtures of pure polymer additives.[10] Electrospray mass spectrometry (ESI-MS and ESI-MS/MS) has also recently been used for the analysis of polymer additive mixtures. Mechanisms and fragmentation pathways for both low- and high-energy CID spectra were investigated in this work.[11]

There are many advantages to be gained in being able to chemically speciate additives *directly* from the polymer matrix. Extraction and separation procedures are often time consuming,

† The University of Edinburgh.

‡ Swiss Federal Institute of Technology.

§ Present address: Analytical Chemistry Group, Department of Chemistry, Swiss Federal Institute of Technology (ETH), 8092 Zürich, Switzerland.

(1) Vimalasiri, P. A. D. T.; Haken, J. K; Burford, P. P. *J. Chromatogr.* **1984**, *300*, 300–315.
(2) Munteanu, D.; Isfan, A.; Isfan, C.; Tincul, I. *Chromatographia* **1987**, *23*, 7–14.
(3) Haney, M. A.; Dark, W. A. *J. Chromatogr. Sci.* **1980**, *18*, 655–659.
(4) Sevini, F.; Marcato, B. *J. Chromatogr.* **1983**, *260*, 507–512.
(5) Raynor, M. W.; Bartle, K. D.; Davies, I. L.; Williams, A.; Clifford, A. A.; Chalmers, J. M.; Cook, B. W. *Anal. Chem.* **1988**, *60*, 427–433.
(6) Lattimer, R. P.; Harris, R. E. *Mass Spectrom. Rev.* **1985**, *4*, 369–390.
(7) Carlson, D. W.; Hayes, M. W.; Ransaw, H. C.; McFadden, R. S.; Altenau, A. G. *Anal. Chem.* **1971**, *43*, 1874–1876.
(8) Lattimer, R. P.; Welch, K. R. *Rubber Chem. Technol.* **1980**, *53*, 151–159.
(9) Lattimer, R. P.; Harris, R. E.; Ross, D. B.; Diem, H. E. *Rubber Chem. Technol.* **1984**, *57*, 1013–1022.
(10) Jackson, A. T.; Buzy, A.; Scrivens, J. H.; Jennings, K. R. *Proceedings of the 43rd ASMS Conference on Mass spectrometry and Allied Topics*, Atlanta, GA, May 21–26, 1995; p 750.
(11) Jackson, A. T.; Buzy, A.; Jennings, K. R.; Scrivens, J. H. Submitted to *Eur. J. Mass Spectrom.*

S0003-2700(96)00429-5 CCC: $12.00

rendering additive characterization a slow and laborious process. Furthermore, there is the possibility that the extraction procedure may compromise the integrity of the additive mixture, leading to an inaccurate picture of the polymer composition. Early attempts at mass spectrometric characterization of bulk polymer samples have centered on direct thermal desorption of additives from the bulk polymer, followed by EI-MS, chemical ionization (CI-MS),[12] or field ionization (FI-MS).[13] However, this approach is limited to polymer additives that are stable or can provide meaningful fragment ions at elevated temperatures. Lattimer[14] has recently reported the use of thermal desorption and pyrolysis mass spectrometry (Py-MS) for the detection and identification of various organic additives in poly(propylene) polymers. Desorption/ionization methods, such as (FAB),[15] laser desorption (LD),[16,17] and secondary ion mass spectrometry (SIMS)[18] have also been applied in the analysis of additives from bulk polymer samples. However, these single-step techniques suffer to varying degrees from matrix interference in the resulting mass spectra.

Laser desorption/laser photoionization time-of-flight mass spectrometry (L2MS) is a technique that has great potential for the direct analysis of molecular species from complex host matrices.[19-22] This two-step approach circumvents many of the problems, described above, that have been encountered with other techniques. In this method, a pulsed CO_2 laser is used to desorb the analyte into the gas phase as a neutral species, *directly* from the sample of interest. A second pulse from a UV laser is then used to postionize these gas phase neutral species, generally using a resonance-enhanced multiphoton ionization (REMPI) scheme. The benefits of this two-step approach lie in the spatial and temporal separation of the desorption and ionization events, thereby enabling the independent optimization of each process. This provides a number of advantages for the in situ analysis of bulk polymer samples: (i) desorption of neutral target molecules from the host polymer matrix with minimal decomposition, (ii) soft ionization of the desorbed neutral species, resulting in readily interpretable mass spectra, (iii) selective ionization of polymer additives which have a significant one-photon absorption cross section at the chosen ionization wavelength, and (iv) highly sensitive detection of many polymer additive species.

The L2MS technique has previously been successfully used for the analysis of polymer systems. Polystyrene samples with molecular weights up to $m/z = 4000$ can be characterized,[23] and low molecular weight electropolymerized indoles have also been readily detected.[24] In recent work, L2MS has been successfully used for the in situ detection of electropolymerized indoles directly from the electrode surface.[25] Lustig and Lubman have used L2MS to selectively detect aromatic polymers in aliphatic polymer blends.[26,27] In addition, Lykke and co-workers have shown that it is possible to selectively detect aromatic polymer additives vaporized from rubber vulcanizates by careful choice of the ionization wavelength.[28]

The present study demonstrates the potential of L2MS for rapid generation of readily interpretable mass spectra of polymer additives directly from their host polymer matrices. The polymer additives that have been studied consist of two main classes: antioxidants and UV stabilizers. The antioxidants are either phenolic or phosphite antioxidants, while the UV stabilizers all belong to the Tinuvin class of molecules (hydroxyphenylbenzotriazoles). Mass spectra were initially recorded for the pure additives, using 266 and 193 nm laser photoionization. The two different ionization laser wavelengths result in markedly different mass spectra. These mass spectral differences are a valuable aid in the unambiguous identification of the additives. The use of L2MS for in situ analysis of some additives directly from industrial poly(oxymethylene) (POM) and poly(propylene) (PP) formulations is also reported. The spectra obtained show not only that it is possible to directly detect these additives in the polymer formulations, but also that chemical changes undergone by antioxidants, due to either processing or aging, can also be observed. Finally, the potential of L2MS for depth profiling of polymers from the surface into the bulk is discussed.

EXPERIMENTAL SECTION

Samples. *Pure Polymer Additives.* Ten pure polymer additives consisting of a series of antioxidants and UV stabilizers were examined during this work. Their trade name, chemical name, and structure are given in Table 1. Irganox 1076, Irganox 1330, Irgafos 168, Tinuvin 326, Tinuvin 327, and Tinuvin P were obtained from ICI Materials (Wilton, UK) and used without further purification. Tinuvin 326, Tinuvin 329, and Tinuvin 343 were obtained from Ciba-Geigy (Marly, Switzerland). Santo White powder was obtained from DuPont (Geneva, Switzerland). In preparing the samples, a small amount (~20 mg) of material was dissolved in ~1 cm^3 of acetone. Approximately 100 μL of this solution was deposited onto a 5 mm diameter circular stainless steel sample probe and the solvent allowed to evaporate. The sample covered the entire area of the disk, ~75 mm^2. A typical mass spectrum was obtained from an area of 1.4 mm^2.

Bulk Polymers. A sample of poly(propylene) containing Irganox 1330 (0.15 wt %) and Irgafos 168 (0.05 wt %) was obtained from ICI Materials. This sample was in the form of solid beads, ~3 mm × 2 mm × 2 mm, and was analyzed as received. Three

(12) Rudewicz, P.; Munson, B. *Anal. Chem.* **1986**, *58*, 358–361.
(13) Lattimer, R. P.; Harris, R. E.; Rhee, C. K.; Schulten, H.-R. *Anal. Chem.* **1986**, *58*, 3188–3195.
(14) Lattimer, R. P. *J. Anal. Appl. Pyrol.* **1993**, *26*, 65–92.
(15) Barber, M.; Bordoli, R. S.; Sedgwich, R. D.; Taylor, A. N. *J. Chem. Soc., Chem. Commun.* **1981**, 325–327.
(16) Furstenau, N.; Hillenkamp, F.; Nitsche, R. *Int. J. Mass Spectrom. Ion Processes* **1979**, *31*, 85–91.
(17) Johlman, C. L.; Wilkins, C. L.; Hogan, J. D.; Donovan, T. L.; Laude, D. A.; Youssefi, M.-J. *Anal. Chem.* **1990**, *62*, 1167–1172.
(18) Mawn, M. P.; Linton, R. W.; Bryan, S. R.; Hagenhoff, B.; Jürgens, U.; Benninghoven, A. *J. Vac. Sci. Technol.* **1991**, *A9*, 1307–1311. Linton, R. W.; Mawn, M. P.; Belu, A. N.; Desimone, J. M.; Hunt, M. O.; Menceloglu, Y. Z.; Cramer, H. G.; Benninghoven. A. *Surf. Interface Anal.* **1993**, *20*, 991–999.
(19) Dale, M. J.; Jones, A. C.; Pollard, S. J. T.; Langridge-Smith, P. R. R.; Rowley, A. G. *Environ. Sci. Technol.* **1993**, *27*, 1693–1695.
(20) Dale, M. J.; Jones, A. C.; Pollard, S. J. T.; Langridge-Smith, P. R. R. *Analyst* **1994**, *119*, 571–578.
(21) Dale, M. J.; Downs, O. H. J.; Costello, K. F.; Wright, S. J.; Langridge-Smith, P. R. R.; Cape, J. N. *Environ. Pollut.* **1995**, *89*, 123.
(22) Zhan, Q.; Voumard, P.; Zenobi, R. *Rapid Commun. Mass Spectrom.* **1995**, *9*, 119–127.
(23) Redpath, C. R. Ph.D. Thesis, The University of Edinburgh, 1995.
(24) Mackintosh, J. G.; Redpath, C. R.; Jones, A. C.; Langridge-Smith, P. R. R.; Mount, A. R. *J. Electroanal. Chem.* **1995**, *388*, 179–185.
(25) Wright, S. J.; Mount, A. M.; Langridge-Smith, P. R. R. Unpublished results, The University of Edinburgh, 1996.
(26) Lustig, D. A.; Lubman, D. M. *Laser Photoionization and Desorption Surface Analysis Techniques*; SPIE: Bellingham, WA, 1990; pp 1208, 170.
(27) Lustig, D. A.; Lubman, D. M. *Int. J. Mass Spectrom. Ion Processes* **1991**, *107*, 265.
(28) Lykke, K. R.; Parker, D. H.; Wurz, P.; Hunt, J. E.; Pellin, M. J.; Gruen, D. M. Hemminger, J. C. *Anal. Chem.* **1992**, *64*, 2797–2803.

Table 1. Nomenclature and Structure of Polymer Additives

Trivial Name	Chemical Name	Structure	MW
Irganox 1330	1,3,5,-tris(3,5-di-*tert*-butyl-4-hydroxybenzyl)-2,4,6,trimethylbenzene	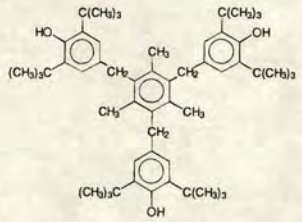	774
Irganox 1076	octadecyl-3-(3,5-di-*tert*-butyl-4-hydroxyphenyl) propionate	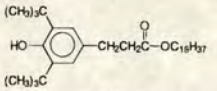	530
Irgafos 168	tris(2,4-di-*tert*-butylphenyl) phosphite	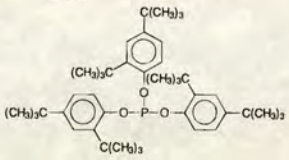	646
Santo White	4,4'-butylidene bis-6-(4-methyl-2-*tert*-butylphenol)	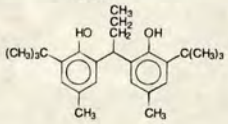	382
Tinuvin P	2-(2'-hydroxy-5'-methylphenyl)-2*H*-benzotriazole	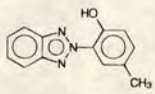	225
Tinuvin 326	2-(2'-hydroxy-3'-methyl-5'-*tert*-butylphenyl)-2*H*-5-chlorobenzotriazole	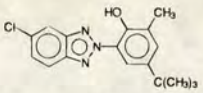	315
Tinuvin 327	2-(2'-hydroxy-3',5'-di-*tert*-butylphenyl)-2*H*-5-chlorobenzotriazole	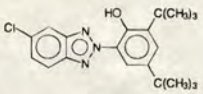	357
Tinuvin 320	2-(2'-hydroxy-3',5'-di-*tert*-butylphenyl)-2*H*-benzotriazole	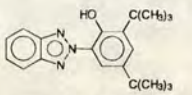	323
Tinuvin 343	2-(2'-hydroxy-3'-*tert*-butyl-5'-(1-methyl)-propylphenyl)-2*H*-benzotriazole	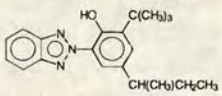	323
Tinuvin 329	2-(2'-hydroxy-5'-(1,1,3,3-di-methyl)-butylphenyl)-2*H*-benzotriazole	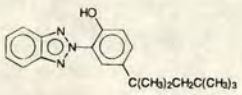	323

samples of poly(oxymethylene) (POM) obtained from DuPont were also examined. These samples had been injection moulded and were in the form of solid rods ~125 mm × 13 mm × 3 mm. One reference sample contained no additives, one contained only Santo White powder (0.1 wt %), and a third contained only Tinuvin 320 (0.3 wt %). For analysis, a section of these polymers ~25 mm × 5 mm × 3 mm in size was cut from the rods and placed directly onto the sample probe.

Instrumentation. The mass spectrometer used in these experiments has been described in detail elsewhere.[21] It consists of two differentially pumped chambers: a desorption/ionization chamber and a second chamber housing a reflection time-of-flight (RETOF) mass spectrometer. The sample probe, which is mounted on an *XYZ* manipulator, was situated approximately one-third of the distance between the repeller and the draw-out grid of the modified Wiley–McLaren ion-extraction optics.[29] To minimize field distortions, the sample probe was floated at two-thirds of the potential difference between these electrodes.

Infrared (IR) laser desorption was carried out using a pulsed TEA CO_2 laser (Alltec 854MS). The CO_2 laser beam was introduced directly above the sample and orthogonal to the sample probe. The output from the CO_2 laser was focused to a spot size of 1.4 mm^2 on the sample probe using a 20 cm focal length NaCl lens. For the analysis of the polymer additives, either as pure compounds from the stainless steel probe or directly from the POM samples, typical laser desorption power densities of ~6–10 MW cm^{-2} were employed. Higher laser desorption power

(29) Wiley, W. C.; McLaren, I. M. *Rev. Sci. Instrum.* **1955**, *26*, 1150.

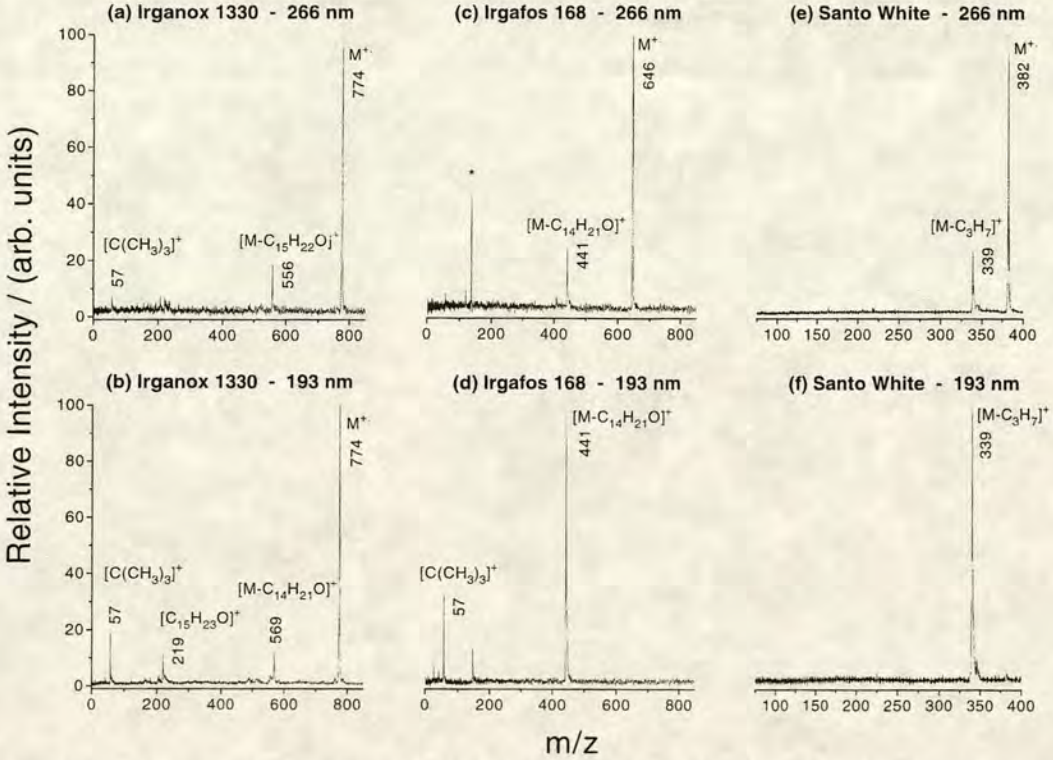

Figure 1. Photoionization mass spectra for Irganox 1330 at (a) 266 and (b) 193 nm; Irgafos 168 at (c) 266 and (d) 193 nm; and Santo White powder at (e) 266 and (f) 193 nm. The peak marked with an asterisk in spectrum c is due to an internal mass standard, 4-aminobenzoic acid ($m/z = 137$).

densities were required for the in situ analysis of additives from the PP sample.

The desorbed neutral species were photoionized ~5 mm above the sample surface using one of two lasers operating at either 193 (Lumonics TE-860T excimer laser, ArF line) or 266 nm (JK HY750 Nd:YAG laser, fourth harmonic). The ionization laser power density was chosen to maximize the intensity of the molecular ion signal while minimizing fragmentation. Typical power densities were ~0.8 MW cm^{-2} when using 193 nm photoionization and ~2 MW cm^{-2} for photoionization at 266 nm.

Vertical deflection plates were used to steer the ions into the reflection time-of-flight mass spectrometer (RETOFMS). Ions were detected using a dual-chevron-type microchannel plate detector (R. M. Jordon), and the signal was further amplified by a factor of 10. Spectra were collected using a CAMAC-based data acquisition system, employing a 200 MHz transient digitizer (Joerger TR200) interfaced to a Dell Model 325 PC with custom in-house software. Only positive ion spectra were acquired in these experiments.

The mass resolution of the RETOFMS, $R = m/\Delta m = t/2\Delta t$, has been measured to be 1200 at $m/z = 477$. However, the observable mass range at the highest time resolution of the digitizer, equivalent to the highest sampling speed (200 MHz, 5 ns/point), is limited because of the finite digitizer memory that can be stored (2K points). The spectra displayed here were recorded using either a 50 (20 ns) or 25 MHz (40 ns) sampling speed and are bandwidth limited. Experiments were carried out at a repetition rate of 10 Hz. For the pure additives, data from ~100 laser shots were accumulated in order to enhance the signal-to-noise ratio. For in situ analysis of the bulk polymers, typically 200 laser shots were accumulated. Generally, a three-point mass calibration was employed using indole ($m/z = 117$), carbazole ($m/z = 167$), coronene ($m/z = 300$), phthalocyanine ($m/z = 514$), or magnesium phthalocyanine ($m/z = 536$) as standards. Mass measurement accuracy is 200 ppm. All peaks are quoted as integer nominal mass.

RESULTS AND DISCUSSION

Pure Polymer Additives. The ultimate aim of using L2MS for polymer additive characterization was to provide a means for direct detection of these compounds in polymers. As a preliminary to undertaking such experiments, L2MS spectra were first recorded for samples of the pure additives. The additives examined are shown in Table 1; they consist of phenolic and phosphite antioxidants and Tinuvin UV stabilizers. These additives were all studied using both 266 and 193 nm photoionization.

Antioxidants. The mass spectra obtained for Irganox 1330, Irgafos 168, and Santo White using 266 and 193 nm photoionization are shown in Figure 1. In the case of Irganox 1330, the spectra at both these wavelengths are dominated by the molecular ion peak at $m/z = 774$. However, it is evident that 266 nm photoionization results in the production of fragment ions different than those observed at 193 nm. At 266 nm, a fragment is observed at $m/z = 556$. This is thought to result from loss of a 3,5-di-*tert*-butyl-4-hydroxybenzyl side group, with a concomitant hydrogen rearrangement. A weaker fragment peak at $m/z = 57$, due to the *tert*-butyl ion, can also be seen.

Photoionization of Irganox 1330 at 193 nm produces fragments at $m/z = 57$, 219, and 569. The fragment at $m/z = 569$ corresponds to the loss of a 3,5-di-*tert*-butyl-4-phenol side group via direct cleavage rather than rearrangement. The peak at $m/z = 219$ is characteristic of positive ion mass spectra of dibutyl phenols and corresponds to the 3,5-di-*tert*-butyl-4-hydroxybenzyl

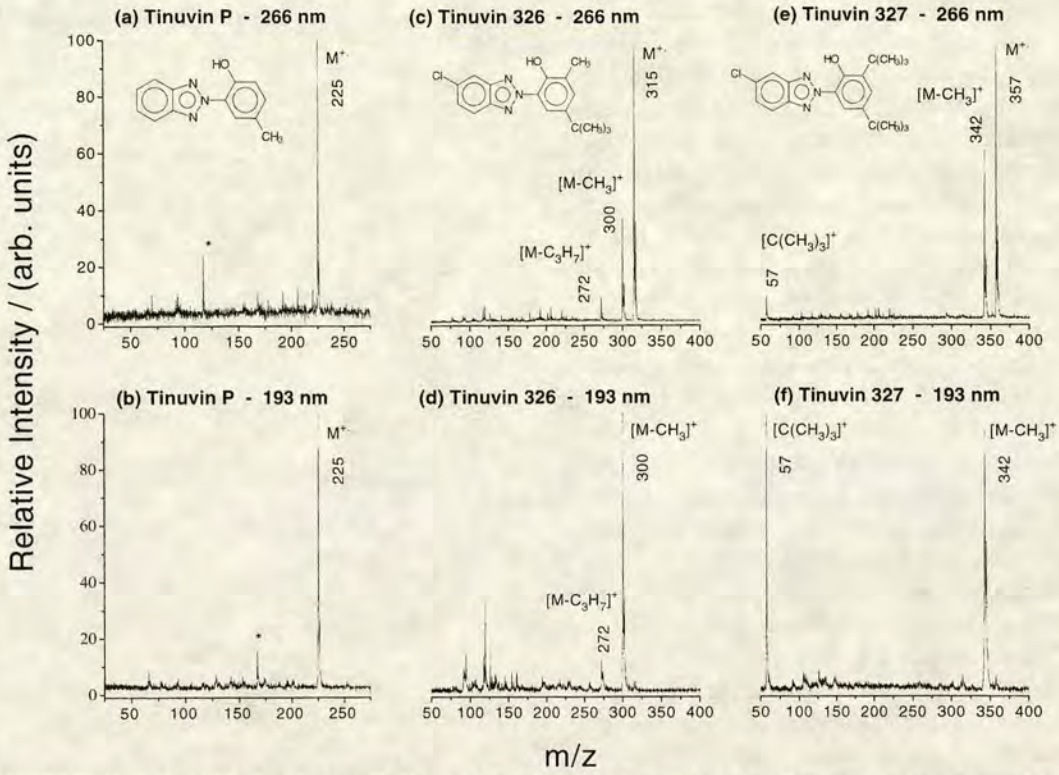

Figure 2. Photoionization mass spectra for Tinuvin P at (a) 266 and (b) 193 nm; Tinuvin 326 at (c) 266 and (d) 193 nm; and Tinuvin 327 at (e) 266 and (f) 193 nm. Peaks marked with an asterisk are due to the internal mass standards indole ($m/z = 117$) and carbazole ($m/z = 167$).

ion.[11,30] The peak at $m/z = 57$ corresponds to the *tert*-butyl ion.

Similar characteristics were observed in the mass spectra for Irganox 1076 (not shown). When 266 nm radiation is used, the molecular ion can be clearly identified at $m/z = 530$. At 193 nm, no molecular ion peak is seen. Instead, the base peak of the mass spectrum is at $m/z = 515$, corresponding to the loss of a methyl radical from the molecular ion.

For Irgafos 168, which is a phosphite antioxidant, there is once again a marked difference in the mass spectra obtained using photoionization at 266 versus 193 nm. At 266 nm, the molecular ion at $m/z = 646$ is the base peak in the mass spectrum. A less intense fragment peak is also observed at $m/z = 441$, which corresponds to the loss of a 2,4-di-*tert*-butylphenyl−O side group via direct cleavage. However, for photoionization at 193 nm, this fragment ion is the base peak in the spectrum, and there is no signal corresponding to the molecular ion. A prominent fragment peak at $m/z = 57$, due to the *tert*-butyl ion, can also be seen.

Figure 1e shows the mass spectrum obtained for Santo White powder using 266 nm photoionization. The molecular ion at $m/z = 382$ is the base peak in the spectrum, with the fragment peak at $m/z = 339$ corresponding to the loss of a propyl radical, [$^{\bullet}C_3H_7$], from the molecular ion. The 193 nm photoionization mass spectrum is shown in Figure 1f. Once again, no molecular ion signal is observed. The only significant peak in this mass spectrum is due to the fragment at $m/z = 339$, which is assigned, as before, to the loss of a propyl radical, [$^{\bullet}C_3H_7$], from the molecular ion.

In summary, for all the antioxidants studied, the mass spectra obtained using photoionization at 266 nm are dominated by molecular ion signals, with very little fragmentation. With the exception of Irganox 1330, photoionization using 193 nm radiation generated little or no molecular ion signal. There are two possible explanations for this apparent wavelength dependence. Most organic molecules have ionization potentials (IP) in the range 7−10 eV. The energy of 266 nm photons is ~4.66 eV, whereas a 193 nm photon has an associated energy of 6.42 eV. In both cases, therefore, absorption of two photons is required in order to achieve ionization. However, absorption of the first 193 nm photon can result in different intermediate electronic states being accessed compared to excitation at 266 nm, such as Rydberg states. It is possible that this may lead to different ionization pathways being promoted, resulting in differing mass spectra at 193 versus 266 nm.[31] Alternatively, the difference may simply be due to the difference in excess energy deposited initially in the molecular ion. Assuming an ionization potential of 8 eV, photoionization at 266 nm will produce a molecular ion with up to 1.32 eV of excess energy. This is small compared to the excess energy of up to 4.84 eV possible following photoionization at 193 nm. This larger excess energy may be sufficient to exceed the appearance potential for the production of the most facile fragment ions. Therefore, at 193 nm, ionization would be accompanied by facile fragmentation. Our data at present do not enable us to identify which of these two mechanisms may be responsible for the different fragmentation patterns observed.

UV Stabilizers. The 266 and 193 nm photoionization mass spectra of the UV stabilizers Tinuvin P, Tinuvin 326, and Tinuvin 327 are shown in Figure 2. For Tinuvin P, the base peak in the mass spectra at both wavelengths is due to the molecular ion, with essentially no fragmentation occurring. However, for Tinuvin 326 and Tinuvin 327, significant differences were found in the mass spectra obtained at these two photoionization wavelengths. For

(30) Asamoto, B.; Young, J. R.; Citerin, R. J. *Anal. Chem.* **1990**, *62*, 61−70.

(31) Jones, A. C.; Dale, M. J.; Keenan, G. A.; Langridge-Smith, P. R. R. *Chem. Phys. Lett.* **1994**, *219*, 174−180.

photoionization of Tinuvin 326 at 266 nm, the molecular ion is the base peak in the spectrum (see Figure 2c). Fragment ions were observed at $m/z = 300$ and 272, which can be attributed to the loss of a methyl radical, [$^{\bullet}CH_3$], and [$-C_3H_7$] group, respectively, from the molecular ion. In contrast, for photoionization at 193 nm, no molecular ion signal is detected (see Figure 2d). The principal peaks at $m/z = 300$ and 272 can be assigned to the same fragment ions as in Figure 2c. At both 266 and 193 nm, it is possible to resolve the doublets characteristic of the two naturally occurring isotopes of chlorine.

The spectra for Tinuvin 327 are similar to those obtained for Tinuvin 326. At 266 nm, the molecular ion is the base peak in the spectrum (see Figure 2e), with a less intense fragment ion observed at $m/z = 342$ due to the loss of a [$^{\bullet}CH_3$] radical from the parent molecular ion. A weaker peak at $m/z = 57$, due to the *tert*-butyl ion, can also be observed. Figure 2f shows the spectrum obtained at 193 nm. Again, no molecular ion peak is observed, only a strong fragment peak due to the loss of the [$^{\bullet}CH_3$] radical from the molecular ion, together with a very prominent fragment peak at $m/z = 57$ due to the *tert*-butyl ion.

In general, the photoionization mass spectra of the Tinuvin UV stabilizers examined differ markedly at 266 and 193 nm. At 266 nm, the mass spectra are dominated by molecular ion signals, with very little associated fragmentation. This nicely illustrates the advantage of L2MS as a soft ionization technique, enabling readily interpretable mass spectra to be generated. Photoionization at 193 nm, however, results in mass spectra in which the base peaks are fragment ions. This difference in behavior may be due either to the difference in excess energy deposited in the molecular ion or to excitation via different intermediate states, as discussed earlier.

Isomeric UV Stabilizers. The marked wavelength dependence of these photoionization mass spectra can be exploited for the unambiguous identification of many polymer additives. A particularly useful application is the differentiation between isomeric additives. The mass spectra of three such isomeric species, Tinuvin 320, Tinuvin 343, and Tinuvin 329, were recorded using photoionization at both 266 and 193 nm. The spectra are shown in Figures 3 and 4, respectively.

The 266 nm photoionization mass spectrum for Tinuvin 320, shown in Figure 3a, consists of a base peak at $m/z = 323$, corresponding to the molecular ion. A less intense fragment ion at $m/z = 308$, consistent with the loss of a methyl radical from the molecular ion, is also observed. The mass spectrum of Tinuvin 343, shown in Figure 3b, also contains these two peaks. However, a further fragment peak is observed at $m/z = 294$, which can be assigned to the loss of an ethyl radical, [$^{\bullet}C_2H_5$], from the molecular ion. The 266 nm photoionization spectrum of Tinuvin 329, shown in Figure 3c, is markedly different, however. While a peak corresponding to the molecular ion is observed, the base peak in the spectrum is at $m/z = 252$. This fragment ion can be attributed to the loss of a 2,2-dimethylpropyl radical, [$^{\bullet}CH_2C(CH_3)_3$], which results from direct cleavage at the tertiary substituted carbon atom in the alkyl side chain of the molecular ion.

Photoionization of these isomers at 193 nm produced mass spectra similar to those previously observed for the other Tinuvin UV stabilizers. For Tinuvin 320, no molecular ion is observed in the spectrum (see Figure 4a). The base peak is at $m/z = 308$, which was previously attributed to loss of a methyl radical from the molecular ion. The intense fragment peak at $m/z = 57$ is

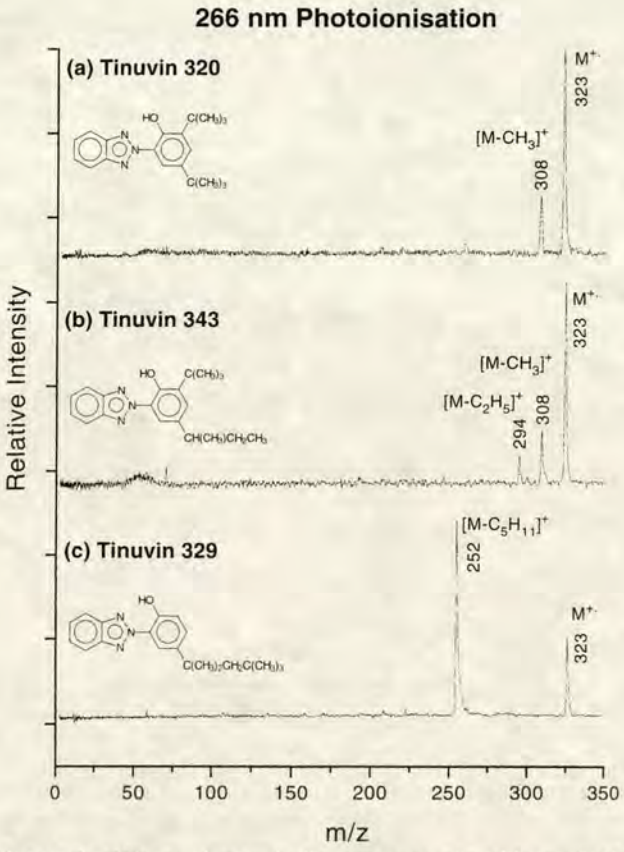

Figure 3. 266 nm photoionization mass spectra of isomeric UV stabilizers (a) Tinuvin 320, (b) Tinuvin 343, and (c) Tinuvin 329.

due to the *tert*-butyl ion. The assignment of the other low-mass fragment peaks at $m/z = 29$ and 41 is less certain, but they may correspond to $[C_2H_5]^+$ and $[C_3H_5]^+$, respectively. The weaker, and somewhat broader, peaks in the middle mass range may be due to fragmentation of the benzotriazole skeleton. The 193 nm photoionization mass spectrum of Tinuvin 343 is shown in Figure 4b. Again, no molecular ion signal was detected. The fragment ions at $m/z = 308$ and 294 are assigned as $[M - CH_3]^+$ and $[M - C_2H_5]^+$, respectively. The peaks to low mass, and those in the middle mass range, are assigned as above. The mass spectrum of Tinuvin 329 obtained using 193 nm photoionization is shown in Figure 4c. The base peak in the mass spectrum is at $m/z = 252$, which is assigned as loss of the 2,2-dimethylpropyl radical from the molecular ion. Interestingly, no prominent fragment peak at $m/z = 57$ for the *tert*-butyl ion is observed for this isomer.

In the case of these isomeric Tinuvin UV stabilizers, the nature of the substituent groups can affect the fragmentation and allow for differentiation between isomers. For example, Tinuvin 320 has two *tert*-butyl substituents, and so it may lose a methyl radical from either, but not both, of its substituent groups. This results, therefore, in a single fragment ion corresponding to $[M - CH_3]^+$ (see Figures 3a and 4a). Alternatively, Tinuvin 343 contains only one *tert*-butyl substituent along with a [$-CH(CH_3)CH_2CH_3$] group. Again, it is possible to lose a methyl radical at the *tert*-butyl substituent, as before. However, the most stable carbocation that can be formed by a fragmentation at the other substituent corresponds to the loss of an ethyl radical, to leave the ion $[M - C_2H_5]^+$. Therefore, in this case, a mass spectrum is produced that contains two high-mass fragment ions (see Figures 3b and 4b), which allows this molecule to be differentiated from its isomer Tinuvin 320. In the case of Tinuvin 329, there is only one alkyl

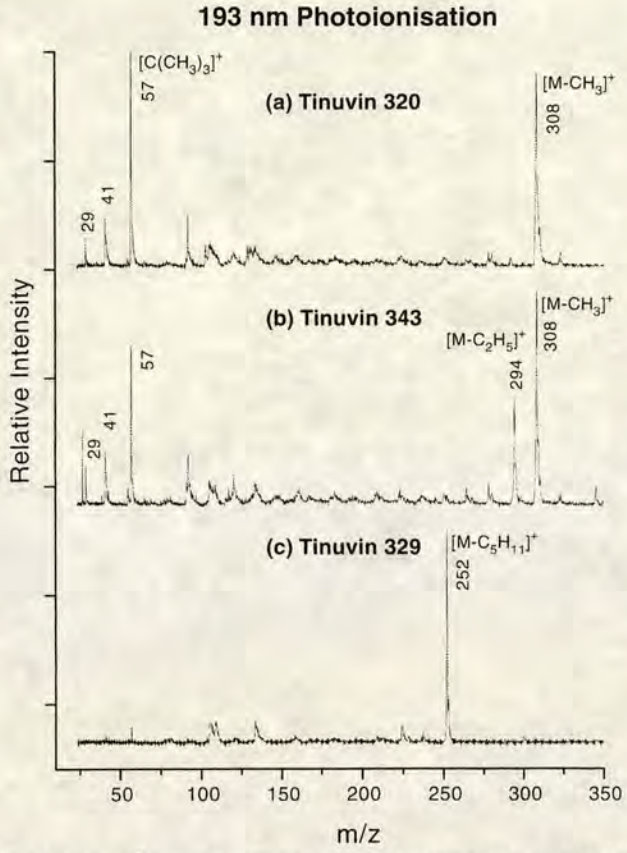

Figure 4. 193 nm photoionization mass spectra of isomeric UV stabilizers (a) Tinuvin 320, (b) Tinuvin 343, and (c) Tinuvin 329.

substituent, and so the most stable radical that can be lost is a 2,2-dimethylpropyl radical, [$^{\bullet}CH_2C(CH_3)_3$]. This results in a mass spectrum that contains the molecular ion and a single fragment at $m/z = 252$ (see Figures 3c and 4c).

At each of the two photoionization wavelengths employed, it is possible to distinguish between all three of these Tinuvin isomers. However, by comparing the spectra obtained at both of these wavelengths, one can also unambiguously identify each isomer from its fragmentation patterns, which are characteristic of the hydroxyphenylbenzotriazole compound class.

Photofragmentation of UV Stabilizers. Tinuvin P displays what, at first sight, appears to be anomalous behavior. In this case, both 266 and 193 nm photoionization result in exclusive detection of the molecular ion (see Figure 2a and b). In this case, this is due to the lack of tertiary substituents in Tinuvin P. All of the other Tinuvin UV stabilizers studied in this work contain tertiary substituent groups. Fragmentation is most likely to occur at these sites, since a stable tertiary carbocation is produced as a result of resonance stabilization. The absence of such tertiary substituents in Tinuvin P, therefore, means that no such facile fragmentation process is possible, and an intact molecular ion is observed.

Apparently anomalous behavior is also observed in the case of Tinuvin 329. In the 266 nm photoionization mass spectrum of this compound, a fragment peak dominates the molecular ion signal (see Figure 3c). Reduction of the ionizing laser fluence failed to enhance the molecular ion signal relative to the fragment ion. This suggests, therefore, that the observed fragmentation is not a stepwise process resulting from absorption of photons by the molecular ion. Once again, therefore, there are two possible mechanisms by which this fragment ion may be produced.

One possibility is that absorption of two 266 nm photons deposits sufficient excess energy to exceed the appearance potential of this fragment ion. However, from the earlier discussion, which assumed an approximate ionization potential of 8 eV for these molecules, only 1.32 eV of excess energy is present in the molecular ion. Typical C–C bond dissociation energies are on the order of 350 kJ mol^{-1}, which is equivalent to around 3.63 eV. Therefore, on energetic grounds, excess energy in the molecular ion is unlikely to be the cause of the observed fragmentation.

Another possibility, as mentioned earlier, is that absorption of the first photon accesses excited electronic intermediate states which promote ionization pathways that do not lead exclusively to the molecular ion, favoring formation of fragment ions, instead. Photoionization of Tinuvin 329 at 193 nm produces a similar mass spectrum (see Figure 4c). In this case, the molecular ion is not observed. Once more, it is likely that the fragmentation is caused by accessing an excited intermediate state, which promotes an ionization pathway that does not result in molecular ion production. However, without accurate ionization potentials and more information on the excited states, it is not possible to be certain which of the two alternative explanations is correct.

Such wavelength-dependent photoionization mass spectra can enable important structural information to be obtained about the molecules under study. However, more importantly, they also aid in the unambiguous determination of unknown compounds directly from their host matrices.

In Situ Analysis of Additives Directly from Polymers. Clearly, any technique that can provide chemical analysis of target analytes at trace levels directly from their host matrix represents an attractive and rapid methodology. L2MS has previously been used for in situ analysis of polycyclic aromatic hydrocarbons (PAHs) in atmospheric particulates.[21,22] The feature of the technique that allows this to be achieved is the selectivity provided by the photoionization process. Most organic molecules have ionization potentials between 7 and 10 eV. To achieve ionization, absorption of two or more UV photons is required. For efficient photoionization, a molecule must have a significant absorption cross section at the wavelength of the ionizing radiation employed. Molecules that do not possess a suitable chromophore will not be efficiently ionized. Therefore, by careful choice of the ionization laser wavelength, the target analyte of interest may be selectively detected in preference to other components present in the mixture, including the host matrix. In the present study, it is shown that polymer additives with an appreciable absorption in the UV region of the spectrum can be selectively ionized in preference to the non-UV-absorbing host polymer.

Several polymer formulations were studied using this approach. A sample of poly(propylene) (PP) containing 0.15 wt % of Irganox 1330 and 0.05 wt % of Irgafos 168 was examined first. The mass spectra obtained using 266 and 193 nm photoionization following direct desorption from the PP matrix are shown in Figure 5. To obtain an appreciable signal from this sample, it was necessary to increase the desorption laser power density 4-fold, to ~38 MW cm^{-2}, compared to the value used to desorb the pure polymer additives. The need for increased laser desorption power densities is due to the poly(propylene) matrix having a very low absorbance at the desorption laser wavelength of 10.6 μm.[32] In the spectrum

(32) Zhan, Q.; Zenobi, R.; Wright, S. J.; Langridge-Smith, P. R. R. Submitted to *Macromolecules*.

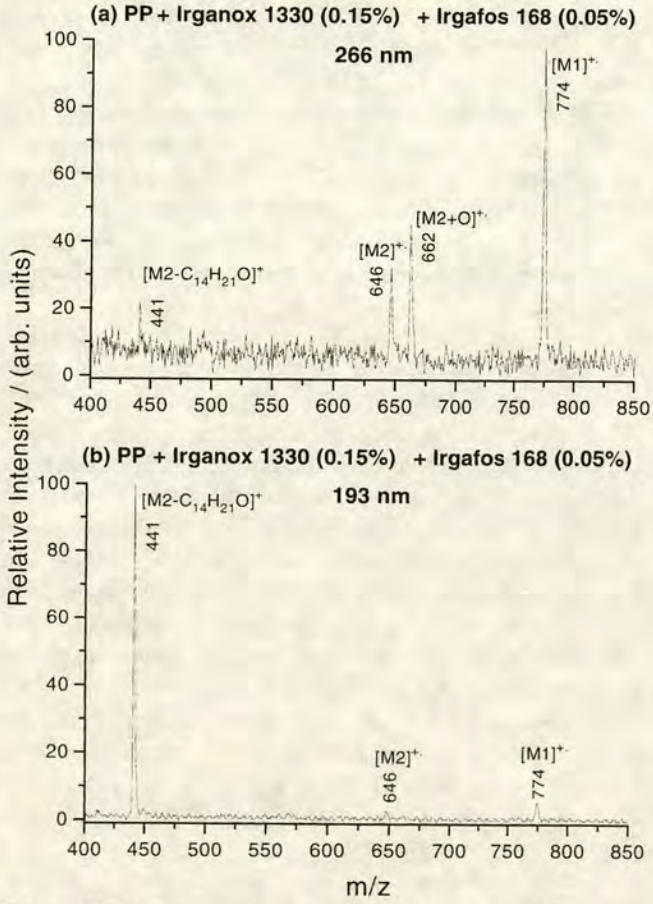

Figure 5. In situ mass spectra of poly(propylene) (PP) sample containing Irganox 1330 (0.15 wt %) and Irgafos 168 (0.05 wt %). Photoionization at (a) 266 and (b) 193 nm. $[M1]^+$ and $[M2]^+$ denote the molecular ions of Irganox 1330 and Irgafos 168, respectively.

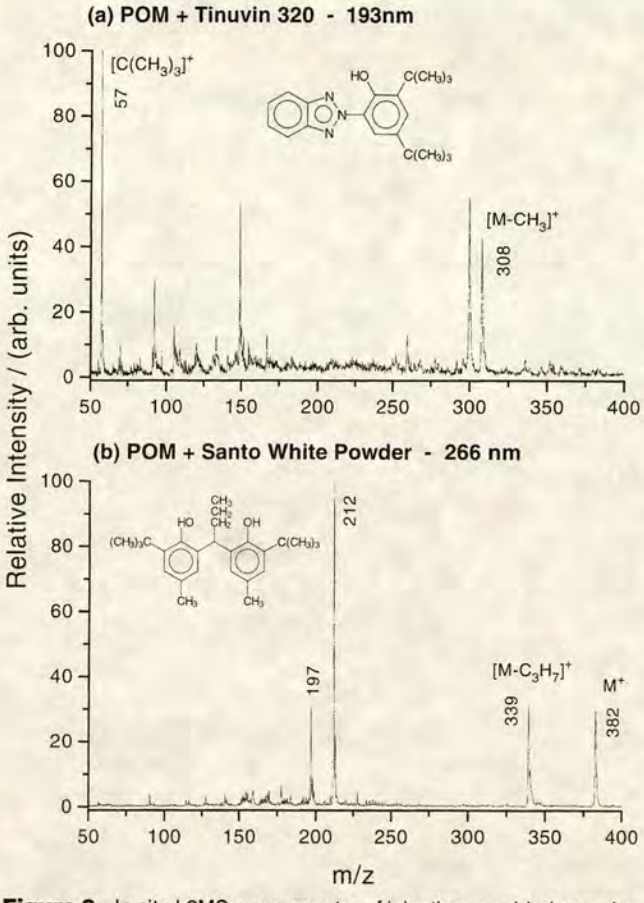

Figure 6. In situ L2MS mass spectra of injection-moulded samples of POM. (a) Sample containing Tinuvin 320 (0.3 wt %); photoionization at 193 nm. (b) Sample containing Santo White antioxidant (0.1 wt %); photoionization at 266 nm.

obtained at 266 nm, the molecular ions for both Irganox 1330 (m/z = 774) and Irgafos 168 (m/z = 646) are present. For ionization at 193 nm, the molecular ion signals are very much weaker. However, a strong characteristic fragment signal at m/z = 441, anticipated from the 193 nm photoionization mass spectrum of pure Irgafos 168 (see Figure 1d), can be seen. This peak is due to the loss of a 2,4-di-*tert*-butylphenyl−O group from the molecular ion, as is seen in the corresponding spectrum for the pure compound. These spectra demonstrate that, by use of two readily available ionization wavelengths, and with reference to the corresponding spectra for the pure additives, it is possible to unambiguously determine the presence of Irganox 1330 and Irgafos 168 directly from the host PP matrix.

An apparently anomalous peak at m/z = 662 is observed in the 266 nm photoionization mass spectrum (see Figure 5a). This can be accounted for by considering the chemistry of Irgafos 168. This compound is a phosphite antioxidant, which is generally considered to be a secondary antioxidant. Phosphite antioxidants react with hydroperoxides, peroxy radicals, alkoxy radicals, and olefinic and carbonyl moieties, thereby controlling polymer molecular weight and color. The level of phosphite additives in polymers affects the stability of the polymer. Although it is very important to be able to determine how much additive is in the polymer, it is equally important to be able to monitor how much the additive remains in the original phosphite form, since it is only in this form that the additive remains useful as an antioxidant. The peak at m/z = 662 in Figure 5b can be attributed to the oxide of Irgafos 168. The ratio of phosphite to phosphate will give an indication of how resistant the polymer will be to further oxidation. Studies of this type have previously been attempted by SIMS[18] and LD-EI-FTICR.[33] The data presented here show that it is possible not only to determine the presence of additive species directly from the polymer but also to monitor chemical changes caused by the polymerization process or subsequent exposure to heat, light, and other conditions which initiate polymer degradation.

The MPI efficiency of the additive under investigation is an important factor. For example, photoionization of pure Tinuvin 320 using 266 nm radiation produced intense signals (see Figure 3a). However, when a sample of POM containing 0.3 wt % of Tinuvin 320 was analyzed using photoionization at 266 nm, no peaks attributable to this compound were observed. This sample was supplied in the form of an injection-moulded bar from which a section was cut and attached to the sample probe. Figure 6a shows a mass spectrum for the same polymer sample obtained using 193 nm photoionization. Intense signals are observed at m/z = 308 and 57, which correspond to the anticipated fragment ions for the 193 nm photoionization of pure Tinuvin 320 (see Figure 4a). It is clear that photoionization at 193 nm is a more efficient and sensitive detection wavelength for Tinuvin 320 than that at 266 nm. The desorption power density used was 7.7 MW cm^{-2}, which is similar to the value used for desorption of the pure

(33) Xiang, X.; Dahlgren, J.; Enlow, W. P.; Marshall, A. G. *Anal. Chem.* **1992**, *64*, 2862−2865.

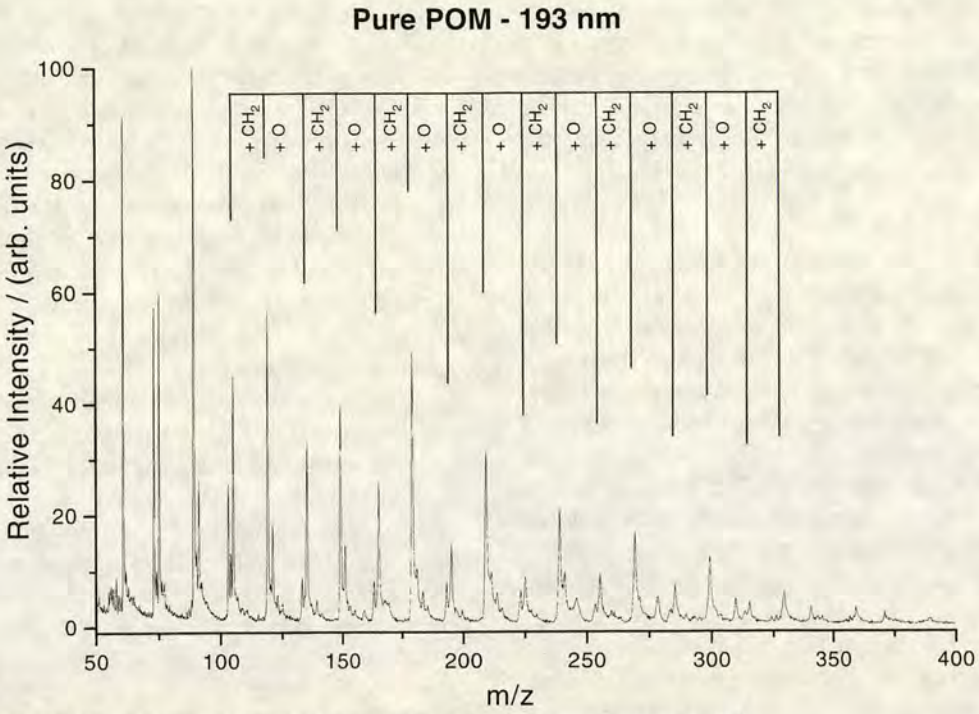

Figure 7. 193 nm photoionization mass spectrum of an injection-moulded sample of pure POM.

additives from a stainless steel substrate. POM has a relatively intense absorption at 10.6 μm; as a result, only moderate desorption powers are required for desorption of the neutral analyte species.[32] It is clear that, provided sufficient material can be liberated from the polymer, the limiting factor for in situ detection of additives at levels typically found in real polymer formulations is the efficiency with which they can be ionized. Provided a suitable wavelength is available, the analysis of bulk polymers with additive concentrations as low as 0.01 wt % should be possible using this technique.

As a further example of the utility of the L2MS technique, another sample of POM, this time containing Santo White antioxidant, was analyzed using 266 nm photoionization. This sample, also cut from an injection-moulded bar of POM, contained 0.1 wt % of Santo White powder. It was attached to the sample probe, such that the polished surface of the polymer was interrogated by the CO_2 laser.

Figure 6b shows the 266 nm photoionization mass spectrum obtained when this finished exterior surface of the polymer sample was exposed to the CO_2 laser. In addition to the peaks at m/z = 382 and 339 observed previously from the pure sample of Santo White, a further intense peak can be seen at $m/z = 212$, together with another peak at $m/z = 197$. It has not proved possible to formally identify these peaks, although it is believed that they may be due to a surface contaminant introduced during the finishing or injection processes. When desorption was carried out on the same location for an extended period of time, the intensities of the peaks at $m/z = 212$ and 197 were observed to diminish relative to those of the peaks associated with the antioxidant. This reinforces the argument that these peaks are due to a species present on the surface of the polymer.

When the interior, unfinished surface of the polymer was interrogated, these peaks were absent. This demonstrates that L2MS can be used to readily detect species from the surface of a polymer. Polymer additives are not uniformly distributed throughout a given polymer matrix. Often, the additives will migrate toward the surface or aggregate into small clusters within the body of the polymer. Both of these effects can alter the chemical and mechanical properties of the material. In addition, trace contaminants may be present on the surface of the polymer introduced during injection moulding and/or finishing processes.

Since this experiment has shown that the L2MS technique is sensitive to surface species, it may be possible to assay for polymer additives as a function of depth within the polymer. This will be the subject of a forthcoming publication.[32] Such studies could also be extended to include two-dimensional imaging of additives on a polymer surface, by utilizing an optical delivery system capable of achieving a desorption spot-size less than 50 μm. This would allow the investigation of inhomogeneous features on polymer surfaces, such as additive aggregation or segregation throughout a polymer formulation. It may also prove possible to monitor time-dependent phenomena, such as the extent of surface migration and segregation of additives as a function of polymer age.

An important feature of the spectra shown in Figures 5 and 6 is that no signals are observed that correspond to the polymer matrix itself. Efficient multiphoton ionization (MPI) requires that the target molecule has a significant absorption at the photoionization wavelength. Neither poly(propylene) (PP) nor poly(oxymethylene) (POM) possesses a UV chromophore. Thus, at low ionizng laser fluences, it is possible to effectively discriminate against material ablated or desorbed from the polymer matrix itself. It has been shown elsewhere[32] that incident infrared radiation at 10.6 μm at laser power densities similar to those employed here results in efficient ablation for POM, due to its relatively high absorption cross section at this wavelength. It is unlikely, therefore, that neutral fragments associated with the polymer are not present in the gas phase in the ionization region. At higher ionizing laser power densities, it is possible to promote nonresonant MPI of nonabsorbing material. At these elevated fluences, the target materials are prone to significant levels of fragmentation. Figure 7 shows such a spectrum for a sample of

pure POM polymer, obtained using photoionization at 193 nm. In this case, the ionizing laser output was focused, resulting in an increased power density of 3.4 MW cm^{-2}. This characteristic spectrum shows two series of low-mass ions separated by units by $m/z = 30$, thereby providing sufficient evidence to identify the polymer as POM, with a repeat unit of $[-CH_2O-]_n$.

CONCLUSION

The analysis of chemical additives within bulk polymers is a complex problem. Extraction-based methodologies are well established, but they are frequently time consuming and laborious procedures. Direct analysis of additives in bulk polymers is an attractive methodology. However, traditional mass spectrometric approaches are not suitable for the analysis of such species, and other more recent techniques such as FAB and SIMS often suffer from considerable matrix interference. This work has demonstrated that L2MS is a powerful technique in that it can generate simple readily interpretable mass spectra for such molecules.

Photionization mass spectra at 266 and 193 nm for a series of phenolic and phosphite antioxidants as well as hydroxyphenylbenzotriazole UV stabilizers have been recorded. Marked differences in the photofragmentation behavior at these two wavelengths allow unambiguous identification of these additives, even including differentiation between isomeric species. It has also proved possible to detect antioxidants and UV stabilizers in poly(propylene) (PP) and poly(oxymethylene) (POM) polymers at concentrations consistent with commercial polymer formulations. In the case of the PP polymer formulation, it has been possible to detect an oxidation product of the antioxidant Irgafos 168 formed during either processing or natural aging of the polymer. Such measurements could be extended to allow monitoring of additive degradation levels in aged polymer samples.

This study has also demonstrated the potential of L2MS as a surface analytical technique. It has been shown that it is possible to detect species on the surfaces of polymers which are not present in the bulk of the sample. It should prove possible to extend this work using spatially resolved desorption to probe for additive migration and aggregation. Indeed, the use of this technique for depth profiling has recently been demonstrated.[32]

ACKNOWLEDGMENT

S.J.W. thanks the BMSS for a John Beynon Studentship. We are also grateful to Unilever plc for financial support and for the award of a postdoctoral fellowship to M.J.D. We thank Dr. V. Dudler (Ciba-Geigy, Marly, Switzerland) and Dr. J.-M. Philippoz (DuPont, Geneva, Switzerland) for providing samples. We also thank Jim Scrivens, Tony Jackson, and Hilary Yates at ICI for financial support and helpful discussions during this project. This collaborative study was made possible through a CIBA ACE award. P.R.R.L.S. also thanks CIBA for the award of a Senior Research Fellowship.

Received for review May 1, 1996. Accepted July 25, 1996.[⊗]

AC9604292

[⊗] Abstract published in *Advance ACS Abstracts,* September 1, 1996.